Evaluation of a Permittivity Sensor for Continuous Monitoring of Suspended Sediment Concentration

Barbra Crompton Utley

Dissertation submitted to the faculty of the Virginia Polytechnic Institute and State University in partial fulfillment of the requirements for the degree of

Doctor of Philosophy
In
Biological Systems Engineering

Theresa Wynn
W. Cully Hession
Panos Diplas
Carl Zipper
Naraine Persaud
Naiqian Zhang

October 30, 2009
Blacksburg, Virginia

Keywords: sediment, suspended sediment concentration, sediment transport, permittivity, streams

Evaluation of a Permittivity Sensor for Continuous Monitoring of Suspended Sediment Concentration

Barbra Crompton Utley

ABSTRACT

According to the US Environmental Protection Agency (USEPA) sediment is a leading cause of water quality impairment (US EPA, 2002). The annual costs of sediment pollution in North America alone are estimated to range between $20 and $50 billion (Pimentel et al., 1995; Osterkamp et al, 1998, 2004). Due to the large spatial and temporal variations inherent in sediment transport, suspended sediment measurement is challenging.

The overall goal of this research was to develop and test an inexpensive sensor for continuous suspended sediment monitoring in streams. This study was designed to determine if the gain and phase components of permittivity could be used to predict suspended sediment concentrations (SSC). A bench-scale suspension system was designed and tested to guarantee that there were no significant differences in the sediment suspension vertically or horizontally within the system. This study developed prediction models for SSC with input variables of temperature, specific conductivity, and gain and/or phase at multiple frequencies. The permittivity sensor is comprised of an electrode, power source, and a control box or frequency generator.

Fixed and mixed effect, multiple, linear regression models were created and compared for target frequencies. However, it was not possible to meet the normality requirements for prediction accuracy. Partial Least Squares (PLS) regression techniques were also applied to gain and phase data for 127 of the 635 frequencies. The three models with the lowest error between predicted and actual values of SSC for validation were further tested with nine levels of independent validation data. The largest model error (error>50%) occurred for the top three models at 0 and 500 mg/L. At the higher concentrations error varied from 1-40%.
Once the treatment levels, of the independent validation data set, were near 1000 mg/L the prediction accuracy increased for the top three models. Model 3A, a phase based model, preformed the best. Model 3A was able to predict six of the nine independent validation treatment levels within 300 mg/L. Future research will provide additional laboratory and field testing of the prototype sensor.

Dedication

I would like to dedicate this work to my husband and best friend, Sam Utley, for pushing me to believe in my dream.

Acknowledgements

I would like to thank my advisor, Dr. Tess Wynn, for her support and advice throughout my doctoral program. Dr. Wynn has become a mentor, confidant, and a friend during my time at Virginia Tech. Thank you for sharing your time and family with me. I would also like to thank my research committee Cully Hession, Carl Zipper, Naraine Persaud, Naiqian Zhang, and Panos Diplas for their time and thoughts on my dissertation project. I would like to give a special thanks to Naiqian Zhang for allowing me to borrow one of his control boxes for my dissertation work.

This project would not have been possible without the help of Laura Teany and Henry Lehmann. Laura and Henry have offered support, ideas, and sympathy throughout every phase of this project. I would also like to thank a few of the graduate students in our research group: Leslie Hopkinson, Andrea Ludwig, and Kathy DeBusk, for their friendship during these last few years. It has been pleasure struggling through school and life with you ladies.

I have been blessed with a wonderful support system of both family and friends. I would like to thank my family: Katherine and Jim Crompton; Rita Crompton and Ray Burrasca; Sena Zoller; Rennae, Dennis, and William Beilke; Barb, Barry, and Beau Bisbee; and finally Phil and Dot Utley for their support and endless cellular minutes over the last four years. Without your encouragement this would have been a very long four years.

Lastly there has been one man and core group of women with me throughout my undergraduate and graduate school adventures. My husband, Sam, has been gently pushing me to succeed in my chosen area of engineering for nine years. Thank you for every pep talk, hug, and walk in the woods when school became too much and my sensor just didn't work. Lastly, to my UGA girls thank you for every laugh, memory, and adventure over the last ten years. Your support and encouragement has meant everything.

Table of Contents

List of Tables

List of Figures

Chapter 1: Introduction

1.1 Introduction

Suspended sediment is a global problem; annual worldwide suspended sediment yields are estimated at around 20 billion tons (Wren et al., 2002) and the suspended sediment load makes up 70% of the total sediment transported to the oceans (Leopold, 1994). In North America the annual costs due to sediment pollution are estimated to range between $20 billion and $50 billion (Pimentel et al., 1995; Osterkamp et al, 1998, 2004). The US Environmental Protection Agency (US EPA) identified sediment as a leading cause of water quality impairment in 2002 (US EPA, 2002). A survey of streams throughout the United States determined 46% of streams analyzed suffer from excessive siltation (Berkman and Rabeni, 1987).

Section 303(d) of the Clean Water Act requires states to list impaired waters and to establish Total Maximum Daily Loads (TMDL) for watersheds drained by impaired streams. Results of these TMDL plans have wide-ranging impacts on local land use, industry, and development. Currently, many of the water quality assessments for sediment are based on a few grab samples; there is little information on natural levels of suspended sediments or the thresholds at which ecological impairment occurs. Few suspended sediment criteria have been established by the states or the US EPA because the connection between suspended sediment concentrations (SSC) and ecological responses is not clear (Kuhnle and Simon, 2000).

Due to the large spatial and temporal variations inherent in sediment transport, the measurement of suspended sediment is challenging (Wren et al., 2002). The majority of sediment movement occurs infrequently during large rainfall events, leading to the rapid mobilization of field personnel into hazardous flood conditions (Fig. 1.1). Also a large number of samples may be required to see changes in SSC throughout the duration of a storm (Lewis and Rassmussen, 1999). Traditional methods for measuring suspended sediment are also expensive. As of 2006 only a quarter of the USGS stations collecting daily sediment data in 1981 were still in service. The decrease in sediment monitoring stations is due a number of reasons but the primary reason is cost (Gray and Gartner, 2009). For example, in 2000 the annual cost for the United States Geologic Survey (USGS) to collect and publish daily stream flow and suspended sediment data at one station was at least $20,000. Often the price can be as great as $60,000 per station, depending on such factors as the types and frequency of data collected; the size

distribution of the suspended sediment; the hydraulic characteristics of the gaged reach; and, the site location (Larsen et al., 2001). Adjusted for inflation the same cost estimates for maintaining a USGS streamgage in 2008 dollars are from $24,000 to $78,000 (Gray and Gartner, 2009). Currently there are 1,602 USGS sites that monitor suspended sediment daily, requiring up to $96 million annually (USGS, 2007).

Figure 1.1. BSE graduate students sampling suspended sediment and measuring stream discharge during a storm event in June, 2006 on Stroubles Creek in Blacksburg, VA. The wooden bridge spans the bankfull stream channel.

As of 2001, there was no alternative to traditional pump and bottle sampling techniques approved by the Federal Interagency Sedimentation Project (Larsen et al., 2001). Currently the USGS is testing multiple new sensing technologies in U.S. rivers and in laboratories for measuring certain characteristics of suspended sediment, bed load, and bed material. The technologies include: bulk optic or turbidity, laser optic, pressure difference, and acoustic backscatter (Gray and Gartner, 2009). The informal Sediment Monitoring Instrument and Analysis Research Program with the USGS is working to determine if the above technologies can make the shift from research to operational applications (Gray and Gartner, 2009). The new technologies are being rigorously tested for accuracy and reliability across the range of

physiographic conditions. Also their performances must be compared to the tradition pump and bottle sample techniques.

An alternative to measuring SSC would have to be cost-effective and autonomous and have increased temporal and spatial resolution. High-quality suspended sediment data will allow researchers to better quantify soil losses due to hillslope and channel erosion, the rate of reservoir sedimentation and the results of landuse and climate change, management actions, and restoration efforts on aquatic systems (Wren et al., 2002).

1.2 Goals and Objectives

The overall goal of this research was to develop and test an inexpensive sensor for continuous suspended sediment monitoring in streams. Specific objectives include the following:

1. Develop a prototype permittivity electrode for use in stream systems and a bench-scale, re-circulating sediment system;
2. Develop and assess a prediction model for SSC; and,
3. Develop a preliminary, qualitative conceptual model of sediment suspension response to electrical fields.

1.3 Research Questions

Five questions were initially identified for this research project. The work presented here answers the first three questions. Unfortunately it is not possible to answer the fourth and fifth question with the data collected during this study.

1. Can the gain and phase components of permittivity as measured by the KSU BAE control box be used to predict SSC?
2. What is the accuracy of SSC predicted with gain and phase for the concentrations analyzed in this study?
3. Conceptually, how do gain and phase change with increasing frequency and concentration?
4. Why do gain and phase change with increasing frequency and concentration?
5. How does the dielectric constant of the sample medium change with the addition of sediment?

Chapter 2: Background

There are three main categories of rocks: igneous, metamorphic, and sedimentary. The rock cycle describes the dynamic movement of mass from one type of rock to another driven by the water cycle and plate tectonics over geologic time (Waltham, 2002). Igneous rocks are formed under two different environments. Formation of all igneous rocks begins when rock material is pushed deep under the Earth's surface, where it melts into magma. As conditions change and the magma is no longer able to remain in liquid state it cools to form igneous rocks. The differences in the two types of igneous rocks arise due to cooling conditions. Igneous rocks that cool slowly within the Earth have a coarse-grained structure. Igneous rocks that form under rapidly cooling conditions at the Earth's surface are fine-grained and in some cases glassy (Waltham, 2002). Sedimentary rocks are formed when pieces of different types and sizes of rock material are deposited, compacted together, and the cemented over time. Sedimentary rocks are often found in ancient sea floors or lake beds. Metamorphic rocks are formed when any type of rock material is subjected to heat and pressure from burial or contact igneous rocks (Waltham, 2002). Heat and pressure from the burial causes the molecules of the mineral to line up with a different orientation. This research is more closely associated with the formation sedimentary than igneous or metamorphic minerals. The following paragraphs will describe sources of sediment, how it is transported, and why excess sediment can be a concern in aquatic ecosystems.

2.1 Sediment Sources

Sediment is formed by three different processes. First bedrock must weather to soil, and then soil must detach from the soil matrix and be transported into a water body. A brief summary of these processes follows.

Five factors influence soil formation: climate, living organisms, relief, time, and the parent material (McBride, 1994). Climate is an important factor because it determines air and water temperatures and the quantity and timing of runoff a system conveys. The system relief is the change in elevation per unit change in planform distance and thus dictates upland and channel slope. For example, gravity will play a much larger part in physically weathering rocks in the mountains than in the coastal plain. The weathering of parent material/bedrock to create soil takes time. It is important to understand where the study system is with in the rock cycle; for instance, were the mountains just formed (geologically) or are the mountains in an older system

like the Appalachians. Given the same parent material and climate, time will determine what mineral will be present (McBride, 1994). Parent material can be residual, organic, or transported from someplace else in the system (McBride, 1994). Colluvial parent material is moved by gravity from a higher elevation in the watershed; alluvial material is deposited by fluvial processes. Therefore, soil can become sediment and sediment can become soil again if it is deposited on a floodplain connecting the stream to the landscape. Parent material can also be ocean deposits (marine), wind deposits (aeolian), lake deposits (lacustrine), or glacial deposits (McBride, 1994). Soil can be created by precipitation, heat, and/or organic matter. It can be lost by leaching of soil bases from the matrix, erosion, and seepage. Soil can be transformed by mineral weathering and organic matter decay.

Minerals and soil weather physically and chemically. Weathering is the response of materials to physical and chemical conditions at or near the earth surface (McBride, 1994). Physical weathering is the breakdown of materials by mechanical processes, including changes in pressure or temperature, mechanical collapse, abrasion, and other disturbances (McBride, 1994). Regardless of the process, the result is a smaller particle size with the same chemical composition. Chemical weathering involves chemical reactions of the minerals with air and aqueous solutions (McBride, 1994); therefore, the result of chemical weathering depends on many factors, such as duration of the conditions and the chemical constituents present in the soil water. Chemical weathering reactions include oxidation/reduction, hydrolysis/hydration, and ion exchange/chelation (McBride, 1994).

Soil mineralogy is related to soil particle size (McBride, 1994). Particles greater than two millimeters in diameter are mostly primary minerals, such as quartz, feldspars, and micas (McBride, 1994). Particles less than two millimeters are mostly secondary minerals, such as layer silicate clays, oxides, and non-crystalline aluminosilicates (McBride, 1994).

Soil is detached from the soil matrix by raindrop impact, surface water runoff, channelized flow, gravity, wind, ice, and chemical reactions (Novotony, 2003). Each agent releases the soil particle or aggregate into one of the following flow conditions: sheet, inter-rill, rill, ephemeral gully, or classic gully (Novotony, 2003). However, detachment of a soil particle or aggregate from the matrix does not guarantee transport to a water body. Soil transport is dependent on particle size, shape, density, and structural arrangement (Knighton, 1998). Research has found

that particle size has a direct relationship to transport for non-cohesive materials (Knighton, 1998).

Sub-aerial processes also erode soil by weakening the soil structure near the surface, making the particles more susceptible to transport during the next rainfall event. Sub-aerial processes include freeze-thaw cycling, soil wetting and drying, and the shrinking and swelling of clay minerals. Anthropogenic activities can also weaken the soil structure causing erosion. Examples of activities that induce erosion include: agriculture, urban development, silviculture, highways, and surface mining practices (Novotony, 2003). Row-crop agriculture, where plant refuse is tilled under the soil after harvest, is a leading cause of soil loss.

Soil detached from streambanks also becomes sediment. Streambank erosion and retreat are complex processes that depend on the materials present, antecedent moisture conditions within the streambank, and the flow conditions within the stream on both local and watershed scales. The streambank materials of natural channels are highly variable, but in many cases the banks are made of cohesive materials. Depending on the local climate, the banks may be reinforced by the roots of riparian vegetation (Knighton, 1998). The detachment of sediment from streambanks is due to hydraulic action, subaerial processes, and mass failure. Mass failure of streambanks depends on the geometry, structure, and material properties of the bank (Knighton, 1998).

Hydraulic action is described by the near bank velocity and shear stress. The dominant removal mechanism of non-cohesive material is hydraulic action. However, the effectiveness of hydraulic action on cohesive banks depends on the antecedent moisture content and degree of preconditioning of the material (Knighton, 1998). The resistance of cohesive material to erosion also depends on the strength of cohesive bonds between particles in the soil matrix instead of the physical properties of the particles themselves (Knighton, 1998). For example, wet banks erode with relative ease if the bank has been subjected to numerous wetting and drying events. A dry, hard bank is frequently more resistant (Knighton, 1998).

Channel sources of sediment are the bed and banks of the river and its tributaries. These sources are strongly controlled by the stream discharge and the stability of the bank material. Specific channel sources of sediment are: 1) river banks subject to high shear stresses, such as meander bends, and/or extended exposure to water; 2) mid-channel and point bars; 3) fine bed material stored within the interstitial spaces of large substrate particles or in the sub pavement; 4)

natural backwaters where sediment may accumulate during periods of low flows; 5) fine particles trapped within stands of macrophytes or associated with the seasonal growth and decline of aquatic vegetation (Wood and Armitage, 1997).

Non-channel sources of sediment in rivers are bare hillslope soils that are susceptible to increased erosion within the watershed. Examples of sediment sources within a watershed include: 1) mass failures, such as landslides and soil creep; 2) urban areas due to increased volume and timing of runoff from rainfall events; 3) anthropogenic activities, such as development; and, 4) atmospheric deposition, due to aeolian processes and precipitation (Wood and Armitage, 1997). Stream sediment load can be dramatically increased by anthropogenic activities such as agriculture, mining, forestry operations, construction of roads and reservoirs, and flow regulation (Wood and Armitage, 1997). These activities alter the physical environment of a stream by increasing runoff and by affecting both the volume and timing of sediment delivery stream to the stream (Wood and Armitage, 1997). All of these processes are influenced by land use, soil type, and ground cover vegetation.

2.2 Sediment Composition

Depending on the particle size and material, sediment may have cohesive or non-cohesive properties. For example, sand-sized or larger sediment (0.062 – 2 mm) is non-cohesive (Knighton, 1998). Physical weathering due to abrasion and freeze-thaw cycling will decrease the particle size while the particles are within the channel but the particles will be resistant to changing chemical composition.

Gravels (2-64 mm), cobbles (64-256 mm), and boulders (>256 mm) are normally present in headwater streams (Knighton, 1998) and are mainly weathered bedrock from within the channel or parent material that fell or rolled directly into the channel during a mass wasting event or was deposited during glacial movement. Stream bedload consists of sands, gravels, cobbles, and boulders that move along the bed by rolling, sliding, or hopping. (Knighton, 1998). The bedload transport rate is mostly a function of the flow transport capacity, but the development of an armor layer on the bed surface can decrease the bed material supply (Knighton, 1998).

Sand-size particles (0.062-2 mm) are comprised mainly of quartz and feldspars minerals and thus are very resistant to chemical weathering (McBride, 1994). Feldspars are less resistant to chemical weathering than quartz due to impurities within the structure from isomorphic substitution (McBride, 1994).

Silt- and clay-size sediment are cohesive materials primarily composed of clay minerals. Clay minerals have many distinct and complex characteristics. One such characteristic is surface charge density. Surface charge density allows cohesive materials to adhere to each other; charge varies from 0 to -2 charges per unit volume (McBride, 1994). Under most conditions clays are negatively charged, attracting cations and organic matter to neutralize the surface charge. Due to this negative surface charge, clay aggregates adsorb heavy metals, trace elements, pesticides, hormones, and any other positively charged ion in the environment.

Clay minerals have many different structural configurations; however, the most resilient and stable are sheet silicates, or phylosilitcate minerals (McBride, 1994). Phylosilicate minerals are composed of combinations of tetrahedral and octahedral sheets. Tetrahedral sheets are coordinated around silica atoms; octahedral sheets are either dioctahedrals with aluminum as the base cation or trioctahedral with magnesium as a base cation (McBride, 1994). When there is one tetrahedral layer joined to one octahedral layer the structure is a 1:1 clay mineral. Kaolinite is the dioctahedral, 1:1 clay mineral (fig. 2.1). Its ideal structure has no charge, and the layers are held together by hydrogen bonds between an OH^{-1} of one layer and the O_2^- ions of another layer. The strong hydrogen bonds between the layers prevent kaolinite from swelling with waters of hydration. Kaolinite has a very low surface area and cation exchange capacity (CEC) compared to other clay minerals (McBride, 1994). The low CEC is due to the ideal structure with very little isomorphic substitution in either the tetrahedral or octahedral layers (McBride, 1994).

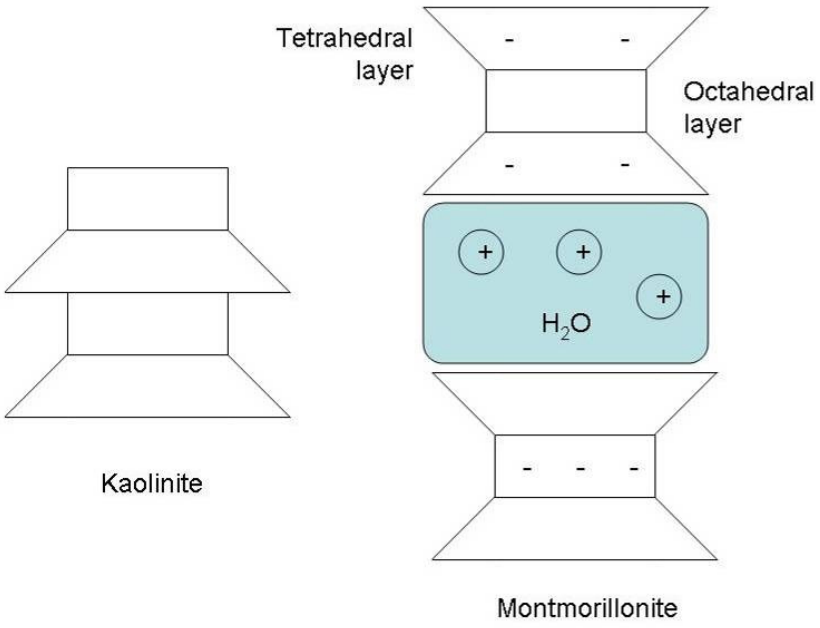

Figure 2.1. Layered silicates have two main configurations, 1:1 and 2:1. Kaolinite and montmorillonite are shown in terms of tetrahedral and octahedral layers. The locations of structural charge and exchange cations are represented by + and – signs (After McBride, 1994).

The other major category of clay minerals is composed of two tetrahedral layers sandwiching one octahedral layer (fig. 2.1). These minerals are known as 2:1 layer silicates and can be neutral when there is no isomorphic substitution in any of the layers. In most 2:1 layer silicates it is more common to have substitution. For example, montmorillonite is a dioctahedral, 2:1 clay mineral. Montmorillonite can have isomorphic substitution of magnesium for aluminum in the octahedral layer and aluminum for silica in the tetrahedral layer (McBride, 1994). The substitutions create a net negative charge within the mineral structure that is neutralized by adsorbed base cations from the soil solution. The cations are adsorbed by the interlayer and are normally hydrated. The adsorbed cations can easily be displaced by other cations within the soil solution and the ease at which this is occurs determines the mineral CEC. Montmorillonite has a low layer charge compared to other 2:1 clays, allowing the mineral to expand significantly with increasing water content (fig. 2.1; McBride, 1994).

Suspended sediment is comprised mainly of washload and suspended bedload. The wash load is fine material (silt and clay fractions) transported over the landscape or eroded from the stream channel. The washload concentration is constant over the depth of the water column due to in-stream turbulent mixing and the low settling velocity of these sediments (Knighton, 1998).

Suspended load is comprised of sand and finer sized particles (<2 mm) entrained from the stream bed during increased flows. Suspended fine sediment (<0.062 mm) in streams tends to be well mixed across the stream cross section and water column, varying little over time (Wren et al., 2000). However, sand transport (0.062-2 mm) can fluctuate significantly with time due to the high settling velocities of sand-sized particles (Wren et al., 2000). Suspended sediment concentration increases with increasing depth and, in most cases, a stream is supply-limited for suspended load (Knighton, 1998).

Dissolved material is also part of the suspended load. Specifically, the dissolved load consists of material transported in solution. The dissolved load and wash load are typically the sediment components from landscape runoff (Knighton, 1998). The dissolved load varies in magnitude and composition depending on the route traveled within the watershed, the dominant sources, and the rates of solute mobilization (Knighton, 1998). During low flow conditions, the dissolved load can be relatively high since the lower soil profiles are draining to the stream, but the dissolved load will generally decrease with increasing flow rate (Knighton, 1998).

2.3 Sediment Fate and Transport

Erosion of sediment from landscape surfaces and sediment transport to and from storage zones are rarely in a steady state (Trimble, 1975; Trimble, 1999). Research has shown that culturally accelerated erosion has overloaded streams with sediment to the extent that most of the excess sediment has been deposited on floodplains (Trimble, 1975). Therefore, a sediment budget is required to monitor environmental changes. This budget accounts for changes in storage flux throughout the watershed (Trimble, 1999). Trimble (1999) completed a long-term study on Coon Creek, in the Driftless Area of Wisconsin, USA. The study estimated the 140-yr sediment budget starting during European settlement. In 1938, 150 stream and valley cross-sections on Coon Creek were surveyed and monumented. There were also extensive stratigraphic data along the selected cross-sections for the agriculture period (Trimble, 1999). The final study sites, 92 of the original 150, were resurveyed from 1991-1995. Trimble (1999) concluded that sediment fluxes (sources and amounts) changed significantly over the past 140 years for Coon Creek, but sediment yield, or the efflux of sediment, has remained relatively constant. Therefore, estimating sediment yield alone does not provide an accurate picture of sediment movement within a watershed (Trimble, 1999). Trimble (1999) also found that the

majority of sediment is stored on floodplains: the rate of floodplain sediment accretion decreased from 15 cm/yr during the 1920s and 1930s to 0.53 cm/yr from 1975 to 1993.

Trimble (1975) also assessed ten river basins in the piedmont of the southeastern United States and found that only around 5% of the sediment eroded during European settlement had actually left the river systems. The study estimated gross erosion at around 95 mm/100 years on average for the ten river basins and average sediment yields of 4.5 mm/100 years. These average values translated into an average weighted delivery ratio of only 4.7% with a range of 3-10%. The remaining 95% of the sediment eroded during European settlement remained within the river system as either alluvium or colluvium (Trimble, 1975). The alluvium was up to six meters deep on the floodplains of second to fifth order streams within the assessed watersheds (Trimble, 19750). Deposits of this magnitude indicated a departure from steady state conditions. Due to increased erosion control practices and declining agricultural land use, streams are regaining their transport capacity and transporting the large historic deposits (Trimble, 1975). Currently the movement of the historic deposits is now limited by the reservoirs present on most river systems (Trimble, 1975).

2.4 Environmental Impacts

Aquatic ecosystems fall into two major categories based on how water moves through the system. Lotic systems are moving systems such as steams and rivers, while lakes are considered lentic systems. The impacts of sediment are similar to both systems, but there are more physical impacts on a lotic system than a lentic system. Sedimentation and increased turbidity are the two major physical impacts common to both systems. Sedimentation decreases water depth and increases flooding in lakes, reservoirs, and large rivers. Sedimentation is a costly annoyance to human society since we use reservoirs and lakes for storing irrigation and drinking water, recreation, and transportation (Wood and Armitage, 1997). Increased sedimentation in large rivers, such as the Mississippi, is also a problem for flood protection and navigation throughout the interior of the United States.

Excessive sediment has many other physical impacts on lotic systems. Excess sedimentation shifts the median particle size of many streambeds toward finer material (Wood and Armitage, 1997). For example, a gravel-bed river may become a predominantly sand-bed river. In dramatic cases, this shift can actually change the stream morphology; for example, a riffle-pool morphology could shift to a plane bed morphology (Wood and Armitage, 1997). Changes in

morphology can also be considered from an energy view point. Large increases in sediment load can shift a supply-limited stream to a transport-limited system. A shift in the particle size distribution toward finer material also reduces habitat variety along the stream bed by filling the interstitial spaces of larger substrates (Wood and Armitage, 1997).

Increased sediment also decreases the depth of sunlight penetration within the water column by increasing turbidity (Wood and Armitage, 1997). A change in the amount of sunlight is a physical impact; however, it leads to important chemical and biological changes. Sediment reduces the biological energy available for photosynthesis, thereby altering the foundation of the food web (Wood and Armitage, 1997). While the transmission of solar radiation may be decreased by increased sediment, increased sediment will also increase heat radiation to the water column. Increases in water temperature decrease dissolved oxygen levels at saturation and increase carbon dioxide, leading to decreases in pH.

Chemical changes within the water column cause changes in the chemical composition of the sediment. Different minerals have unique chemical and physical characteristics which determine weathering rates and particle size. Clay- and silt-size fractions are mainly clay minerals which have varying surface charge density. The surface charge allows sediment particles to adsorb solution cations and anions depending on the pH of the system. Therefore, soil particles eroding from hillslopes have the capacity to carry substances such as heavy metals, pesticides, pharmaceuticals, and bacteria over the landscape and into the water column (Larsen et al., 2001). For example, sediments less than 63 μm in size are by nature cohesive and move in marine and freshwater systems as composite or aggregate particles (McConnachie and Petticrew, 2006). The increased adsorption and transport of contaminants is due to the large surface area and geochemical composition of the particles (Wood and Armitage, 1997). As the water column chemistry changes, these compounds desorb at different rates and depths in the water column. For example, pH is one of the factors that can shift a sediment particle from a negative to positive surface charge, releasing sorbed cations, such as lead.

The release of toxic chemicals and heavy metals from the sediment surface does more than change water chemistry. At toxic levels the release of contaminants from sediment particles can have extreme environmental results, such as fish kills. The consequences of long- and short-term changes in water chemistry can often be detected more accurately by changes in the biological community. Excessive sediment shifts the entire biological community to species which are

more tolerant of physical and chemical changes and reduces the abundance and diversity of the aquatic biota.

Changes in water chemistry alter competition between pollutant-tolerant and intolerant species. For example, large blooms of cyanobacteria can result from increased phosphorus within the system. The bacteria can fix atmospheric nitrogen, thereby allowing the organism to out-compete algae within the same system. As the bacteria surge out of control, they use all the dissolved oxygen within the system, leaving the system anoxic and killing other organisms.

Excessive sediment directly affects both fish and macroinvertebrates within the ecosystem, reducing the diversity and abundance of aquatic organisms (Berkman and Rabeni, 1987). If the ecosystem is inundated with fine particles, the gills of benthic macroinvertebrates can be clogged. Also the habitat required to support many benthic macroinvertebrates can be destroyed when fine sediment fills the interstitial spaces of the stream bed. Once the interstitial spaces are filled, macroinvertebrates have difficulty feeding and are unable to escape predation by birds, fish, and other macroinvertebrates. Many fish species are also negatively impacted by stream bed siltation since it reduces spawning habitat quality (Wood and Armitage, 1997). For example, salmonids require clean gravel for their redds. During the spawning process, salmonids are able to clean off the sediment before laying their eggs; however, if the fine material is replaced after the eggs are laid, the eggs will die. Increased turbidity can also affect fish by reducing visibility and making it more difficult to feed and hide from predators (Wheeler et al., 2005; Wood and Armitage, 1997).

In conclusion, excessive sediment does not change just one aspect of a stream. Any disturbance radiates throughout the ecosystem, changing the physical, chemical, and biological characteristics. Therefore, the extent of the damage sediment has on an ecosystem varies from stream to stream and with the duration of the disturbance. For example, road construction will negatively impact an aquatic ecosystem over a relatively short duration, allowing the stream to recover (Wheeler et al., 2005). On the other hand, if the road leads to the removal of all the trees from the watershed the effects from excessive sedimentation will last longer as the stream has a constant source of new sediment with each rainfall event. Therefore predicting ecosystem response to excessive sediment requires a detailed picture of the entire watershed and aquatic system.

2.5 Sensor Design

Means for measuring sediment movement through a watershed have taken numerous physical and electrical forms. Regardless of what parameter is measured, design considerations are universal. These considerations are introduced in the following paragraphs.

Measurand

A measurand is a physical quantity, property, or condition that is measured. The physical property measured by the design sensor can take many forms. For example, a turbidity probe senses changes in the optical backscatter of light within a sample volume.

Sensor

A sensor was defined by Carr (1993) as a "device that converts energy derived from a physical phenomenon into an electric current or voltage, for purposes of measurement, control, or information."

Signal and signal processing

The direct output from a sensor is not always suitable for immediate display; therefore, the signal is conditioned (Carr, 1993). Processing or conditioning may include amplification, frequency-selective filtering; simple DC level translation; or, mathematical operations. Common mathematical operations are differentiation, integration, "logging", or "anti-logging" (Carr, 1993).

Sensor response and calibration

Calibration of the measurement system is the development of a relationship between the input value and the system output value (Figliola and Beasley, 2000). Calibration is defined by Figliola and Beasley (2000) as the "act of applying a known value of input to a measurement system for the purpose of observing the system output." The known value used during calibration is the *standard*. It is important when calibrating a sensor to calibrate it over the known range of the measurement system (Figliola and Beasley, 2000). The sensor range is the maximum and minimum values of an applied parameter than can be measured (Carr, 1993), while the dynamic range is the total range of the sensor from minimum to maximum (Carr, 1993).

There are both static and dynamic calibration procedures. Static calibration is the most common calibration procedure; it involves recording system output for a series of known input

values or standards. The data are used to develop a calibration curve which describes the static input-output relationship. The relationship forms the logic by which the indicated output can be interpreted during an actual measurement. When the variables of interest are time-dependent and time-based conclusions are desired, a dynamic calibration is required. Dynamic calibration determines the relationship between an input of known dynamic behavior and the measurement system output (Figliola and Beasley, 2000).

Signal display and recording

For a system to be useful it must output the measurements to a display or recording device. The output can be in analog, digital, visual display, or a paper recording depending on the need or application.

Interferences

Interference and noise measure the effects of extraneous variables on the measured parameter (Figliola and Beasley, 2000). Noise is a random variation in the measured signal as a consequence of change in the extraneous variables (Figliola and Beasley, 2000). In natural systems, noise is the normal, random variations in environmental conditions that affect the measured parameter (Figliola and Beasley, 2000).

Interference produces detrimental deterministic trends on the measured value because of extraneous variables (Figliola and Beasley, 2000). Interference can be especially damaging if the interference period is longer than the sampling period, which will superimpose a false trend in the behavior of the measured variable (Figliola and Beasley, 2000). To overcome interference on the measured parameter it is important to perform the measurement in a manner that will break up interference trends such that they appear as random variations in the data set (Figliola and Beasley, 2000).

Accuracy and Error (systematic and random)

Sensor accuracy is the maximum difference that will exist between the actual value (which must be measured by a primary or good secondary standard) and the indicated value at the output of the sensor (Carr, 1993). Accuracy can be expressed as a percentage of full scale or in absolute terms (Carr, 1993). Accuracy is measured during sensor calibration (Figliola and Beasley, 2000

All sensors have some errors. Error is defined by Carr (1993) as the "difference between the measured value and the true value". Carr (1993) classifies error into five basic categories:

dynamic errors, application errors, characteristic errors, insertion errors, and environmental errors. Dynamic errors occur when a sensor response is much slower or damped compared to changes in the environment. For example, it often takes many seconds for a thermistor to change resistance in response to a change in temperature, but the change in temperature can occur abruptly (Carr, 1993). Application errors are due to the operator ignorance, such as incorrect placement of the probe or incorrect insulation of the probe. One example of application error for a capacitance sensor would be installing the probe perpendicular to the primary flow direction instead of parallel, effectively making the probe much more flow intrusive.

Characteristic errors are inherent in the device itself for example, when a linear transfer function is applied to a non-linear response (Carr, 1993). An insertion error occurs when the act of inserting the sensor into the measurement systems changes the parameter being measured (Carr, 1993). Environmental errors are derived from the environment in which the sensor is used (Carr, 1993). The error may be due to temperature, vibration, shock, altitude, chemical exposure, or other factors. Environmental errors are often lumped into the sensor characteristic error.

2.6 Sediment Monitoring Technologies

In addition to traditional field methods of bottle and pump sampling, SSC can be monitored with a variety of techniques. Current sensing technologies available on the market today or under evaluation are optical backscatter, acoustic, and laser diffraction. Other technologies currently under development include: nuclear, differential pressure, optical transmission, focused-beam reflectance, spectral reflectance, digital optical, vibrating tube, impact sampler, capacitance, fiber optic transmissometer, and photo-optic imaging. Specific sensor characteristics are discussed below and summarized in table 2.1. Wren et al. (2000) and Wren and Kuhnle (2002) provided extensive reviews of current technology for measuring SSC and, except where indicated, the discussion in section 2.6 is based on these papers.

2.6.1 Bottle Sampling

Bottle sampling is a standard sampling technique for suspended sediment (fig. 2.2). One requirement for accurate bottle sampling of suspended sediment is the proper use of the isokinetic sampler. Proper use of an isokinetic depth-integrating sampler entails lowering and raising the bottle on a rod at the same rate at five positions across a stream. The rate is set such

that the sample bottle is just filled at the deepest and fastest point in the river. However, setting this rate is completely subjective and difficult to repeat without significant field experience. With isokinetic sampling, the fluid entering the bottle has the same velocity as the local stream velocity. Both isokinetic point and depth-integrating samplers are available. Isokinetic point samplers sample at discrete depths using an electronically controlled valve.

Figure 2.2. Barbra Utley and Alan Simpson during a training seminar in March 2006. Simpson was demonstrating proper usage of a depth-integrated D-48 isokinetic bottle sampler.

When done correctly, bottle sampling is a well documented, reliable, and widely used technique. Many other monitoring systems, such as optical backscatter probes, require the development of a rating curve using the bottle sampling method. Depth integrating and point samplers are two of the few systems that sample most of the water column. This advantage must be balanced against the fact that bottle sampling requires the mobilization of field personnel into the field during storm events, often at night. Also, since the inlet nozzle on most isokinetic samplers is below the lowest part on the bottle it is unable to sample the lowest 0.10-0.15 m of the water column. Bottle samplers do not actually measure suspended sediment but collect a sample. Suspended sediment concentration and particle size are actually measured in the

laboratory via standard filtration and sedimentation methods. The laboratory analysis is time-consuming and expensive. Additionally, bottle sampling has poor temporal resolution and is flow intrusive.

2.6.2 Pump Sampling

Pump sampling is also considered a standard technique for measuring SSC. An advantage of pump sampling is that it is possible to measure both sediment concentration and particle size if over 100 g of sediment is collected for the particle size analysis. During pump sampling, a vacuum is applied to a submerged line in the channel, and a fluid and sediment sample is collected and stored until laboratory analysis. The intake nozzle is pointed upstream under most circumstances. To minimize sampling bias, the intake velocity must be the same as the local stream velocity. Unfortunately, pump sampling only collects the water sample. The sample must then be analyzed in the lab for both particle size and concentration by standard methods.

Pump sampling is a reliable and standard method for sampling suspended sediment that works well for fine sediments (<0.062 mm; Wren et al., 2000). Automated samplers can be programmed to sample at discrete intervals or, when outfitted with additional depth or flow sensors, to sample with changes in discharge or stage. A major advantage of pump samples over bottle sampler is that the automated sampling does not require the deployment of field personnel during storm events. However, pump sampling has poor temporal resolution, takes only point measurements, is flow intrusive, and requires personnel to collect and analyze the samples. Also, the amount and size of sediment sampled depends on the orientation of the nozzle with respect to the flow direction and the speed of the pump (Wren et al., 2000).

Wren et al. (2000) measured errors as large as 20% between known conditions and ex-situ sampling techniques, such as bottle and pump sampling techniques. The error in manual sampling techniques varies with sampling rate, sediment size, and the angle of the sampler relative to the flow velocity (Admiraal and Garcia, 2000). Therefore, the development of inexpensive field-based suspended sediment sensors will allow tremendous advances in research on the identification of background sediment levels and thresholds for ecological impact, stream channel instabilities, and stream restoration.

2.6.3 Optical Backscatter Sensors

Optical backscatter sensors, commonly called turbidity sensors, have been commercially available for estimating SSC since the 1980's (fig. 2.3; Gartner et al., 2001) and are the most common means for estimating SSCs in U.S. rivers (Gray and Gartner, 2009). SSC is determined from the strength of the backscatter from an infra-red or visible light source within a sample volume (Agrawal and Pottsmith, 2001; Wren and Kuhnle, 2002). The backscatter is measured by a series of photodiodes positioned around the emitter. The backscatter signal is converted to voltage output response that is proportional to the SSC. However, this relationship is only valid when the size and optical properties of the sediment do not vary during the measurement time (Schoellhamer, 2001).The measurement volume of the sensor varies with the turbidity of the water (Wren and Kuhnle, 2002). For example, blackwater systems have a higher background turbidity, which may reduce the sample volume for SSC.

Optical backscatter systems are calibrated empirically on a site specific basis (Agrawal and Pottsmith, 2001; Gray and Gartner, 2009). The calibration curve or transfer function is developed by sampling SSC by pump or bottle technique and relating the turbidity measurements to the known sediment concentration. Development of the transfer function for turbidity to SSC must be site specific because the strength of the backscatter signal is a function of the local suspended solids properties, such as composition, geometry, and size-distribution of the sediment as well as algae, plankton, micro-organisms, and organic matter (Minella et al., 2008). Also errors associated with optical backscatter measurements can be due to changes in composition, geometry, or size distribution of the sediment during the measurement interval of the sensor (Gartner et al., 2001).

The maximum SSC limit for turbidity sensors depends in part on the particle size distribution at the study site (Gray and Gartner, 2009). Optical backscatter systems are most accurate for particle sizes from 200-400 μm and concentrations up to 500 g/L for optimum performance (Wren and Kuhnle, 2002; Gray and Gartner, 2009). Advantages of these probes include the ability to deploy the probes remotely and log the data, relatively low cost, and simple operation. Turbidity probes have three main disadvantages: 1) particle size dependency (Black and Rosenberg, 1994); 2) biofouling of the optical window (Gartner and Gray, 2002); and, 3) the required calibration. Multiple studies have shown that a measured concentration may increase by an order of magnitude when compared to readings of the same concentration at a different

particle size (Wren et al., 2000; Agrawal and Pottsmith, 2001). The probes are also sensitive to low particle concentrations and provide only point measurements. Caution should be exercised in using turbidity sensors at sites with varying particle size and particle color conditions, unless the instrument is recalibrated for ambient conditions (Gray and Gartner, 2009).

Figure 2.3. Eureka Manta sondes with turbidity probes in Stroubles Creek, on the Heth Farm, Blacksburg, VA. Two sensors are deployed to measure suspended sediment near the bed and near the surface of the water column.

2.6.4 Acoustic Sensors

Acoustic sensors determine SSC by monitoring the strength of the backscatter from short bursts (~10 μs) of high frequency sound (1-5 MHz). The concentration and size of sediment present and the acoustic frequency determine the backscatter voltage amplitude (fig. 2.4; Thorne et al., 1991). However, in some systems (single or mutli-frequency) changes in measurements may be due to increased concentration or changes in particle size (Gartner and Cheng, 2001; Gartner, 2002). Acoustic systems are a non-intrusive technology and can measure over a vertical range of one to two meters; this depth can be increased by submerging the transducers to the desired depth. The water column is sampled in discrete sections based on the return time of the echo; this is known as range gating and is shown in figure 2.5. A measurement is comprised of

all the reflections that occur within the measuring volume and return to the transducer at the same time (Admiraal and Garcia, 2000).

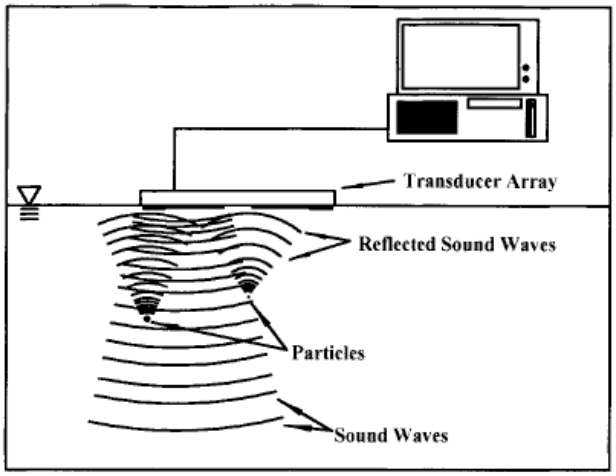

Figure 2.4: Acoustic Backscatter (Wren et al., 2000 with permission from ASCE).

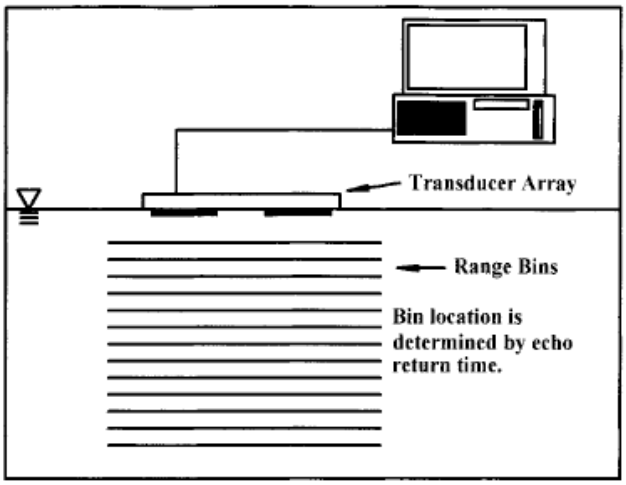

Figure 2.5: Range Gating (Wren et al., 2000 with permission from ASCE).

Estimating SSC with acoustic backscatter technology is based on the active sonar equation (Reichel and Nachtnebel, 1994):

$$EL = SL - 2TL + TS \tag{2.1}$$

where, *EL* is the echo level, or intensity, *SL* is the source level, *TL* is the transmission loss, and *TS* is the target strength, or the intensity of the signal echoed by a target.

The source level is specific to the equipment, and transmission loss explains the decreasing strength of the acoustic signal on its path between desired distance and the sound source. The target strength is affected by the presence of suspended sediment. It is dependent on the concentration and size distribution of the particles and their physical characteristics; for example, density, shape, compressibility, rigidity, and particle size can all affect the reading. The system is calibrated to toconcentrations from physical samples in mass units (Gray and Gartner, 2009).

Transforming acoustic backscatter data into SSC has been done empirically with iterative methods (Thorne et al., 1991) and explicitly based on measured samples from each bin depth. The empirical approach iteratively calculates the concentration for each range bin based on the

attenuation data. This process can be done without any previous knowledge of the sediment concentration. In contrast the explicit approach determines the concentration in one range bin based on the concentration information for the previous bin, requiring the assumption or measurement of SSC (Wren et al., 2002). Laboratory experiments by Wren et al. (2002) found a 39% error when estimating average SSC by the empirical method, and 20% error with the explicit method. The authors believed these errors were due to transducer calibration, the high voltages used in the sonar system, or data processing techniques. They concluded the errors for both methods could be reduced with improved hardware and algorithms. Wren et al. (2003) attempted to predict SSC from the backscatter data with a simple linear regression approach. This approach required the measurement of the actual concentration with pump samplers. The regression was successful but only accurate for the measured SSC range.

Typical ultrasonic frequencies can measure particle sizes from approximately 62-2000 μm and concentrations up to 30 g/L. As the concentration increases the sampling depth decreases. Research is ongoing to distinguish particle size using different acoustic frequencies (fig. 2.6). Currently ultrasonic devices provide an improved temporal (~0.1 s) and spatial resolution (~1 cm); however, increased resolution of single frequency measurements requires either detailed knowledge of the sediment characteristics or the sediment concentration at some known range from the acoustic transducer (Wren et al., 2002). One benefit of the increased resolution is the ability to study sediment movement under turbulent conditions since the system is not flow intrusive.

Acoustic systems are not susceptible to biofouling, but they are difficult to use due to the complexity involved with interpreting the backscatter signal. The system also has a strong particle size dependency and is difficult to calibrate. Calibration of an acoustic system is challenging because uniform concentrations of large diameter sediment are difficult to attain due to the tendency of the sediment to settle out of suspension wherever turbulence decrease (Admiraal and Garcia, 2000). Currently the hardware for acoustic systems is commercially available; however, there is not a commercially available hardware/software package to measure suspended sediment concentration profiles (Wren and Kuhnle, 2002).

Figure 2.6. In-stream acoustic and depth-integrated pump sampling system developed by the U.S. Department of Agriculture, Agricultural Research Service in Gibson Creek near Oxford, MS, USA.

2.6.5 Laser Diffraction Sensors

Laser diffraction measures multi-angle scattering of light particles at small angles, which is used to compute sediment size distribution and concentration. The scattered laser light is collected by a detector or array of detectors. An array of detectors is ring-shaped with progressive diameters (fig. 2.7). Laser systems are not particle-size dependent or affected by particle composition. The particle size can be calculated from knowledge of the scattering angle, using the Fraunhofer approximation or the exact Lorenz-Mie solution (Wren et al., 2000). The Mie solution is based on the concept that sediment particles will diffract light at a specific angle. This angle increases with decreasing particle size (McCave and Syvitski, 2001).

Measurements made by laser diffraction systems are not affected by the refractive index of the particles; however, without specific site data, the particle density must be assumed. The optical path length for the laser diffraction systems is either 2.5 cm or 5.0 cm. Depending on the optical length the particle size range is limited to either 1.25-250 μm or 2.5-500 μm, respectively.

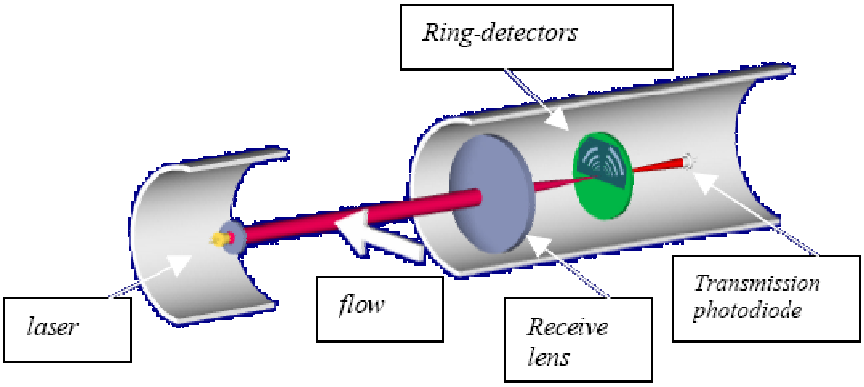

Figure 2.7. Laser diffraction principles – a cut away view of the basic LISST-100 instrument. A collimated laser beam illuminates particles (left to right). Multi-angle scattering is sensed by a specially constructed photo-diode array placed in the focal plane of the receiving lens. The array detector has 32 concentric rings, placed in alternate quadrants. A hole in the center passes the attenuated beam for measurement of optical transmission (Agrawal and Pottsmith, 2001).

Laser systems can only measure concentrations up to 2 g/L (Gray and Gartner, 2009). The systems can be automated for remote applications and are available commercially in multiple configurations. Laser diffraction techniques are also used to measure particle sizes of cements, chocolates, and microbes (Wren et al., 2000). There are multiple laser diffraction systems commercially available for use in both laboratory and field environments. One of the most common field systems is the LISST-100 developed by Sequoia Scientific Inc.(Laser In-Situ Scattering and Transmissometry; fig. 2.7).

Laser diffraction systems are expensive and flow intrusive, provide only point measurements, and require special training for technicians. Unfortunately, the statistical algorithms used to translate the data do not arrive at a unique concentration measurement, and the process works better when there is a uniform sediment distribution (Wren et al., 2000). Laser diffraction systems also have a limited particle size range (<250 μm) and are susceptible to biofouling (Wren and Kuhnle, 2002). Also deviation of particle shape from spherical may bias the measurement results (Gray and Gartner, 2009).

2.6.6 Optical Transmission

In optical transmission systems light is sent into the sample volume where a portion of the light will be reflected back if particles are in suspension (Agrawal and Pottsmith, 2001; Wren and Kuhnle, 2002). A sensor on the opposite side of the sample volume measures the transmission of the light beam. The concentration of sediment present in the sample volume is

calculated based on an empirical calibration to known SSC. The known SSC are determined by a standard bottle or pump method. The sample volume size varies between devices, and the devices are relatively inexpensive.

Optical transmission sensors have good temporal and spatial resolution, are more sensitive to lower concentrations of suspended sediment than optical backscatter probes, and are also commercially available (Gray and Gartner, 2009). For example, the upper limit for optical transmission sensors can be as low as 0.05 g/L (Gartner and Gray, 2002). Optical transmission systems are dependent on particle size and the refractive index of the particles (Agrawal and Pottsmith, 2001; Wren et al., 2000). Research has shown that optical transmission sensors have a nonlinear response to increasing particle concentrations: large changes in SSC produce only small output change. While the response can be corrected by using a shorter optical path, this results in decreased path length and increased flow disturbance. Therefore optical transmission systems typically require an array of sensors with varying path lengths to measure large variations in sediment concentration.

2.6.7 Nuclear

Nuclear sampling relies on the attenuation or backscatter of radiation by sediment within the sample volume. There are three methods for nuclear sediment measurement: 1) those that measure radiation emitted naturally by sediments; 2) those that measure backscattered radiation from an artificial source; and, 3) those that measure radiation transmission from an artificial source. The last two techniques have the broadest application and are described the most in the literature.

Backscatter gages direct radiation into the sample volume from the radioactive source or emitter, which is isolated from the detector or sensor by lead. The sensor is placed in the same plane as the emitter to measure radiation backscattered from the sediment. Usually X or gamma rays are used in nuclear systems**.** An empirical calibration is required to convert between backscatter and SSC.

Transmission gages measure the radiation attenuation due to sediment particles within the sample volume between the emitter and the transmission gage. SSC is determined with a ratio of the attenuation of the radiation within sediment suspension to the attenuation due to just distilled water. The ratio approach used in transmission gages removes errors associated with drift in

electronic components, shifts in water density due to changes in temperature, and radioactive decay (Tazioli, 1980).

Nuclear systems are not affected by the color of the water or the amount of suspended organic matter present within the system. Nuclear systems have low power consumption requirements and have the ability to measure over a wide range of concentrations and particle sizes; however, there are many disadvantages to the system at this time. The system is flow intrusive and expensive, provides only point measurements, has low sensitivity, and must be frequently recalibrated. Nuclear systems can only measure concentrations between 0.5 and 12 g/L. The system also requires special training and regulations. Research completed by Tazioli (1980) concluded that a transmission gage measuring Cesium-137 could not maintain precise results, but the system could successfully measure SSC during highly critical flood conditions. The system is unable to measure low concentrations, and it is affected by sediment composition, sea water, and organic matter, requiring field calibration. It is also impossible to use in streams less than a meter and half deep due to the geometry of the gamma backscatter instruments. Finally, nuclear systems have poor temporal resolution since a single measurement takes a few minutes of observations (Wren et al., 2000).

2.6.8 Differential Pressure

Differential pressure transducers can be used to determine differences in the specific weight of water. The specific weight of water is a function of the water density and is affected by SSC. Specifically the difference in pressure is measured between two points on a sedimentation column, one with high SSC and another with cleaner water near the surface of the sedimentation column. The change in pressure between the sedimentation and reference columns is used to determine the average SSC. The sample volume size depends on the distance between the inlets of the reference column to the sedimentation column. Differential pressure transducers were able to measure both SSC and the particle size distribution, but the concentration range is dependent on the transducer sensitivity (Lewis and Rasmussen, 1999). The system is relatively inexpensive, all the elements are available commercially, and the technology is not prone to signal drift of biofouling (Gray and Gartner, 2009). Also the accuracy of the system should theoretically improve with concentration increasing above 10-20 g/L (Gray and Gartner, 2009). However, the system is flow intrusive and affected by temperature changes, turbulence, and concentration of dissolved solids (Lewis and Rasmussen, 1999; Wren and Kuhnle, 2002). This

system is currently under development and has not been tested extensively in the field (Gray and Gartner, 2009).

2.6.9 Fiber-Optic Transmissometer

Fiber-optic transmissometers (FIT) measure the transmittance of a continuous light source through the water suspension using a photodetector. The photodetector measures the amount of radiant power and uses this to calculate the total transmission. The total light intensity measured by the photodector is less than the intensity emitted from the light source due to sediment particles between the source and detector absorbing or scattering light. Fiber-optic systems require a fiber-optic probe with access to flowing stream water (fig. 2.8). The Campbell et al. (2005) system used a red light emitting diode (LED) as a constant light source for the fiber-optic array. The source optic fiber and the detector are place on opposing sides of the water sample volume. The light signal is converted by the photodetector to an electrical signal and recorded by a data logger or computer (Campbell et al., 2005). The data can then be transferred to SSC with the Beer-Lambert transfer function. The Beer-Lambert law is a logarithmic relationship between the radiant power detected and the particle concentration between the source and the detector (Campbell et al., 2005). Campbell et al. (2005) utilized a linear form of the Beer-Lambert Law to calculate SSC from transmittance. Campbell et al. (2005) maximized the linear active area by optimizing the light source intensity and the path length between the source and detector.

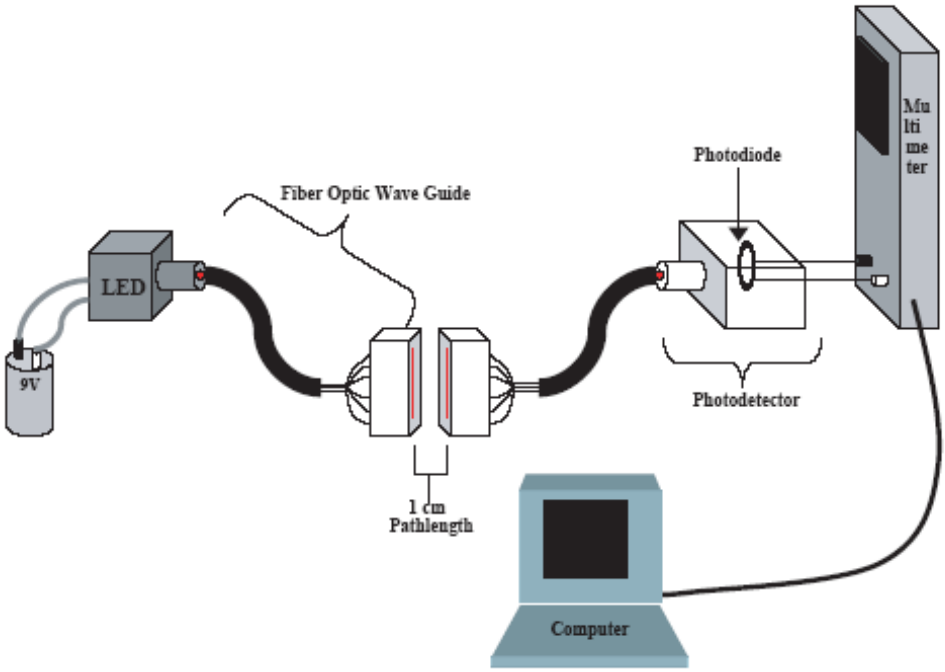

Figure 2.8. Schematic diagram of the FIT including the LED source powered by the 9V battery, fiber optic waveguides, sensor end and pathlength, photodetector, and multi-meter interfacing with a computer. Reprinted from Journal of Hydrology, vol. 311, Chris G. Campbell, Danny T. Laycak, William Hoppes, Nguyen T. Tran and Frank G. Shi, High concentration suspended sediment measurements using a continuous fiber optic in-stream transmissometer, 244-253, Copyright (2005) with permission from Elseivier.

Fiber-optic transmissometer measurement is inexpensive and simple and has the potential for continuous monitoring. It can distinguish changes in concentration over a wide range, including high concentrations. Single-point calibration is possible, and elements of the system are commercially available. Unfortunately, the system is particle size dependent, sensitive to sediment color, and flow intrusive. Campbell et al. (2005) compared the fiber-optic tranmissometer to two optical backscatter probes. The study concluded the fiber-optic transmissometer was precise for SSC up to 10 g/L with errors of ±1-2% for lower concentrations and up to ±4% at 10 g/L (Campbell et al., 2005). The authors also found that varying sediment color still resulted in a linear relationship between SSC and transmittance; however, the experiment did not exclude sediment geometry as a source of variation in the color study. Campbell et al. (2005) concluded the main source of variability in the study was associated with particle size dependency. The linear assumption for the Beer-Lambert Law began to degrade at very large (>710µm) or small (<45 µm) particle sizes. The fiber-optic transmissometer was

found to be more accurate and precise than the optical backscatter probes at both high and low concentrations. It was also sensitive to the optical fibers arrangement. Further development is needed as it has not been field-tested.

2.6.10 Photo-Optic Imaging

Photo-optic imaging systems measure SSC and sediment size distribution. Originally applied in the medical field during the 1980s, photo-optic imaging was used to determine the concentration of red blood cells in the bloodstream by delineating, characterizing, and counting organic particles (Gray et al., 2003). The photo-optic imaging system consists of a lens, fiber-optic cable, flow-through area, and a camera with a frame grabber (Gray et al., 2003). Once the flow-through area is illuminated the frame grabber is able to capture a high-quality two dimensional image of the suspended particles (Gray et al., 2003). Next, image analysis techniques are used to enhance particle boundaries and characterize the particle size and shape (Gooding, 2001; Gray et al., 2003).

Elements of the systems are commercially available at this time; however, further research is needed and the system has not been field-tested. The accuracy of photo-optic imaging decreases when transparent particles are present in the sample volume, and in turbid systems with organic and colloidal particles (Gray et al., 2003). Photo-optic imaging also requires post processing image software to optimize the image quality and to calculate sediment quantity and size distribution. Currently, the post-processing software needs to be refined to decrease errors from the automated analysis of aggregates (Gray et al., 2003).

2.6.11 Focused Beam Reflectance

Focused beam reflectance has not been extensively studied. The system uses a laser beam focused on a very small spot within the sample volume (fig. 2.9). The beam is then rotated extremely fast (many times per second). As the beam rotates it encounters particles that reflect a portion of the beam. The system then determines the size of the particles in the path of the laser by relating the beam reflectance time to the chord length of the particle(s) in the beam path. The volume of the sphere representing this particle is then calculated using the chord length.

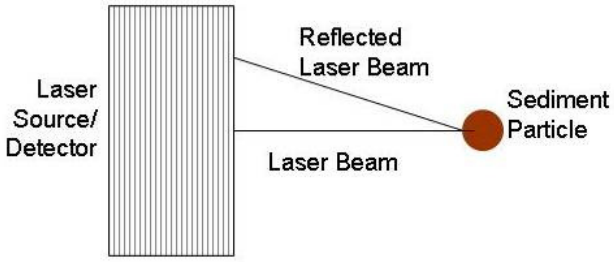

Figure 2.9. Focused beam reflectance (based on Wren et al., 2000 with permission from ASCE).

Focused beam reflectance systems are accurate for particle diameters of 1-1000 μm and concentrations of 0.01-50 g/L. It is accurate at very high sediment concentrations and is not particle size dependent because concentration is calculated based on particle size. The system is easily portable and has had good results in the field.

The main drawback of focused beam reflectance systems is they do not work well when particles have little or no reflectance, such as organic matter. Also at concentrations less than one gram per liter, long counting times are required for accuracy. Poor readings also occur when particles deviate from spherical geometry. The system is both flow intrusive and expensive (Wren et al., 2000).

2.6.12 Spectral Reflectance

Spectral reflectance is based on the relationship between the properties of water within the sample volume and the amount of radiation reflected from that water (fig. 2.10). Most spectral reflectance systems use radiation within the visible or infrared range. The relationship between SSC and reflected radiation is dependant on the optical properties of the sediment type, solar zenith angle, spatial resolution of the measurements, and the sensor observation angle.

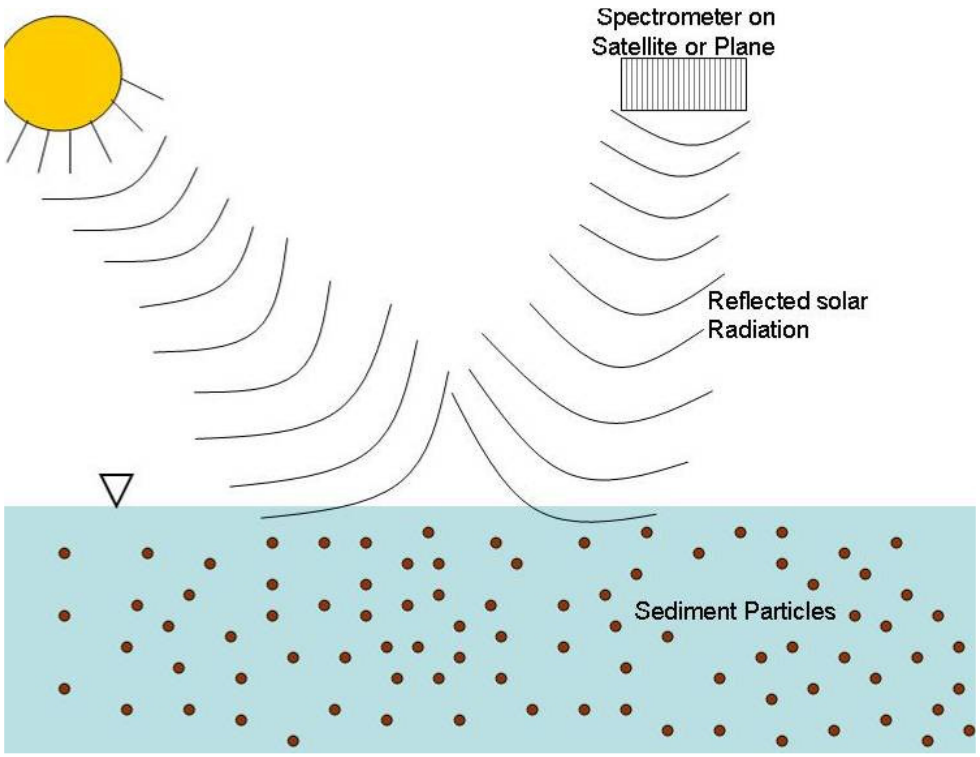

Figure 2.10. Remote spectral reflectance (after Wren et al., 2000 with permission from ASCE).

The radiation can be measured by hand-held, airborne, or a satellite-based spectrometer. Sample area ranges from m^2 to km^2 of the water body; therefore, spectral reflectance is better suited for marine applications than streams. Spectral reflectance distinguishes changes in concentration over time, which could be valuable information for government agencies that monitor the effectiveness of best management practices or restoration activities within watersheds with high sediment loading. This method is particle size dependent, and has low sensitivity; a large range in suspended sediment concentrations produces only a small range in reflectance.

2.6.13 Digital Optical

A digital optical sensor uses a charge-coupled device to digitally record an image of the sediment and water mixture in-situ. The recording can then be analyzed to determine the size and concentration of the suspended particles. This technology will continue to expand with improvements in computer and imaging technology. The sample volume for digital optical systems depends on light penetration into the water column.

2.6.14 Vibrating Tube

A vibrating tube system pulls water from the stream to a housing located on the bank. The water is passed through a vibrating tube and the water density is related to the vibration frequency to determine the average concentration of sediment within the tube. The vibrating tube most accurately measures concentrations greater than 1 g/L. Vibrating tube measurements are adversely affected by temperature, debris on the tube walls, and dissolved solids concentration which can change the background water density.

2.6.15 Impact sampler

An impact sampler is based on the principle of momentum transfer**.** The sensor measures the rate of impacts by sediment particles. An impact is dependent on the velocity, mass, and angle of particle impact. This device is not recommended for fluid environments and requires more research.

Reid et al. (2007) installed ten impact samplers measuring particles larger than 20 mm in the Upper Wharfe catchment of Yorkshire Dales National Park in northern England. The instruments were installed flush with the channel bed or gravel surface to ensure the detection of only bedload movement. The impact samplers were found to obtain reliable estimates of the timing of sediment entrainment and transfer cessation and a less reliable estimate of relative transport intensities (Reid et al., 2007). However installation location is vital to obtain representative data since bedload movement often follows preferential flowpaths. The impact samplers could record three impacts per second and up to 255 impacts within the sampling window of five minutes (Reid et al., 2007).

2.6.16 Conclusions on existing technologies

A few studies have been completed comparing new technologies (acoustic and laser diffraction systems) to more common optical backscatter techniques. One study conducted by Creed et al. (2001) compared SSC measurements from the LISST-100 (laser diffraction) to optical backscatter and acoustic technologies. The authors concluded the optical backscatter system preformed similarly to the LISST-100 when the distribution of the fine sediments was uniform (0.014-0.17mm). Creed et al. (2001) also concluded the backscatter data from the Sontek Acoustic Doppler profiler (ADP) was effective in determining sediment size for fine, uniform distributions ranging from 0.075 to 0.25 mm. The ADP was not used to estimate

suspended sediment by Creed et al. (2001), instead the data were analyzed for correlation between the reported sediment size classes for the ADP backscatter and LISST. Another study completed by Gartner et al. (2001) found that the LISST-100 consistently underestimated the size of mono-sized particles by 10-20%, and that the error increased with increasing particle size. Thus, when properly calibrated the LISST-100 has accuracy similar to optical backscatter sensors.

Multiple options are available for measuring suspended sediment (table 2.1). Only pump and bottle sampling are considered standards by the monitoring community. Unfortunately both techniques require laboratory analysis to quantify SSC. Many of the other techniques available on the market today also require sample collection via a standard method to correlate sensor output to SSC, including optical backscatter and optical transmission sensors. Particle size dependency and/or flow-intrusive geometries plague many of the commercially available (optical backscatter and transmission probes, laser diffraction systems, spectral reflectance) and research technologies (acoustic and fiber-optic transmissometers). Systems independent of particle size require specialized training and complex data analysis to tease out changes in both particle size and SSC (nuclear and acoustic). In conclusion, an ideal solution for continuous *in-situ* SSC measurement is not currently available. To be widely adopted and utilized, an SSC sensor will need to be cost effective, automated, and not require field calibration.

Table 2.1. Comparison of suspended sediment concentration measuring techniques.

Sensor	Advantages	Disadvantages
Bottle Sampling	Standard method Measures concentration	Ex-situ technique Poor temporal resolution Flow intrusive Requires on-site personnel
Pump Sampling	Standard method Able to measure concentration	Ex-situ technique Poor temporal resolution Flow intrusive Point sampling Does not usually sample isokinetically
Optical Backscatter (Turbidity)	Simple Good temporal resolution Remote deployment and data logging Relatively inexpensive Commercially available	Empirical calibration based on pump or bottle sampling required Strong particle-size dependency Flow intrusive Biofouling Point measurement only Sensitive to low particle concentration
Acoustic	Good spatial and temporal resolution Nonintrusive Measures over wide vertical range Measures concentration and size distribution (multi-frequency) Time-series profile Commercially available Not affected by biofouling	Backscatter signal difficult to convert Signal attenuation at high concentration Strong particle size dependency Unable to differentiate between changes in size distribution and concentration (single frequency) Calibration difficult
Laser Diffraction	No particle size dependency Measures concentration and size distribution Not affected by particle composition Can be automated Possible for remote application Commercially available-many versions	Expensive Flow intrusive Limited particle-size range Biofouling Requires special training and regulations Point measurement only
Optical Transmission	Good temporal and spatial resolution Sensitive to SSC < 0.05 g/L Commercially available	Empirical calibration based on pump or bottle sampling Dependent on particle size and refractive index
Nuclear	Low power consumption Wide particle concentration and size range	Radioactive source decay Requires special training and regulations Flow intrusive Point measurement only Low sensitivity Expensive Recalibration often needed Unable to measure low concentrations Affected by sediment composition, sea water, and organic matter
Differential Pressure	Measures concentration and size distribution Relatively inexpensive Commercially available elements	Flow intrusive Further research needed Affected by temperature changes

Table 2.1 cont. Comparison of suspended sediment concentration measuring techniques.

Sensor	Advantages	Disadvantages
Fiber Optic Transmissometer	Inexpensive Simple Possible continuous monitoring Wide particle concentration range Capable of measuring high concentrations Possible single-point calibration Commercially available elements	Particle-size dependency Flow intrusive Sensitive to optical fiber arrangement Further research needed No field tests performed
Photo-Optic Imaging	Able to measure concentration and size distribution Commercially available elements	Further research needed No field tests performed
Focused Beam Reflectance	Measures particle size to calculate concentration Accurate for diameters of 1-1000 μm & concentrations of 0.001-50 g/L Portable	Only accurate for fine sand particles or smaller Does not work well when particles have little or no reflectance (organic matter) Concentrations <1g/L require long counting times for accuracy Accuracy decreases when particles are not spherical Flow intrusive Expensive
Spectral Reflectance	Can be measured by hand-held, airborne, or satellite-based spectrometers Sample Area of m^2 to km^2	Better suited for marine applications Particle size dependent Small range of reflectance values represents a large range of SSC
Digital Optical	Determines size and concentration	Sample volume depends on light penetration Accuracy depends on quality of computer & imaging technology Requires more research
Vibrating Tube		Accurate for concentration > 1 g/L Affected by temperature, debris on tube wall, and high dissolved solids Requires more research
Impact Sampler		Dependent on velocity, mass, and angle of the particle impact Not recommended for fluid environments Requires more research
Capacitance	Simple and small Inexpensive Possible continuous monitoring Not affected by flow velocity	Flow intrusive Affected by temperature changes Site-specific soil texture calibration required Further research needed

2.7 Permittivity Sensors

2.7.1 Capacitance Theory

A capacitor is an energy storage device, and capacitance is a measure of the ability of a capacitor to store electrical charge. A basic capacitor design includes a pair of facing metallic plates separated by an insulating material (Carr, 1993). Each metal plate is a conductor (O'Malley, 1992). If the potential difference between the two conductors is *V* volts, where there is a positive charge of *Q* coulombs on one conductor and an equal and opposite charge on the other, the capacitance is determined as follows:

$$C = \frac{Q}{V} \tag{2.2}$$

where *C* is the capacitance in farads (Carr, 1993; O'Malley, 1992).

The main feature of the capacitor is its ability to hold charge on the insulating material, with negative charge on one of its two conductors and positive charge on the other. The capacitor then releases the stored energy. Capacitance is measured in farads (F), where one farad is the capacitance that will store one coulomb (Q) of electrical charge ($6.28 * 10^{18}$ electrons) at an electrical potential of one volt (Carr, 1993). A farad is too large for most electronics applications; therefore, micro- and pico farads are the more common units of measure.

The insulator between the two conductors is called the *dielectric*. The dielectric can be a gas, liquid, or a solid, and consists of atoms with an electric dipole structure (Diefenderfer, 1998). The dipole structure requires a physical separation between positively and negatively charged entities on an atomic level (fig. 2.11). These charges are bound by atomic forces and are unable to move. In the case of ideal dielectrics there are no free charges and the material is neutrally charged on a molecular level (Diefenderfer, 1998). In the case of soils the dielectric is a mixture of soil, water, and air (Munoz-Carpena et al., 2005). For a parallel plate capacitor the capacitance is expressed as follows:

$$C = \varepsilon_r \varepsilon_0 \frac{A}{d}(n-1) \tag{2.3}$$

where C is the capacitance in picofarads, *A* is the area of either plate in square meters, *d* is the distance between the plates in m, *n* is the number of plates, ε_r is the relative permittivity in farads per meter of the dielectric, and ε_0 is the electric constant or permittivity of free space (8.854 pFm^{-1}; Nelson, 1991; Robinson et al., 2005). Therefore, system capacitance increases with increasing plate surface area or dielectric permittivity of the insulator and decreasing distance between the conductors (O'Malley, 1992; Carr, 1993).

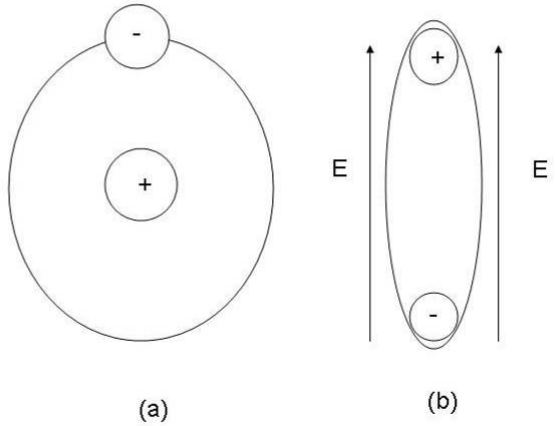

Figure 2.11. Typical atom in (a) absence of and (b) under an applied field (after Diefenderfer, 1998).

The permittivity or dielectric constant is a property of the insulating material and is related to atomic characteristics of the insulating medium that support electric flux (Carr, 1993). The standard reference for dielectric constant is 1.000 for a perfect vacuum (Carr, 1993). Some other common dielectric constants are shown in table 2.2. When an electrical field is applied to the conductors, the charges on the conductors distort the surface charge on the atoms of the insulating medium, resulting in a net negative charge on one side of the dielectric surface and a net positive charge on the opposite side (fig. 2.11 and 2.13). This dipole-effect partially neutralizes the effects of the surface charge on the insulating medium, permitting an increase in electrical charge for the same voltage (O'Malley, 1992). The permittivity of a material has also been described as the extent to which the charge distribution within the materials is polarized in an external electric field (Robinson et al., 1999). Natural soils have an apparent dielectric constant of 2-20 depending on the air and water content within the soil matrix. Therefore, the soil minerals do not polarize as well as water, which has an apparent dielectric around 80 (Hasted, 1973).

A defining characteristic of dielectric materials is polarization or their ability to store energy when an external electric field is applied (Diefenderfer, 1998). There are four ways for a material to polarize once an electric field is applied: ionic, electronic, dipole, or heterogeneous (fig. 2.12). Ionic polarization (fig 2.12a) occurs when an external electrical field is applied to a material that contains positive and negative ions, and the ions are displaced (Diefenderfer, 1998). Induced dipoles can be created by ionic polarization, but the ionic bonds of the material strongly resist the rotational forces induced by the electric field. Ionic polarization is harder to detect at microwave frequencies (300 MHz – 300 GHz; Diefenderfer, 1998).

Electronic polarization (fig. 2.12b) occurs in materials that respond to an applied electrical field by shifting the electron cloud in the center of the molecule which surrounds the nucleus of the atom, relative to the center of the nucleus (Diefenderfer, 1998). Electronic polarization can also induce dipoles. The magnitude of electronic polarization is a function of the strength of the electric field and the attraction forces the nucleus of the molecule imposes on the electron cloud (Diefenderfer, 1998).

Substances composed of polar molecules, such as water, also undergo dipole polarization (fig. 2.12c). Polar molecules are permanent dipoles, and when there is not an external electric field applied to the system, the molecules are randomly oriented. Once an electrical field is applied to the system the molecules then orient themselves in the direction of the field. Dipole polarization is temperature- and phase-dependent. Lattice structures restrict the rotation of molecules to the applied electrical field (Diefenderfer, 1998). For example, the dielectric constant of liquid water is eight times greater than the dielectric constant of ice.

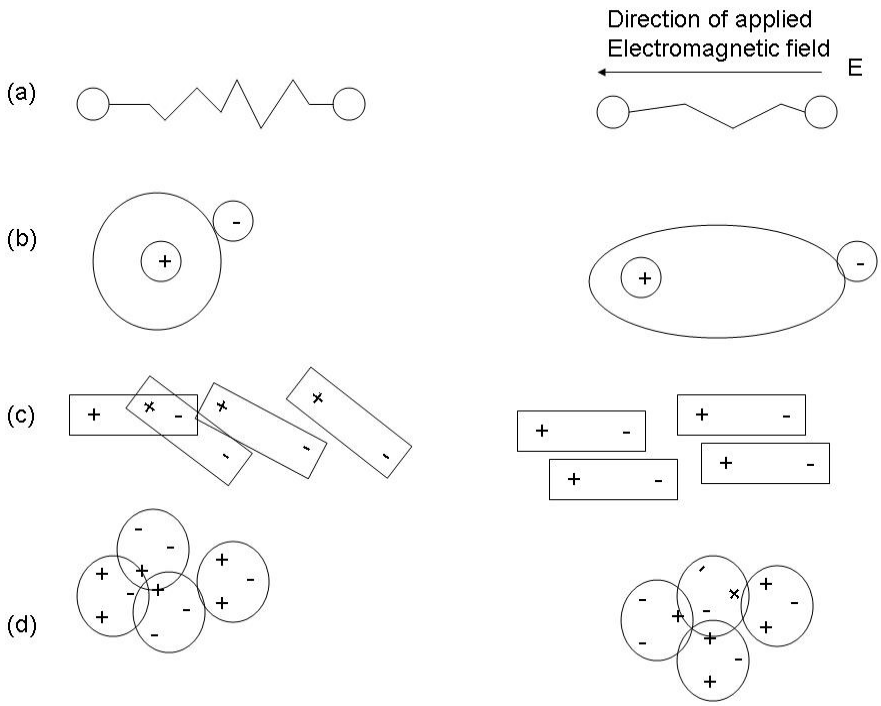

Figure 2.12. Representation of the four types of polarization: (a) ionic, (b) electronic, (c) dipole, (d) heterogeneous (after Diefenderfer, 1998).

The last polarization type is heterogeneous polarization, which occurs when conducting volumes are distributed over the dielectric material such as in soils or a concrete mixture (Diefenderfer, 1998). The specifics of the polarization are a function of a critical frequency or the dielectric relaxation frequency. When the frequency is less than the critical frequency, the charge carriers can redistribute within the conductive particles yielding an artificially high dielectric constant (Diefenderfer, 1998). However, when the applied frequency is greater than the critical frequency the charge carriers are unable to fully redistribute leading to a reduced dielectric constant and an increase in conductivity (Diefenderfer, 1998). The frequency at which the dielectric constant decreases is known as the dielectric relaxation point.

Table 2.2. Common insulating materials and their dielectric constants (Carr, 1993; Hasted, 1973)

Dielectric media	Dielectric Constant
Dry air	1.0006
Wax paper	3.5
Glass	5-10
Mica	3-8
Rubber	2.5-35
Dry Wood	2.5-8
Dry Clay	4
Clay (50 % water)	30
Quartz & Feldspar	4.5-5
Granite	7-12
Limestone	15
Sandstone	9-11
De-ionized Water	81

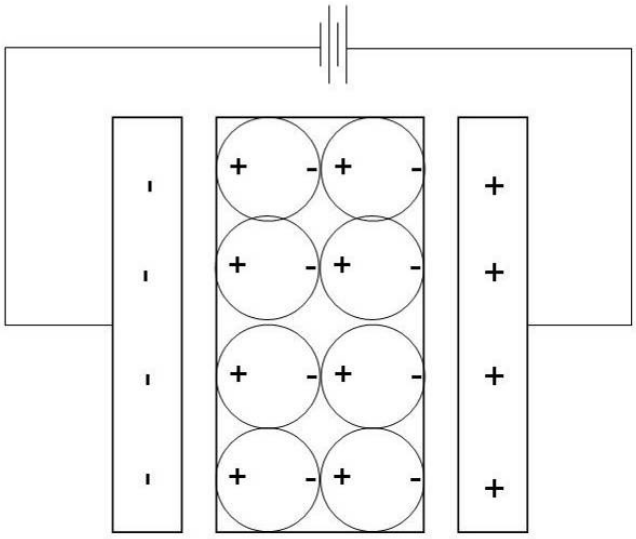

Figure 2.13. Parallel plate capacitor with charged conductors and oriented insulating medium.

2.7.2 Composite Dielectric Materials

Interpreting the measured dielectrics of soil systems theoretically is often difficult (Hasted, 1973). The complexity is due to the interactions between the solid, liquid, and gaseous phases within a soil matrix. The irregular shapes of the solid soil particles also increases the difficulty of applying information from measured dielectrics (Hasted, 1973). The liquid component of the

sample volume can have varying electrolytic conductivity, changing the interaction at the solid-liquid boundary (Hasted, 1973). In the past, the soil system has been simplified by studying only purified sand or clay mixed with air and water (Hasted, 1973).

Conceptual models of composite dielectrics have been developed (Fig. 2.14). Hasted (1973) described the dielectric of a heterogeneous, two-component mixture as a volume-weighted average of the two extremes. Equations 2.4 and 2.5 are valid for a two-component, heterogeneous mixture if the conducting plates are filled with either mixed fibers stretching from plate to plate (equation 2.4), or interleaved sheets parallel to the conducting plates (equation 2.16; Hasted, 1973):

$$\varepsilon_m = \varepsilon_0 + \nu_i \left(\varepsilon_i - \varepsilon_0\right) \tag{2.4}$$

where ε_m is the mixed dielectric constant, ε_0 is the dielectric constant of component one, υ_0 is the volume of component one, υ_i is the volume of component two, and ε_i is the dielectric of component two.

$$\frac{1}{\varepsilon_m} = \frac{\nu_i}{\varepsilon_i} + \frac{\nu_0}{\varepsilon_0} \tag{2.5}$$

The dielectric properties of agricultural products have also been studied extensively (Nelson (1991). The dielectric properties of agricultural products were initially studied to determine moisture content in storage containers. Research focused on grain, wheat, barley, and other materials in both the U.S. and Russia and determined the dielectric properties of these grains depended mainly on water content, but also on temperature of the materials, the frequency of the applied alternating electric field, the structure and density of the products, the chemical composition of the materials, and finally on any permanent dipole moment due to water and any other molecules within the sample volume (Nelson, 1991).

Nelson (1991) also presented equations for estimating the dielectric constant of a solid and liquid mixture (fig. 2.14). To utilize the following mixture equations one must know four of the following variables: complex permittivity of the mixture (ε_m), complex permittivity of the liquid (ε_1), complex permittivity of the solid (ε_2), volume of the liquid (υ_1), or volume of the solid (υ_2; Nelson, 1991).

Table 2.3. Composite Dielectric Equations for a mixture of solid particulate and a liquid (Nelson, 1991)

Equation Name	Equation	Equation number
Complex Refractive Index Mixture	$\varepsilon_m^{1/2} = v_1(\varepsilon_1)^{1/2} + v_2(\varepsilon_2)^{1/2}$	6
Landau & Lifshitz, Looyenga	$\varepsilon_m^{1/3} = v_1(\varepsilon_1)^{1/3} + v_2(\varepsilon_2)^{1/3}$	7
Böttcher	$\frac{\varepsilon_m - \varepsilon_1}{3\varepsilon_m} = v_2\left(\frac{\varepsilon_2 - \varepsilon_1}{\varepsilon_2 + 2\varepsilon_m}\right)$	8
Bruggeman-Hanai	$\frac{\varepsilon_m - \varepsilon_2}{\varepsilon_1 - \varepsilon_2}\left(\frac{\varepsilon_1}{\varepsilon_m}\right) = 1 - v_2$	9
Rayliegh	$\frac{\varepsilon_m - \varepsilon_1}{\varepsilon_m + 2\varepsilon_1} = v_2\left(\frac{\varepsilon_2 - \varepsilon_1}{2\varepsilon_1 + \varepsilon_2}\right)$	10
Lichtenecker	$\ln \varepsilon_m = v_1 \ln \varepsilon_1 + v_2 \ln \varepsilon_2$	11

ε_m= complex permittivity of the mixture, ε_1= complex permittivity of the liquid, ε_2= complex permittivity of the solid, υ_1= volume of the liquid, and υ_2= volume of the solid.

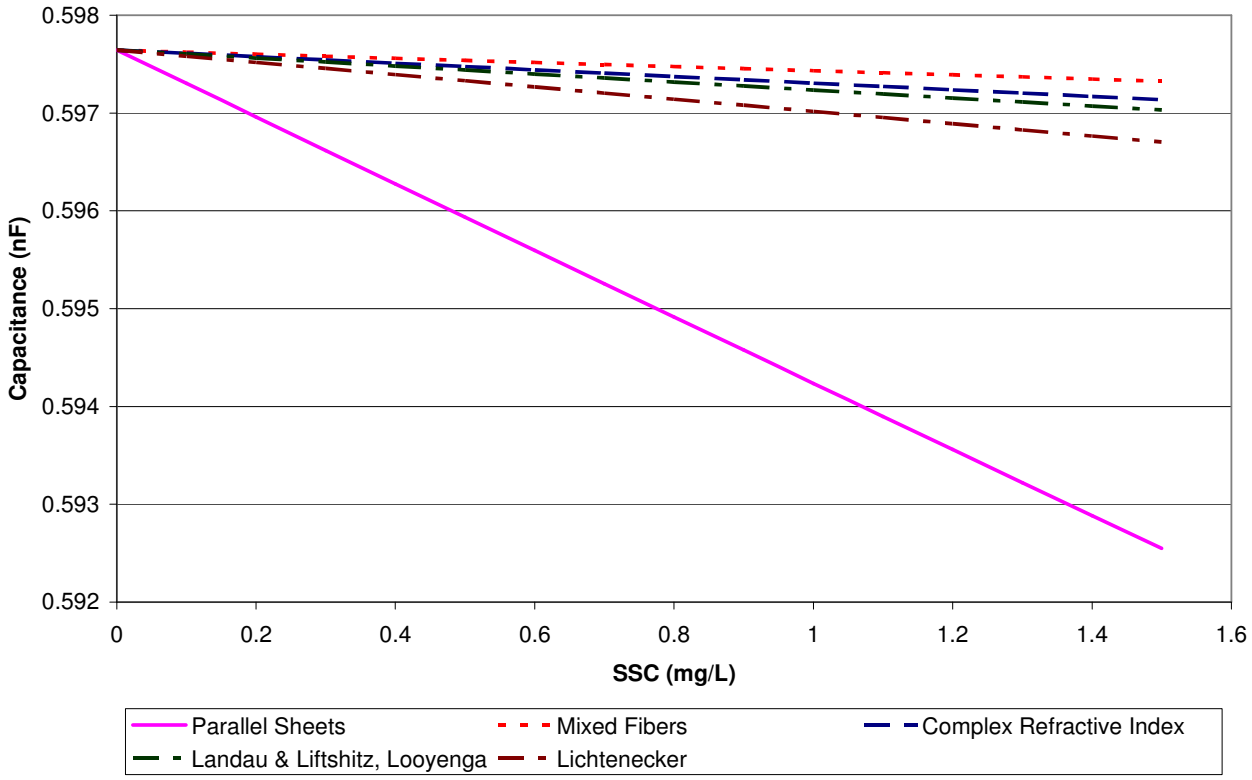

Figure 2.14. Capacitance versus suspended sediment concentration (SSC) for sand using mixture equations 2.4-7 and 2.11.

2.7.3 Application of Capacitance Theory

Capacitance sensors are used in many different applications. For example, a capacitance sensor can monitor fluid depth within a reactor. The sensor is placed above the normal fluid operating depth but below a critical depth for the reactor. Under normal operating conditions the insulating material will be air ($\varepsilon = 1.0006$) and the capacitance reading will be relatively low. The capacitance reading will increase when the solution depth increases and the insulating material shifts from air to the solution. The increase in capacitance is due to increases in the dielectric constant of the insulating material (Carr, 1993).

Capacitance sensors have also been applied to environmental monitoring of natural systems. When applied in systems such as a soil environment, the dielectric constant describes the soil permittivity to an electrical field (Munoz-Carpena et al. 2005; Robinson et al., 2005). Capacitance sensors measure the varying capacitance of the soil and relate that change to changes in the dielectric constant of the soil matrix. In a soil system, the value of the dielectric constant is dominated by the presence of water ($\varepsilon = 80$), as compared to soil and air (ε_{soil} = 2-20 and $\varepsilon_{air} = 1$). The dielectric constant increases with increasing proportions of water to soil. Therefore, capacitance is often used to measure the water content of a soil matrix. The measured capacitance is used to calculate the apparent or relative dielectric constant of the medium based on the known surface area of the conducting plate and the distance between the plates (equation 2.13).

Most capacitance sensors have two or more electrodes in parallel plates, rods or metal rings along a cylindrical configuration. When the probe is inserted into the soil and an electrical field is applied to the conducting plates, the soil in contact with the electrodes forms the dielectric of the capacitor and completes the oscillating circuit (Munoz-Carpena et al. 2005). Some of the advantages of using a capacitance sensor over other soil moisture measurement techniques are because the sensor:

- Can read at high salinity values;
- Can be connected to a data logger;
- Is flexible in application; and,
- Is relatively inexpensive.

Disadvantages of capacitance sensors include a small sensing sphere; the need for good contact with the medium; and, sensor sensitivity to temperature, bulk density, and clay content of the

soil, as well as air gaps. Additionally, calibration to specific soil conditions is required for the highest accuracy (Munoz-Carpena et al. 2005).

2.7.4 Capacitance Sensors and Suspended Sediment

Li et al. (2005) hypothesized that the relationship between soil and increasing water content could be utilized to measure increases of sediment content in a water sample. The authors inferred that the sediment suspension had two electric fields: 1) the electrical field supplied by the negative surfaces of the clay particles in suspension; and, 2) the electrical field applied by the sensor electrodes. The first electrical field was perpendicular to the sediment surface and affected the orientation of the sediment platelets. The interaction between the two fields depended on the sediment concentration in suspension. As the sediment concentration increased above 70% by mass the water was isolated in the soil pore space instead of a continuous stream and the capacitance decreased.

Li et al. (2005) tested both parallel and cylindrical capacitor geometries with brass conductors and an AC power source of 3 V at 10 kHz (fig. 2.15). Li et al. (2005) coated one of the two conductor plates with a think layer of electric-insulating paint to reduce the amount of energy lost due to the conductance of water. The authors found the capacitance outputs from both sensor geometries increased linearly with increasing sediment concentration up to 70% sediment by mass, and then the outputs started to decrease linearly. The study also considered the effects of salinity, flow velocity, soil texture, and temperature on the accuracy of the capacitance sensor SSC predictions. The study found that temperature and salinity increased the output linearly, while flow velocity (0-2 m/s) and soil texture (sandy loam and loam) did not cause a significant difference in sensor output. Specifically, the error of the unified calibration curves was ±0.3% for non-saline soils (NaCl <0.2%) and ±1.1% for saline soils (NaCl>0.2%). Li et al. (2005) measured changes in SSC; however, more research on capacitance sensors for suspended sediment concentration is needed to better understand how environmental factors affect capacitance measurements within a range of SSC values more commonly found in US streams.

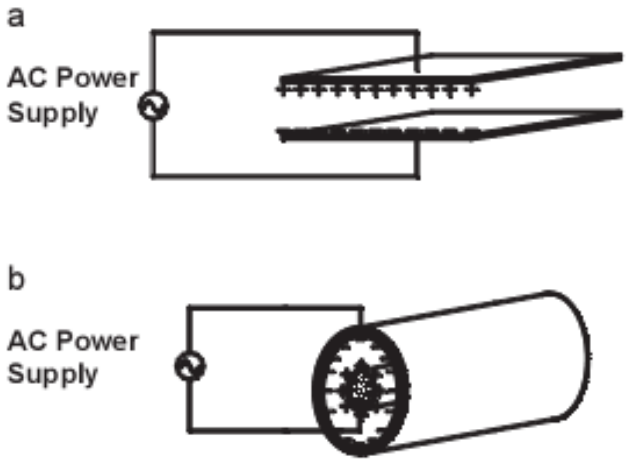

Figure 2.15. Diagrams of the capacitance sensors developed by Li et al. (2005). The study compared parallel plate (a) and cylindrical (b) sensors. Reprinted from Catena, vol. 60(3), Xiaoyu Li, Tingwu Lei, Wei Wang, Qichuan Xu, and Jun Zhao, Capacitance sensors for measuring suspended sediment concentration, 227-237, Copyright (2005) with permission from Elseivier.

2.7.5 Permittivity Theory

Permittivity is a physical description of the effects of an electric field on a dielectric medium and how the medium then affects the electric field (Robinson et al., 1999). It is analogous to impedance since both describe conductive and reactive behaviors, can be expressed in complex form, and, change with frequency (Lee et al., 2007). Permittivity is measured indirectly with an impedance sensor by monitoring the sensor and sample volume, and then removing the known geometric factors of the sensor to calculate permittivity of the sample volume (Lee et al., 2007; Lee and Zhang, 2007). The following equations are necessary to calculate permittivity from impedance measurements:

$$\varepsilon_r^{'} = \frac{C}{\varepsilon_0} g \tag{2.12}$$

$$\varepsilon'' = \frac{G}{2\pi f \varepsilon_0} g \tag{2.13}$$

where $\varepsilon_r^{'}$ is the real part of the relative permittivity, C is the capacitance between the plates (F), ε_0 is the permittivity of free space (8.85X 10^{-12} F m^{-1}), g is the geometric factor of the sensor (m^{-1}), ε_r" is the imaginary part of relative permittivity, G is the conductance between plates (S), and f is frequency (Hz). Equations 2.14 and 2.15 describe the impedance (Z_{load}) of the design sensor,

assuming a parallel connection of a resistor (R) and a capacitor (C). The theory and application of both capacitance and conductance are discussed in the following sections.

$$\left|Z_{load}\right| = \frac{R}{\sqrt{1+(2\pi fRC)^2}} \tag{2.14}$$

$$\angle(Z_{load}) = -\tan^{-1}(2\pi fRC) \tag{2.15}$$

The two factors being measured and recorded by the Lee et al. (2007) microcontroller within the sensor are the ratio of the magnitude of the reference voltage to the voltage signal from of the control volume (*Magnitude_ratio* with units of dB) and the difference in signal phase (*Phase_difference* with units in degrees; equations 2.16 and 17).

$$magnitude\_ratio(dB) = 20\times\log\left(\frac{\left|Z_{load}\right|}{100}\right) \tag{2.16}$$

$$Phase\_difference(\deg) = \angle(Z_{load})\times\left(\frac{180}{\pi}\right) \tag{2.17}$$

The capacitance is estimated from the frequency response and the conductance (which is the reciprocal of resistance) by substituting equation 2.15 into equation 2.17:

$$C = -\frac{G\tan\left(Phase(\deg)\times\frac{\pi}{180}\right)}{2\pi f} \tag{2.18}$$

and then substituting equation 2.14 into equation 2.16:

$$\frac{R^2}{1+(2\pi fR)^2C^2} = \left(100\times10^{\frac{mag(dB)}{20}}\right)^2 \tag{2.19}$$

Finally, by substituting equation 2.18 into equation 2.19 and rearranging the equation, the conductance can be derived from the frequency response. Therefore, $\varepsilon_r`$ and $\varepsilon_r``$ of a soil can be calculated with the magnitude and phase data measured with the sensor and the geometric factor of the sensor (equations 2.12, 13, 18, and 20; Lee et al., 2007).

$$G = \frac{1}{\left\{\left[1+\left\{\tan\left(Phase(\deg)\times\frac{\pi}{180}\right)\right\}^2\right]\times\left(100\times10^{\frac{mag(dB)}{20}}\right)^2\right\}^{\frac{1}{2}}} \tag{2.20}$$

To complete the analysis above the geometric factor of the sensor must be determined by relating resistance (R) and conductivity (σ). The geometric factor (g) of the sensor can be found with the conductivity of the medium surrounding the sensor and the load resistance measured between senor electrodes:

$$R = \rho g = \frac{1}{\sigma} g \tag{2.21}$$

$$g = R\sigma \tag{2.22}$$

where ρ is the material resistivity (Ω-m), and σ is the material conductivity (S m^{-1}). The geometric factor is solved for by submersing the sensor in KCl solution of different known concentrations and completing another frequency test.

2.7.6 Permittivity and Conductance

A disadvantage of optical backscatter, optical transmission, acoustic, fiber-optic transmissometer, and spectral reflectance technologies for measuring SSC is particle-size dependency. For example, optical backscatter or turbidity probes can not distinguish between a change in sediment concentration and change in sediment size. The proposed suspended sediment sensor will also be able to measure the conductance between the electrodes. It is hypothesized that a solution with the same salt content and mass of sediment but with differing particle sizes will have different conductivities. Therefore, measuring both sample permittivity and conductance will allow for predictions of concentration and particle size. Specifically, measuring both magnitude ratio and phase difference may allow particle size to be determined.

Sediment size is closely connected to sediment mineralogy. Sand-sized particles are mostly quartz and feldspar minerals, which have insignificant surface charge density and low conductance. Silt- and clay-sized particles are mainly clay minerals. Clay minerals have a range of surface charge density, depending on the chemical properties of the mineral. For example, kaolinite is a 1:1 clay mineral, with very little isomorphic substitution within its structure, and a surface charge just above zero. Therefore, kaolinite would have a slightly lower resistance than quartz. Montmorillinite is another common clay mineral. It is a 2:1 mineral with significant isomorphic substitution and a surface charge density between 0.4 and 1.20. Two to one clay minerals have surface charge densities up to -2 units of charge per unit cell of mineral, and thus have lower resistance and higher conductance than kaolinite.

2.7.7 Application of Permittivity

Multiple permittivity sensors have been designed to measured soil water content (Lee et al., 2007; Robinson et al, 1999; Klein and Santamarina, 1997). Soil permittivity is the ability of a soil to resist the formation of electric fields within the soil matrix when an electromagnetic wave is applied. Both capacitive and conductive behaviors of the soil matrix affect the amount of current from the electromagnetic wave that can move through the soil matrix (Lee et al., 2007). Water content is one of the dominant soil properties affecting permittivity. Previous studies have shown that when the loss tangent of soil, or the ratio of the imaginary to real part of the relative soil permittivity (eq. 2.25) was assumed to be small, that the real part of relative permittivity, called the apparent dielectric permittivity (ε_a), is a function of water content (Lee et al., 2007).

The soil response to the electric field is dependent on the frequency of the electrical field. For example, at low frequencies soil permittivity is dominated by the capacitive behavior of the soil matrix because the polarity of the applied field is changing slowly enough to allow the dipole molecules in the soil to align in the opposite directions (Lee et al., 2007). As described above this alignment is called polarization. Polarization of the soil particles slows the passage of current through the soil matrix by storing electrical energy and then releasing it once the field is removed. The opposite is true at high frequencies where the electric field is changing too rapidly for the dipole molecules to respond to the alternating current due to the binding forces between atoms (Lee et al., 2007). Therefore, at high frequencies the energy is passed through the system and the system is in a state of dielectric relaxation. Energy from the applied electric field can also be lost due to two conductive aspects of the soil matrix: conduction due to electrical charges on the surface of the solid particles and liquid ionic conduction by electrolytes dissolved in the pore water (Topp et al., 2000; Robinson et al., 2003).

The capacitive behavior of the soil creates a phase lag between the applied field and the measured output. The phase lag is dependent on the frequency of the applied field and allows soil permittivity to be expressed in complex form (Topp et al., 2000). Combining the effects of polarization, conduction, and relaxation on permittivity Topp et al. (2000) and Robinson et al. (2003) represented permittivity with the following equations:

$$\varepsilon_r = \frac{\varepsilon}{\varepsilon_0} = \varepsilon_r' - j\varepsilon_r'' \tag{2.23}$$

$$\varepsilon_r'' = \varepsilon_d'' + \frac{\sigma_{DC}}{2\pi f \varepsilon_0} \tag{2.24}$$

$$\tan\delta = \frac{\varepsilon_r''}{\varepsilon_r'} \tag{2.25}$$

where ε_r is relative permittivity, ε is permittivity (Fm^{-1}), ε_0 is the permittivity of free space (8.85 x 10^{-12} Fm^{-1}), ε_r' is the real component of relative permittivity (energy storage due to polarization), $j = \sqrt{-1}$, ε_r'' is the imaginary component of relative permittivity, ε_d'' is the energy loss due to dielectric relaxation, σ_{DC} is the DC electrical conductivity, f is the applied frequency (Hz), and $\tan\delta$ is the loss tangent.

As for capacitance sensors, salinity and temperature of the soil matrix affect permittivity measurements. Soil texture can also affect permittivity readings for a given water content and salinity combination, depending on the frequency of the electromagnetic field applied to the system (Lee et al., 2007). Therefore, the soil sample must be tested at multiple frequencies to tease apart the complex interactions between multiple soil properties (Lee et al., 2007). By testing a soil sample at multiple frequencies both physical and chemical soil properties may be determined (Lee et al., 2007). Multiple soil properties can detected due to the soil responding differently at low and high frequencies. For example, at low frequencies the permittivity is dominated by capacitive behavior of the soil or its physical properties. In contrast, at high frequencies the capacitive behavior decreases, since the molecules can not polarize at the higher frequency, allowing the conductive behavior of the soil to become apparent. The conductive behavior describes the chemical properties of the soil, such as the concentration of electrolytes in the pore water.

Lee et al. (2007) modified a permittivity sensor designed by Zhang et al. (2004) to simultaneously measure multiple soil properties. Major modifications to the sensor included extending the frequency range from 15 MHz to 100 MHz, changing the probe geometry to further enlarge the capacitive effect and reduce the contact resistance, designing a control system to maintain constant current amplitude through the frequency range, integrating the system using an embedded microcontroller to allow real-time measurement, and adding phase measurement (Lee et al., 2007). The modified sensor was then tested using samples of three soil textures at multiple levels of salinity, density, water content, and probe penetration depth.

The sensor structure was based on a modified four-electrode Wenner-array (Lee et al., 2007). The four electrodes were made of brass alloy and shaped as tapered rectangular plates (80 mm long and 28 mm tall). The plates were tapered to an angle of 76° to allow for better contact between the soil and plates. Distance between the plates varied from 8 to 12 mm, as a function of the plate height. The contact area between the electrodes and soil and the separation between the electrodes were designed to increase the capacitive effect of the sensor (Lee et al., 2007). The electrodes were assembled on a Garolite plate, which is a solid material comprised of a non-conductive, synthetic resin that is resistant to heat, moisture, and oil (Lee et al., 2007). The other main components of the sensor are described in detail by Lee et al. (2007).

The study completed by Lee et al. (2007) tested combinations of three soil textures (very fine sandy loam, silt loam, and silty clay loam), five gravimetric water contents (12%-22%), five salinities (1.90-11.15 dS m^{-1}), and five bulk densities (1.05-1.30 g cm^{-3}). Each combination was tested with 111 different frequencies ranging from 200 Hz to 100 MHz. Conclusions regarding the combinations of soil properties and frequencies tested included the following: magnitude and phase difference data were accurate indicators for multiple soil properties; under the same levels of volumetric water content, electrical conductivity and temperature, only soil density affected the magnitude and phase responses (a lower density increased the phase difference and decreased the magnitude ratio); sensor penetration depth had a significant effect on both the magnitude and phase responses (increasing penetration depth caused a decrease in magnitude ratio and an increase in phase difference); and, the effect of temperature on both the magnitude ratio and phase difference was variable.

Lee and Zhang (2007) used a locally weighted learning (LWL) statistical tool to conduct a piecewise linear regression of the frequency response data to calibrate the sensor. The study concluded that models established using the frequency response data obtained at the deeper soil penetration depth performed better than the shallower penetration depths. As soil clay content increased, the R^2 values of models predicting volumetric water content increased, while model accuracy for predicting conductivity decreased. Models had R^2 values greater than 0.90 for all three soil textures at all the tested water contents, bulk densities, and salinities, while model results for predicting salinity were not as consistent, with R^2 ranging from 0.4-0.8.

2.7.8 Permittivity Sensors and Suspended Sediment

As pointed out by Lee and Zhang (2007), applying permittivity measurements to complex, heterogeneous systems is still a very "black box" approach. This statement also applies to measuring SSC via a permittivity method. However, figures 2.16-18 detail the potential reactions of multiple scenarios to low, medium, and high frequencies. High frequencies will be greater than or equal to the dielectric relaxation point of water (17 GHz as stated by Robinson et al., 2003). Medium frequencies will be less than or equal to the relaxation point for soils (<1 GHz as stated by Robinson et al., 2003). Low frequencies will be less than 10 MHz. The scenarios are designed to move from an ideal liquid system with no ions to a water-sediment suspension to predict how the output signal will change with variations in the heterogeneous mixture within the sample volume. The scenarios include an ideal de-ionized water with no extra ions present (fig. 2.16), water with ions present (fig. 2.17), and water with sediment present (fig. 2.18). The reaction of the sample volume to high, medium, or low frequency in each scenario will be discussed in terms of equations 2.23 and 24, where signal loss can be due to ionic conductivity and dispersion.

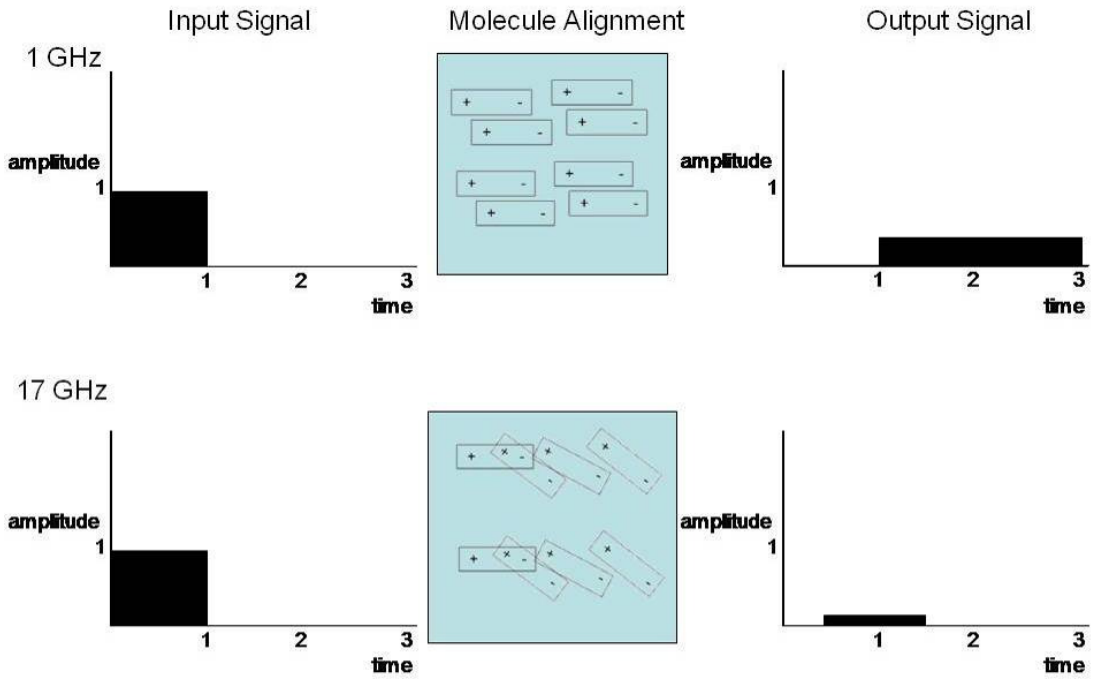

Figure 2.16. Predicted response of de-ionized water to the application of high and low electromagnetic currents. Input signals, molecular response to the signal, and the signal transmitted through the media are shown for both frequencies.

At 1 GHz both the gain and phase values will be greater than due to storage within the sample volume. At 17 GHz the water molecules will be unable to polarize. No energy will be stored within the sample volume because the dielectric relaxation point of water has been exceeded. An ideal, de-ionized volume of water will have no ions present and act as an insulator. Therefore, very little energy will pass through the sample volume due to the reduced conductivity of DI water. This will cause gain to be greater than one and a small phase shift.

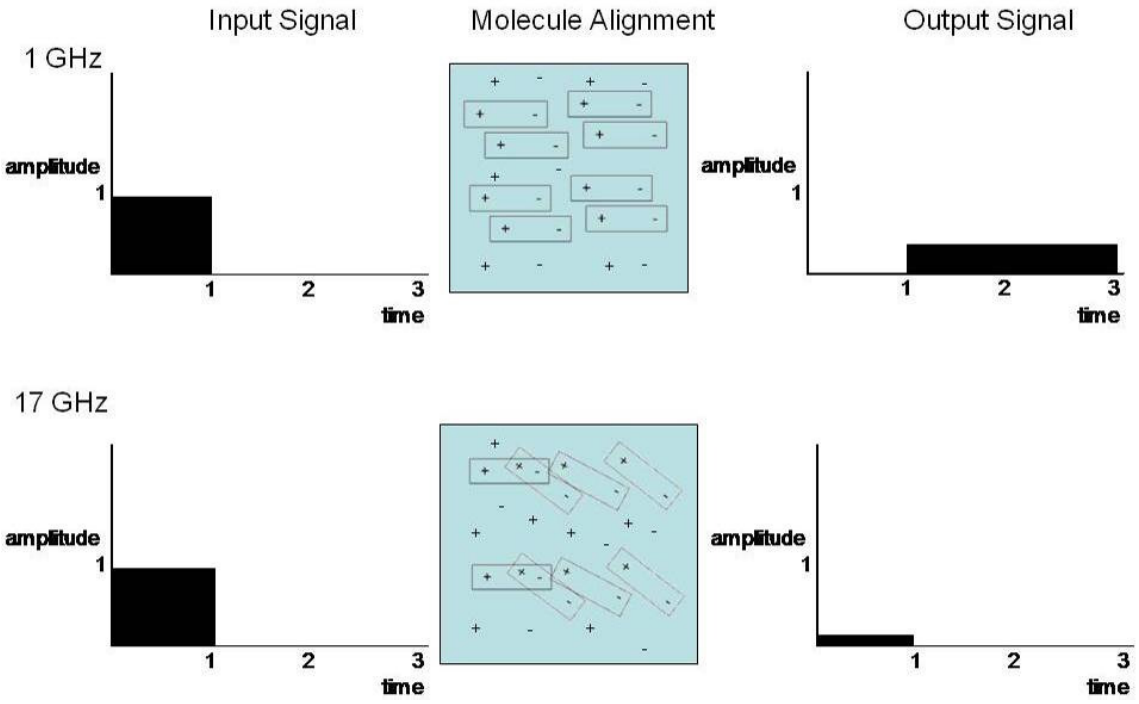

Figure 2.17. Predicted response of water with ions to the application of high and low electromagnetic currents. Input signals, molecular response to the signal, and the signal transmitted through the media are shown for both frequencies.

At 1 GHz both gain and phase will be greater than one as energy is stored in the sample volume. At 17 GHz gain will be greater than one due to conductive losses but phase will be near zero as the ions in the water increase the conductive properties of the water.

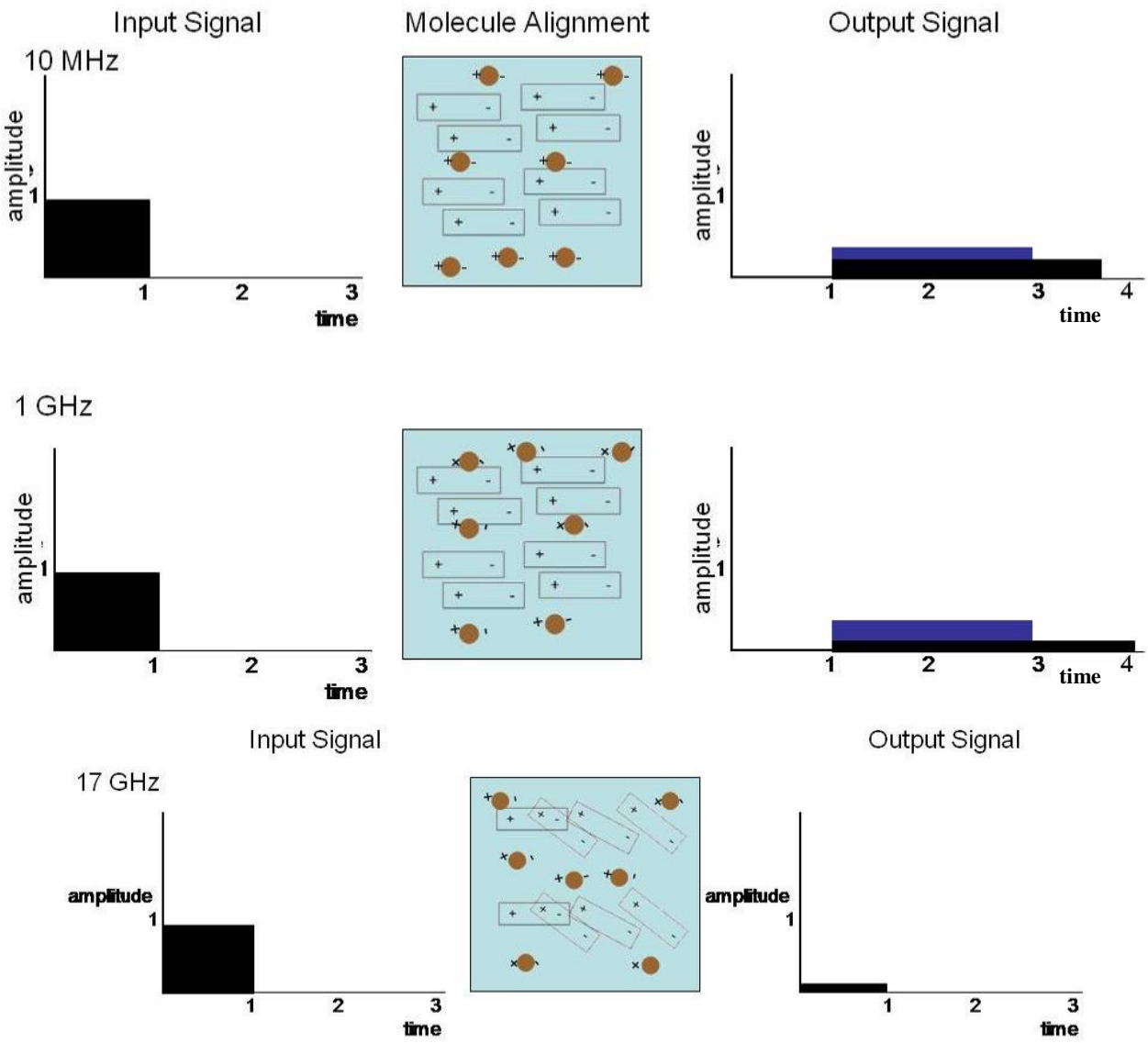

Figure 2.18. Predicted responses of water with suspended sediment to the application of low (10 MHz), medium (1 GHz), and high (17 GHz) electromagnetic currents. Input signals, molecular response to the signal, and the signal transmitted through the media are shown for all three frequencies. The medium and high frequencies correspond to the dielectric relaxation frequencies for sediment and water. Brown signifies soil molecules and blue represents water. Also the blue bars on the output signal represent the response of just water as expressed in figure 2.17.

At 10 MHz gain will be greater than one and phase will be much greater than one because both sediment and water will polarize and store energy within the system. However it will take longer for the system to discharge increasing the difference in phase between the input and output signals. At 1 GHz both gain and phase will be significantly greater than one. Only water will be able to polarize and store energy. The storage is less than pure water because it is believed that

sediment will inhibit the polarization of water. At 17 GHz gain will be greater than one due to conductive losses. Phase will be close to zero due to the conductive properties of water.

Chapter 3: Development of Sediment Suspension System

A sediment suspension system was developed for testing the permittivity sensor. The system was designed to maintain a constant suspension of kaolinite over time and in the space of the container. The following chapter describes the hardware of the suspension system and the results of quality control testing.

3.1 Methods

The sediment suspension system consisted of three clear plastic cylindrical containers, three submersible pond pumps, and three plumbing networks (fig. 3.1). The plumbing networks were comprised of 1.91-cm and 2.54-cm diameter PVC piping (¾" and 1"; fig. 3.2). The pumps were submersible pond pumps from Harbor Freight (Ogden, UT) and had the capacity to move 5991 L/hr (model 47138; 1585 gal/hr). The cylindrical containers had to be large enough to fit the electrode through the opening and provide adequate space so the electrode did not touch the container walls during data collection. The containers had an effective volume of 14 L.

Figure 3.1. Sediment suspension system consisted of three plastic chambers, three submersible pond pumps, and three PVC piping networks.

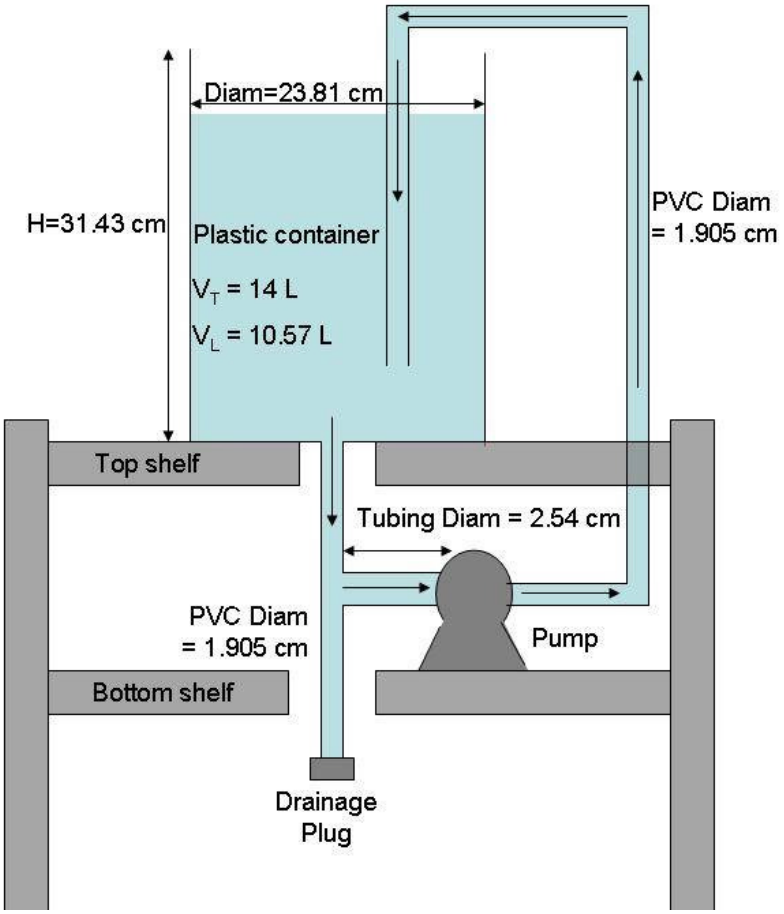

Figure 3.2. Schematic of the suspension system for a single chamber including the pump, container, and piping network. The suspension chamber was 31.4 cm tall and had a diameter of 23.8 cm (12.375" and 9.375"). The chamber volume was approximately 14 liters.

All statistical analyses for this project except the Partial Least Squares regression analysis were conducted in R: A Language and Environment for Statistical Computing version 2.6.2 (R Development Core Team, Vienna, Austria; http://www.R-project.org).

3.2 Results for Quality Control Testing of Suspension System

3.2.1 Homogeneous Mixing

The suspension system was tested to determine if the sediment was homogeneously suspended. Initially 32, 100-mL samples were systematically collected from a cylindrical container for three concentrations (500, 2500, and 5000 mg/L). The sample region of each container was divided horizontally into quadrants and vertically into eight layers (1-cm spacing). Samples were collected with a 25-mL pipette for each horizontal/vertical slice of the sample volume and filtered following a standard SSC filtration method (APHA, 1998). The filters used

throughout the quality control procedures were a glass fiber filter specific for gravimetric analyses in sanitary water analysis procedures (Fisher Scientific, Type AE 4.7 cm dia., 0.3 μm pore size).

The filtered concentrations for all three treatment levels had a non-normal distribution based on the Shapiro-Wilk test ($p << 0.05$) and graphical analysis. The suspension system was tested both vertically and horizontally in all three containers by a Kruskal-Wallis rank sum test ($\alpha = 0.05$) to determine if the distributions for each vertical or horizontal slice were centered on the same median. Statistical results indicated the four vertical sections (n=8) and the eight horizontal slices (n=4) were not statistically different; therefore, the suspension was assumed homogenous at all three treatment levels. Each vertical slice had a sample size of eight and each horizontal slice had a sample size of four. Specifically, it was assumed that the differences between the median filtered concentration for each vertical or horizontal slice was zero for each treatment level (500, 2500, and 5000 mg/L). Since the p_{value} for each test was great than 0.05 the null hypothesis was accepted and the suspension was considered homogeneous.

Table 3.1. Summary of p_{values} for vertical and horizontal testing at three concentration levels.

Concentration Treatment Level (mg/L)	Pvalue for Vertical Test	Pvalue for Horizontal Test
500	0.1152	0.9568
2500	0.0856	0.4074
5000	0.8103	0.765

3.2.2 Comparison between treatment level and filtration level

The filtration data were tested to determine if the median filtered concentration was significantly different than the treatment level ($\alpha = 0.05$) using a one sample, two-sided Wilcoxon signed rank test for each concentration (with μ set as the treatment level: 500, 2500, and 5000 mg/L). Overall three sampling techniques were compared to identify the best sampling method to determine if the suspension within the container measurement volume was equal to the assigned treatment level. The sample techniques included pipette (100 mL), pump sampling (135 mL and 28 mL), and grab samples (28 mL). It was determined that filtered values for all three sampling techniques and sample volumes were significantly different than the treatment levels ($\alpha = 0.05$). Therefore, the following comparisons were completed to determine which sampling technique and sample volume recovered the most of the known concentration.

Initially, 100-mL samples volumes were taken using both a pipette and pump sampler. The median concentration collected from the pipette (n=32) and pumping methods (n=10) was significantly less than the assigned treatment level for all three treatments, based on the Wilcoxon signed rank test (α=0.05; fig. 3.3). The pipette samples analyzed here are the same samples collected for the tests described in section 3.2.1. The pump samples were systematically collected with a pump sampler via 0.95-cm vinyl tubing (ISCO model 6712C; 3/8" tubing) at random locations within the sample volume for the three concentration levels of the study (500, 2500, and 5000 mg/L).

Sample concentrations for the pipette sample method with a volume of 100 mL ranged from 473 to 503 mg/L at 500 mg/L, 2240 to 2458 mg/L at 2500 mg/L, and 3516 to 5322 at 5000 mg/L. Sample concentrations for the pump sample method with a sample volume of 135 mL ranged from 450 to 470 mg/L at 500 mg/L, 2218 to 2440 mg/L at 2500 mg/L, and 4514 to 4788 mg/L at 5000 mg/L. Further investigations revealed increased sample loss with increased concentration level due to the high sediment mass in each 100-mL sample (fig. 3.3). At the lowest concentration level the pipette method was the best at collecting a representative sample; however, the pump sampling technique at the lower sample volume was more accurate at all treatment levels, collecting 97% of the sample for each treatment level. To eliminate this problem, a 30-mL sample volume was used (fig 3.3).

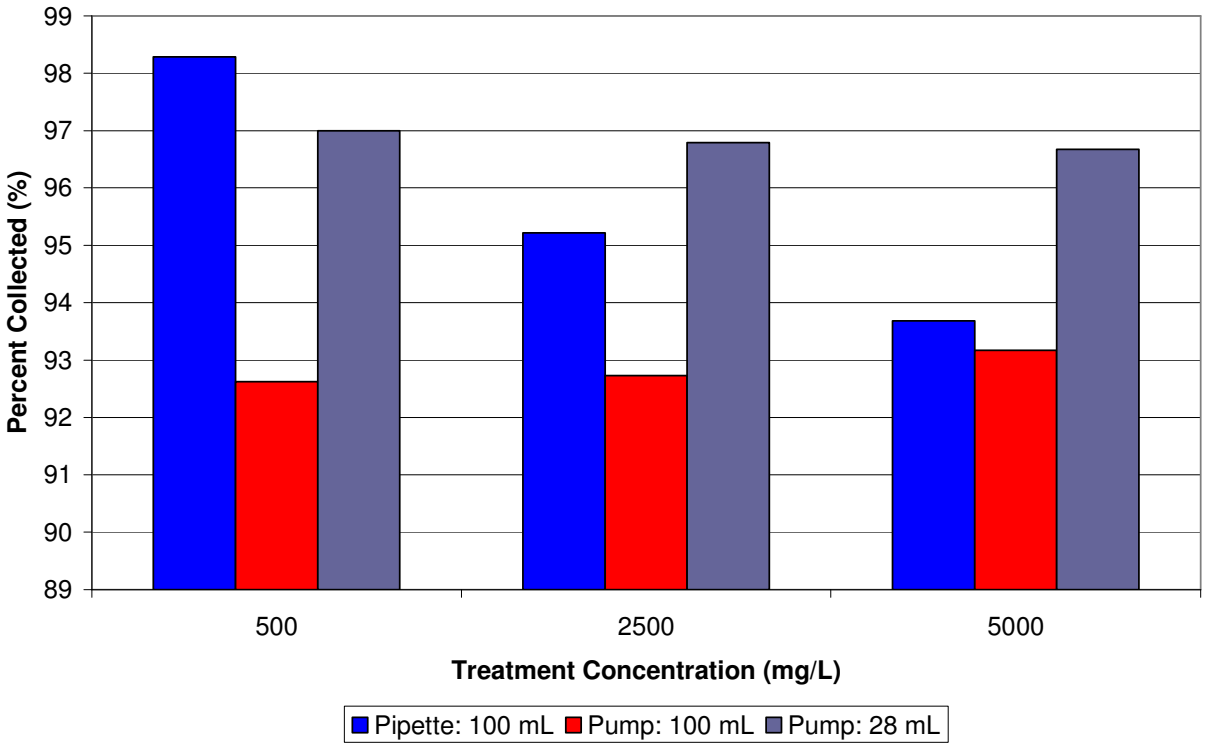

Figure 3.3. Percent of the treatment concentration collected by two collection methods and two different volumes.

One other collection technique was explored to reduce the time required to collect the samples and sample loss at the higher concentration levels during filtration. Five, 28-mL samples were systematically collected with a pump sampler via 0.95-cm vinyl tubing (ISCO model 6712C; 3/8" tubing) and as grab samples at random locations within the sample volume for four concentration levels of the study (1000, 2000, 3000, and 5000 mg/L). Grab samples were pulled randomly from the sample volume at the same depth as the permittivity electrode. The vial was first filled with sample and then emptied and then filled again before capping the sample. The median sample concentrations for the 28-mL samples were compared using a one sample, two-sided Wilcoxon signed rank test for each concentration to the treatment levels and the percent difference between the filtered and treatment concentrations were calculated (fig. 3.4). The median filtered concentration for both pump and grab sample techniques were significantly different than the treatment level (α=0.05). Statistical results indicated the grab sample technique was as accurate as the pump sampling since the grab samples had a higher mean filtered concentration than the pump samples for all concentrations but 5000 mg/L. The

grab samples technique also required less time to collect the samples. Therefore throughout the study 28-mL grab samples were collected.

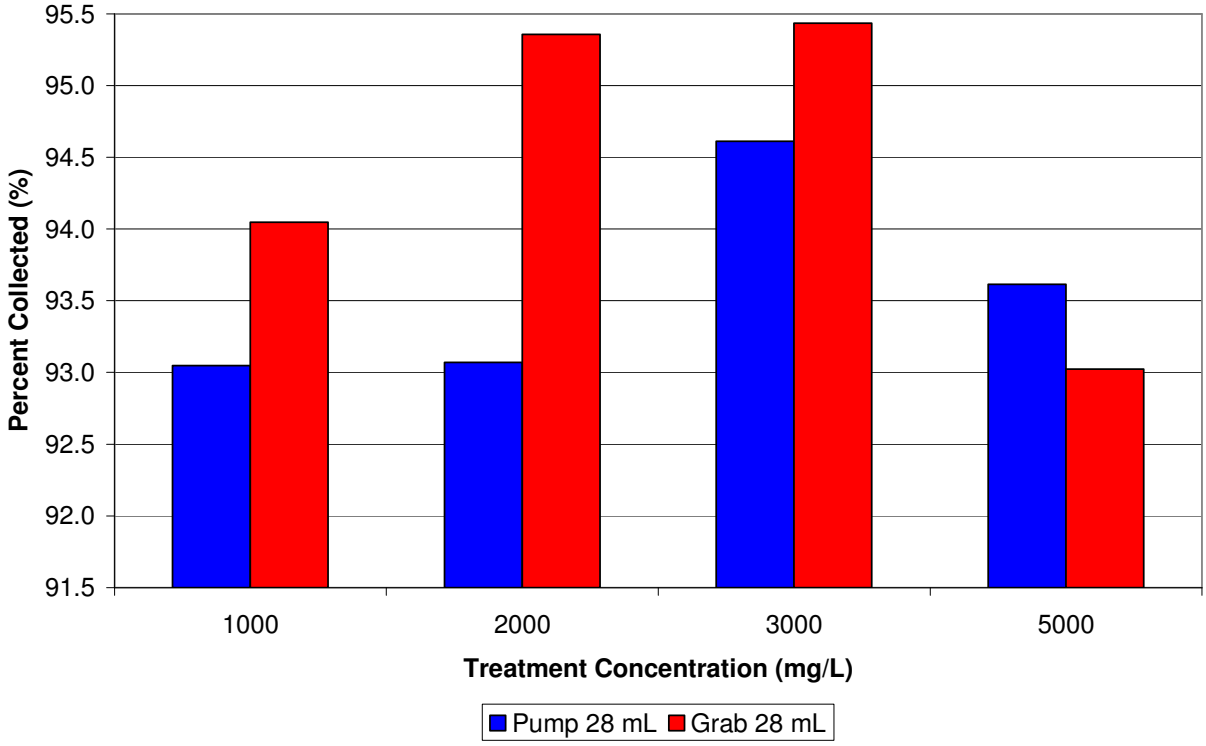

Figure 3.4. Percent of the treatment concentration collected by two collection methods.

3.3 Conclusions for the Suspension System

Statistical tests of the suspension system provided substantial evidence that the suspension system produced a homogeneous sediment suspension. These results indicate preferential flow patterns or sediment settling were not present within the system. Three sampling methods and two sampling volumes were tested for accuracy. It was determined that a 28 mL grab sample would reduce sampling time and maintain accuracy. Also, the filtered concentration did not equal the treatment value within the sampling region of the container for any of the sampling techniques or volumes for an alpha of 0.05. Therefore, during model development it was necessary to use the filtered concentrations instead of the treatment levels. Table 3.2 provides summarized results for all the filtration methods and volumes.

Table 3.2. Summary of filtration methods results.

Sampling Technigue	Study type	# of Samples	Volume of Sample (mL)	Treatment Level (mg/L)	Mean SSC (mg/L)	Median SSC (mg/L)	Stand. Deviation (mg/L)
Grab	Study 2[1]	5	28	500	433.8	439.3	16.53
Pipette	Preliminary QC[2]	32	100	500	491	491.5	7.8
Pump	Preliminary QC	10	135	500	463.1	464.1	7.37
Pump	Preliminary QC	4	28	500	485	481.1	30.7
Pump	Study 1[3]	15	28	500	467.6	467.9	29.5
Grab	Study 1	3	28	1000	940.5	942.9	42.9
Grab	Study 2	5	28	1000	913.8	907.1	48.48
Pump	Study 1	15	28	1000	930.5	935.7	21.2
Grab	Study 1	3	28	2000	1907.1	1907.1	15.2
Grab	Study 2	5	28	2000	1844.0	1846.4	42.53
Pump	Study 1	15	28	2000	1861.4	1860.7	53.6
Pipette	Preliminary QC	32	100	2500	2380	2386.5	46.9
Pump	Preliminary QC	10	135	2500	2318.2	2321.9	66.2
Pump	Preliminary QC	4	28	2500	2419	2419.7	47.1
Grab	Study 1	3	28	3000	2863.1	2825.0	85.2
Grab	Study 2	5	28	3000	2787.6	2778.6	115.68
Pump	Study 1	15	28	3000	2838.3	2835.7	55.3
Grab	Study 2	5	28	4000	3686.0	3685.7	82.66
Pump	Study 1	15	28	4000	3643.3	3621.4	93.9
Grab	Study 1	3	28	5000	4651.2	4685.7	62.9
Grab	Study 2	5	28	5000	4590.7	4585.7	114.53
Pipette	Preliminary QC	32	100	5000	4684	4747	304.8
Pump	Preliminary QC	10	135	5000	4658.4	4676.3	90
Pump	Preliminary QC	4	28	5000	4833.7	4891.1	179.6
Pump	Study 1	15	28	5000	4680.7	4717.9	126.9

[1]Study 2 was the final collection of prediction model data and collected only grab samples.

[2]Preliminary QC was the preliminary analysis comparing pipette and pump sampling methods. The preliminary work also determined that the system was homogeneously suspended.

[3]Study 1 was the first attempt at collecting prediction model data and compared grab and pump samples.

3.3.1 Final quality control sampling protocol

Five 28-mL grab samples were collected for each concentration-conductivity. For example, five samples were collected from the container with 500 mg/L at 0 μS/cm and another five samples from the container with 500 mg/L and 250 μS/cm. Therefore 15 samples were collected for each concentration level. The samples were pulled randomly from the sample volume at the same depth as the permittivity electrode. The vial was first filled with sample and then emptied and then filled again before capping the sample. The five samples were collected after all the permittivity data for that concentration level had been collected. All samples were refrigerated at

5°C in a walk-in cooler. The samples were then filtered following a standard SSC filtration method (APHA, 1998). The filters used throughout the quality control procedures were a glass fiber filter specific for gravimetric analyses in sanitary water analysis procedures (Fisher Scientific, Type AE 4.7 cm dia., 0.3 μm pore size).

Chapter 4: Permittivity Sensor Testing

Laboratory experiments were conducted to create a prediction model to accurately convert measured changes in solution permittivity to changes in sediment suspension of varying concentrations. The experiments took place in the Ecological Engineering Laboratory in the Department of Biological Systems Engineering at Virginia Tech. The study evaluated possible interactions between SSC, specific conductance, and temperature.

The permittivity sensor was comprised of an electrode, power source, and a control box or frequency generator. To complete the study, a bench-scale suspension system was built to maintain a homogeneous suspension throughout the testing period. The suspended sediment sensor was calibrated with a static calibration procedure using known concentrations over the required sensor range. The prediction model was verified by randomly generating nine concentrations, measuring the permittivity of each suspension, and predicting the SSC with the transfer function. The results were compared to the known starting concentrations, and tested to see if the difference between the known concentration and the predicted concentration was significantly different than zero.

4.1 Bench-Scale Apparatus

4.1.1 Electrode design and manufacturing

The electrode consists of four, 22 gauge, stainless steel plates (fig. 4.1) constructed to make a parallel plate capacitor. The top of the electrode was fabricated from a small plastic container with casting resin as the insulating medium to ensure the wire contact points with the plates remained dry. The plates had a surface area of 59.78 cm^2 (fig. 4.2) with a 3-mm spacing between the plates to allow suspended sand grains to flow between the plates. The wiring of the plates (fig. 4.3) followed an alternating plate polarity pattern.

Figure 4.1. Permittivity electrode with plates made of 22 gauge, stainless steel with a plate spacing of 3 mm.

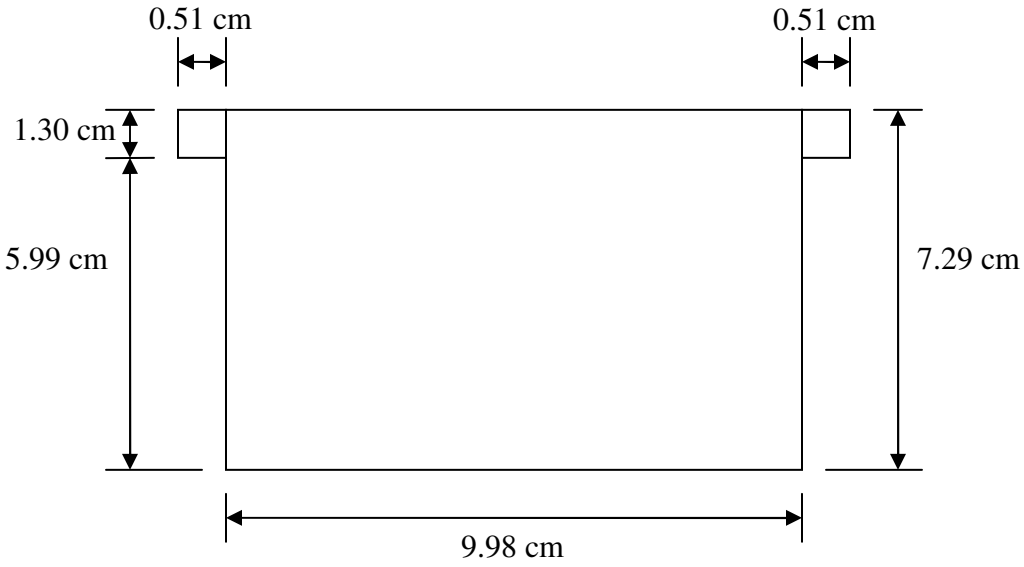

Figure 4.2. Dimensional drawing of a single stainless steel plate.

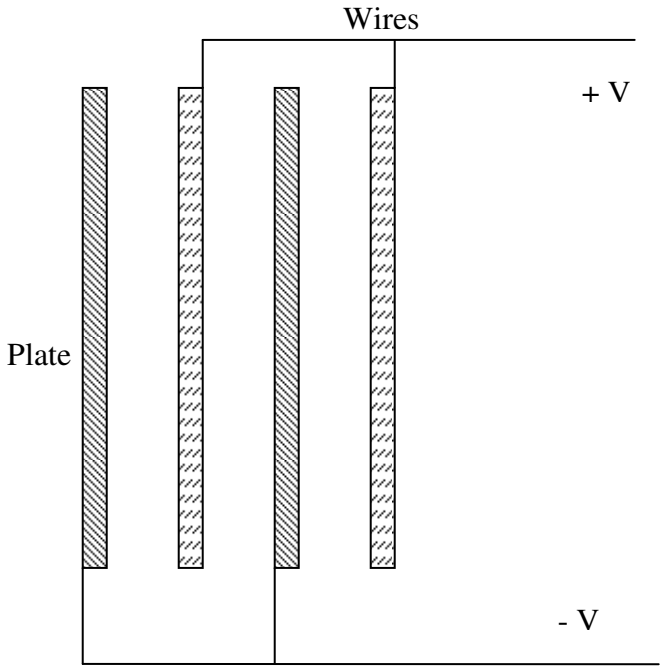

Figure 4.3. The electrode follows an alternating plate polarity pattern.

4.1.2 Kansas State Control Box and Power Source

The Biological and Agricultural Engineering (BAE) Department at Kansas State University (KSU) is developing a frequency response (FR) permittivity sensor for water quality and soil applications. For this study a control box (2005 version) from KSU was borrowed to serve as the frequency generator and microcontroller for the sediment electrode described above (fig. 4.4). The control box was designed, built, and tested by Dr. Naiqian Zhang and his graduate students with BAE at KSU. The control box used in this study generated 635 frequencies between 50 Hz and 120 MHz and monitored two output variables comparing the input voltage signal to the output signal at each frequency. The first output variable was the ratio of the input voltage magnitude to the output voltage measured in decibels (referred to as gain). The second variable was the difference in signal phase from the input signal to the output signal measured in degrees (referred to as phase). Detailed information regarding the control box is available in Tang (2009).

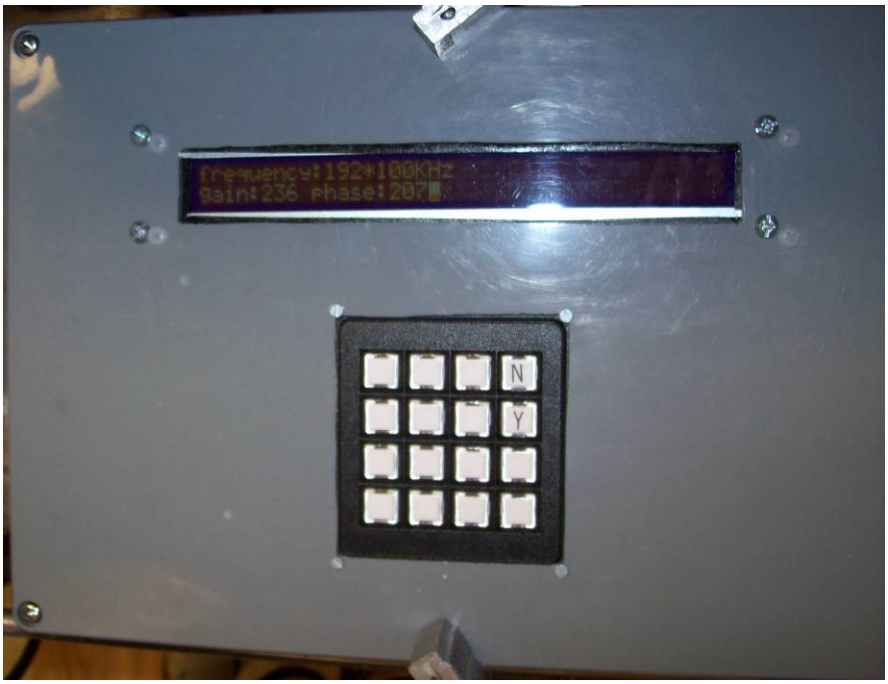

Figure 4.4. Permittivity control box from KSU BAE.

The power supply for the permittivity sensor was an Extech Instruments, 80 watt switching DC power supply (model 382260; Waltham, MA). The Extech power supply provided the required maximum voltage of 9 V and the maximum current of 4 amps.

4.2 Permittivity Data Collection and Analysis

4.2.1 Factorial Design

The study was conducted using 10.57-L solutions at three different conductivities (0, 250, 500 µS/cm), seven different sediment concentrations of kaolinite (0, 500, 1000-5000 mg/L), and three temperatures (10, 20, 30°C). Kaolinite is a 1:1 clay with a low surface charge and does not shrink or swell appreciably due to changes in moisture content. The kaolinite used in this study was from the Kaolin Company (Thiele B-80, Kaolin Filler Grade, CAS #1332-58-7) and contains crystalline silica (CAS #14808-60-7). Specific conductivity and temperature were monitored independently of the permittivity sensor. Temperature was monitored using a digital, traceable thermometer (Traceable Control Company, VWR model 61220416, Friendswood, Texas). Specific conductivity was monitored with a conductivity meter specifically calibrated for levels under 1990 µS/cm (EC Testr waterproof microcontroller series, model 296102). For each conductivity, temperature, and SSC combination the suspension was analyzed at 635 frequencies from 50 Hz to 120 MHz to test the response behavior over a range of frequencies.

The sample volume was analyzed by measuring gain and phase for each of the 635 frequencies. SSC was also measured for each SSC-treatment level using five, 28-mL aliquots removed from the sample volume to determine the exact SSC within the sensor measurement volume.

4.2.2 Data Collection

The KSU control box collected three full sets of data with each run. In this study six runs or 18 individual replicates of gain and phase data were collected per treatment level. An individual data set was collected in about 30 seconds. Data were automatically logged to a laptop computer using a hyper-terminal connection and a serial to USB cable. Gain and phase data were stored in a text file format with frequency indicators.

4.2.3 Data Post-processing

Once collected, the data were post-processed via a series of Excel macros. The gain and phase data were transformed from digital units to measurement units by equations 4.1 and 4.2 (dB; deg):

$$gain = \frac{digitaloutput}{30} \tag{4.1}$$

$$phase = \frac{digitaloutput}{10} \tag{4.2}$$

where digital output is the value provided by the control box for either gain or phase. The frequency indicator values were transformed to actual frequencies (Hz). The transformation equations are listed below:

$$freq = 50(f_i - 50) + 50 \tag{4.3}$$

$$freq = 10^{[0.15(f_i - 69)+13]} \tag{4.4}$$

$$freq = 200000(f_i - 89) + 1000000 \tag{4.5}$$

where *freq* is the calculated frequency (Hz), f_i is the frequency indicator value provided by the control box that ranges from 50 to 684. Equation 4.3 is a linear scale valid for frequency indicator values between 50 and 69. Equation 4.4 is a log scale for frequency indicator values between 70 and 89. Finally, equation 4.5 is a linear scale for frequency indicator values between 90 and 684.

The gain and phase data were then processed and transposed to the correct format for traditional regression and Partial Least Squares (PLS) regression analyses. Data processing for the traditional regression analysis required reducing the data to pre-identified target frequencies from the original 635 frequencies. The data were not averaged over the 18 replicates.

Data processing included collapsing the 18 replicates to three test data files by averaging six replicates of data into tests A, B, and C for the Partial Least Squares regression analysis. Data sets 1-6 were averaged to create test A, 7-12 were averaged to create test B, and 13-18 were averaged to create test C. The data set was also reduced to prevent model "over-fitting" by selecting gain and phase data for every fifth frequency instead of all 635 frequencies. The PLS regression analysis required explanatory (X) and predictor (Y) variables and the data had to be designated as training or validation data. Tests A, B, and C were designated as training data but gain and phase values for all three replicates (test A, B, and C) of seven treatment levels were removed and set aside for model validation. The seven levels set aside for validation were selected via a stratified, random sampling procedure. The sampling scheme was stratified because it was user determined that there would be one validation point per concentration level. The combination of temperature and conductivity treatments was randomly selected. Multiple combinations of explanatory variables were analyzed to find the best combination for the prediction of SSC (Y). The PLS analysis was conducted in SAS JMP version 8.0 (2008 SAS Institute Inc., Cary, NC)

4.2.4 Prediction Model Development

Traditional Regression Analysis

Specific frequencies were initially identified through graphical analysis of the gain and phase data over the 635 frequencies to be included in the initial regression analysis. During the graphical analysis, frequencies were selected where the output exhibited a relatively constant behavior of either gain or phase over multiple treatment levels (temperature, conductivity, or concentration). Ideally, monotonic behavior would have occurred, where a constant relationship

in the magnitude of either the gain or phase signal across sediment concentrations was present. Unfortunately, such behavior was not present in the sensor output. Typical responses of gain and phase output over changing input frequency are shown in section 4.3.2. A target frequency range was identified for the traditional regression analysis as 1-1000 kHz, due to the relatively constant response of gain and phase at these input frequencies.

Once a target frequency range was identified, linear regression models were systematically produced with different combinations of independent variables (concentration, conductivity, and temperature) explain the variance of either gain or phase. The same models were produced as fixed and mixed effect models. For fixed effect models, the gain and phase data were averaged over the 21 target frequencies, but not averaged over the replicates of the data. Mixed effect models included frequency as a random effect to explain the small amount of variance in the signal over the 21 frequencies. The strength of the mixed and fixed effect models were compared with Akaike's Information Criterion (AIC) and Bayesian Information Criterion (BIC), where the lowest metric identifies the strongest model (Wang and Liu, 2005).

Although strong correlation was found between the independent variables and both gain and phase data, model residuals did not meet the normality assumption required for prediction accuracy. The normality of the model residuals was tested with a Shapiro-Wilk test and analyzed graphically with a quantile-quantile plot. Log normal and power transformations on the gain and phase data were attempted. Unfortunately the distribution for both gain and phase data for many of the target frequencies was bi-modal.

Partial Least Squares (PLS) Regression Analysis

Partial Least Squares regression balances two priorities, explaining predictor variation (x-variable) and response variation (y-variable). PLS maximizes the variation explained by both predictor and response variables by generalizing and combining features from principle component analysis (PCA) and multiple regression (Abdi, 2003). It is most appropriate to use in cases where there are more x- variables than observations because it is not affected by multicollinearity in the ways that plague traditional regression techniques (SAS JMP help, 2009; Abdi, 2003). PLS originated in the social sciences but has also become very popular in chemometrics and sensory evaluation (Abdi, 2003).

PLS eliminates some of the predictor variables by creating principle components or latent variables. Latent variables are created from the predictor matrix (X) and used as regressors on

the response matrix (Y). The orthogonality of the latent variables eliminates the multicolinearity problem (Abdi, 2003). PLS regression differs from traditional PCA because it finds latent variables that simultaneously decompose X and Y with the constraint that these components explain as much as possible of the covariance between X and Y. PLS regression follows up the generalized PCA with a regression step where the latent variables of X are used to predict Y (Abdi, 2003).

The PLS regression for this project was conducted in SAS JMP version 8.0 PLS platform. For all models created, the X-matrix was composed of temperature, conductivity, and either gain and/or phase values for 127 frequencies. As described above, the number of frequencies included in the PLS analysis was reduced from 635 to 127 by including only every fifth frequency in the analysis. The data was reduced in this manner following similar PLS modeling work done by Sarah Schultz at Kansas State University. This was done to prevent model over-fitting. Also, as described above, the data were reduced from 18 replicates to three test data sets (A, B, and C). Tests A, B, and C for 56 of 63 treatment levels were used for training data, and seven treatment levels (one for each concentration) were used for validation data. The treatments removed for validation were chosen randomly through a stratified sampling protocol. Table 4.1 summarizes the treatment levels selected for validation.

Table 4.1. Treatment levels randomly selected for validation.

Concentration (mg/L)	Treatment #	Temperature level (°C)	Conductivity level (µS/cm)
0	2	10	250
500	17	30	250
1000	19	10	0
2000	33	20	500
3000	43	30	0
4000	49	20	0
5000	60	20	500

The X and Y matrices were also normalized based on A and B data sets for each model; means and standard deviations for each variable were calculated based on data sets A and B only. Individual data values were normalized by subtracting the mean for that variable and dividing by the standard deviation of the variable. The data were normalized to compare variable importance or significance. Normalizing all the data allows a “unit” change in one

variable to equal the "unit" change in another. As the phase data were an order of magnitude larger than the gain data, this was a necessary step.

Models were created for three scenarios where gain, phase, and gain and phase data at the 127 frequencies were entered in the X matrix. Two models were created for each scenario. The first model used a "leave one out" cross validation procedure to select the number of latent variables to be included in the model. The cross validation selection procedure tries to minimize the Root Mean Square Error (RMSE) independent of the amount of variation explained in Y. For the second model the number of latent variables was selected by the user. The selection was made by the comparing the RMSE and the cumulative percent variation in Y explained by that number of latent variables. The training and validation predictions for both models for the three scenarios were then compared graphically. The percent error between the treatment value and the predicted value was calculated.

The six models created during the first analysis were repeated with one significant difference: all data for 0 mg/L were removed from the analysis to determine the change in accuracy by removing the concentration with the highest prediction error.

4.2.5 Validation Data Collection and Analysis

Two types of validation procedures were completed on the prediction models. The first was briefly described above and was completed as part of the PLS analysis. The second validation procedure was completed on the three prediction models with the lowest overall validation error for concentrations between 433.8 and 5000 mg/L with an independent data set. The three containers and suspension system developed for the main study were used to collect the validation data. Nine treatment combinations of concentration, temperature, and conductivity were randomly selected and organized for the validation study. The range for each independent variable remained constant between model development and validation studies. Suspended sediment concentration, specific conductivity, and temperature ranged from 0-5000 mg/L, 0-500 µS/cm, and 10-30°C, respectively. Treatment levels are shown in table 4.2, while table 4.3 indicates the treatment levels assigned to a specific container. Nine sets of data were collected for each treatment. The number of replicates was lower between the prediction and validation data to maintain a more precise temperature in the system over the data collection period. For example, during the collection of 18 replicates at a specific treatment level for the prediction model, the solution temperature varied by 2-3°C, primarily due to heat input from the pump.

Since temperature was set in 10°C blocks during prediction model data collection, a variation of a few degrees was not considered significant To reduce measurement variance, temperature was maintained within a narrower range during validation; this required a reduction in sample number per treatment.

The validation data were post-processed following the procedure discussed earlier for PLS model development. Following post-processing, SSC levels were predicted using the top three models developed in Section 4.3.4. Prediction values for the nine treatment levels were calculated for each data set (A, B, and C) and then averaged for the final prediction value. Model validation was evaluated graphically.

Table 4.2. Nine treatment levels randomly generated for the validation study.

Concentration (mg/L)	Conductivity (μS/cm)	Temperature (deg C)
2000	230	25
3800	330	25
800	80	12
3200	230	27
100	220	15
3000	350	25
4800	420	27
2400	280	19
1500	130	18

Table 4.3. Treatment levels assigned to each container.

Container 1			Container 2			Container 3		
Conc.* (mg/L)	Cond (μS/cm)	Temp (deg C)	Conc. (mg/L)	Cond (μS/cm)	Temp (deg C)	Conc. (mg/L)	Cond (μS/cm)	Temp (deg C)
100	220	15	800	80	12	1500	130	18
2000	230	25	2400	280	19	3000	350	25
3200	230	27	3800	330	25	4800	420	27

*Conc. = Concentration

4.3 Results from Permittivity Sensor Testing

4.3.1 Quality Control for Suspension System

Once a collection technique was identified, five subsamples were collected to determine the actual concentration within the sample volume of the suspension system. Figure 4.5 shows the average results of five subsamples for each treatment concentration level. In general, greater than 90% of the treatment level was recovered in the subsamples for each concentration level

except the 500 mg/L treatment level (fig. 4.6). The sub-samples for each concentration were normally distributed based on Shapiro-Wilk test (α=0.05). Sample means for each concentration were significantly different than the treatment levels based on student t-test (α=0.05). Therefore the measured concentration was used for model development instead of the treatment level.

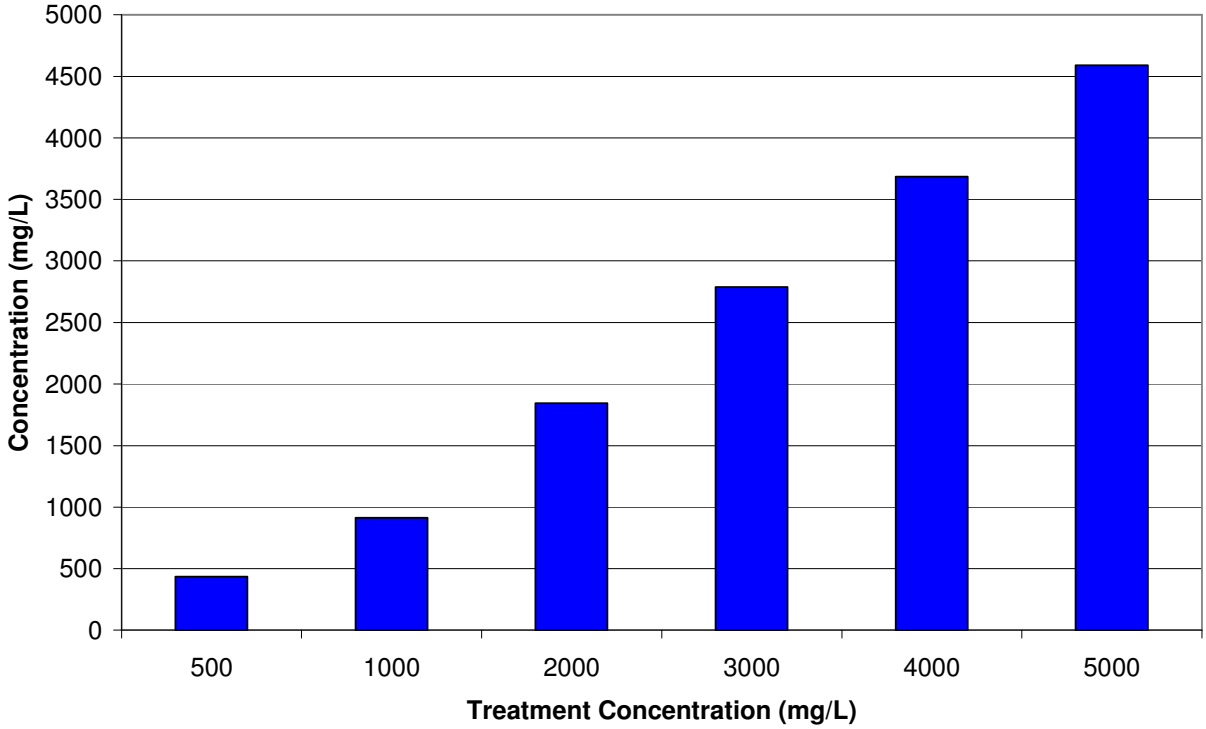

Figure 4.5. Average concentration collected from five grab samples at each treatment concentration (mg/L).

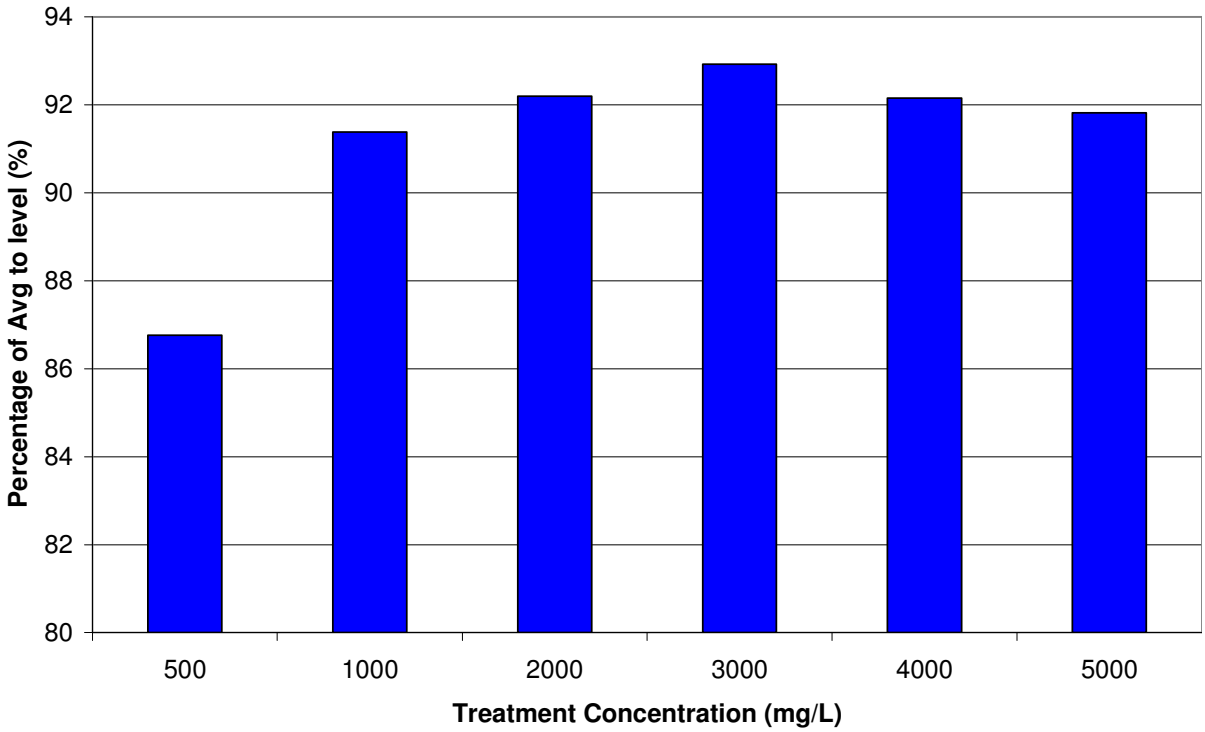

Figure 4.6. Percent of treatment concentration collected via 30-mL grab samples during the pilot study at the seven concentration levels. Five sub-samples were collected from each treatment concentration level.

4.3.2 Typical Data from Permittivity Sensor

The KSU BAE control box outputs gain and phase data for 635 frequencies. Permittivity is frequency-dependent; therefore, the gain and phase attributes of the sample volume varied with frequency. Figures 4.7 and 4.8 show the change in gain and phase as frequency increases. Both plots show the variation in gain or phase for three of the seven treatment concentrations under the same conductivity and temperature conditions.

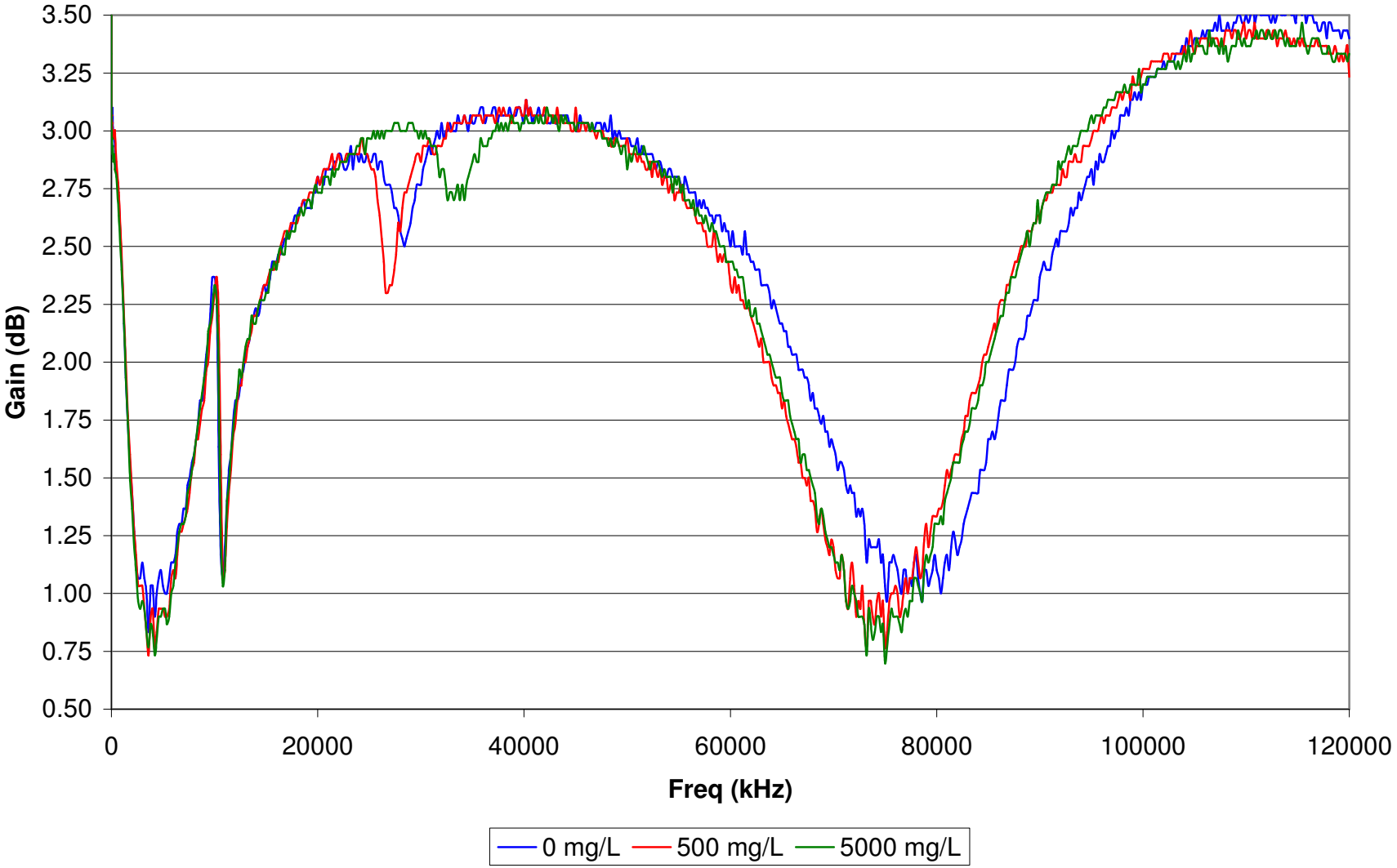

Figure 4.7. Example of typical gain (dB) data collected from the permittivity sensor. Gain data for 0, 500, and 5000 mg/L are shown for a specific combination of specific conductivity and temperature (0 µS/cm and 10°C).

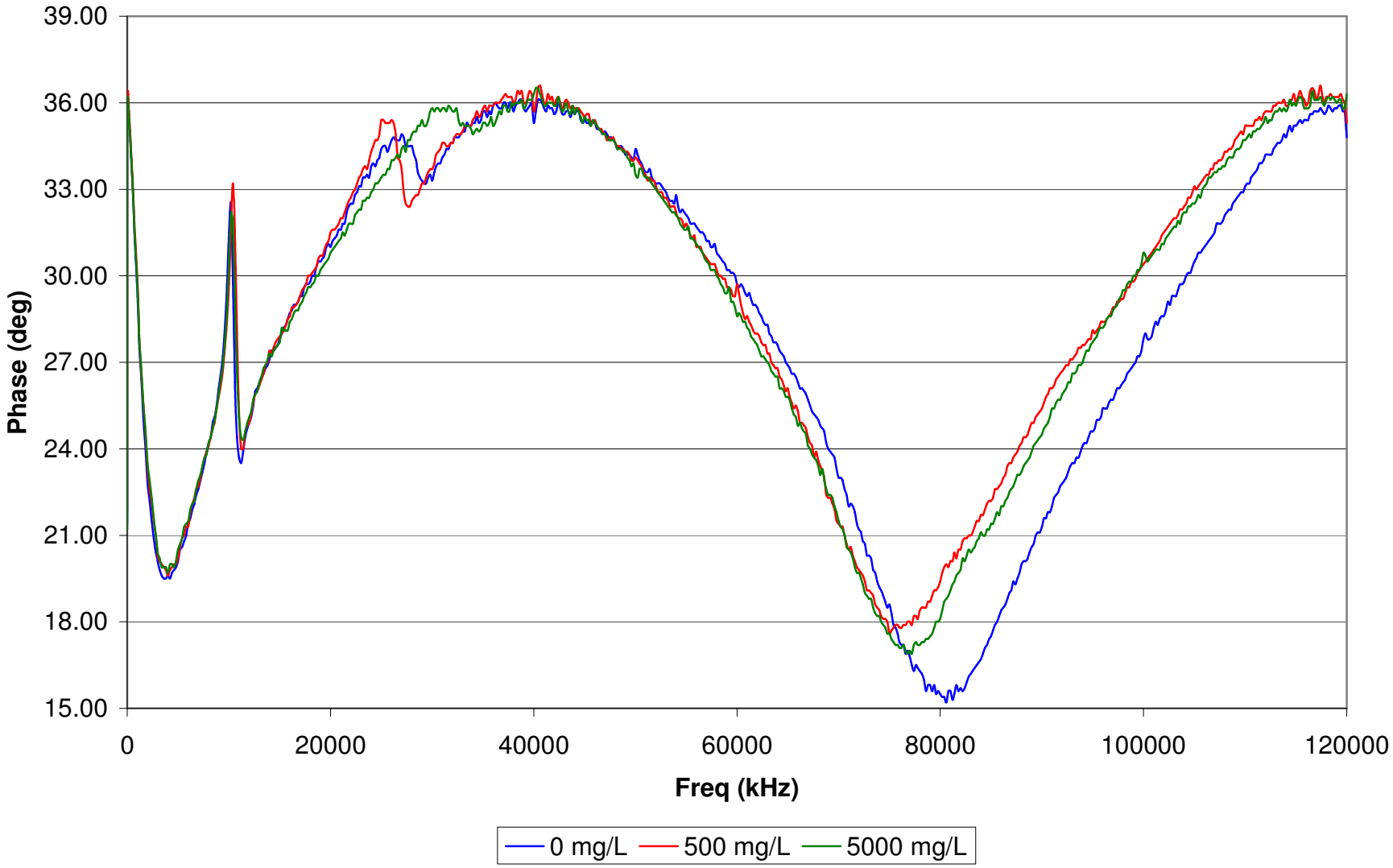

Figure 4.8. Example of typical phase (deg) data collected from the permittivity sensor. Phase data for 0, 500, 5000 mg/L is shown for a specific combination of specific conductivity and temperature (0 µS/cm and 10°C).

4.3.3 Traditional Regression Results

Frequencies included in a traditional regression analysis were initially identified through graphical analysis of the gain and phase data over the 635 frequencies. Figures 4.8-10 show trends in the data that were used to identify the frequency range (landscape version of plots are available in Appendix A.1 for gain and A.2 for phase). Frequencies of 1-1000 kHz were identified due to the lack of change of the gain or phase values over the target range. However the magnitude of the signal over that range varied by treatment level. For example the magnitude of the signal is higher over the target range under the 0 µS/cm condition than the higher conductivity levels. Compared to the following three figures (4.8-4.10) the magnitude of the gain reading was significantly reduced over the frequency range of 1-1000 kHz, as the conductivity increased from 0 to 250 µS/cm and then reduced slightly as conductivity increased to 500 µS/cm.

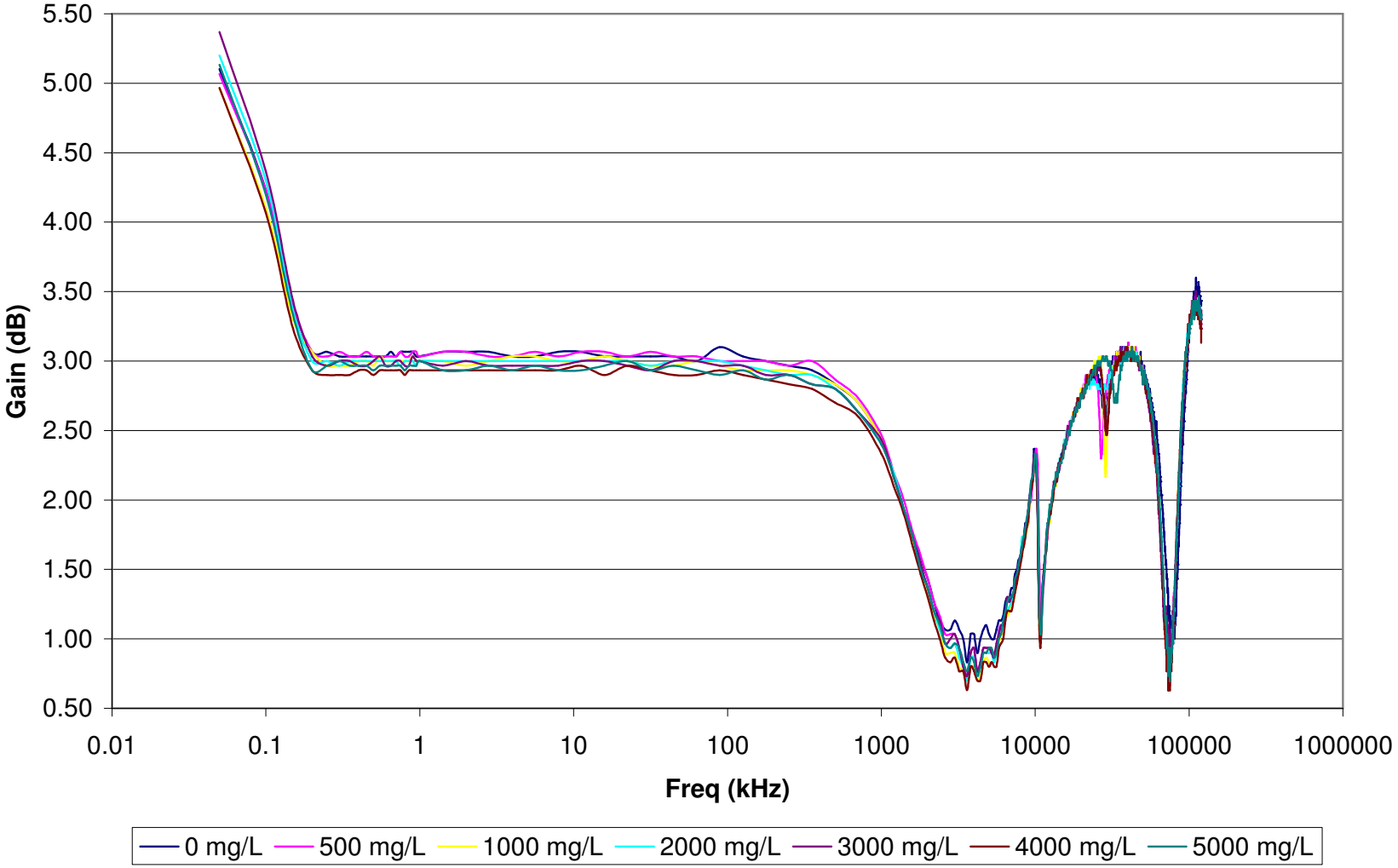

Figure 4.8. Gain data as shown above in figure 4.7 with a log scale on the x-axis. Gain data for the seven treatment concentrations are shown for a specific combination of specific conductivity and temperature (0 µS/cm and 10°C).

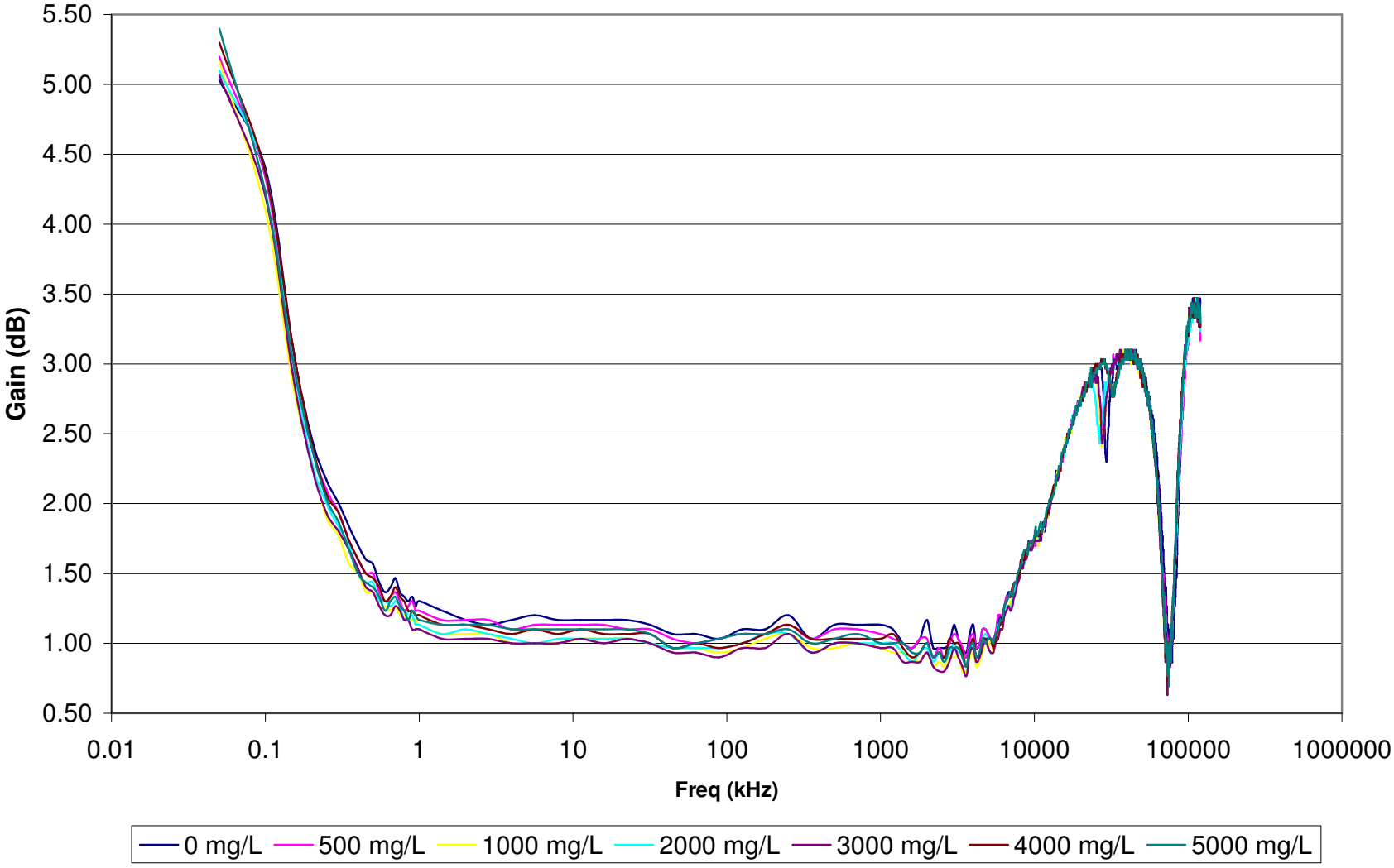

Figure 4.9. Gain data for the seven treatment concentrations are shown for a specific combination of specific conductivity and temperature (250 µS/cm and 10°C).

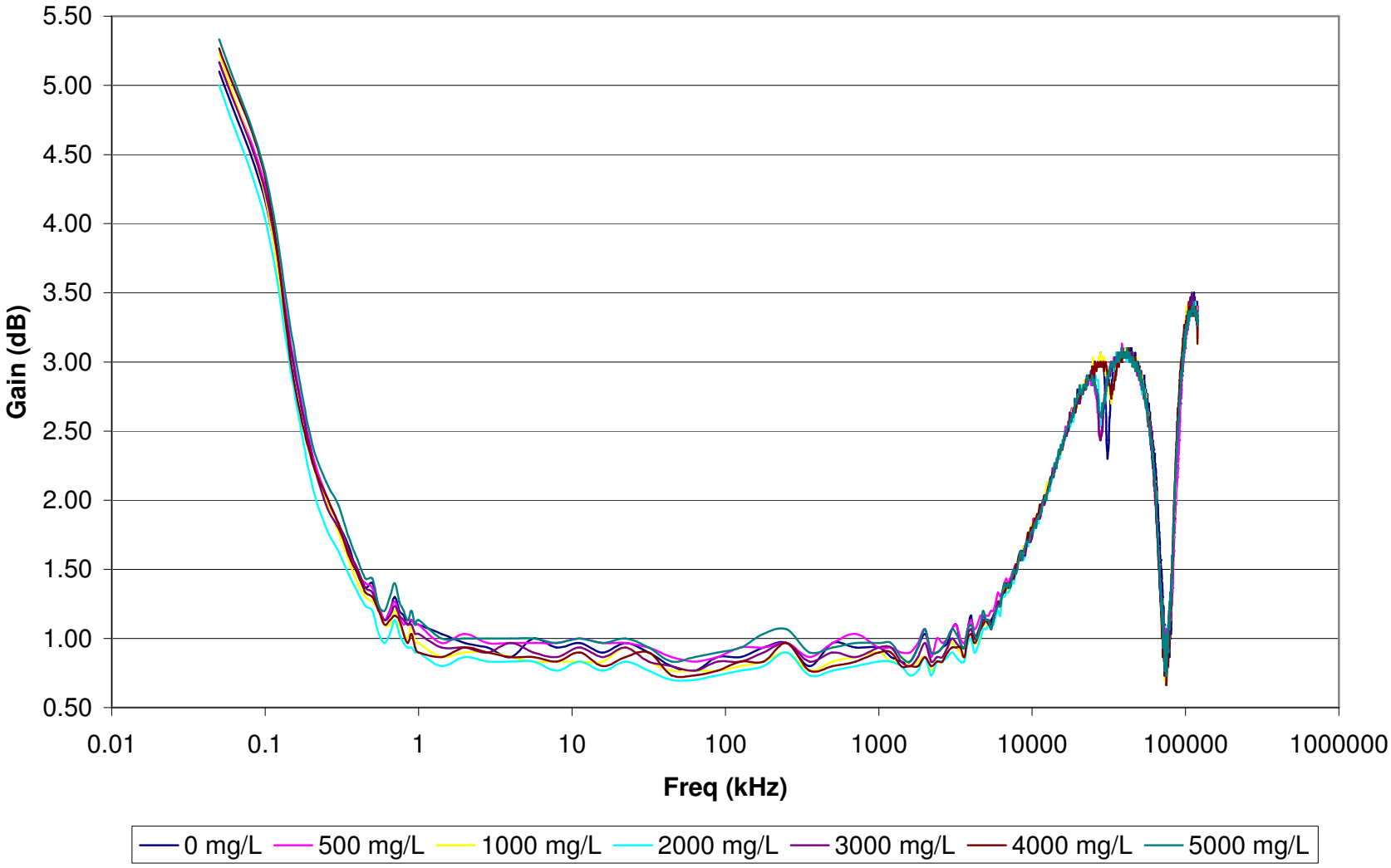

Figure 4.10. Gain data for the seven treatment concentrations are shown for a specific combination of specific conductivity and temperature (500 µS/cm and 10°C).

After isolating the target frequencies of 1-1000 kHz, fixed and mixed effect, multiple, linear regression models were developed. Gain and phase were used as dependent variables. The independent variables were various combinations of concentration, conductivity, and temperature. Frequency was included as a random effect within the mixed effect models. During the analysis over 30 mixed and fixed effects models were tested. However, the residuals were not normally distributed even with power law or logarithmic transformations of the gain and phase data. With further investigation it was evident that multiple of the individual frequencies within the target frequency range had bimodal distributions, making normality impossible to achieve using transformations. Although normality is not necessary to develop a basic linear relationship between dependent and independent variables, it is required to test hypotheses and estimate confidence and/or prediction intervals (Helsel and Hirsch, 1992). Non-parametric methods were also investigated; however, a normal distribution of the residuals is required for most common non-parametric algorithms as well. Therefore PLS regression was conducted and is described in the next section.

4.3.4 Partial Least Squares Regression Results

Twelve PLS regression models were developed, four for each set of input variables. Half of the models had the 0 mg/L treatments removed from the analysis because 0 mg/L had the highest error. Each model was based on three sets of training data. Seven treatment levels (conductivity, temperature, and concentration combination) were excluded from the training data and were used as validation data. The following plots show the average predicted value for both training and validation data sets at each level of concentration. In general, 500 mg/L and 5000 mg/L were the most difficult levels to predict both with training and validation data when 0 mg/L was included in the analysis. A best-fit linear trend line was also included on the plot based on the training data. The black line represents a perfect prediction at all concentration levels. For all models the X and Y matrices were scaled and centered. The first two models for each input category used a cross validation procedure to determine the number of latent variable to include in the model, while for the third and fourth models the number of latent variables was specified by the user. A summary of the twelve PLS models is available in table 4.3.

Table 4.4. Summary of input variables, number of latent variables, and percent variation in Y explained for the 12 PLS regression models.

Model Name	Input variables	Cross Validation	# of Latent Variables	% of Y variation explained
Model 1A	gain	yes	8	83.33
Model 1B	gain	yes	6	78.48
Model 2A	gain	no	15	90.83
Model 2B	gain	no	15	93.39
Model 3A	phase	yes	3	49.29
Model 3B	phase	yes	8	77.23
Model 4A	phase	no	15	86.43
Model 4B	phase	no	15	88.48
Model 5A	gain and phase	yes	10	87.36
Model 5B	gain and phase	yes	5	76.24
Model 6A	gain and phase	no	15	92.65
Model 6B	gain and phase	no	15	95.99

Model 1A with gain as an input variable used eight latent variables. Three sets of training data (blue diamonds) and one set of validation data (red triangles) were included in the model development. The training data had an R^2 value of 0.9405 (fig. 4.11). Model 2 used 15 latent variables. The blue line shows the "best fit" line for model 2 based on the training data set and had an R^2 of 0.9814 (fig. 4.12). The amount of error between the predicted and actual values for both the training and validation data sets was calculated for models 1 and 2 (fig. 4.13). Model 2A was orders of magnitude more accurate at predicting 0 mg/L. Models 1A and 2A had similar accuracy for predicting the other six concentration levels.

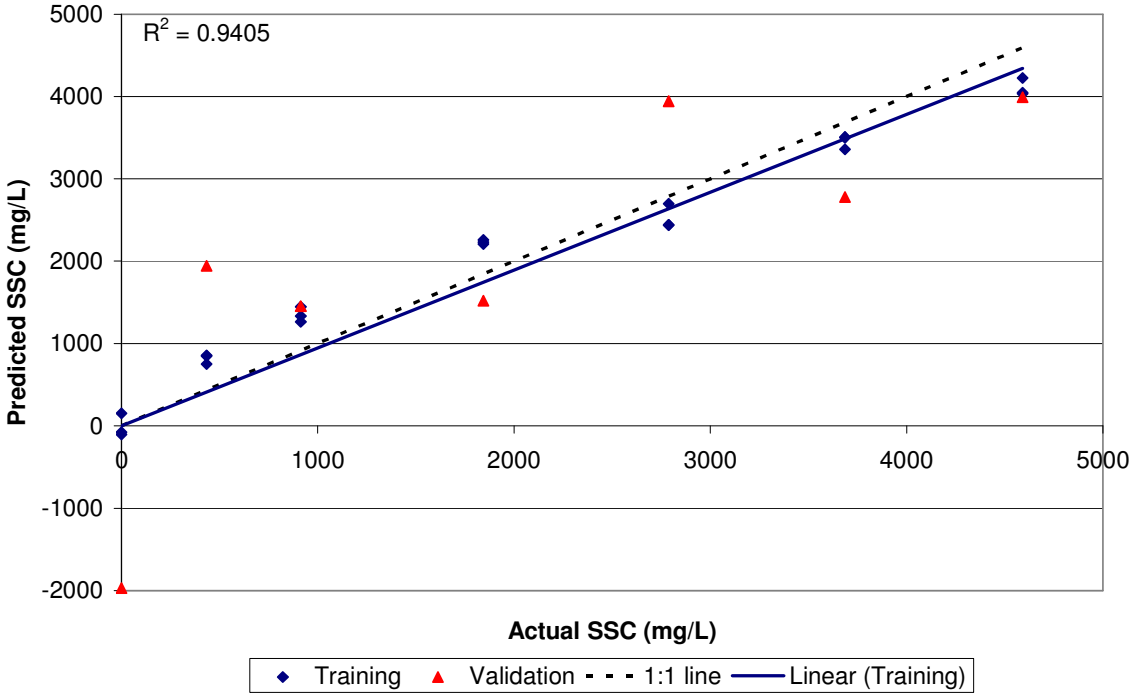

Figure 4.11. PLS model 1A generated with conductivity and temperature data combined with gain data for 127 frequencies. The blue line shows the "best fit" line for model 1A based on the training data set and has an R^2 of 0.9405.

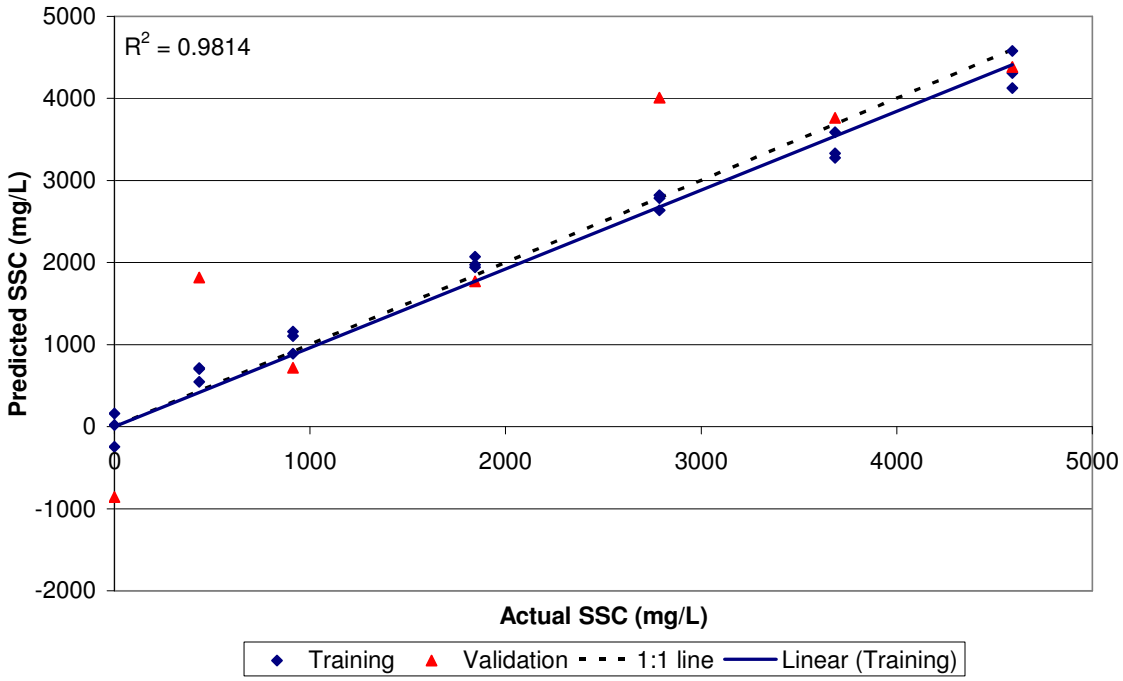

Figure 4.12. PLS model 2A generated with conductivity and temperature data combined with gain data for 127 frequencies. The blue line shows the "best fit" line for model 2 based on the training data set and has an R^2 of 0.9814.

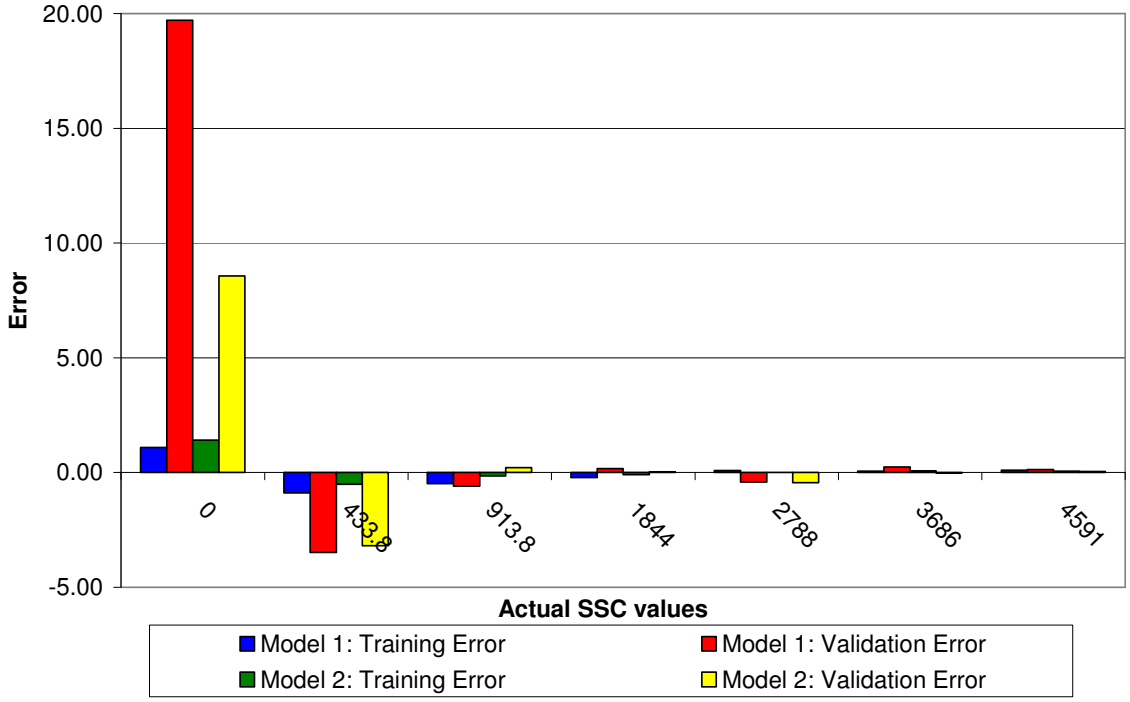

Figure 4.13. Comparison of error between the predicted and expected values of concentration for models 1A and 2A generated with gain data.

Model 3A with phase as an input variable used three latent variables. The training data had an R^2 value of 0.2483 (fig. 4.14). Model 4A used 15 latent variables and had an R^2 of 0.9604 (fig. 4.15). The blue line shows the "best fit" line for model 3A and 4A based on the training data set. The amount of error between the predicted and actual values for both the training and validation data sets was calculated for models 3A and 4A (fig. 4.16). Model 4A was at least an order of magnitude more accurate at predicting the actual SSC value when the treatment level was near 0 mg/L. However at the higher concentration levels model 3A had lower validation errors.

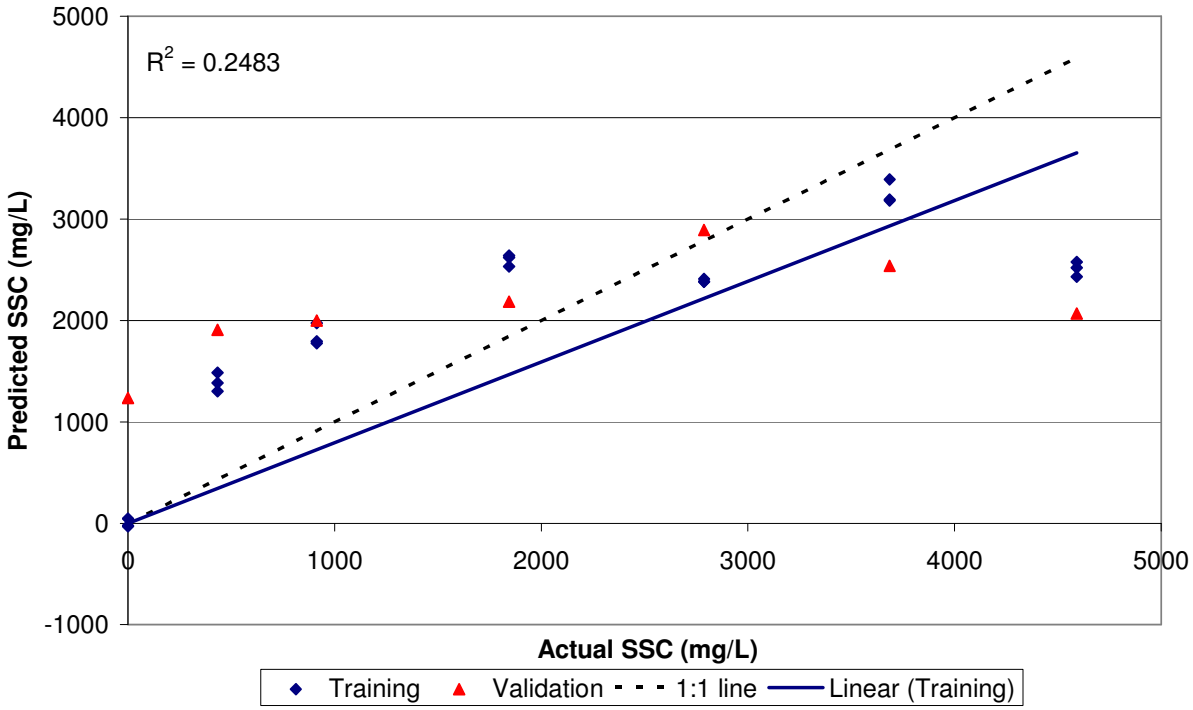

Figure 4.14. PLS model 3A generated with conductivity and temperature data combined with phase data for 127 frequencies. Model 3A used three latent variables. The blue line shows the "best fit" line for model 3A based on the training data set and has an R^2 of 0.2483.

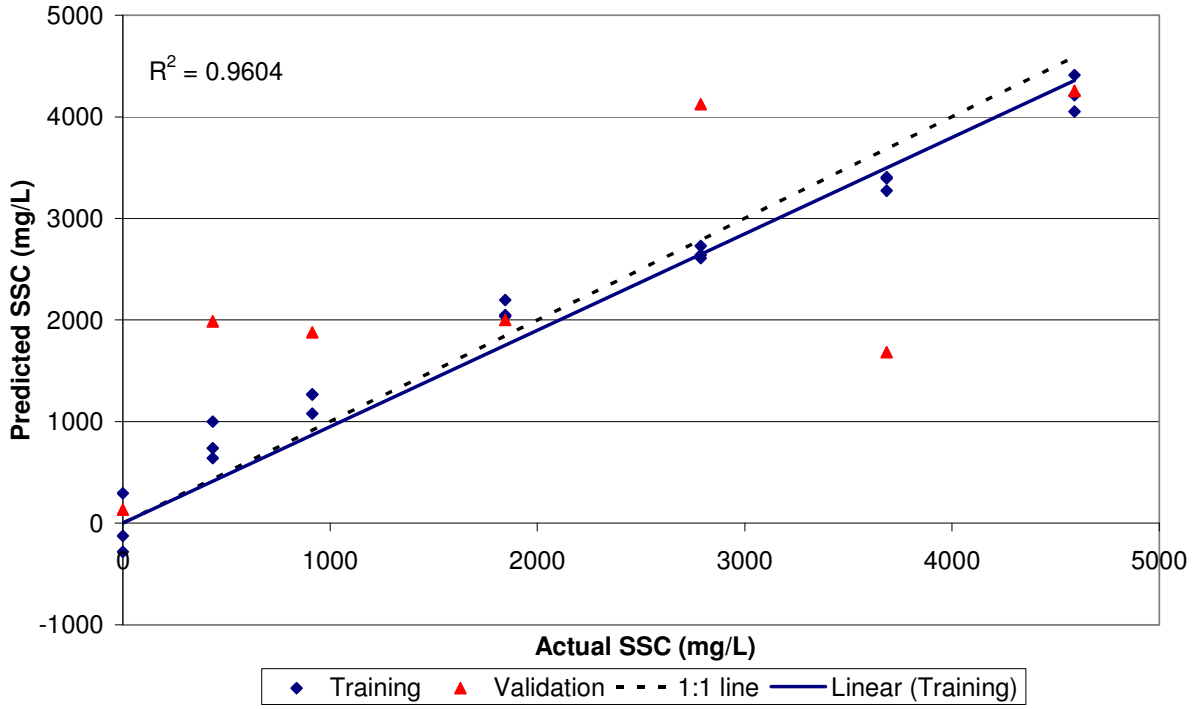

Figure 4.15. PLS model 4A generated with conductivity and temperature data combined with phase data for 127 frequencies. Model 4A used 15 latent variables. The blue line shows the "best fit" line for model 4A based on the training data set and has an R^2 of 0.9604.

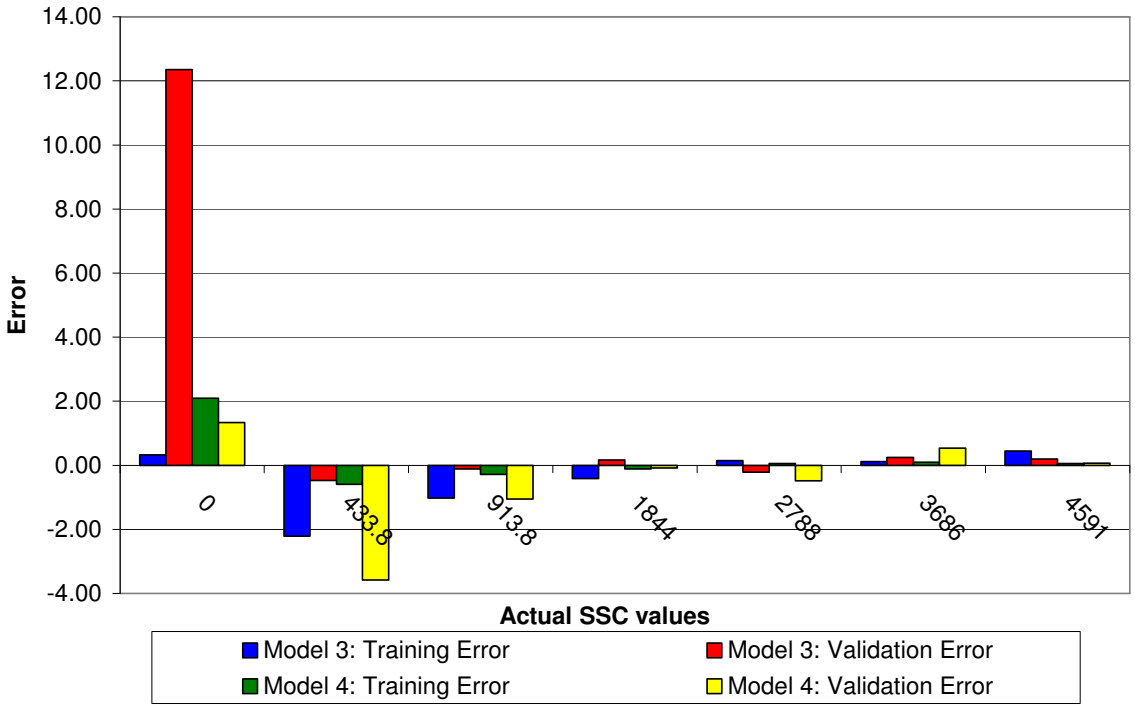

Figure 4.16. Comparison of error between the predicted and expected values of concentration for models 3A and 4A generated with phase data.

Model 5A with gain and phase as input variables used ten latent variables. The training data had an R^2 value of 0.968 (fig. 4.17). Model 6A used 15 latent variables, and the training data had an R^2 of 0.9865 (fig. 4.18). The amount of error between the predicted and actual values for both the training and validation data sets was calculated for models 5A and 6A (fig. 4.19). Model 6A was more accurate at predicting the actual SSC value for all concentration levels except 2787.6 mg/L.

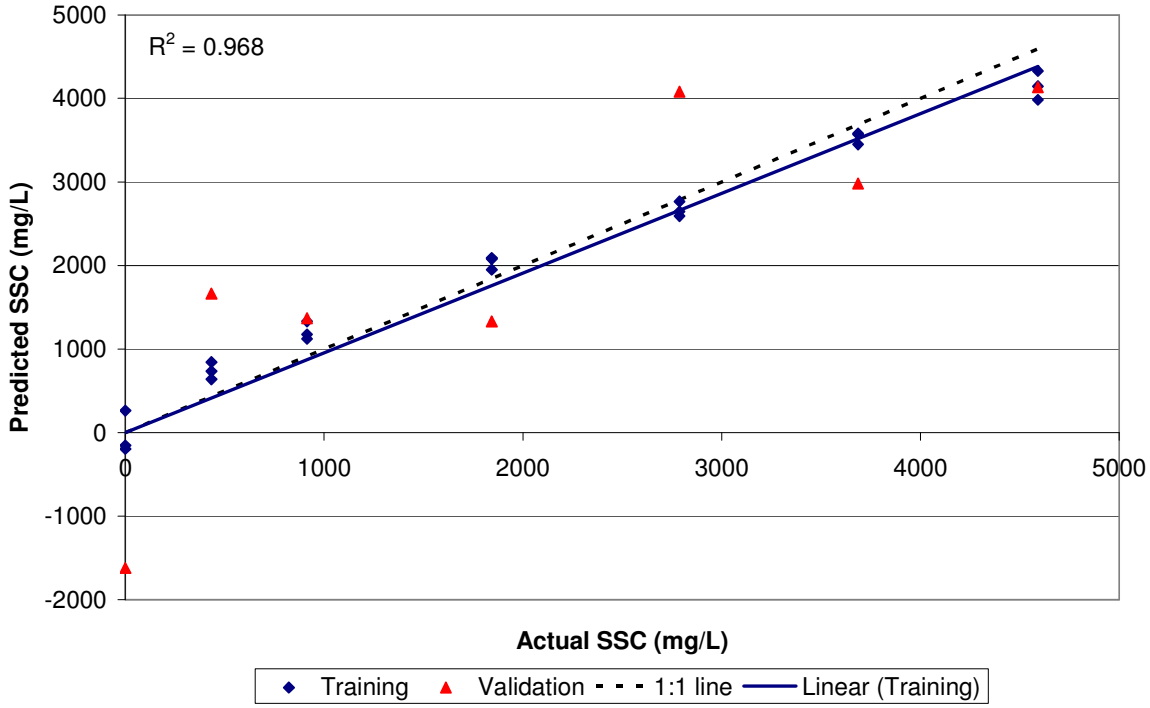

Figure 4.17. PLS model 5A generated with conductivity and temperature data combined with gain and phase data for 127 frequencies. Model 5A used ten latent variables. The blue line shows the "best fit" line for model 5A based on the training data set and has an R^2 of 0.968.

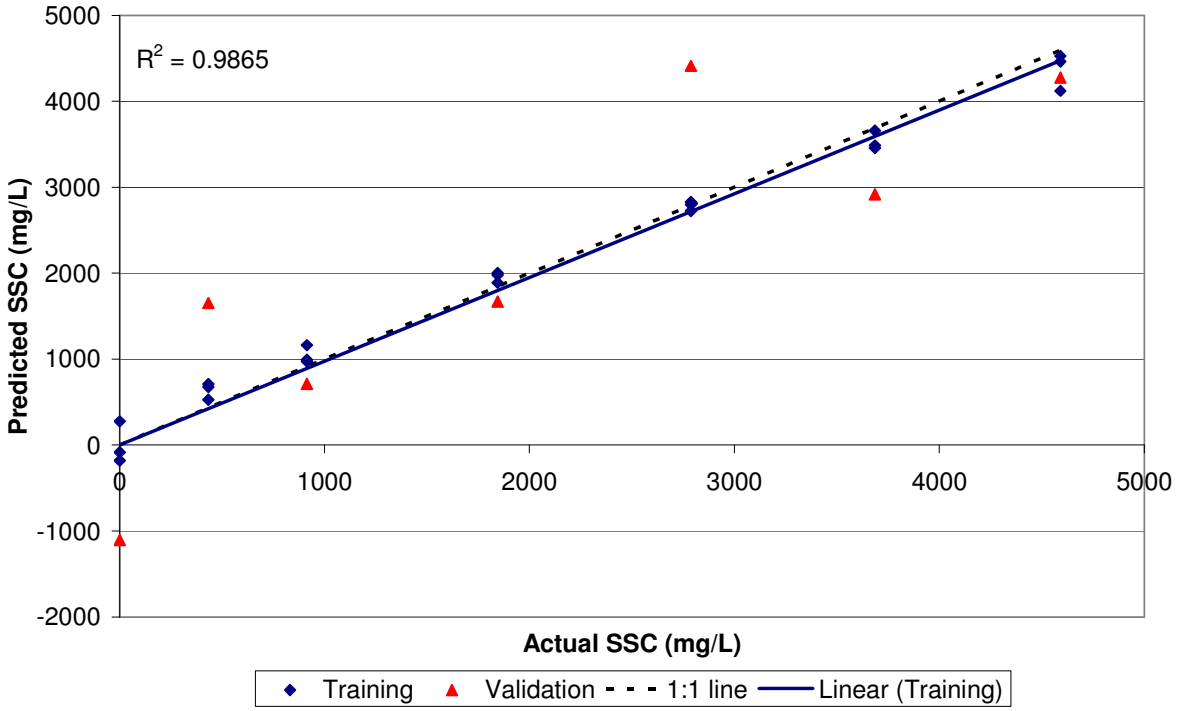

Figure 4.18. PLS model 6A generated with conductivity and temperature data combined with gain data for 127 frequencies. Model 6A used 15 latent variables. The blue line shows the "best fit" line for model 6A based on the training data set and has an R^2 of 0.9865.

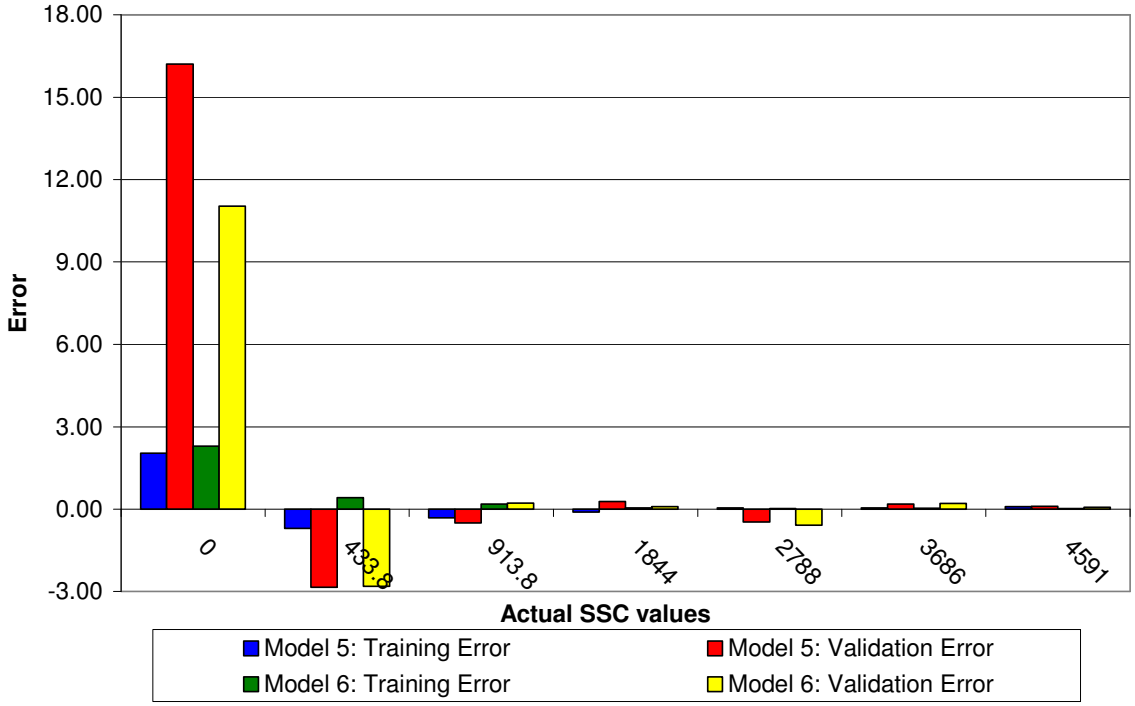

Figure 4.19. Comparison of error between the predicted and expected values of concentration for models 5A and 6A generated with gain and phase data. Both models developed with gain and phase values as explanatory variables have similar error over the treatment concentrations.

The following six PLS models only predict six of the original seven concentration treatment levels. The 0 mg/L treatment level was removed to see if over all model accuracy increased or the error decreased for the both training and validation data sets. Model 1B with gain as an input variable used six latent variables. Three sets of training data (blue diamonds) and one set of validation data (red triangles) were included in the model development. The training data had an R^2 value of 0.9689 (fig. 4.20). Model 2B used 15 latent variables. The blue line shows the "best fit" line for model 2B based on the training data set and had an R^2 of 0.9929 (fig. 4.21). The amount of error between the predicted and actual values for both the training and validation data sets was calculated for models 1B and 2B (fig. 4.13). Models 1B and 2B had similar accuracy for predicting all six concentration levels.

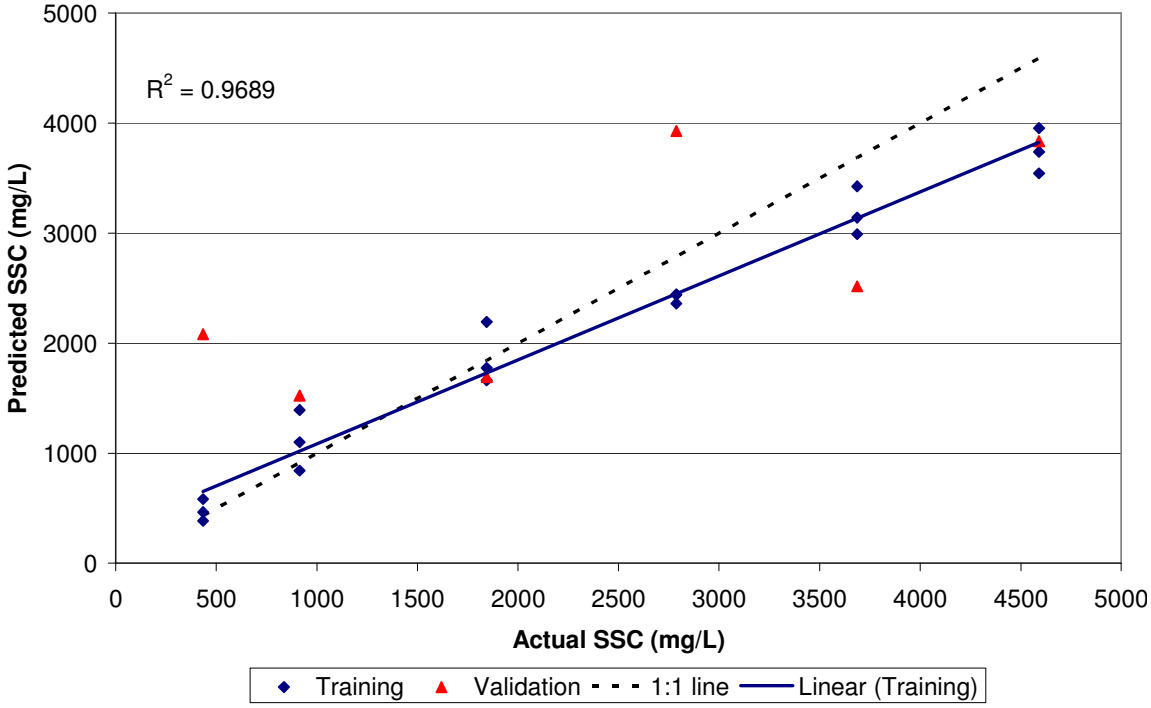

Figure 4.20. PLS model 1B generated with conductivity and temperature data combined with gain data for 127 frequencies but all data with a concentration level of 0 mg/L was removed from the analysis. The blue line shows the "best fit" line for model 1B based on the training data set and has an R^2 of 0.9689.

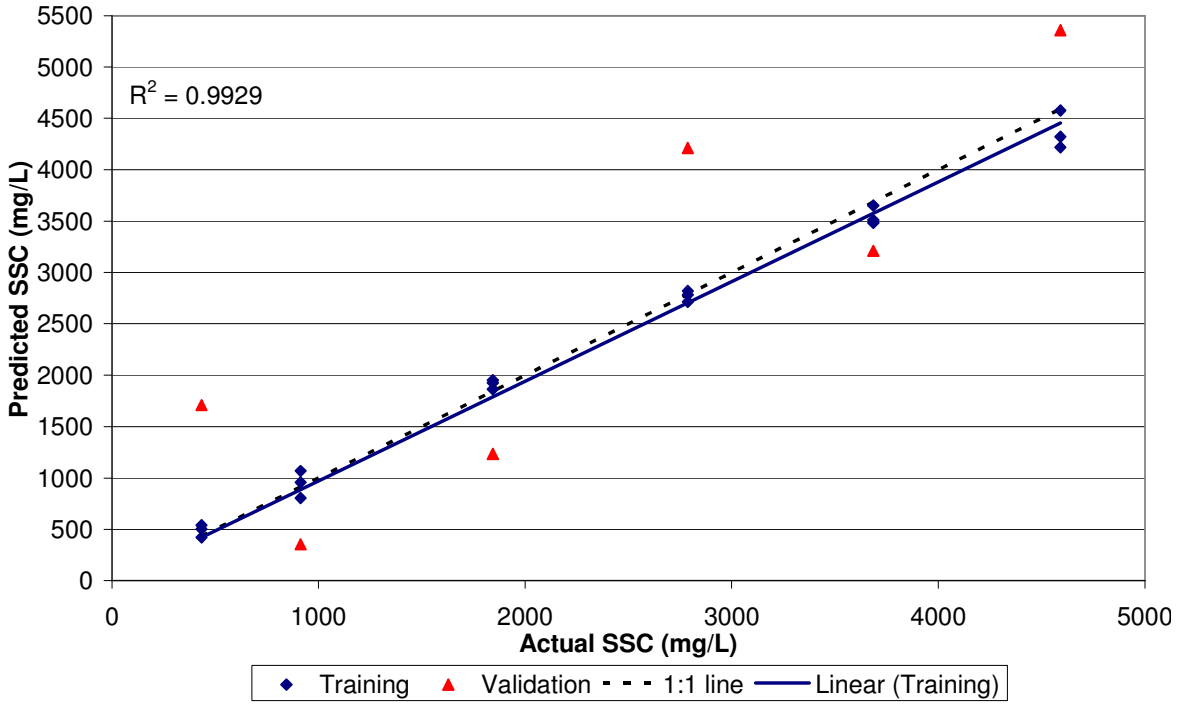

Figure 4.21. PLS model 2B generated with conductivity and temperature data combined with gain data for 127 frequencies but all data with a concentration level of 0 mg/L was removed from the analysis. The blue line shows the "best fit" line for model 2B based on the training data set and has an R^2 of 0.9929.

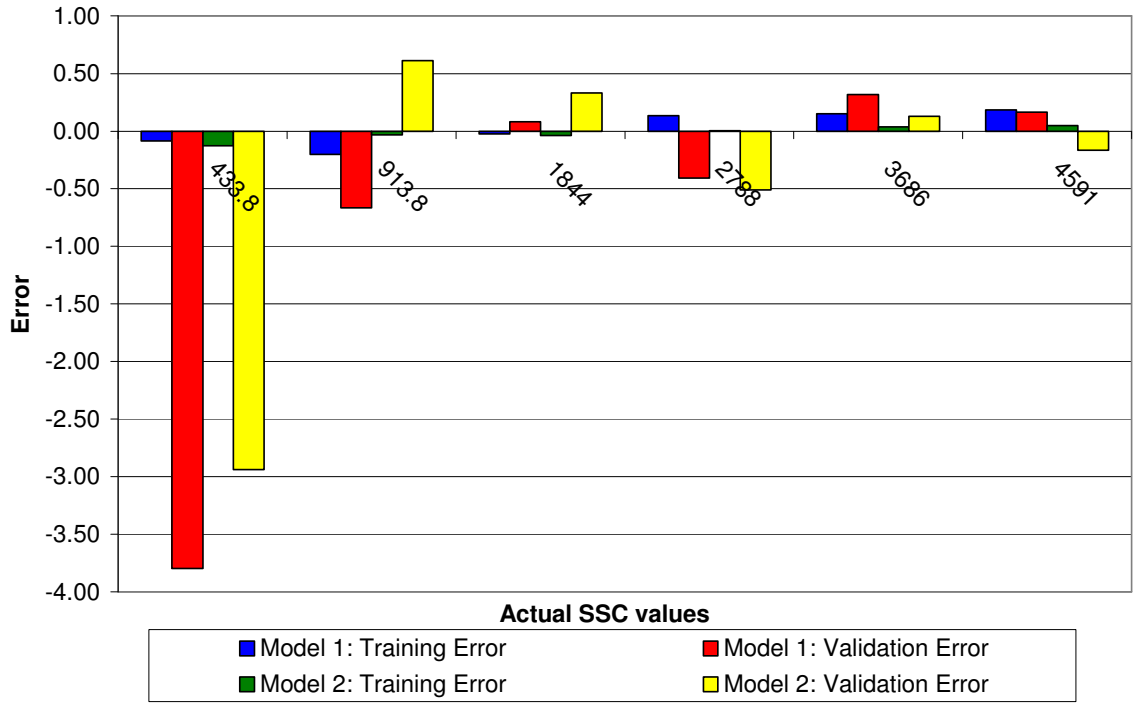

Figure 4.22. Comparison of error between the predicted and expected values of concentration for models 1B and 2B generated with gain data.

Model 3B with phase as an input variable used eight latent variables. The training data had an R^2 value of 0.9401 (fig. 4.23). Model 4B used 15 latent variables and had an R^2 of 0.9745 (fig. 4.24). The blue line shows the "best fit" line for model 3B and 4B based on the training data set. The amount of error between the predicted and actual values for both the training and validation data sets was calculated for models 3B and 4B (fig. 4.15). Model 4B was almost two times more accurate at predicting the actual SSC value when the treatment level was near 500 mg/L. However at the higher concentration levels models 3B and 4B had similar validation errors.

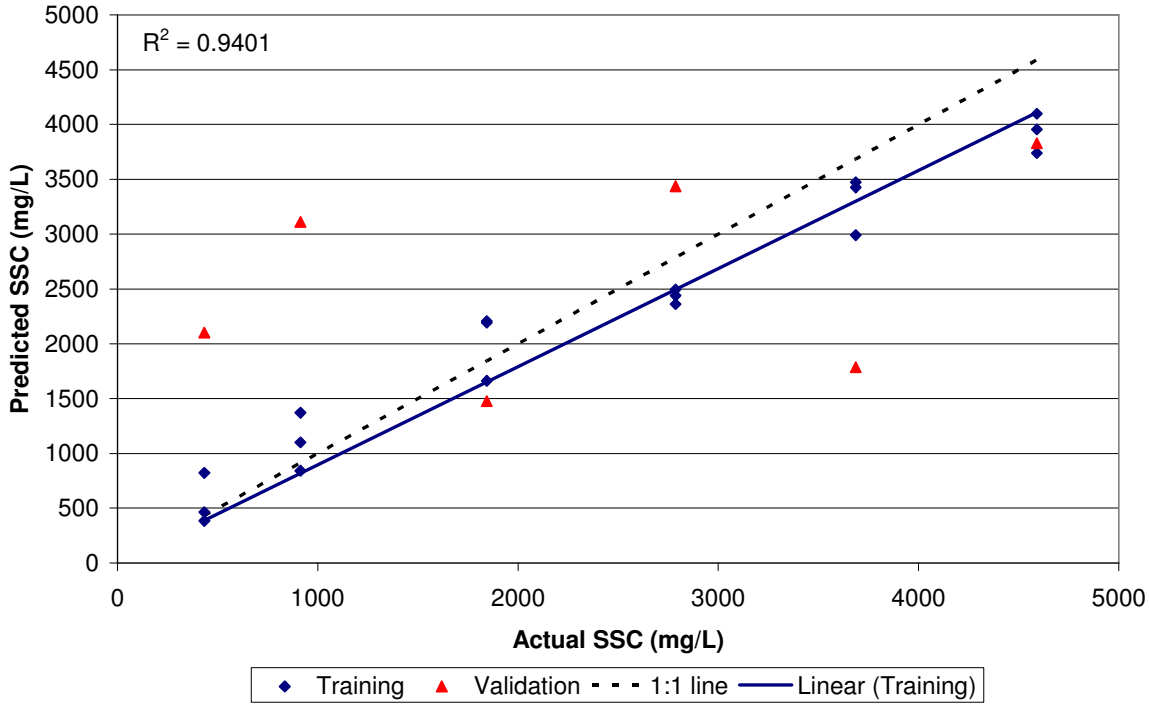

Figure 4.23. PLS model 3B generated with conductivity and temperature data combined with phase data for 127 frequencies. Model 3B used eight latent variables. The blue line shows the "best fit" line for model 3B based on the training data set and has an R^2 of 0.9401.

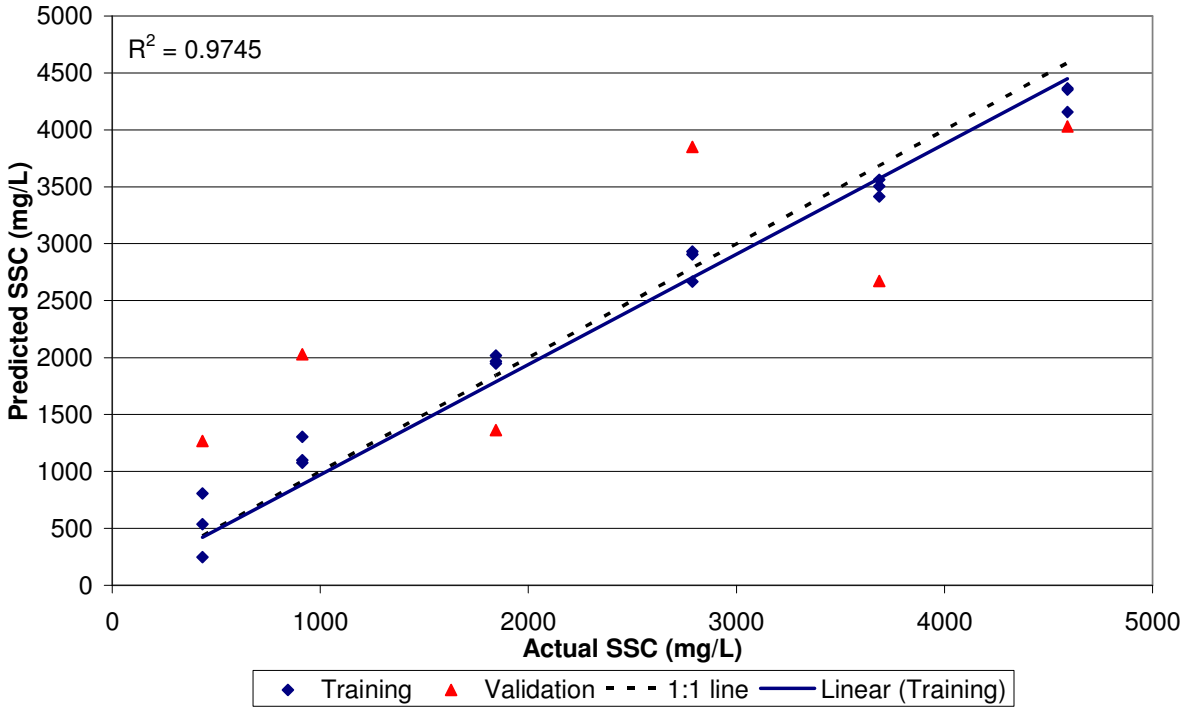

Figure 4.24. PLS model 4B generated with conductivity and temperature data combined with phase data for 127 frequencies. Model 4B used 15 latent variables. The blue line shows the "best fit" line for model 4B based on the training data set and has an R^2 of 0.9745.

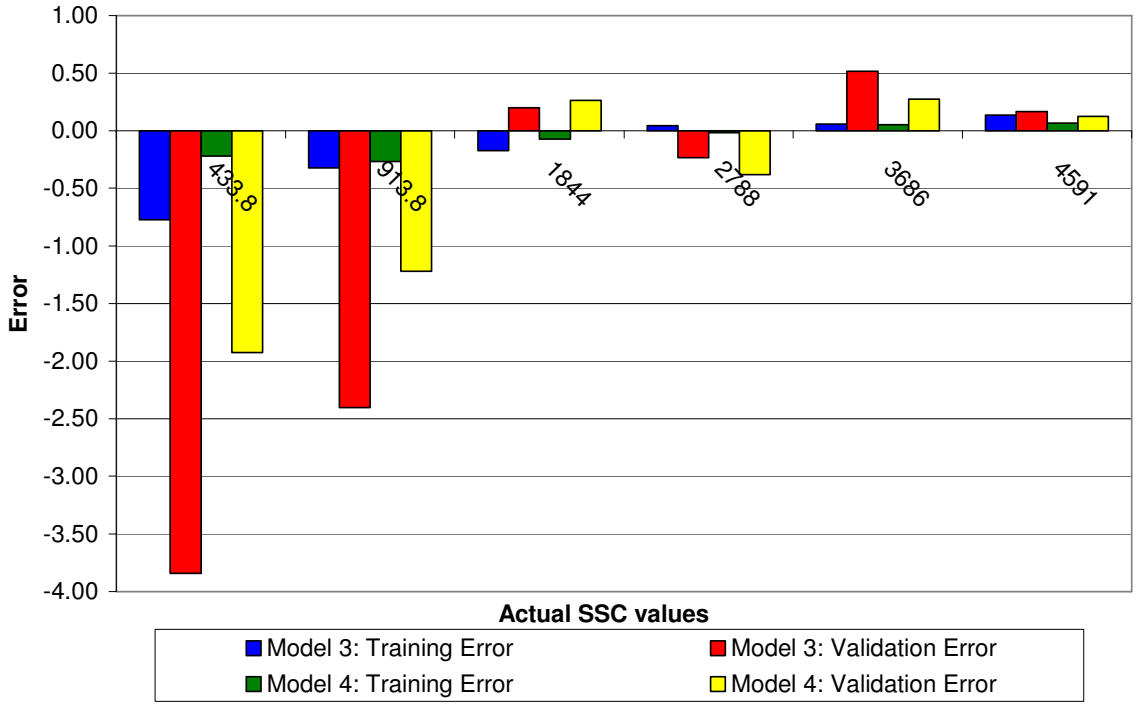

Figure 4.25. Comparison of error between the predicted and expected values of concentration for models 3B and 4B generated with phase data.

Model 5B with gain and phase as input variables used five latent variables. The training data had an R^2 value of 0.9224 (fig. 4.26). Model 6B used 15 latent variables, and the training data had an R^2 of 0.9943 (fig. 4.27). The amount of error between the predicted and actual values for both the training and validation data sets was calculated for models 5B and 6B (fig. 4.28). Model 6B was more accurate at predicting the actual SSC value for all concentration levels except 1844 and 2787.6 mg/L.

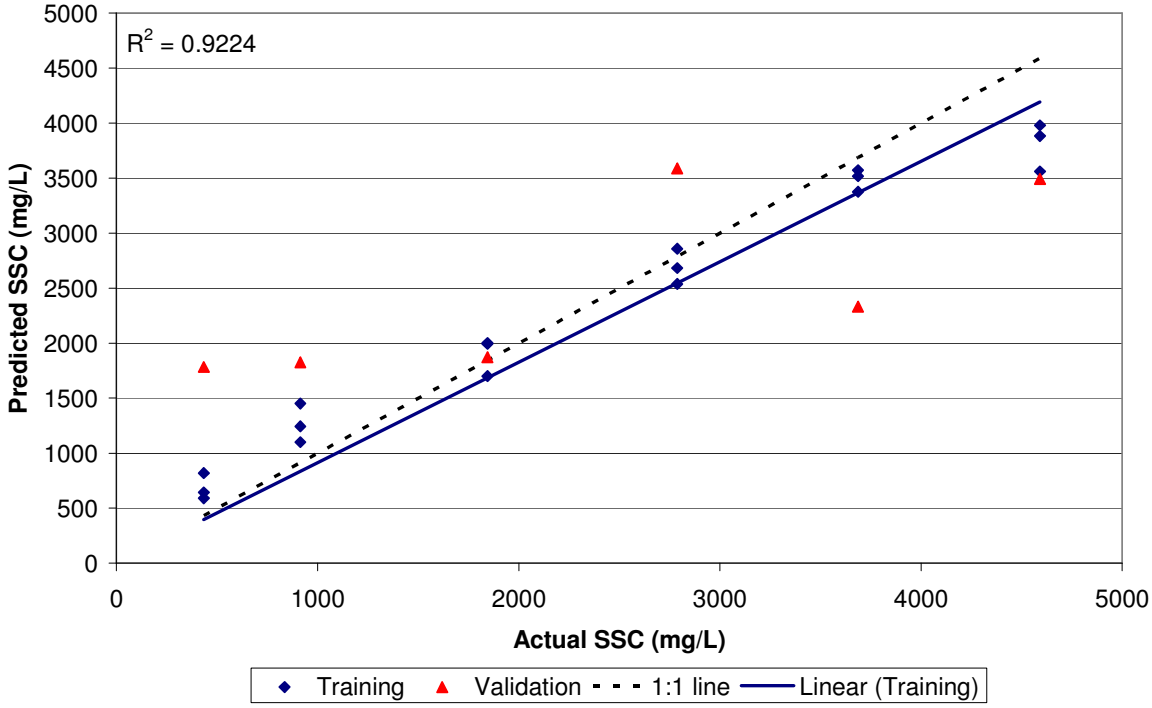

Figure 4.26. PLS model 5B generated with conductivity and temperature data combined with gain and phase data for 127 frequencies. Model 5B used five latent variables. The blue line shows the "best fit" line for model 5B based on the training data set and has an R^2 of 0.9224.

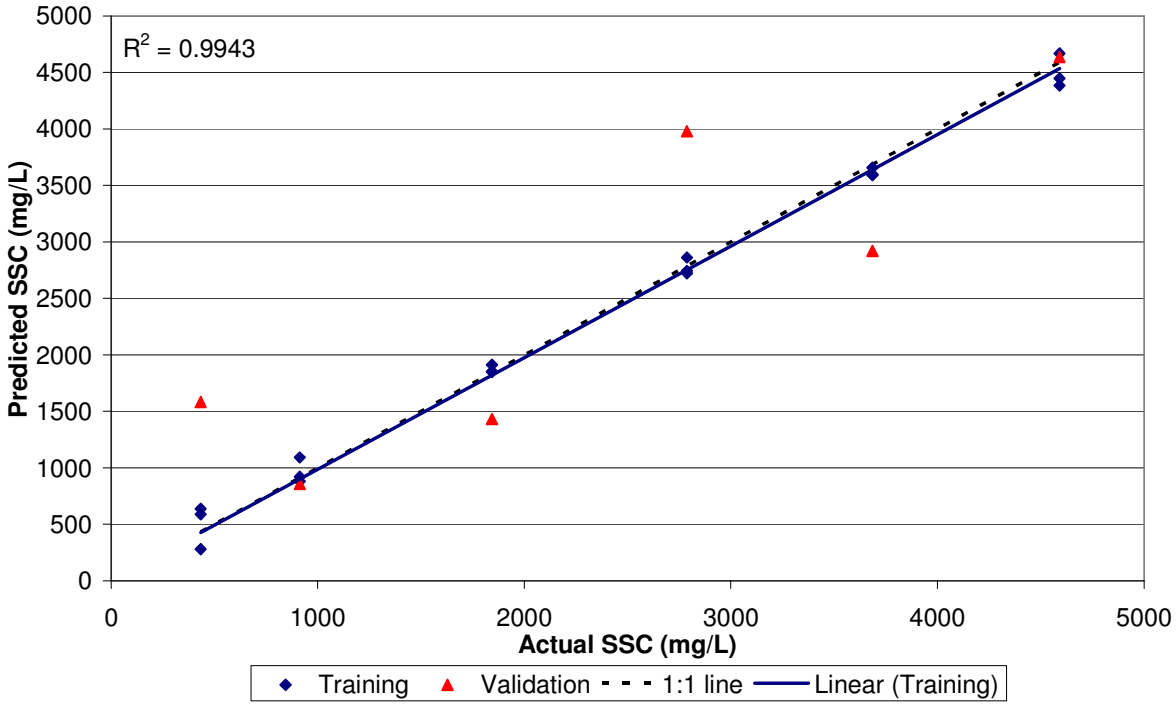

Figure 4.27. PLS model 6B generated with conductivity and temperature data combined with gain data for 127 frequencies. Model 6B used 15 latent variables. The blue line shows the "best fit" line for model 6B based on the training data set and has an R^2 of 0.9943.

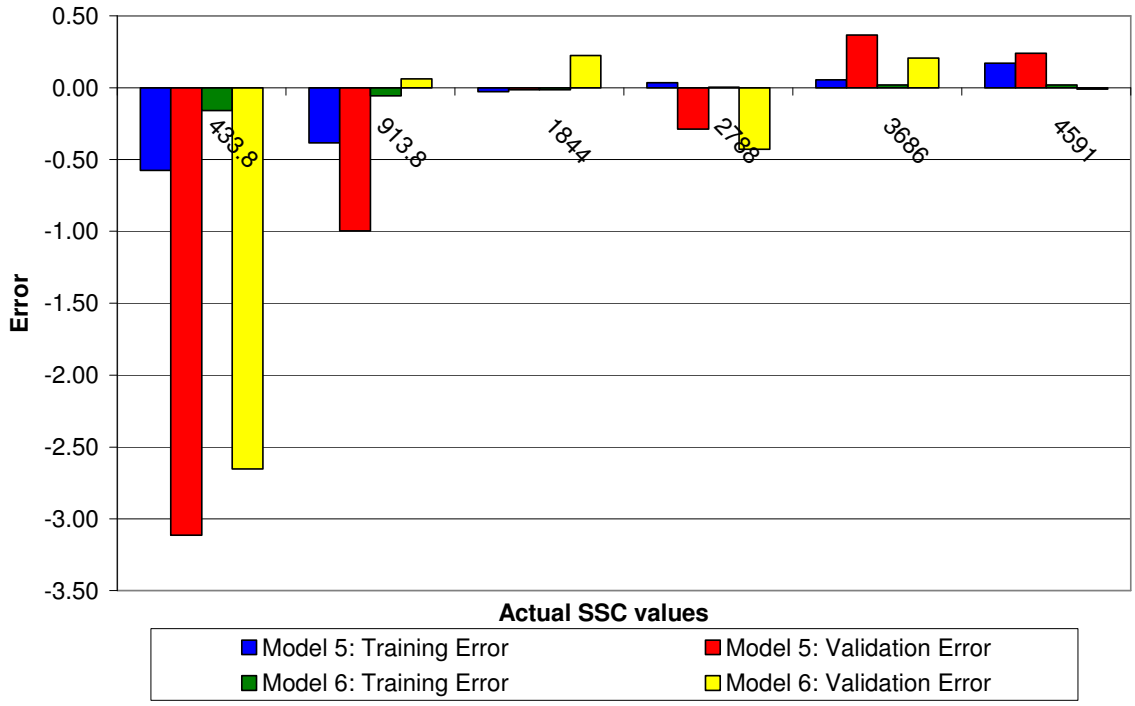

Figure 4.28. Comparison of error between the predicted and expected values of concentration for models 5B and 6B generated with gain and phase data. Both models developed with gain and phase values as explanatory variables have similar error over the treatment concentrations.

The three models with the lowest overall validation error between predicted and actual SSC values from the 12 models described above were selected to test with the second set of validation data (table 4.5 and 4.6). Figure 4.29 compares the prediction error of both training and validation data sets for the three selected models: model 2A with gain input, model 3A with phase input, and model 6B with gain and phase data as input variables and no zero values included in the analysis. Models 2A and 3A had prediction errors greater than 50%at SSC of zero mg/l; however, validation errors over the rest of the concentrations were less than most of the other models. The large error for 0 mg/L may be due to human error in cleaning the system between runs or may be an effect of conductivity when no sediment was present. All of the models performed best at concentrations from 1000 to 5000 mg/L with an accuracy of ± 140 mg/L for model 2A, ± 560 mg/L for model 3A, and ± 320 mg/L for model 6B. However the error for models 2A and 6B increased for concentration around 3000 mg/L to ± 1200 mg/L.

Table 4.5. Summary of error for the training data of the 12 PLS models

Model	1		2		3		4		5		6	
Conc. (mg/L)	A	B	A	B	A	B	A	B	A	B	A	B
0.0	1.10	N/A	1.41	N/A	0.33	N/A	2.09	N/A	2.04	N/A	2.29	N/A
433.8	-0.88	-0.08	-0.51	-0.13	-2.21	-0.77	-0.59	-0.22	-0.70	-0.58	0.42	-0.16
913.8	-0.48	-0.20	-0.15	-0.03	-1.02	-0.32	-0.28	-0.27	-0.32	-0.38	0.18	-0.06
1844.0	-0.21	-0.02	-0.08	-0.04	-0.41	-0.17	-0.11	-0.07	-0.11	-0.03	0.05	-0.02
2787.6	0.09	0.13	0.01	0.01	0.14	0.04	0.06	-0.02	0.04	0.03	0.02	0.00
3686.0	0.06	0.15	0.08	0.04	0.12	0.06	0.10	0.05	0.04	0.05	0.04	0.02
4590.7	0.11	0.18	0.06	0.05	0.45	0.14	0.06	0.06	0.10	0.17	0.02	0.02

Table 4.6. Summary of error for the validation data of the 12 PLS models

Model	1		2		3		4		5		6	
Conc. (mg/L)	A	B	A*	B	A*	B	A	B	A	B	A	B*
0.0	19.71	N/A	8.57	N/A	12.35	N/A	1.34	N/A	16.20	N/A	11.03	N/A
433.8	-3.48	-3.80	-3.19	-2.94	-0.47	-3.84	-3.58	-1.92	-2.84	-3.11	-2.81	-2.65
913.8	-0.59	-0.67	0.22	0.61	-0.11	-2.40	-1.06	-1.22	-0.50	-1.00	0.22	0.06
1844.0	0.18	0.08	0.04	0.33	0.17	0.20	-0.09	0.26	0.28	-0.02	0.09	0.22
2787.6	-0.41	-0.41	-0.44	-0.51	-0.21	-0.23	-0.48	-0.38	-0.46	-0.29	-0.58	-0.43
3686.0	0.25	0.32	-0.02	0.13	0.25	0.52	0.54	0.27	0.19	0.37	0.21	0.21
4590.7	0.13	0.16	0.05	-0.17	0.20	0.17	0.07	0.12	0.10	0.24	0.07	-0.01

*Model selected for further validation testing.

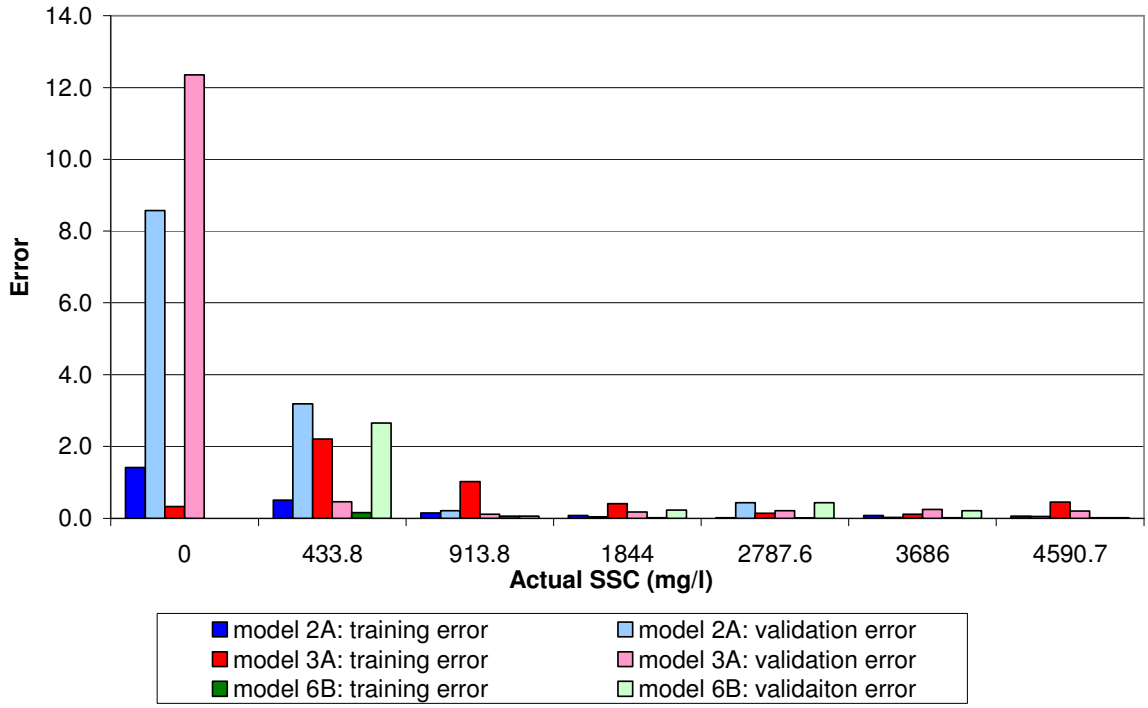

Figure 4.29. Error comparison of the training and validation data for the top three models: Gain model 2A, Phase model 3A, and Gain and Phase model 6B. All three models have the most difficulty predicting concentrations near 0 mg/L and 500 mg/L.

4.3.5 Validation Data Results

Prediction values for nine treatment levels were calculated for each set of data (A, B, and C) and then averaged for the final prediction value (fig. 4.30). Error between the predicted and actual values of SSC was calculated (fig. 4.31). The first level (100 mg/L) was not shown in this plot because the error was orders of magnitude greater than the other concentration levels, greatly exagerating the scale of the y-axis. All three models have the most difficulty predicting concentrations between 100 mg/L and 1500 mg/L. Model 3A does the best job predicting concentration.

The data used to develop the PLS models were normalized; therefore, when using the PLS models for independent validation, the input data must be normalized by the same standard deviation and mean values as used to develop the prediction models. Appendix B.1 provides the variables names, as well as the standard deviation and mean values for each input variable used in the prediction models 2A and 3A. Appendix B.2 provides the variable names, standard deviations, and mean values for model 6B. Appendix B.3 provides the variables and coefficients

for the three models selected from the PLS analysis. The predicted values for the independent validation data were calculated with the following equations:

$$normalized\_input\_value = \frac{\left(x - \bar{x}\right)}{stdev_x} \tag{4.6}$$

$$normalized\_SSC_{predicted} = b + coef_t temp + coef_c cond + \sum_i coef_i x_i \tag{4.7}$$

where *normalized_input_value* is the gain or phase value once normalized; *x* is the gain or phase value measured by the KSU control box at a specific frequency; *x bar* is the mean value of x; $stdev_i$ is the standard deviation of x; $normalized\_SSC_{predicted}$ is the normalized, predicted SSC from model 1, 2, and 3; *b* is the model intercept; $coef_t$ is the coefficient for temperature; *temp* is the temperature recorded during sampling; $coef_c$ is the coefficient for specific conductivity; *cond* is the conductivity recorded during sampling; *i* is a counter variable for the number of frequency-based variables (gain and phase) included in the model (127 variables for model 2 and 254 variables for models 5 and 6); $coef_i$ is the coefficient for variable i; and, x_i is the normalized gain or phase value measured by the KSU control box. Both the explanatory and predicted variables were normalized. Therefore, the predicted SSC must be reverse-transformed. The mean SSC for the models developed with all concentration levels was 2036.6 mg/L and the standard deviation was 1602 mg/L. When 0 mg/L treatments were removed from the analysis (model 6B) the mean was 2375.98 mg/L and the standard deviation was 1477.89 mg/L.

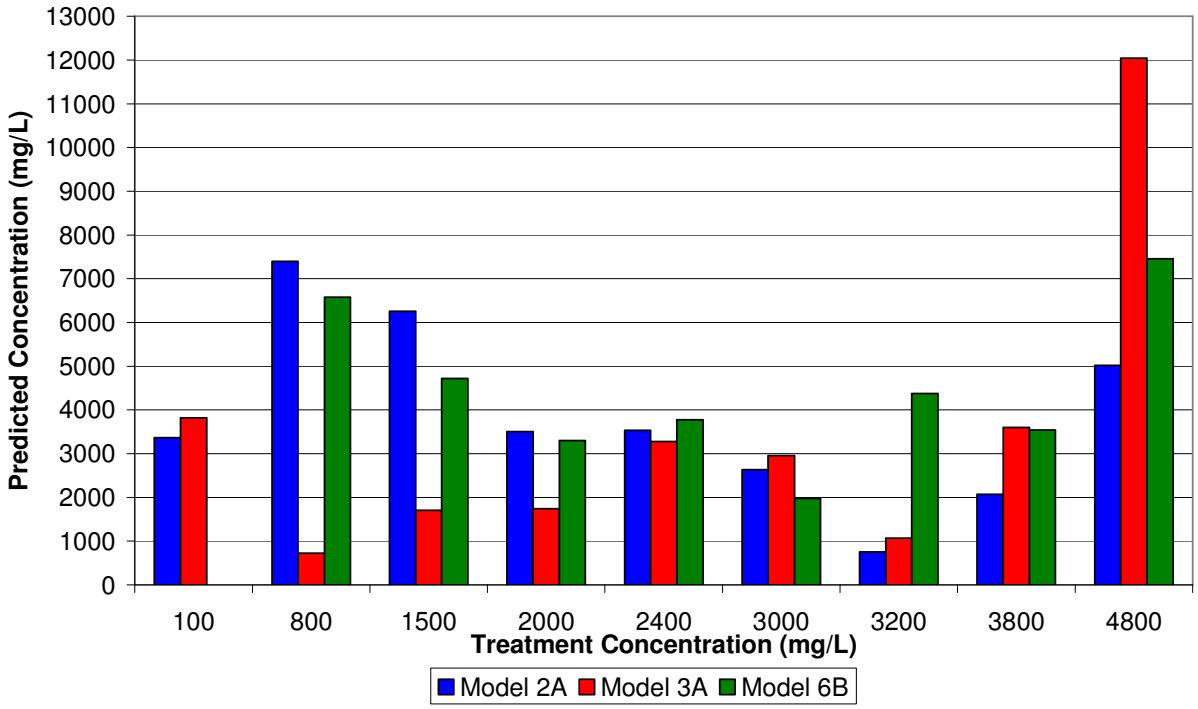

Figure 4.30. Predicted SSC from the three selected PLS models for the nine levels of independent validation data. In general all of the models did a very poor job predicting SSC.

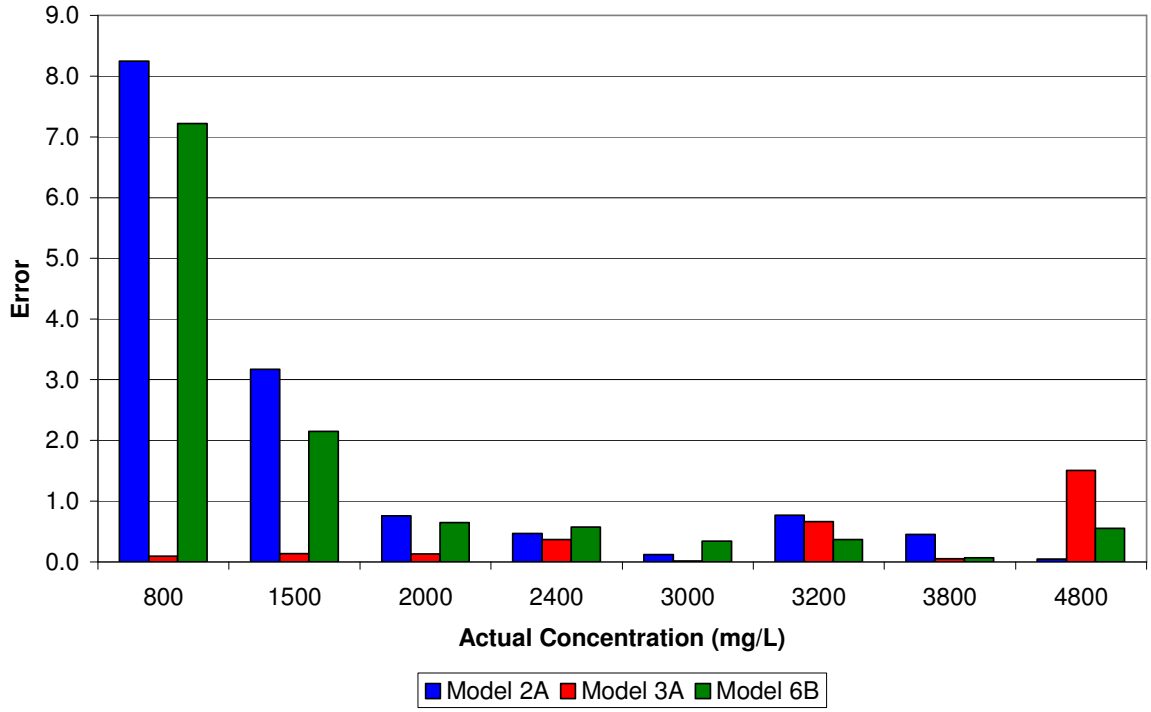

Figure 4.31. Error comparison of the actual and predicted concentrations for eight of the nine validation treatment levels.

Two of the three models selected for prediction with the independent validation data did a poor job of predicting the nine treatment levels. The predicted levels were orders of magnitude higher for 100 and 800 mg/L for all three models. Model 3A did the best job predicting concentration for all treatment levels except 100 and 4800 mg/L. It was expected that model 3A would have a difficult time predicting 100 mg/L based on the earlier validation results. Models 2A and 6B did the best job predicting concentration between 2000 and 4000 mg/L.

Investigations into the source of these poor predictions showed the distribution for many of the gain and phase variables in the independent validation data set had a different distribution than the prediction model data set. For most variables the mean gain and phase values did not vary significantly, but the standard deviation for 40-50 variables was double the size of the standard deviation values of the prediction model. The variation in standard deviations between data sets led to normalized values of gain within the validation data set as high as 20 instead of ranging between -2 and 2.

4.3.6 Summary of Results

Fixed and mixed effect, multiple, linear regression models were created and compared for target frequencies. However, it was not possible to meet the normality requirements for prediction accuracy. Partial Least Squares (PLS) regression techniques were also applied to gain and phase data for 127 of the 635 frequencies. Twelve models were generated for gain and phase individually and a combination of both variables. The three models with the lowest error between predicted and actual values of SSC for validation were further tested with nine levels of independent validation data. The largest model error (error>50%) occurred for the top three models at 0 and 433.8 mg/L. At the higher concentrations error varied from 1-45%.

Error increased significantly for the independent validation data for all models except model 3A. Model 3A had a difficult time predicting 100 and 4800 mg/L with errors greater than 150%. However for concentrations between 500 and 5000 mg/L the error ranged between 1.5-66%. It was determined that the distribution of around 40 gain and phase variables was significantly different than the variable distributions of the prediction model data. Standard deviation values of the independent validation data were double or triple the size of deviations from the prediction model data. This caused normalized values to be significantly greater and lead to significantly higher predicted values. Since model 3A did not seem to have the same over prediction

problems as models 2A and 6B it may be that phase is less susceptible to variations in standard deviation or hard connections within the experimental system.

4.4 Discussion of Prediction models

4.4.1 Accuracy of PLS Regression models

Based on the initial training and validation data for models 2A, 3A, and 6B it was expected that the models would be able to predict SSC to +/- 150-500 mg/l over most of the study range (0-5000 mg/L) except for concentrations at or close to 0 mg/L. However the error for models 2A and 6B increased for concentration around 3000 mg/L to ± 1200 mg/L.

This was not the case as seen in the analysis of the independent validation data set where all of the predicted levels for two of the models (2A and 6B) were significantly greater than the treatment levels (± 2000 mg/L). This drastic decrease in model accuracy was due to differences in the distributions of the gain and phase values between the prediction data and the independent validation data. At this point it is not clear if response to the shifted distribution is a weakness of PLS regression technique or there was a hardware malfunction in the measurement system, resulting in validation data with a significantly different distribution than the prediction data even though similar treatments were applied. However model 3A which was based on temperature, specific conductivity, and 127 frequencies of phase data was able to predict six of the nine independent validation levels within ± 300 mg/L. The increased accuracy of model 3A could mean that phase values are less susceptible to variations within the hardware than gain values.

4.5 Conclusions on Permittivity Sensor

4.5.1 Hardware Comparisons

Traditional bottle or pump sampling techniques for SSC are time consuming, expensive (collection and analysis), and can be dangerous under storm and flood stage conditions. There is also a scale discrepancy between the measurement time-scale and the time-scale at which most desired calculations are completed (Gray and Gartner, 2009). Currently there are three popular, surrogate technologies that are gaining credibility with the USGS: turbidity or optical backscatter sensors, Laser diffraction systems, and acoustic backscatter systems (Gray and Gartner, 2009). No one system provides the solution for all sediment monitoring challenges; therefore the strengths and weaknesses of each measurement system compared to the conditions of the study

site must be taken into account (Gray and Gartner, 2009). Some common weakness include particle size dependency, spatial or temporal resolution, and susceptibility to biofouling (Gray and Gartner, 2009; Wren et al. 2000).

This study was able to support the concept that permittivity measurements can predict SSC. The modeling predictions were most accurate (±150-500 mg/l) from 1000 to 5000 mg/L. This falls within the common measurement range of most turbidity (0-2000 mg/L or 0-5000 mg/L) and laser diffraction systems (0-2000 mg/L) currently available on the market (Gray and Gartner, 2009).

4.5.2 Cost Comparisons

Currently the cost estimate for a common turbidity sensor is $5000 (Gray and Gartner, 2009). Laser and acoustic systems can easily cost two to six times that amount (Gray and Gartner, 2009). It is believed that the permittivity system will be cheap to produce and may even be on the scale of or less than a traditional turbidity sensor. The most expensive components of the system will be the metal plates, molding of the electrode housing unit, and the frequency generator and analyzer. Permittivity electrodes could potentially be multiplexed with one controlling system, allowing the user to deploy multiple electrodes at field site with only one control system.

4.5.3 Conclusions for PLS Regression and Validation

Multiple models generated within this study were able to predict treatment level with errors less than 10% during model development. However, SSC predictions made during a validation procedure were orders of magnitude greater than the treatment levels for concentrations under 1000 mg/L. At this time strong conclusions cannot be drawn regarding the feasibility of using permittivity to predict. It is suspected that differences in the distribution of the validation data compared to the prediction model data set caused the poor predictions. Although two of three models tested with independent validation did not show promise, the phase based model (model 3A) did predict six of the nine treatment levels within 300 mg/L. It would be beneficial to repeat the independent validation portion of this study. First, the control box and all system connectors would need to be tested to determine if the control box contributed to the error in the independent validation predictions for models with gain as input variables (models 2A and 6B).

It may also be necessary, if significant changes are made the KSU control box, for the entire prediction model data set to be collected again.

4.6 Future work on Permittivity Sensor

4.6.1 Future work for sensor development

The primary goal of this study was to determine if it was possible to distinguish between different suspended sediment concentrations using a permittivity sensor. The previous sections presented data and analyses that were able to distinguish differences over a large range of concentrations. It is recommended that future work on the application of permittivity measurements for predicting SSC include designing a more appropriate electrode for the environmental conditions present in lotic systems. For example possible research question would include:

- How can the design of the sensor electrode be manipulated to maximize capacitance and minimize flow effects? Entrance and exit effects should be considered to develop isokinetic conditions within the plates.
- How does the electrode geometry affect sediment movement between the plates? Sensor geometry should not attract or prevent sediment from passing between the plates.
- How can electrode geometry and plate materials be optimized to prevent biofouling? Given the frequent occurrence of biofouling of environmental sensors during long term field deployments, bio-resistant plate material or surface coatings should be researched.
- Can a permittivity sensor predict both SSC and size distribution of the particles in suspension? This could be determined by completing a similar study using multiple mineral types and heterogeneous soil mixtures common in stream systems.
- With the optimal electrode geometry can the accuracy of SSC prediction be increased to the scale necessary for research? This study was unable to distinguish concentration at a resolution necessary for research. For example, changes in concentration of 500 or 1000 mg/L are very large for many stream systems. Ideally the permittivity system will be able to distinguish changes in concentration as low as

100 mg/L. This may be possible by measuring over a higher frequency range or with more accurate gain and phase measurements.

4.6.2 Future Work for PLS Regression and Validation

This project generated a significant amount of data because the exact modeling technique was not known at the onset. Two different modeling techniques were attempted in this study, traditional, multiple linear regression and PLS regression. There are many more options available for modeling frequency based data. Future works for the prediction and validation components of this study include the following:

- How repeatable are the measurements made by the KSU control box when the system is broken down completely between runs? For this study the system was not disconnected in between runs for the prediction model development. The system was reconnected to collect the independent validation data. It was determined that the standard deviation of 40-50 of the frequency-based variables (gain and phase values) doubled or tripled for the validation data. It will be important to determine if this is a problem with the system hardware.
- Can remote sensing analysis techniques be used to predict SSC? Remote sensing data are frequency based and ratios are created to determine differences between treatments. For example a ratio of the reflected light at two different frequencies can determine water surfaces from vegetated surfaces.
- Can other multivariate modeling techniques predict SSC with higher accuracy than the PLS regression completed in this study? Work by Dr. N. Zhang's students in Biological and Agricultural Engineering at Kansas State University is exploring alternate modeling techniques such as neural networks and wavelet transforms for analyzing this type of frequency-based data.
- Are temperature and conductivity not significant in predicting SSC once sediment enters the system? Specific conductivity is fundamentally tied into the theory of permittivity; however, in this study conductivity was not a significant variable in any of the top prediction models (model 2A, 3A, and 6B). Temperature appeared more significant than conductivity based on the magnitude of temperature and conductivity coefficients for the three models. Model coefficient magnitude could be compared because the input and output variables were normalized before the PLS analysis was

completed. The effect of temperature and conductivity on model predictions could be explored by stratifying the prediction models by conductivity and/or temperature.

- Why do the prediction models have a difficult time prediction concentrations at or near 0 mg/L? Currently all of the prediction models have a very difficult time predicting 0 mg/L. Temperature and conductivity had a larger effect on gain and phase measurements at 0 mg/L than over the rest of the concentration range. For example gain measurements taken at 0mg/L, 0 μS/cm, and 10°C were often 0.1-0.2 dB greater than gain measurements taken at the higher conductivity and temperature levels at the same concentration. This bimodal distribution may have reduced the models abilities to predict 0 mg/L. It is believed that sediment dampened the effect of temperature and conductivity on the measurement of gain and phase over the entire frequency range. It will be necessary to increase the accuracy of predicting values at or near 0 mg/L to establish base flow conditions in most streams.

Chapter 5: Conceptual Model

Permittivity is frequency-dependent; therefore, physically significant frequencies were identified to develop a conceptual model. Gain and phase data for 635 frequencies were collected. The number of frequencies was reduced from 635 to 127 during the PLS analysis to prevent model over-fitting. From the 127 frequencies involved in the PLS analysis not all frequencies were significant in the prediction of SSC. Due to system complexity two approaches were identified to develop a conceptual model. At a small scale, specific frequencies with unique patterns were identified to consider how gain and phase changed with increasing SSC. At a larger scale, changes in the gain and phase of pure water and the sediment suspensions with increasing SSC were considered over the entire frequency range. Both discussions are presented below.

5.1 Micro-scale Conceptual Model

First, the 25 most significant (highest absolute value of the coefficient values) frequencies were selected to look for patterns in the change in gain and/or phase with increasing suspended sediment. From the 25 significant frequencies seven frequencies were selected for this conceptual model. These seven frequencies meet unique conditions; such as gain transitions zones which identify changes in energy storage verses discharge or frequencies with maximum values of phase and maximum ranges of values over a single frequency. Figure 5.1 shows a simplified model of the system. It important to reiterate the definition of both gain and phase: for this study gain (dB) was the ratio of the *input* voltage to the *output* voltage (equation 5.1) and phase (deg) was the difference between the phase of the *input* signal to the *output* signal (equation 5.2; Tang, 2009).

$$gain = \frac{V_{in}}{V_{out}} \tag{5.1}$$

$$phase = phase_{out} - phase_{in} \tag{5.2}$$

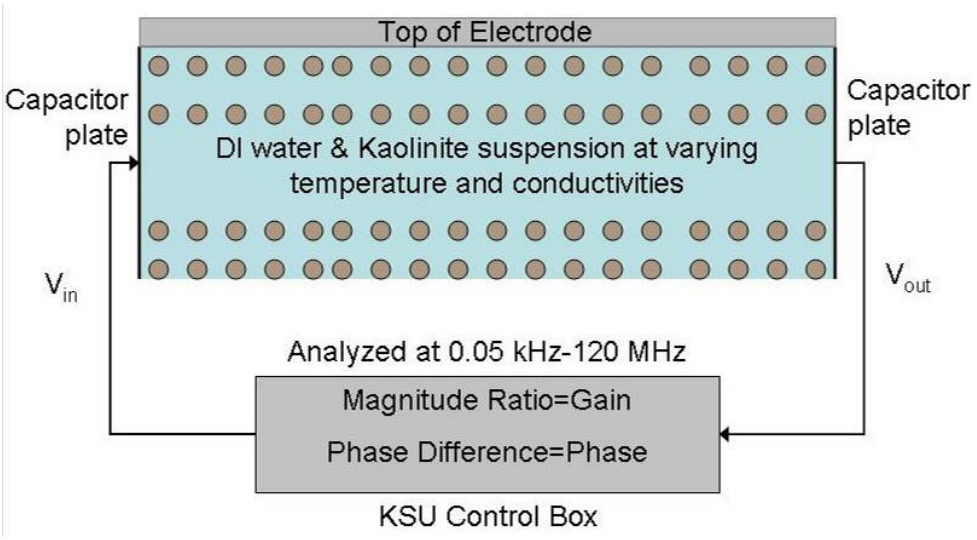

Figure 5.1. Simplified diagram of the KSU control box and the suspension system. The edges of the suspension volume are determined by the distance between the capacitor plates. For this study the plates were 3 mm apart.

The samples have three known components: water, sodium chloride, and kaolinite. These components individually and collectively make a complex circuit equivalent. The sensor electrode used in this study was a parallel plate capacitor; therefore, changes in gain and phase in terms of capacitance are described herein. Also, energy in the system varied with changing temperature and signal frequency. However, the effects of temperature and conductivity on gain and phase measurements seemed most pronounced only when sediment was not present.

It is also important to note that human error and system error may be responsible for some of the anomalies in the data. For example, there could be a property error associated with the control box concerning the spectral performance of digital to analog or analog to digital converters or with improper isolation of the control box power supply. Also the resolution of the gain and phase values is not known; therefore, values below one or close to one may be greater than reported based on measurement error in the system.

As presented in Chapter 2, there are four types of polarization: ionic, electronic, dipole, and heterogeneous (Diefenderfer, 1998). Within the study system the primary means of polarization are believed to be dipole (water) and heterogeneous (kaolinite suspension). It is also important to note the effect of dipole and heterogeneous polarization is theoretically prominent until the dielectric relaxation frequency is applied (Diefenderfer, 1998). For this study neither the dielectric relaxation point of water (17 GHz as stated by Robinson et al., 2003) nor of general soil was reached (<1 GHz as stated by Robinson et al., 2003). Thus, both the water-salt mixture

and the kaolinite should be able to polarize over the frequency range of 0.05 kHz to 120 MHz. However, it is not known at this time if, at certain frequencies, the water and sediment may polarize out of phase with each other, leading to decreasing gain and increasing phase with the increase in sediment concentration.

5.1.1 Gain Transition Zones

Gain is the ratio of input voltage to output voltage; therefore, there are three possible values for gain. When gain is less than one (gain<1) the output voltage from the sample volume is greater than the input voltage. It is not intuitive that the signal coming out of the sample volume would be larger than the signal going in. Traditional amplified circuits require a secondary external excitation to constructively interfere with the input signal, thereby adding to the input signal to amplify it. The experimental set-up for this study did not purposefully add an external excitation to amplify the gain signal. Because the relaxation point for neither water nor soil was reached in the study frequency range, the system has capacitive properties. The primary goal of capacitors is to store energy. Therefore, it is possible that under certain frequencies the system/sample volume may be discharging energy stored from a previous frequency; the probability of this occurring needs to be investigated. This condition occurred under different temperature and conductivity treatments for approximately 1/6 of the input frequencies and the gain ratios were never less than 0.60 dB. It is important to note that gain values less than one decibel may be due to measurement errors within the permittivity system.

The second condition occurred when gain was roughly equal to one (gain~1). When this was true the energy applied to the system continued through the sample volume without dissipating or causing the dipoles to discharge any stored energy. This condition did not occur often in the data collected for this study.

The last possible condition was for gain to be greater than 1 (gain>1), under the definition of gain for this study, when gain was greater than one the input voltage was greater than the output voltage. Therefore, energy was stored or dissipated within the system. The majority of the gain data collected during this study were greater than one.

Two frequencies were identified from the 25 significant frequencies of the PLS analysis that recorded a transition of gain values to greater or less than one with the addition of suspended sediment to water (fig. 5.2). The lowest frequency, 75,200 kHz, decreased to less than one with the addition of sediment. Therefore the addition of sediment to the suspension at this frequency

may have decreased the quantity of charge the system "capacitor" could hold. Or, in other words, the dielectric constant of the system may have decreased with the addition of sediment. The opposite was true for 81,200 kHz, where with the addition of sediment caused gain to increase above one, indicating storage within the system. Thus, the dielectric constant of the mixture was greater than the dielectric constant of the solution alone at this frequency.

Figure 5.2 includes a third frequency, 77,200 kHz, which remained just less than one throughout the addition of sediment (~0.9 dB). Of the 25 analyzed for the conceptual model, 77,200 kHz is the only frequency at which gain remained close to one even with the addition of sediment. At this frequency the system capacitance does not change significantly with more sediment added to the system. It is important to note that, for all three frequencies, phase followed the same trends as gain, although the magnitude of the change was different: phase remained between 15 and 20 degrees. The frequencies presented in figure 5.2 also represent minimum values for both gain and phase compared to gain and phase values measured over the entire frequency range.

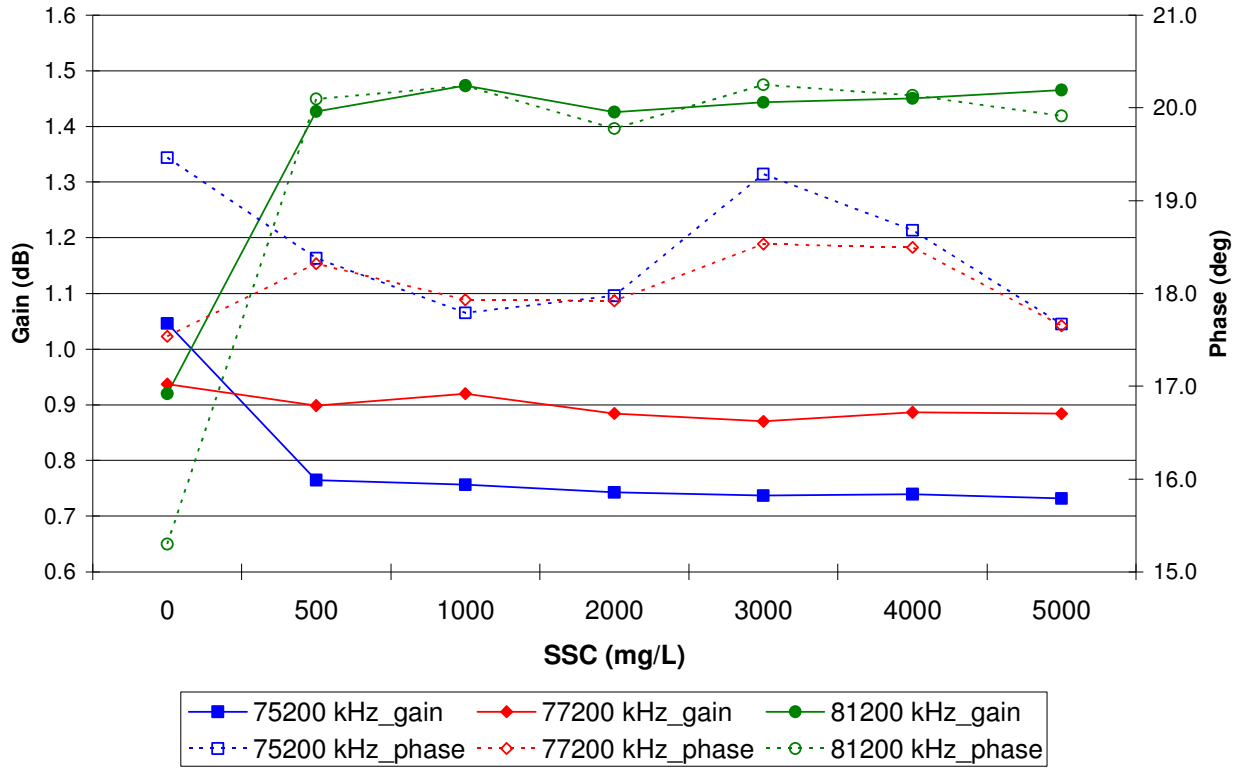

Figure 5.2. Changes in gain and phase with increasing SSC for 75200, 77200, and 81200 kHz. These frequencies show the transition of gain from less than one to greater than 1.

5.1.2 Frequencies with Maximum Phase Change

Of the 25 significant frequencies, six frequencies had a difference between the input and output phase, with the maximum phase change of 36.65 degrees. The six frequencies occurred in two ranges, three frequencies around both 37,200 kHz and 117,200 kHz. Only phase and gain data for 37,200 and 117,200 kHz are shown below in figure 5.3. For both 37,200 and 117,200 kHz, gain values were above average (2.66 dB), although not at the maximum and greater than 1.00 for all concentration levels. Therefore the input voltage was greater than the output voltage and energy was stored within the sample volume "capacitor". Although both frequencies had large changes in phase, compared to the 25 frequencies examined, the response of gain and phase to the two frequencies shown in figure 5.3 was very different. The lower frequency, 37,200 kHz, showed a relatively steady response for both gain and phase with the addition of sediment. This may be due to the ability of the suspension to continue to polarize even with increasing SSC because of the low frequency, or there are no significant changes in gain with increasing SSC because the water is the dominant polarizing component in the system at 37,200 kHz.

In contrast, the higher frequency, 117,200 kHz, had decreasing gain and increasing phase as SSC increased from 0 to 500 mg/L, indicating that by increasing SSC the suspension was unable to polarize as quickly, thereby reducing energy storage but increasing travel time for the current. It is believed that the overall magnitude of gain is greater for the higher frequency (117,200 kHz) because more energy is entering the sample volume due to the higher frequency.

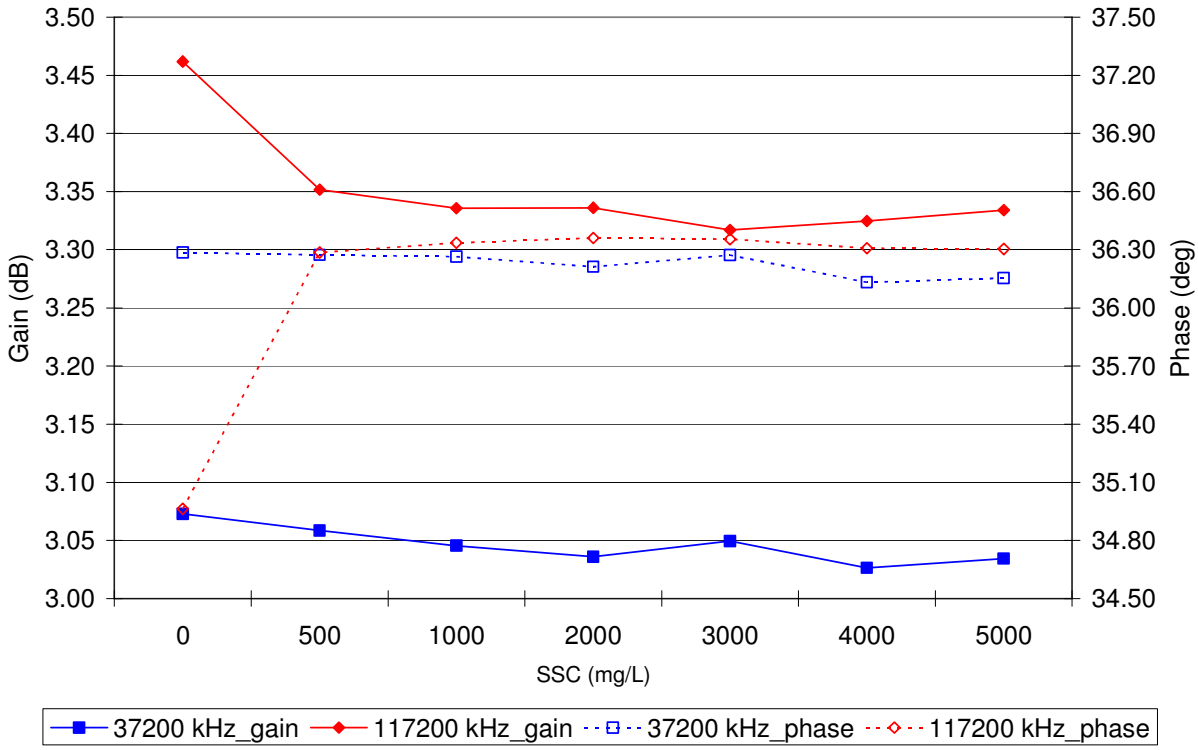

Figure 5.3. Changes in gain and phase with increasing SSC for 37200 and 117200 kHz. Gain and phase data for two frequencies with maximum phase values and gain values significantly above average.

5.1.3 Frequencies with Maximum Range

The final two frequencies (84,200 and 86,200 kHz) examined follow similar patterns with both gain and phase increasing with increasing SSC. There is a slight increase in the magnitude of both gain and phase with the increase of frequency from 84,200 to 86,200 kHz. This increase with increasing frequency could again be due to the higher energy entering the system at a higher frequency. For this study range was defined as difference between the maximum and minimum measurements of either gain or phase for a single frequency. The frequencies presented in figure 5.4 have the highest range for both gain and phase. The range for gain was 1.11 and 1.16 dB, and the range for phase was 9.34 and 9.64 degrees for 84,200 and 86,200 kHz, respectively. With the increase in SSC more energy is stored within the sample volume than in the water sample and it takes longer for the signal to pass through the sample volume. The high phase values may also be due to the time it takes for the larger capacitor of water and sediment to charge and discharge.

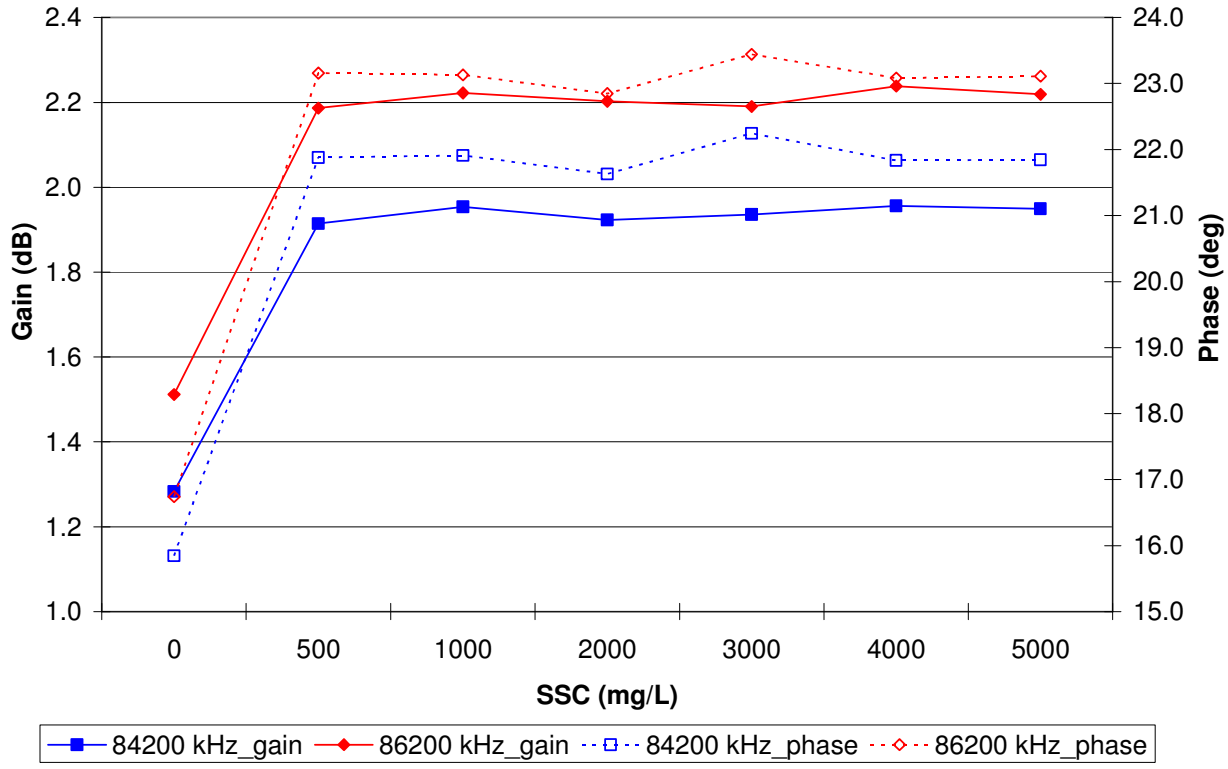

Figure 5.4. Gain and phase data verses SSC for two frequencies, 84,200 and 86,200 Hz. These frequencies were selected because they have the maximum increase in gain and phase measured at a single frequency.

5.2 Macro-scale Conceptual Model

At the larger scale, repeatable trends or signals were present in both gain and phase data. To begin explaining how the signal changed with the addition of sediment, the signal of de-ionized water must be understood. At this time, information is not available to explain all the changes or trends in the water signal (fig. 5.5). Since the study frequency range never reached the dielectric relaxation point of water, it was believed that the gain signal for pure water would be greater than 1 at all frequencies and continue to increase slightly with increasing frequency. This is not the condition of the pure water signal (blue line on figures 5.5-5.8).

Instead the pure water signal decreases and increases across the range of frequencies, and falls below one decibel from 3000-6000 kHz and 78,200-82,800 kHz. To better understand the changes of gain and phase with changing frequency it would be necessary to actually calculate the real and imaginary portions of the dielectric constant. It is not possible to perform these calculations on the data collected for this study because the geometric shape factor of the

electrode used in this study was never determined. Once the geometric shape factor is known it would be possible to study how the relationship between capacitive and conductive effects of pure water changes with increasing frequency and answer the question if increasing gain was actually increasing storage or increasing signal loss.

The same issues plagued understanding the differences between sediment signals and the pure water signal across. Without knowing how the relationship between capacitive and conductive aspects of the dielectric medium changed with frequency it is impossible to predict if changes in gain were the result of increased/decreased storage or increased/decreased losses from conduction. In an attempt to gain further insight into the differences between water and sediment signals and at which frequencies the differences occurred, figures 5.9-12 were created. The pure water signal was subtracted from the signals for each sediment concentration. Therefore values of zero would represent the same condition between the water signal and a sediment signal. The mean and median values for both gain and phase data at all concentrations was greater than zero. Considering how it different the water signal is from the sediment signals it is surprising that the prediction model had such a difficult time of predicting 0 mg/L.

At this time and with the data collected for this study all that can be determine is that the responses of pure water and sediment suspensions were frequency-dependent and seemed to be cyclic. Similar responses occurred over different band width of excitation frequencies.

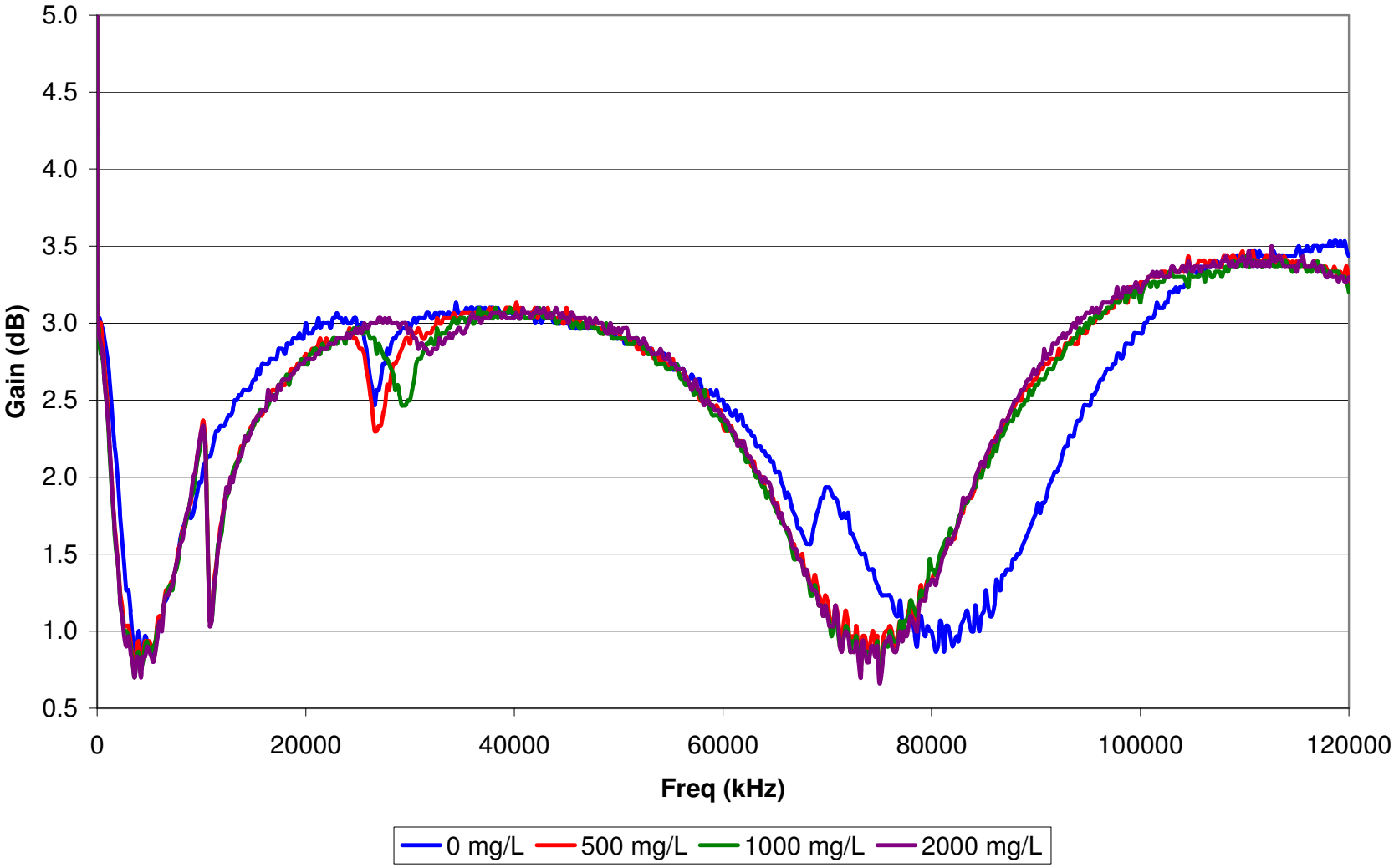

Figure 5.5. Gain data for 0, 500, 1000, and 2000 mg/L at 20°C and 0 µS/cm.

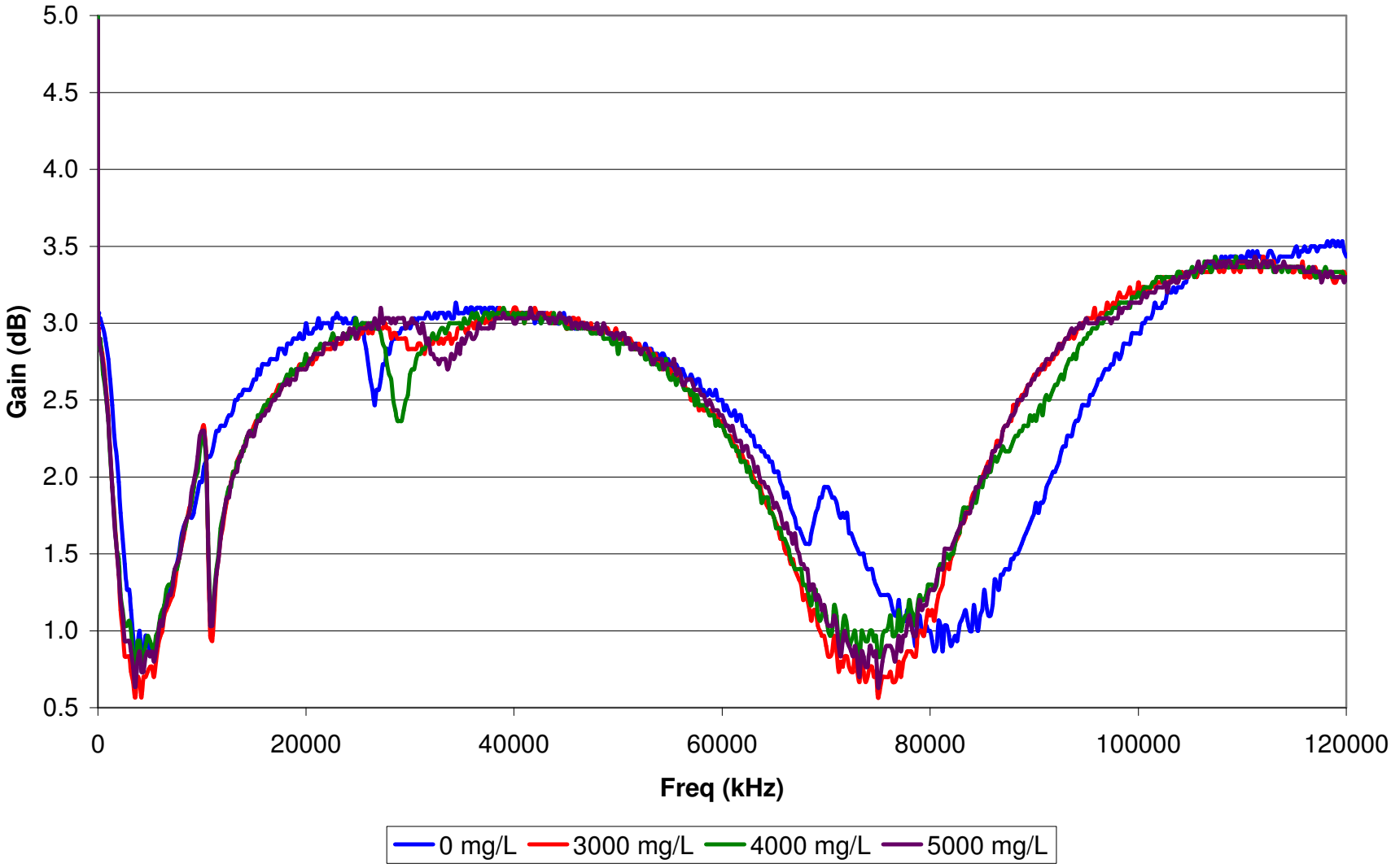

Figure 5.6. Gain data for 0, 3000, 4000, and 5000 mg/L at 20°C and 0 µS/cm.

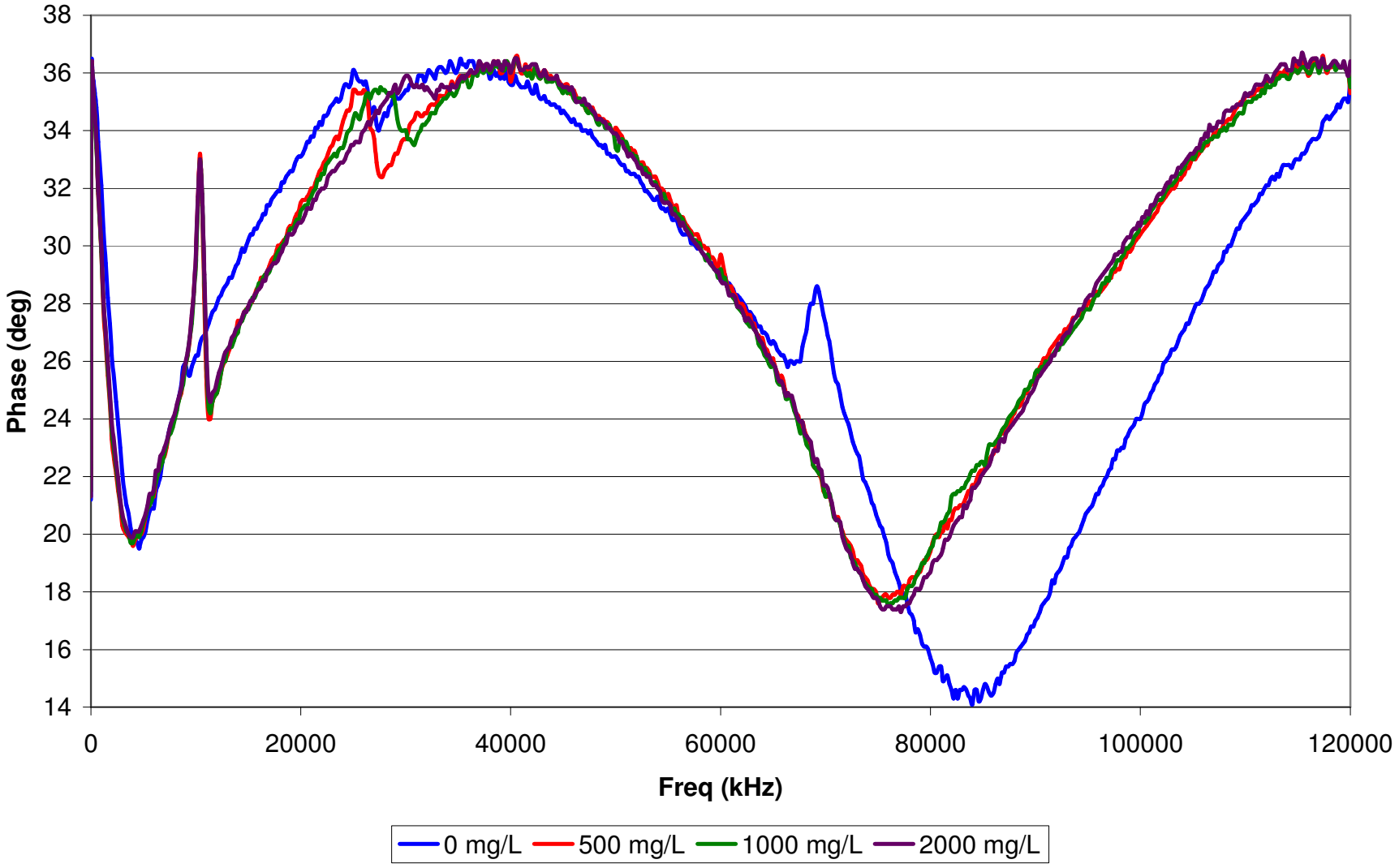

Figure 5.7. Phase data for 0, 500, 1000, and 2000 mg/L at 20°C and 0 µS/cm.

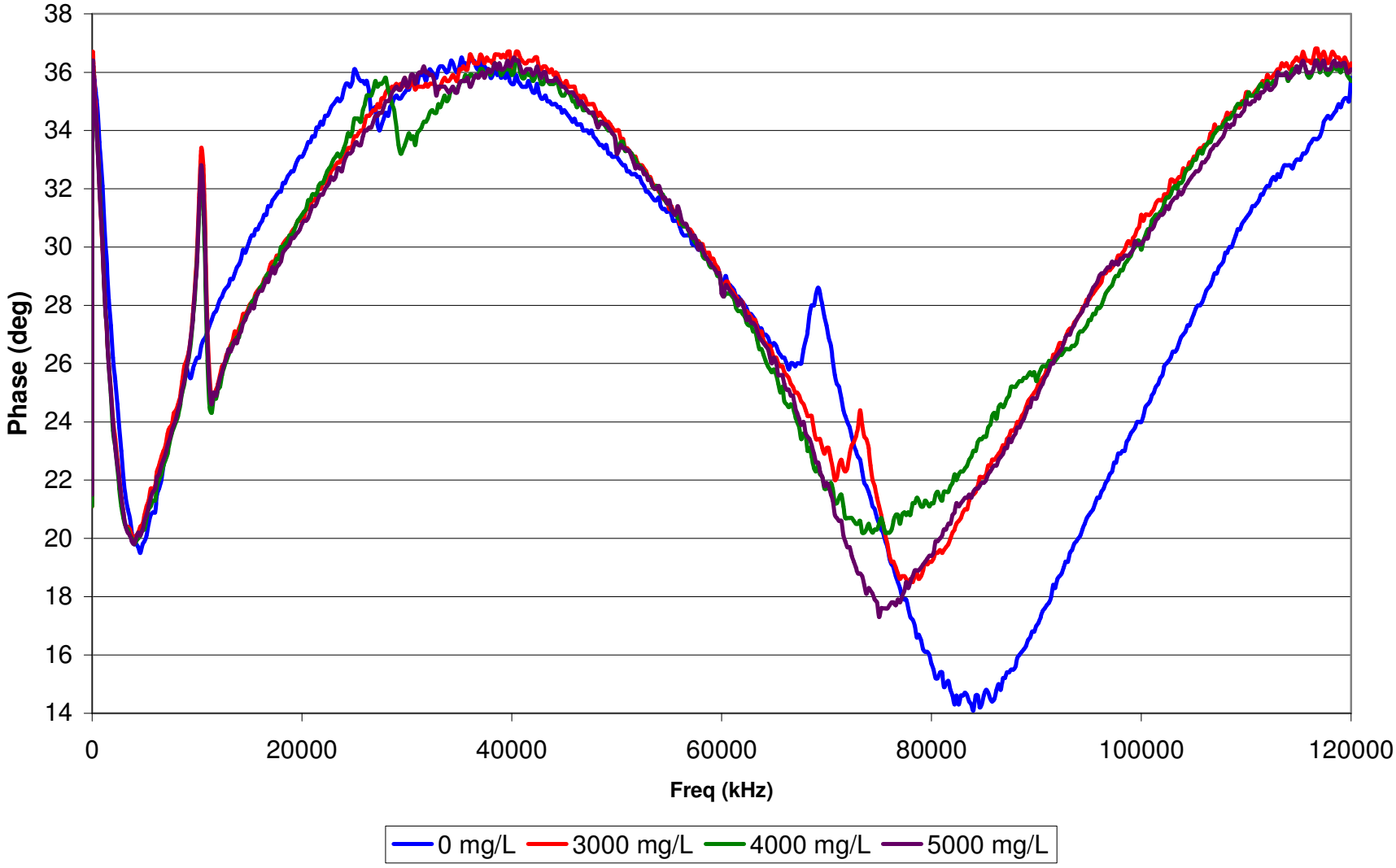

Figure 5.8. Phase data for 0, 3000, 4000, and 5000 mg/L at 20°C and 0 µS/cm.

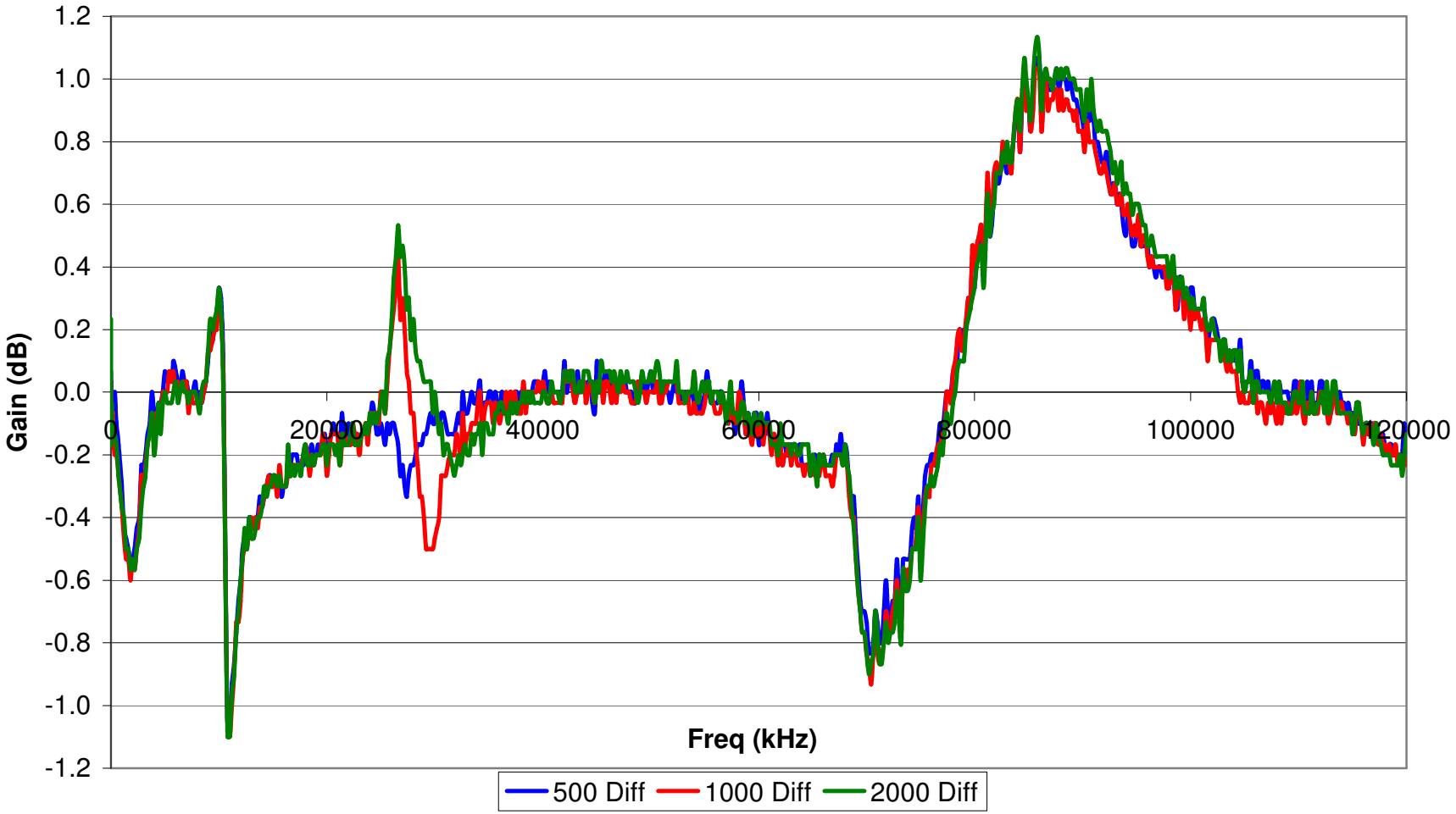

Figure 5.9. Differences between gain data for 500, 1000, and 2000 mg/L and pure water (0 mg/L) over the range of study frequencies.

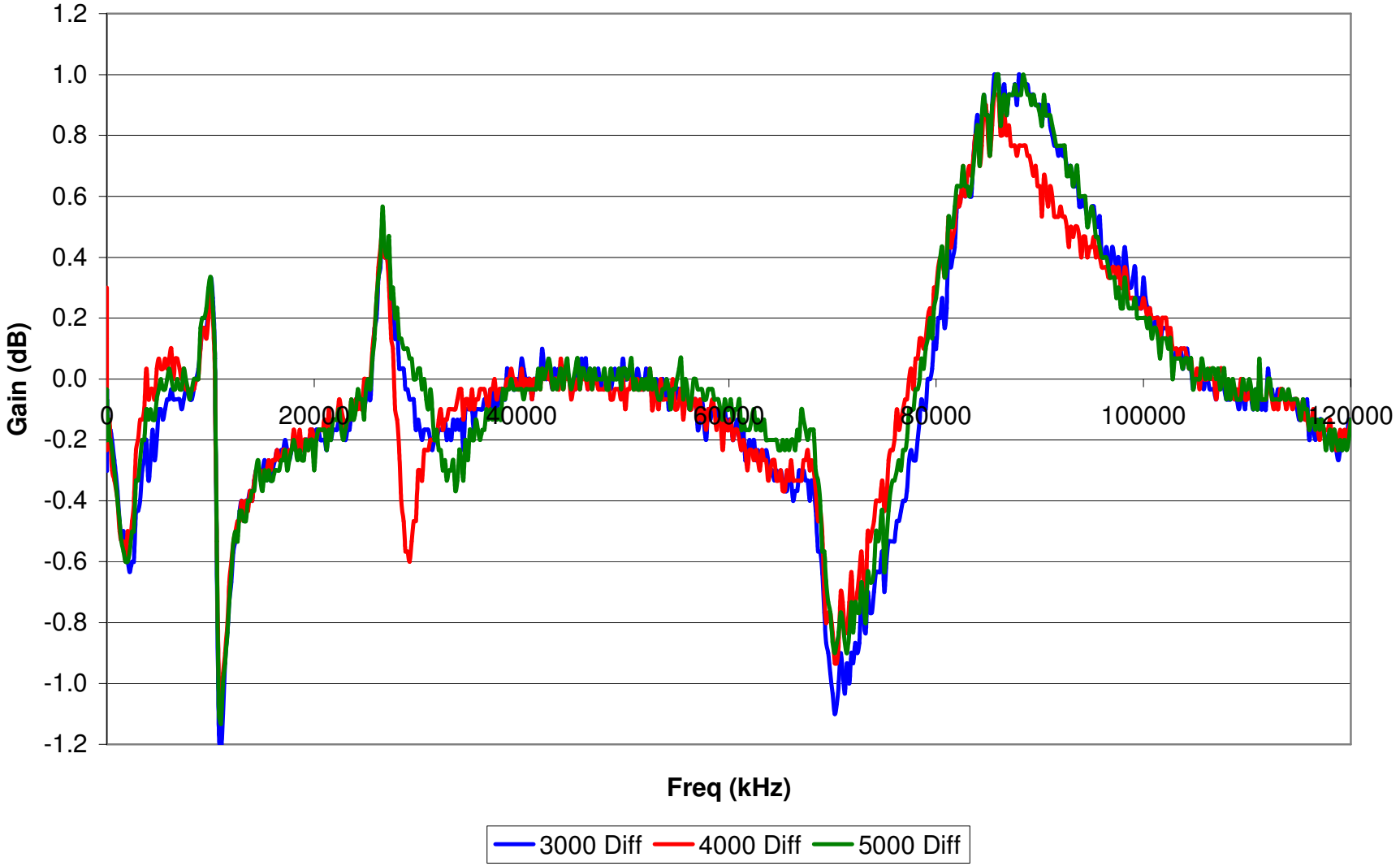

Figure 5.10. Differences between gain data for 3000, 4000, and 5000 mg/L and pure water (0 mg/L) over the range of study frequencies.

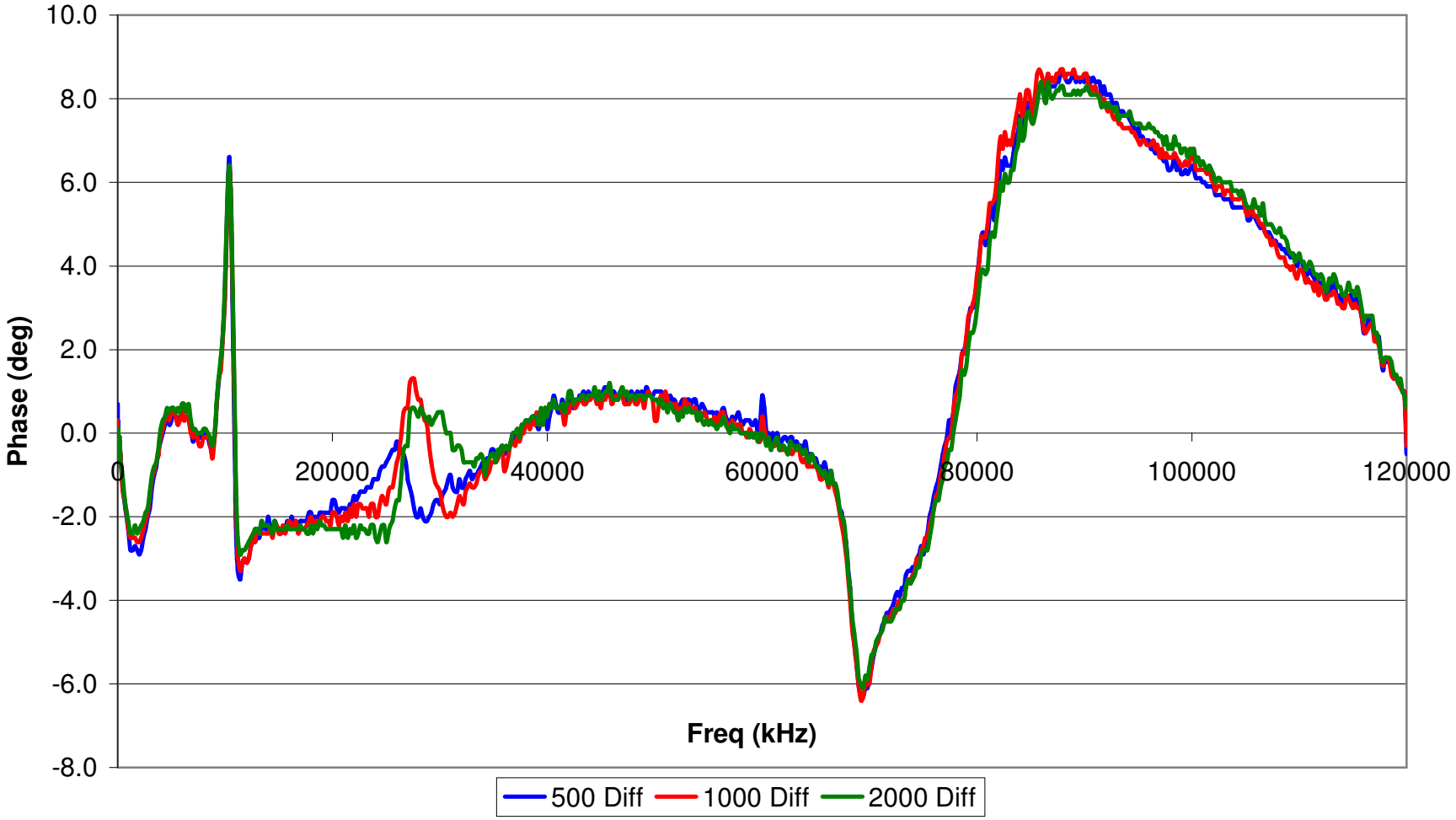

Figure 5.11. Differences between phase data for 500, 1000, and 2000 mg/L and pure water (0 mg/L) over the range of study frequencies.

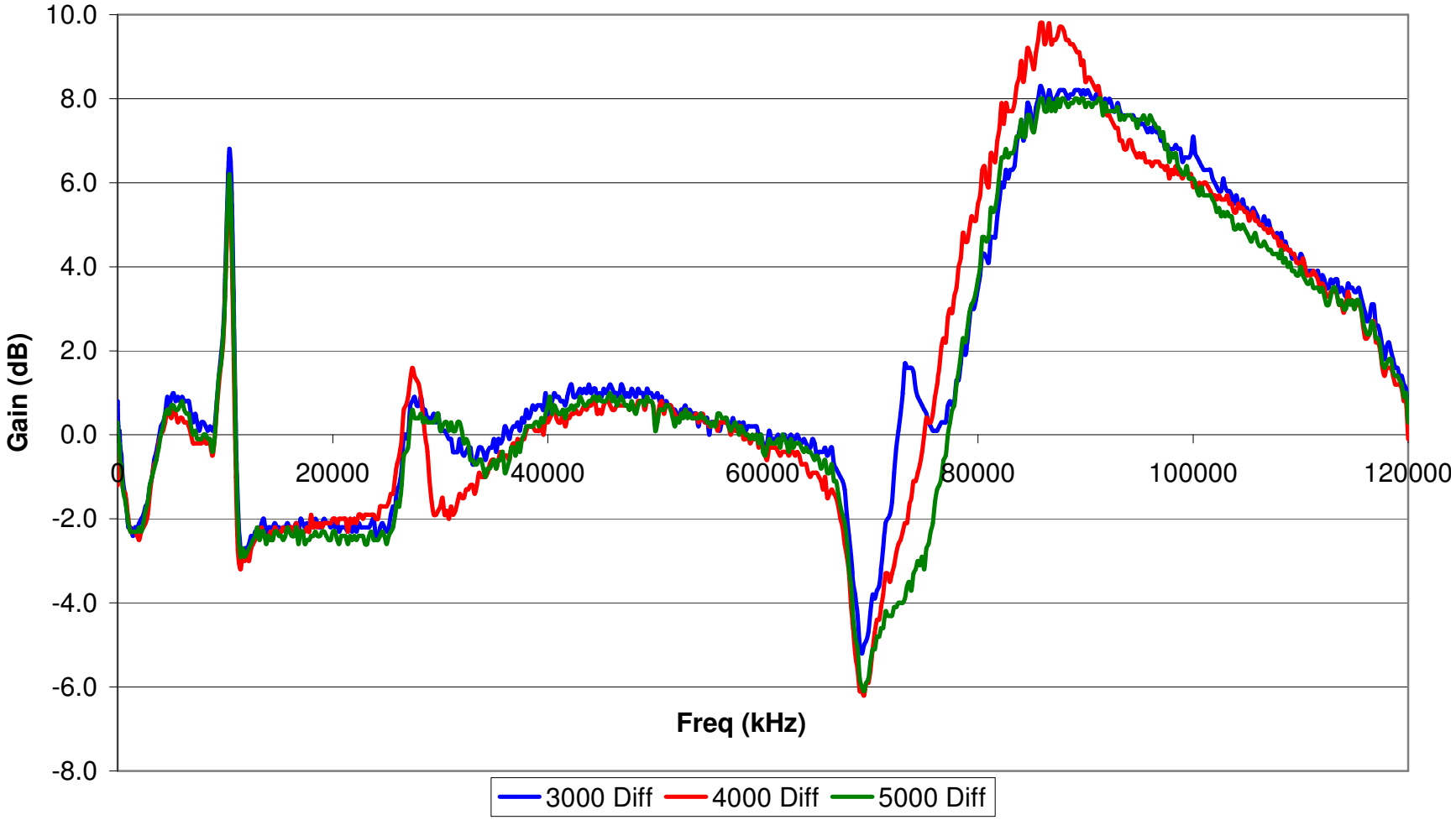

Figure 5.12. Differences between phase data for 3000, 4000, and 5000 mg/L and pure water (0 mg/L) over the range of study frequencies.

5.3 Conceptual Model Conclusions

For five of the seven frequencies described in the above sections the largest change in gain and phase occurred in the transition from 0 to 500 mg/L. System changes at concentrations of 500 to 5000 mg/l were less significant. As the technology continues to move forward, the measurement of gain and phase will become more accurate over the range of concentrations; therefore, prediction accuracy over the range of concentrations will continue to improve. Conceptually the behavior of the sediment suspension was significantly different than that of water with ions over most of the frequencies analyzed in this study.

5.4 Future Work on the Conceptual Model

This project was a "black box" approach to applying permittivity to predicting SSC. There are still many unknowns about how an electric field affects a sample volume of varying sediment suspensions when applied over a range of frequencies. Plus it is believed that changing the mineral in suspension will also affect the permittivity. There are many questions that need to be investigated to design the best possible permittivity sensor for measuring suspended sediment. Some of the questions would include:

- What is the geometric shape factor for the electrode used in this study? How do the conductance and capacitance of the sample volume change with increasing frequency? The geometric shape factor was not determined for the electrode used in this study. Once the geometric shape factor is determined it would be possible to use the gain and phase values at each frequency to see how the capacitance and conductance of the sample volume changes with frequency. This would help explain how the sediment-water suspension behaved differently than water.
- Why does the gain and phase signal for DI water and water with ions cycle? In order to increase the accuracy of predicting 0 mg/L it would be helpful to understand why the response of gain and phase for water without sediment cycles.
- Why is it possible to get gain values less than one? For the hardware used in this study gain values less than one correlate to an output voltage greater than the input voltage. It should not have been possible for this system to return gain values less than one, however all treatment levels (combination of concentration, conductivity,

and temperature) had multiple frequencies with gain values less than one. It may be necessary to monitor gain in the time domain to see why this is occurring.

By understanding the changing response of sediment and water to different frequencies the range of frequencies required for predicting SSC can be narrowed. Also new versions of the KSU control box have an expanded frequency range. It is possible the best frequency range for predicting SSC has not been evaluated at this time.

References

Abdi, H. (2003). Partial least squares regression (PLS-regression). In M. Lewis-Beck, A. Bryman, T. Futing (Eds): *Encyclopedia for research methods for the social sciences*. Thousand Oaks (CA): Sage. pp. 792-795.

Admiraal, D. M., and M. H. Garcia. 2000. Laboratory measurement of suspended sediment concentration using an Acoustic Concentration Profiler (ACP). *Experiments in Fluids*. 28 (2): 116-127.

Agrawal, Y. C., and H. C. Pottsmith. 2001. Laser sensors for monitoring sediments: capabilities and limitations, a survey. *Proceedings of the Seventh Federal Interagency Sedimentation Conference*. Reno, NV; III-144 - 151.

APHA (1998). 20th Ed. Standard Methods for the Examination of Water and Wastewater, 10.18-10.25. Washington, DC.: American Public Health Association.

Berkman, H.E. and C.F. Rabeni. 1987. Effect of siltation on stream fish communities. *Environmental Biology of Fishes*. 18(4): 285-294.

Black, K. P., and M. A. Rosenberg. 1994. Suspended sand measurements in a turbulent environment: field comparison of optical and pump sampling techniques. *Coastal Engineering*. 24(1-2) 137-150.

Campbell, C.G., D.T. Laycak, W. Hoppes, N.T. Tran, F.G. Shi. 2005. High concentration suspended sediment measurements using a continuous fiber optic in-stream transmissometer. *J. Hydrology*: 311: 244-253.

Carr, J. 1993. *Sensors and Circuits*. Englewood Cliffs, New Jersey: Prentice Hall.

Creed, E. L., A. M. Pence, and K. L. Rankin. 2001. Inter-Comparison of Turbidity and Sediment Concentration Measurements from an ADP, an OBS-3, and a LISST. *OCEANS 2001 MTS/IEEE Conference and Exhibition*. Honolulu, HI; 1750-1754.

Diefenderfer, B. 1998. Development and testing of a capacitor probe to detect deterioration in Portland Cement Concrete. MS thesis. Blacksburg, VA: Virginia Polytechnic Institue and State University, Via Department of Civil and Environmental Engineering.

Gray, J.R. and J.W. Gartner. 2009. Technological advances in suspended-sediment surrogate monitoring. *Water Resources Research. 45*, W00D29, doi:10.1029/2008WR007063.

Gartner, J. W., 2002. Estimation of suspended solids concentrations based on acoustic backscatter intensity: theoretical background. *Federal Interagency Workshop on Turbidity and Other Sediment Surrogates*. Reno, NV, 3 pages.

Gartner, J. W. and R. T. Cheng. 2001. The promises and pitfalls of estimating total suspended solids based on backscatter intensity from Acoustic Doppler Current Profiler. *Proceedings of the Seventh Federal Interagency Sedimentation Conference*. Reno, NV; III-119 - 126.

Gartner, J. W., R. T. Cheng, P. F. Wang, and K. Richter. 2001. Laboratory and field evaluation of the LISST-100 instrument for suspended particle size determinations. *Marine Geology.* 175, 199-219.

Gartner, J. W., and J. R. Gray. 2002. Summary of Suspended-Sediment Technologies Considered at the Interagency Workshop on Turbidity and Other Sediment Surrogates. *Federal Interagency Workshop on Turbidity and Other Sediment Surrogates*. Reno, NV, 1-9.

Gooding, D. J. 2001. Photo-Optical Sedimentation Tube. *Proceedings of the Seventh Federal Interagency Sedimentation Conference*. Reno, NV, Poster-29-30.

Gray, J. R., D. J. Gooding, T. S. Melis, D. J. Topping, and P. P. Rasmussen. 2003. U.S. Geological Survey Suspended-Sediment Surrogate Research, Part II: Optic Technologies. *Proceedings of the Virginia Water Research Conference*. Virginia Tech, Blacksburg, VA, 58-64.

Hasted, J.B. 1973. *Aqueous Dielectrics.* London: Chapman and Hall.

Helsel D.R. and R.M. Hirsch. 1992. *Statistical methods in water resources.* New York, N.Y.: Elsevier.

Klein, K. and J.C. Santamarina. 1997. Methods for Broad-band deielctric permittivity measurements (soil-water mixtures, 5 Hz to 1.3 GHz). *Geotechnical Testing Journal*. 20(2):168-178.

Knighton, D. 1998. *Fluvial Forms and Processes.* London: Arnold.

Kuhnle, R. A. and A. Simon. 2000. Evaluation of Sediment Tranpsort Data for Clean Sediment TMDLs. *National Sedimentation Laboratory Report No. 17.* USDA NSL: Oxford, MS.

Larsen, M., C.F. Alamo, J. Gray, and W. Fletcher. 2001. Continuous automated sensing of streamflow density as a surrogate for suspended-sediment concentration sampling. *Proceedings of the Seventh Federal Interagency Sedimentation Conference,* Reno, NV.

Lee, K.H., N. Zhang, W.B. Kuhn, G.J. Kluitenberg. 2007. A frequency-response permittivity sensor for simultaneous measurement of multiple soil properties: Part I. The frequency-response method. *Trans. ASABE.* 50(6): 2315-2326.

Lee, K.H., N. Zhang, and G. Kluitenberg. 2007. A frequency-response permittivity sensor for simultaneous measurement of multiple soil properties: Part II. Calibration model tests. *Trans. ASABE.* 50(6): 2327-2336.

Leopold, L. 1994. *A View of the River*. Cambridge, Massachusetts: Harvard University Press.

Lewis, A.J. and T.C. Rasmussen. 1999. Determination of suspended sediment concentration and particle size distribution using pressure measurements. *Journal of Environmental Quality.* 28(5):1490-1496.

Li, X., T. Lei, W. Wang, Q. Xu, and J. Zhao. 2005. Capacitance sensors for measuring suspended sediment concentration. *CATENA*. 60(3), 227-237.

McBride, Murray B. 1994. *Environmental Chemistry of Soils*. New York, N.Y.: Oxford University Press.

McCave, I. N., and J. P. M. Syvitski. 2001. Principles and methods of geological particle size analysis. *Principles, Methods, and Applications of Particle Size Analysis*. J. P. M. Syvitski, ed., Cambridge University Press, New York, 3-21.

Minella, J. P. G., G. H. Merten, J. M. Reichert, and R. T. Clarke. 2008. Estimating suspended sediment concentrations from turbidity measurements and the calibration problem. *Hydrological Processes*. 22 (12): 1819-1830.

Munoz-Carpena, R., A. Ritter, D. Bosch. 2005. Chapter 5: Field methods for monitoring soil water status. *In Soil-Water-Solute Process Characterization,*167-195. Alverez-Bendedi, J. and R. Munoz-Carpena, ed. Boca Raton, FL.: CRC Press.

Nelson, S.O. 1991. Dielectric-properties of agricultural products-Measurements and applications. *Transactions on electrical insulation.* 26(5):845-869.

Novotony, V. 2003. *Water Quality: Diffuse Pollution and Watershed Management.* Boston, MA: John Wiley & Sons.

O'Malley, J. 1992. Chapter 8: Capacitors and capacitance. In *Schaum's Outlines: Basic Circuit Analysis*, 153-173. New York, NY.: McGraw Hill.

Osterkamp, W. R., P. Heilman, and L. J. Land. 1998. Economic considerations of a continental sediment-monitoring program. *International Journal of Sediment Research.* 13(4): 12-24.

Osterkamp, W. R., P. Heilman, and J. R. Gray (2004), An Invitation to Participate in a North American Sediment-Monitoring Network, *Eos Trans. AGU*, 85(40).

Pimentel, D., C. Harvey, P. Resosudarmo, K. Sinclair, D. Kurz, M. Mcnair, S. Crist, L. Shpritz, L. Fitton, R. Saffouri, and R. Blair. 1995. Environmental and Economic Costs of Soil Erasion and Conservation Benefits. *Science*. 267 (5201): 1117-1123.

Reichel, G., and H. P. Nachtnebel. 1994. "Suspended sediment monitoring in a fluvial environment: Advantages and limitations applying an Acoustic Doppler Current Profiler. *Water Research*. 28, no. 4, 751-761.

Reid, S.C., S.N. Lane, J.M. Berney, and J. Holden. 2007. The timing and magnitude of coarse sediment transport events within an upland, temperate gravel-bed river. *Geomorphology* 82:152-182.

Robinson, D.A., C.M.K. Garnder, and J.D. Cooper. 1999. Measurement of relative permittivity in sandy soils using TDR capacitance and theta probes: comparison, including the effects of bulk soil electrical conductivity. *J. Hydrology.* 223: 198-211.

Robinson, D.A., S.B. Jones, J.M. Wraith, D. Or, and S.P. Friedman. 2003. A review of advances in dielectric and electrical conductivity measurement in soils using time domain reflectometry. *Vadose Zone Journal* 2: 444-475.

Robinson, D.A., T.J. Kelleners, J.D. Cooper, C.M.K. Gardner, P. Wilson, I. Lebron, and S. Logsdon. 2005. Evaluation of a capacitance probe frequency response model accounting for bulk electrical conductivity: Comparison with TDR and network analyzer measurements. *Vadose Zone Journal* 4: 992-1003.

Schoellhamer, D. H. 2001. Continuous monitoring of suspended sediment in rivers by use of optical sensors. *Proceedings of the Seventh Federal Interagency Sedimentation Conference*, Reno, NV, III-160 -167.

Tang, N. 2009. A Real-time control system for a frequency response-based permittivity sensor. MS thesis. Manhattan, KS: Kansas State University, Department of Biological and Agricultural Engineering.

Tazioli, G. S. 1980. The measurement of suspended sediment transport in natural streams using automatic radioisotope gauges. *Journal of Hydrology*. 47: 173-185.

Thorne, P. D., C. E. Vincent, P. J. Hardcastle, S. Rehman, and N. Pearson. 1991. Measuring suspended sediment concentrations using backscatter devices. *Marine Geology*. 98:7-16.

Trimble, S.W. 1975. Denudation studies: Can we assume stream steady state? *Science*. 188 (4194):1207-1208.

Trimble, S.W. 1999. Decreased rates of alluvial sediment storage in the Coon Creek Basin, Wisconsin, 1975-93. *Science*. 285(5431):1244-1246.

USEPA. 2002. National Water Quality Inventory: 2000 Report. *EPA 841-R-02-001*. USEPA: Washington, DC.

USGS. 2007. *http://co.water.usgs.gov/sediment/seddatabase.cfm* May, 9,2007.

Waltham, T. 2002. *Foundations of engineering geology*. 2nd. London ; New York: Spon Press.

Wang, Y., and Q. Liu. 2006. Comparison of Akaike information criterion (AIC) and Bayesian information criterion (BIC) in selection of stock-recruitment relationships. *Fisheries Research*. 77 (2): 220-225.

Wheeler, A.P., P.L. Angermeier, and A.E. Rosenberger. 2005. Impacts of new highways and subsequent landscape urbanization on stream habitat and biota. Reviews in Fisheries Science 13:141-164.

Wood, P.J., and P.D. Armitage. 1997. Biological effects of fine sediment in the lotic environment. *Environmental Management.* 21(2):203-217.

Wren, D., B. Barkdoll, R. Kuhnle, and R. Derrow. 2000. Field techniques for suspended-sediment measurement. *Journal of Hydraulic Engineering-ASCE.* 126(2):97-104.

Wren, D. and R. Kuhnle. 2002. Surrogate techniques for suspended sediment measurement. *Federal Interagency Workshop on Turbidity and Other Sediment Surrogates*. Reno, NV.

Wren, D. G., R. A. Kuhnle, and J. Chambers. 2003. Progress in Acoustic Suspended-Sediment Measurement in Laboratory Flumes. *Proceedings of World Water Congress 2003.* ASCE. Philadelphia, PA. 1-10.

Wren, D., S.Vadakapurapu, J. Chambers, R. Kuhnle, and B. Barkdoll. 2002. Suspended-sediment measurements in laboratory flumes using acoustic techniques. *HMEM* 2002, ASCE.

Appendix A: Raw Gain and Phase Data

A1. Gain Data

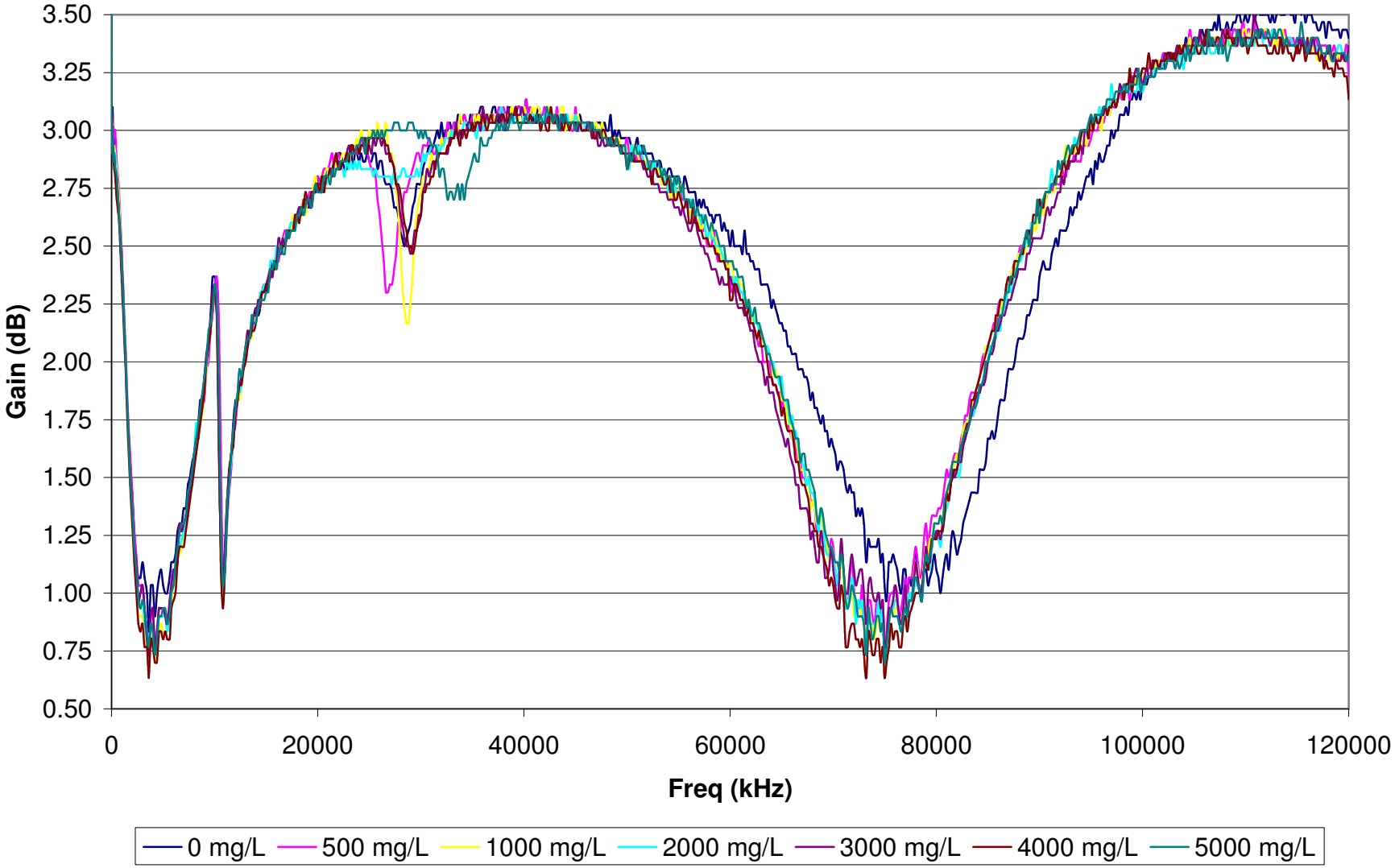

Figure A1.1. Gain data for the seven treatment levels of concentration (0-5000 mg/L) over then entire frequency range at 0 µS/cm and 10°C.

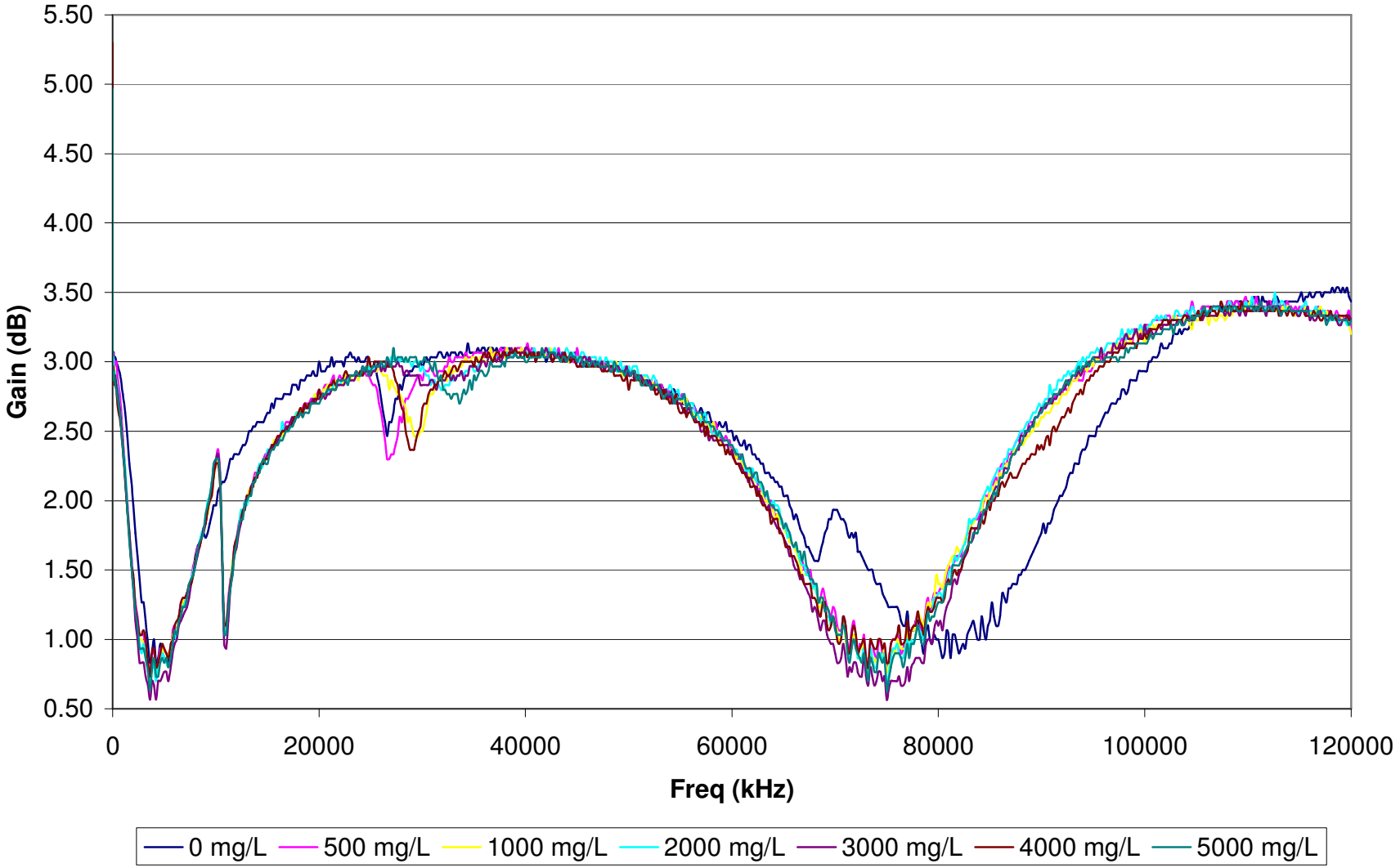

Figure A1.2. Gain data for the seven treatment levels of concentration (0-5000 mg/L) over then entire frequency range at 0 µS/cm and 20°C.

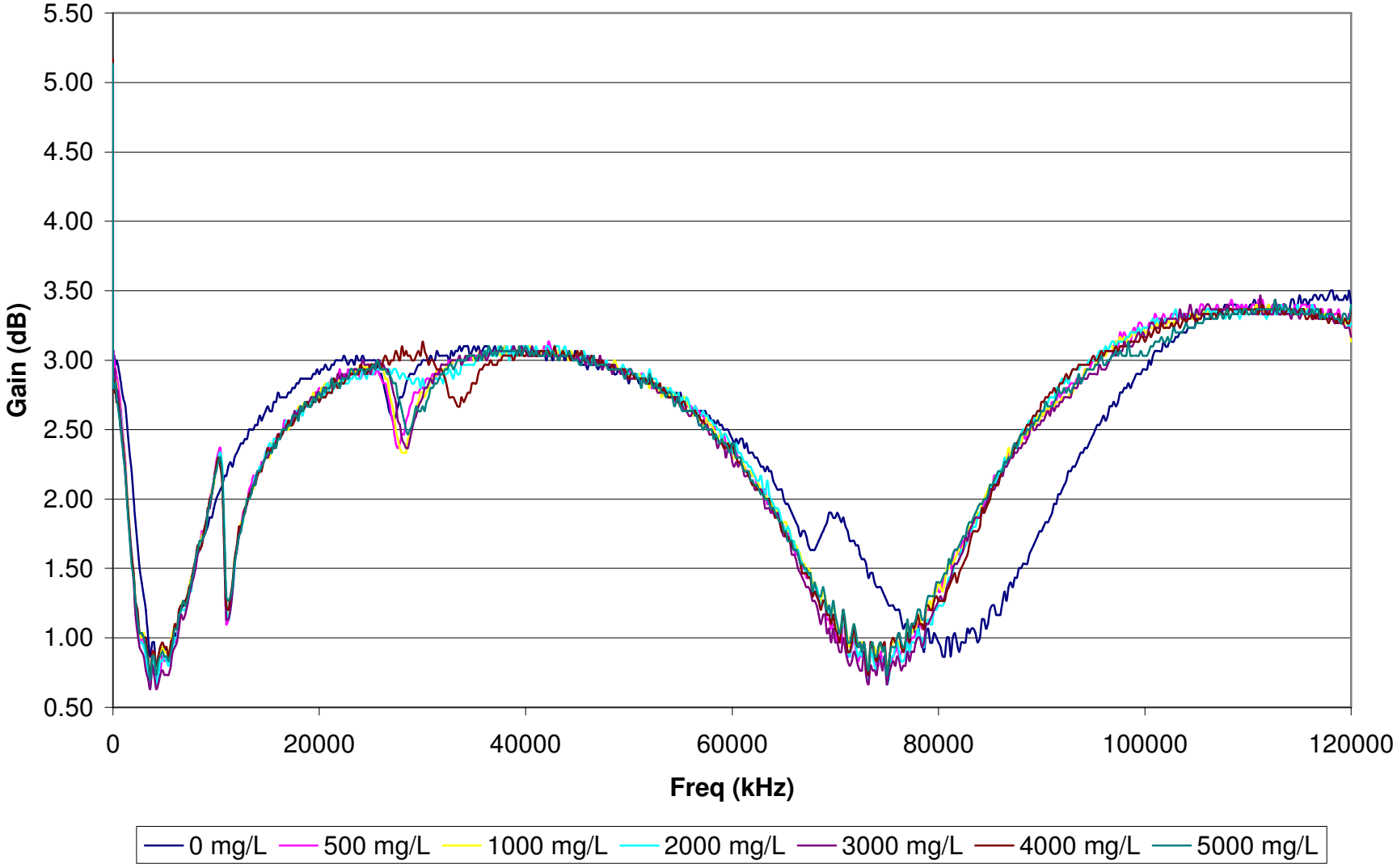

Figure A1.3. Gain data for the seven treatment levels of concentration (0-5000 mg/L) over then entire frequency range at 0 µS/cm and 30°C.

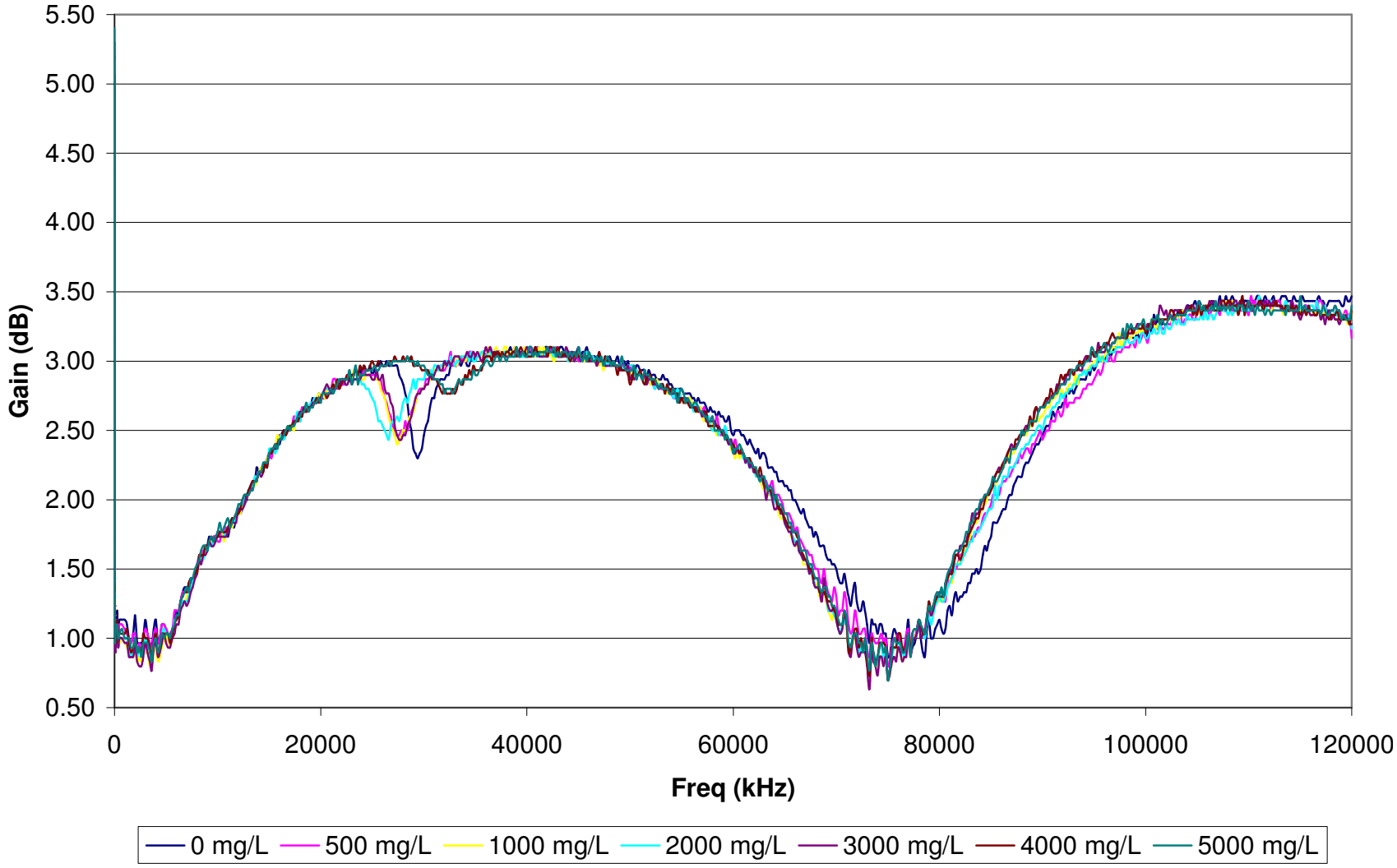

Figure A1.4. Gain data for the seven treatment levels of concentration (0-5000 mg/L) over then entire frequency range at 250 µS/cm and 10°C.

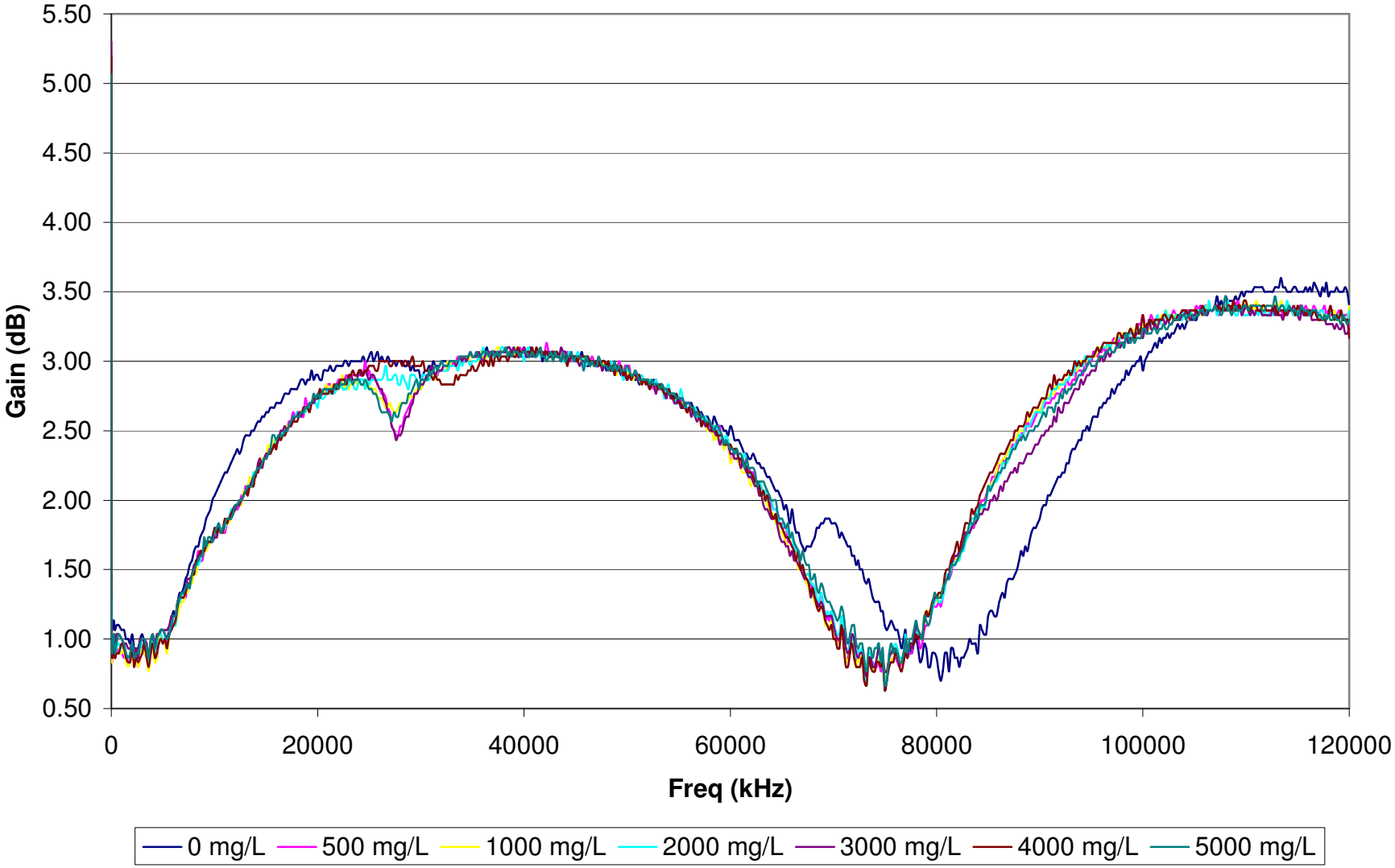

Figure A1.5. Gain data for the seven treatment levels of concentration (0-5000 mg/L) over then entire frequency range at 250 µS/cm and 20°C.

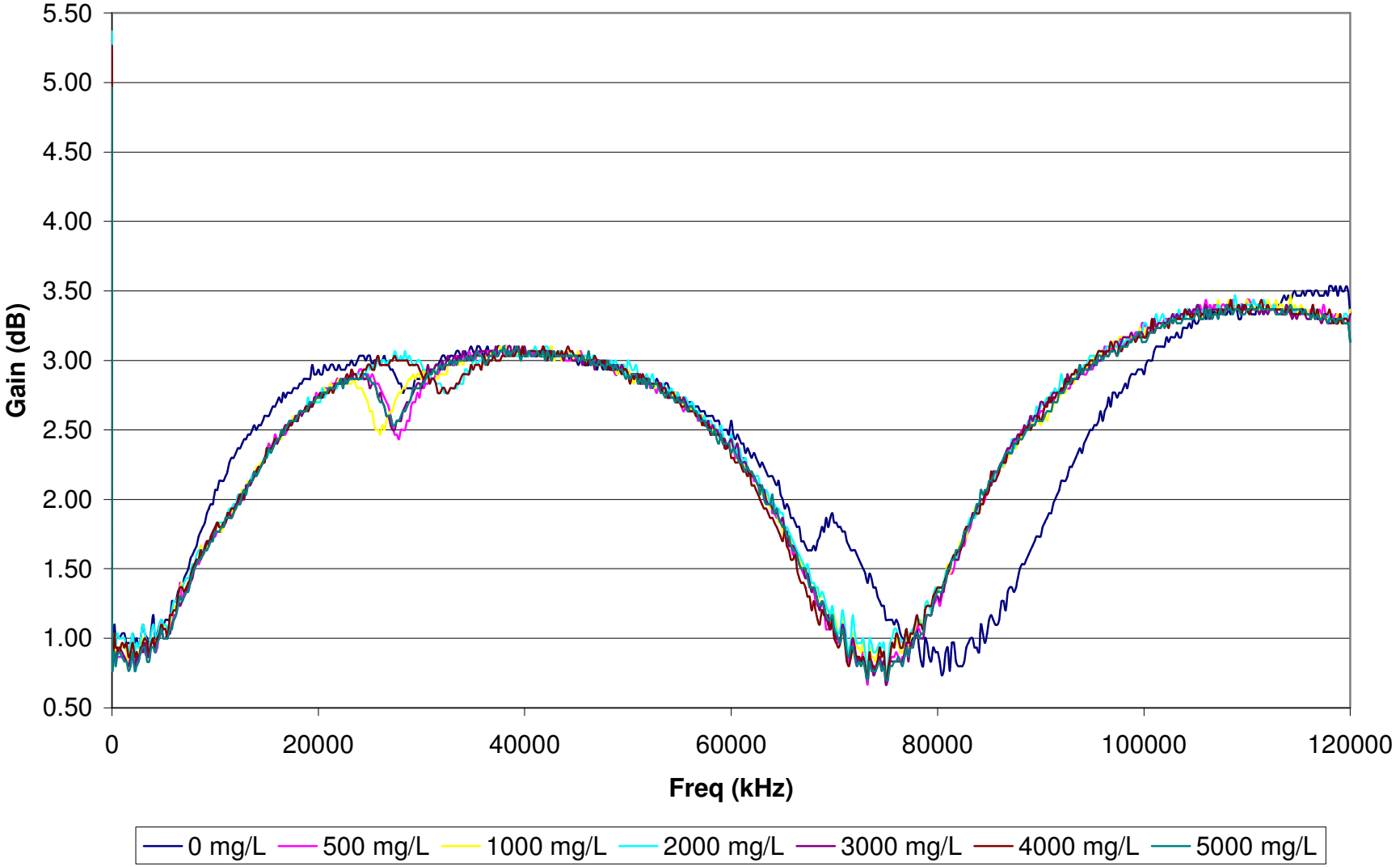

Figure A1.6. Gain data for the seven treatment levels of concentration (0-5000 mg/L) over then entire frequency range at 250 µS/cm and 30°C.

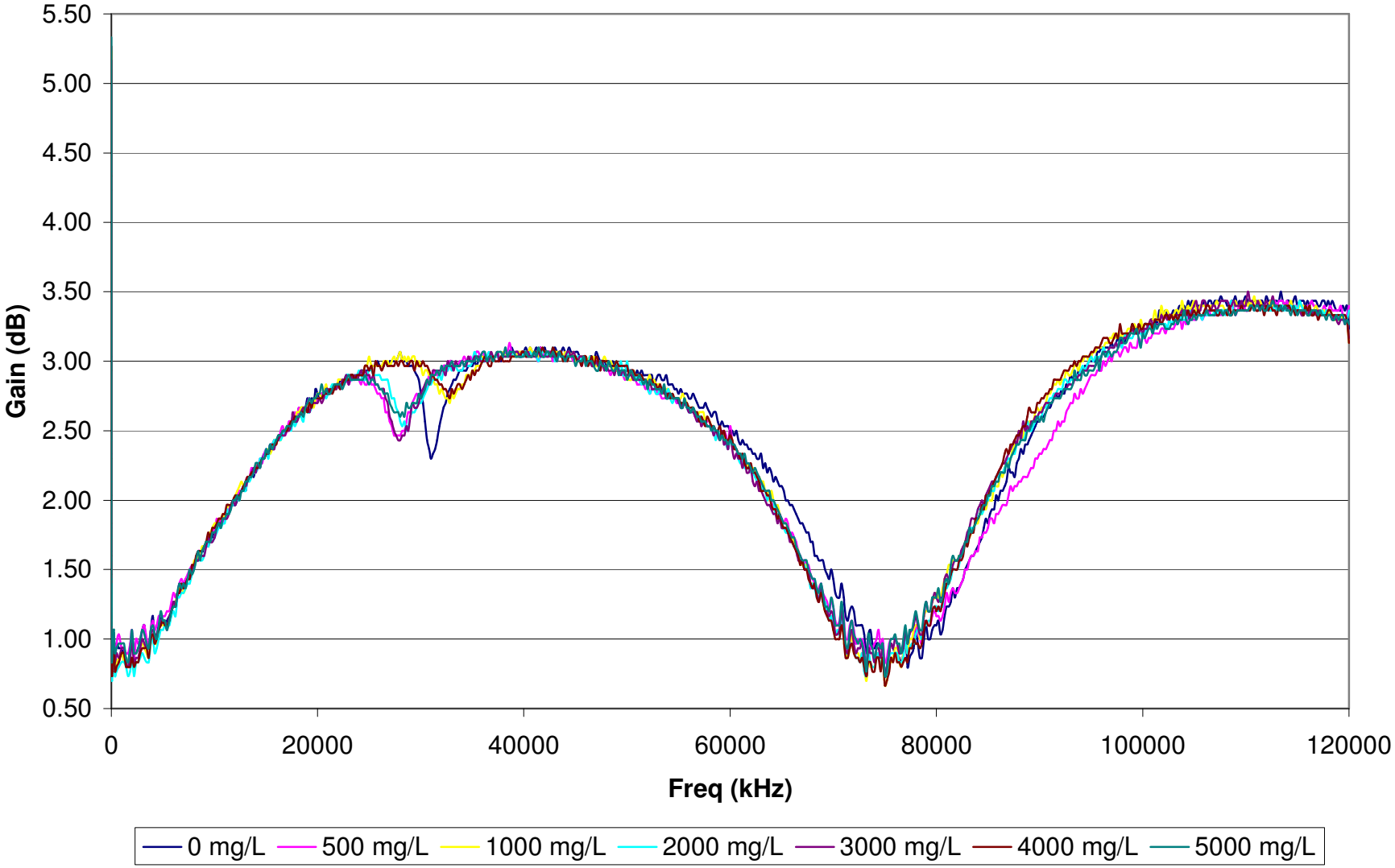

Figure A1.7. Gain data for the seven treatment levels of concentration (0-5000 mg/L) over then entire frequency range at 500 µS/cm and 10°C.

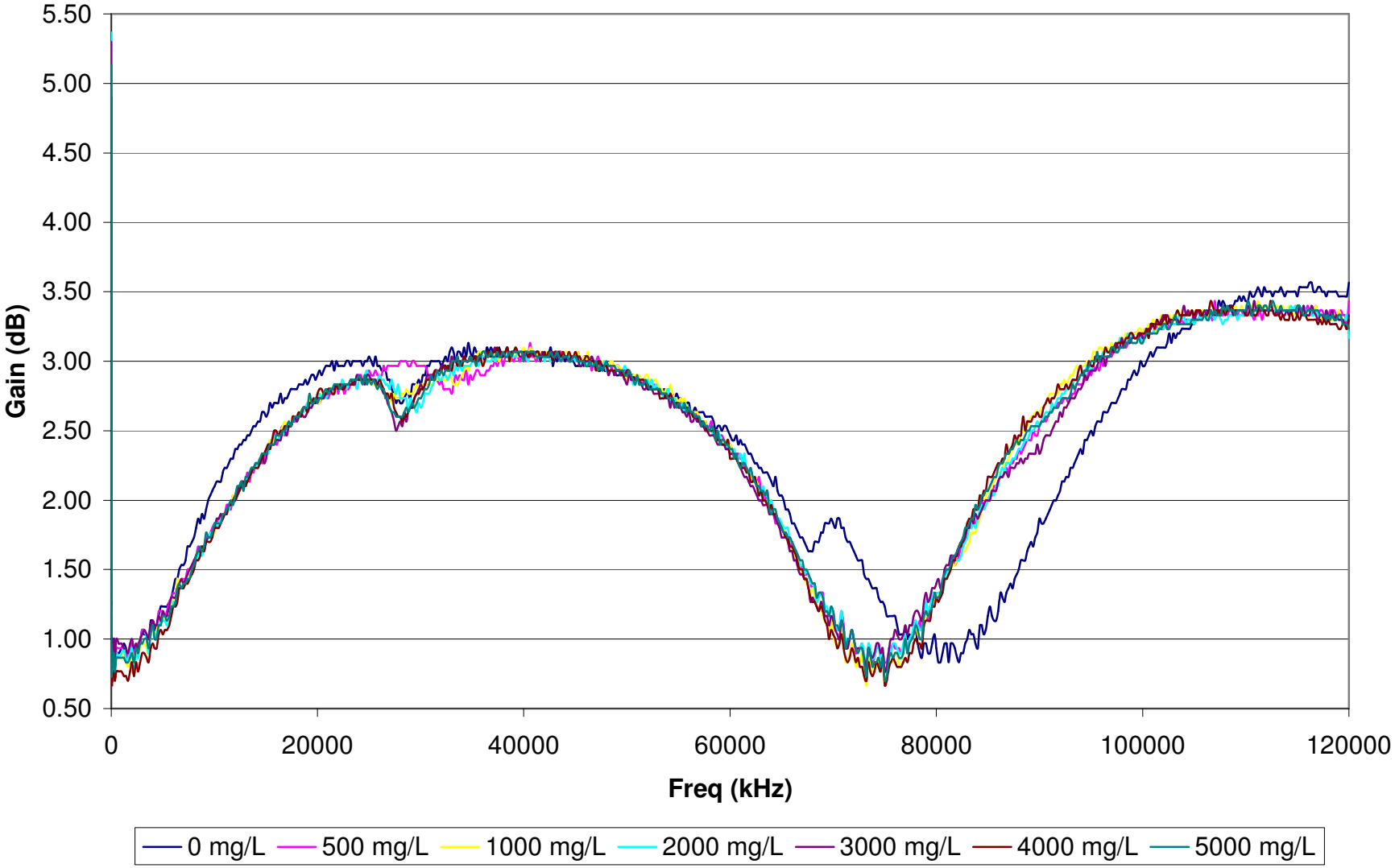

Figure A1.8. Gain data for the seven treatment levels of concentration (0-5000 mg/L) over then entire frequency range at 500 µS/cm and 20°C.

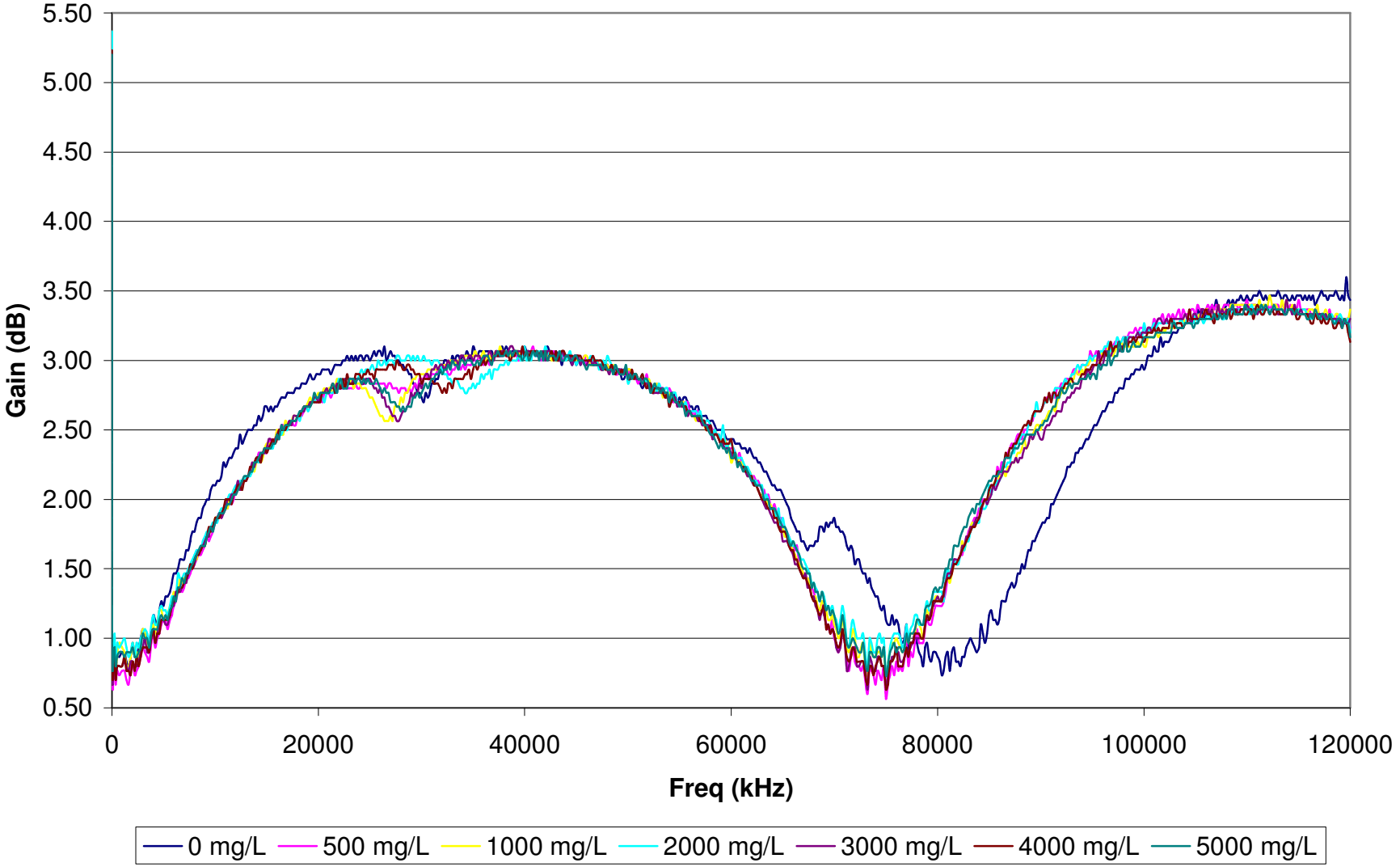

Figure A1.9. Gain data for the seven treatment levels of concentration (0-5000 mg/L) over then entire frequency range at 500 µS/cm and 30°C.

A2. Phase data

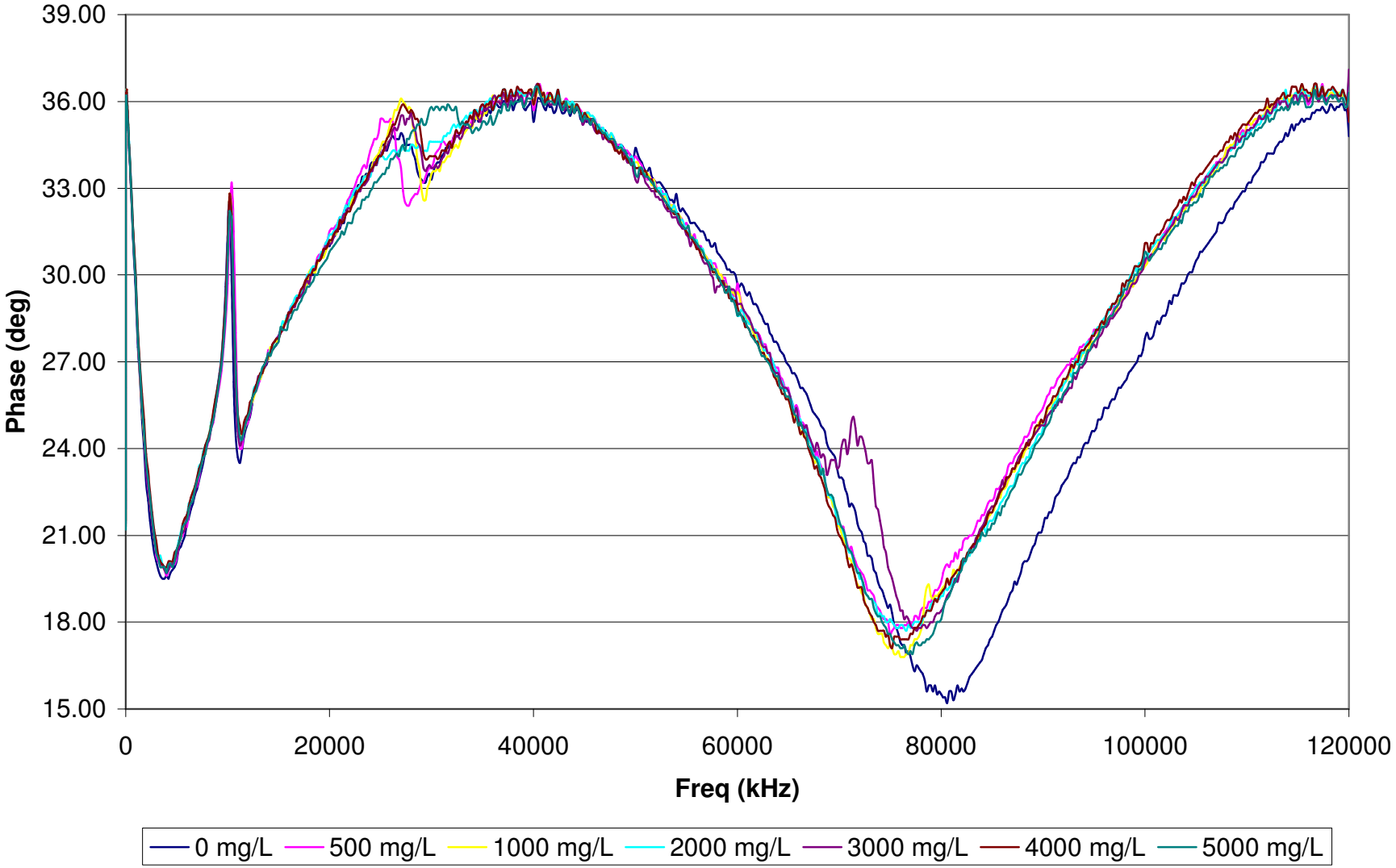

Figure A2.1. Phase data for the seven treatment levels of concentration (0-5000 mg/L) over then entire frequency range at 0 µS/cm and 10°C.

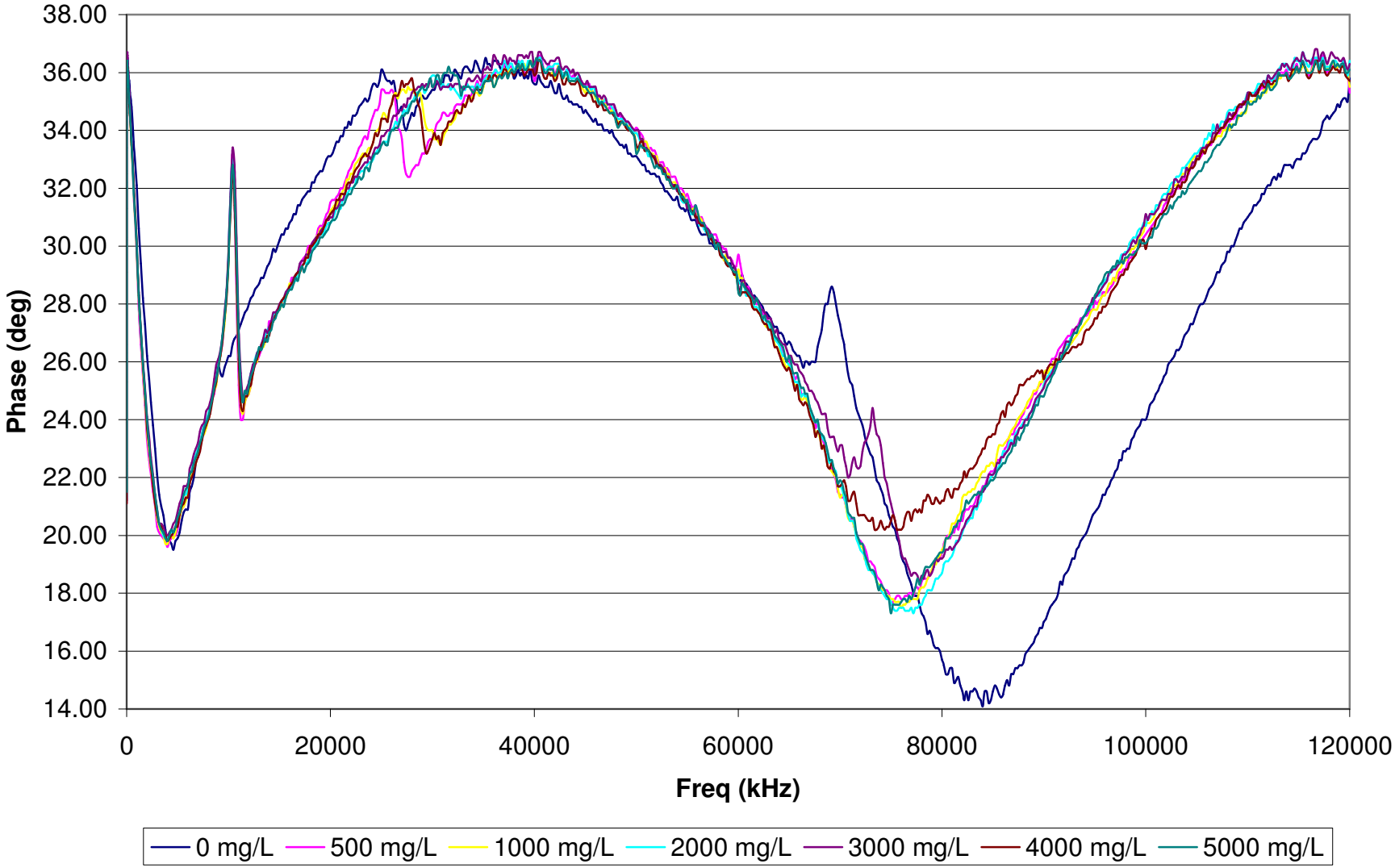

Figure A2.2. Phase data for the seven treatment levels of concentration (0-5000 mg/L) over then entire frequency range at 0 µS/cm and 20°C.

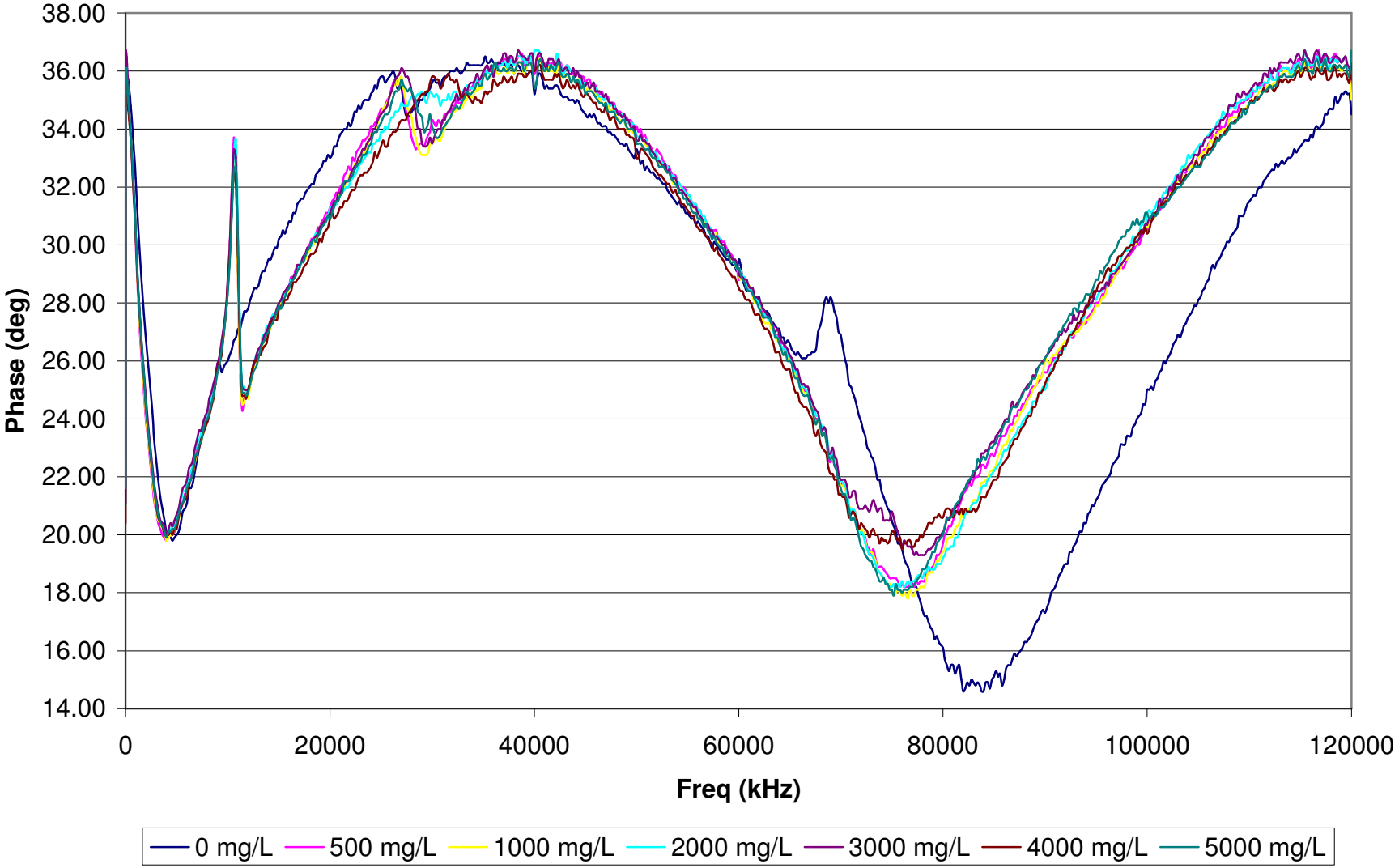

Figure A2.3. Phase data for the seven treatment levels of concentration (0-5000 mg/L) over then entire frequency range at 0 µS/cm and 30°C.

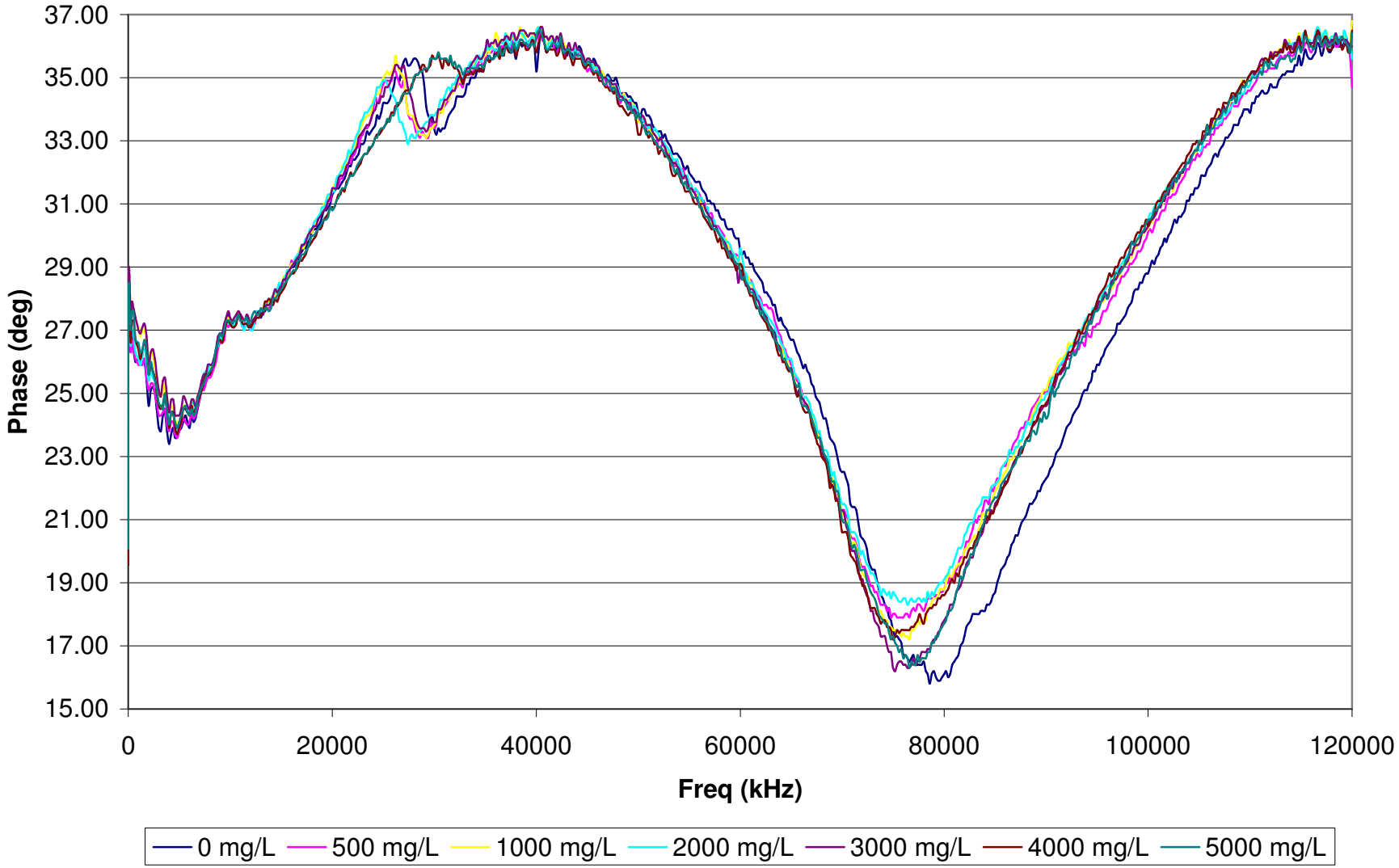

Figure A2.4. Phase data for the seven treatment levels of concentration (0-5000 mg/L) over then entire frequency range at 250 µS/cm and 10°C.

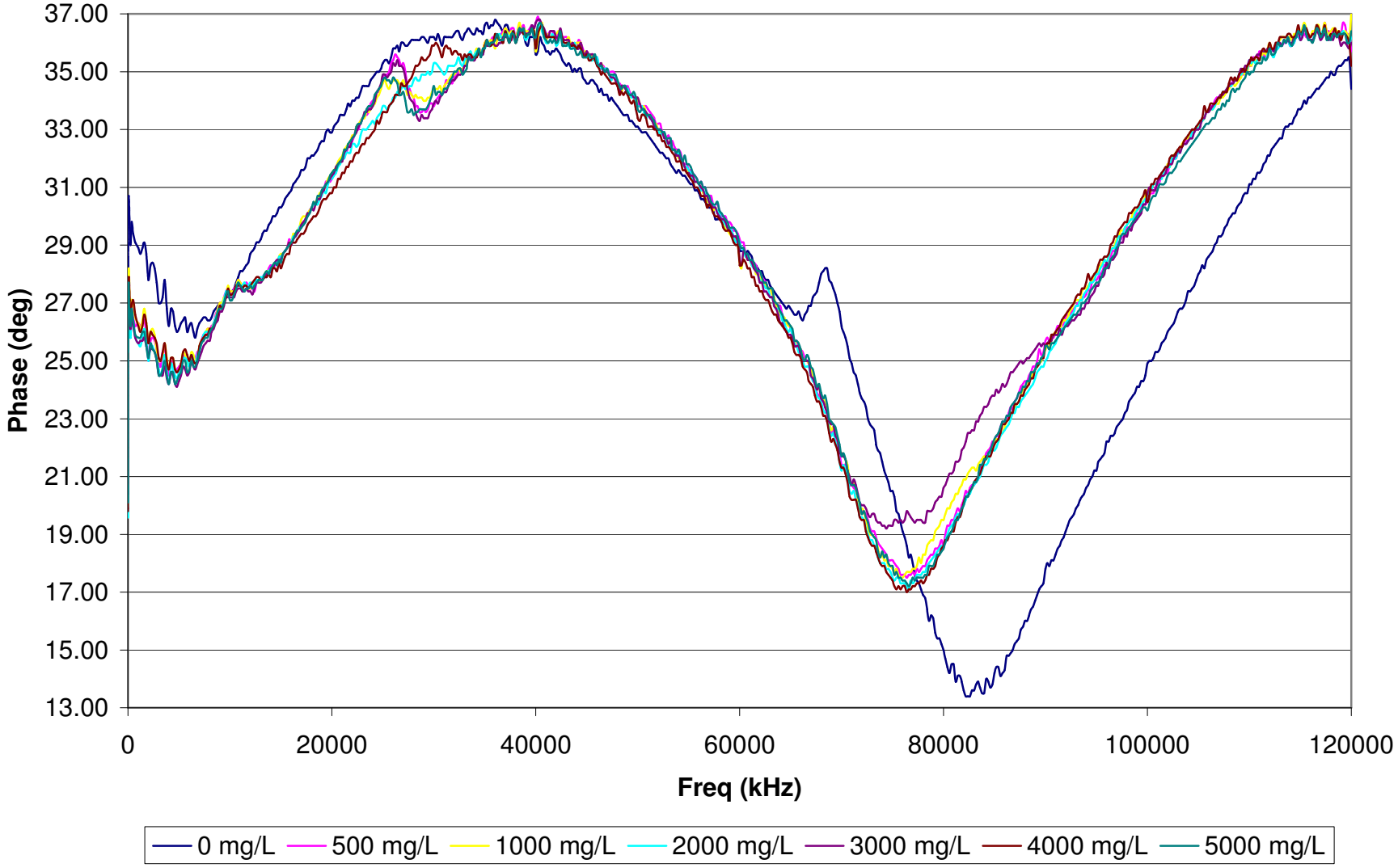

Figure A2.5. Phase data for the seven treatment levels of concentration (0-5000 mg/L) over then entire frequency range at 250 µS/cm and 20°C.

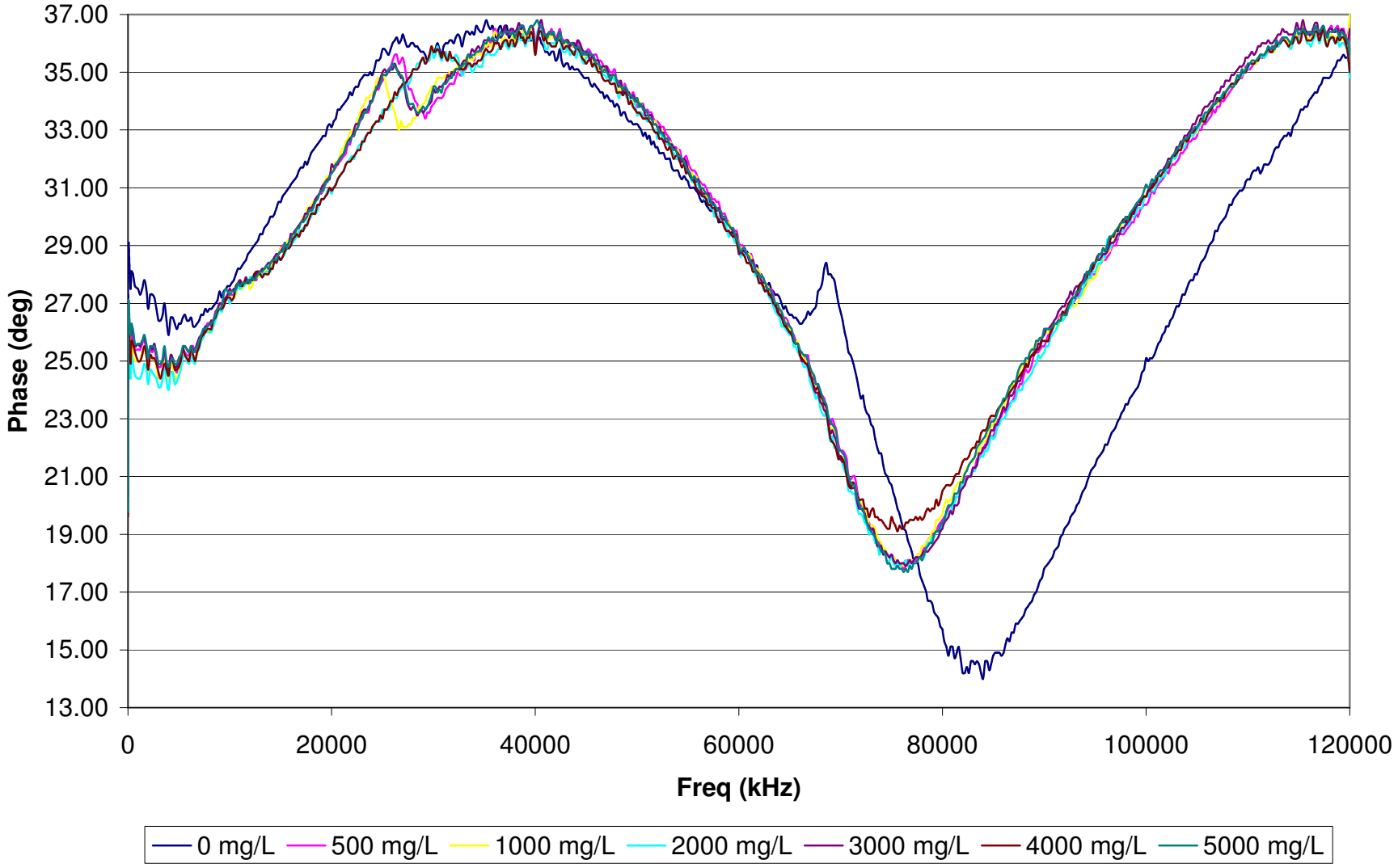

Figure A2.6. Phase data for the seven treatment levels of concentration (0-5000 mg/L) over then entire frequency range at 250 µS/cm and 30°C.

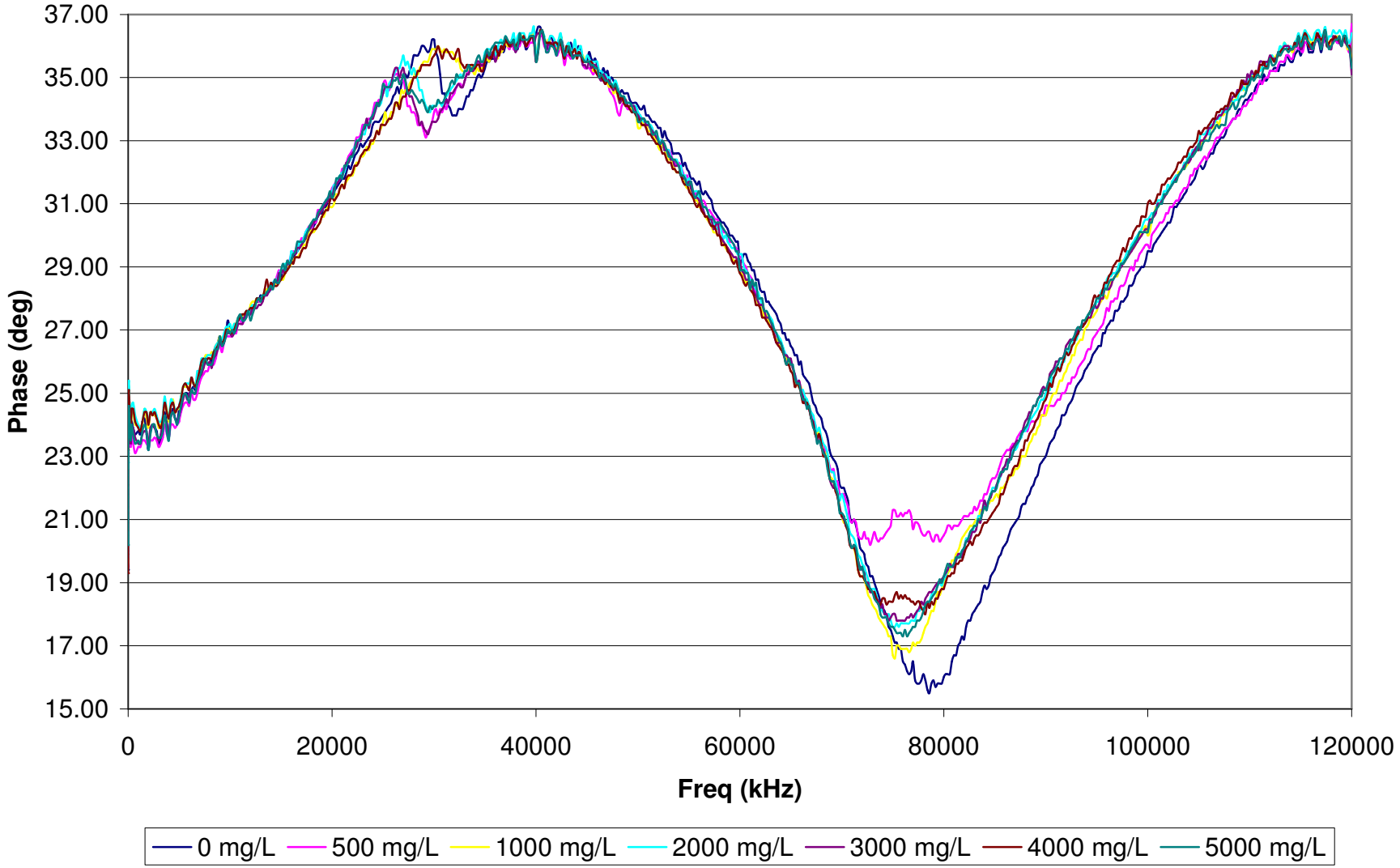

Figure A2.7. Phase data for the seven treatment levels of concentration (0-5000 mg/L) over then entire frequency range at 500 µS/cm and 10°C.

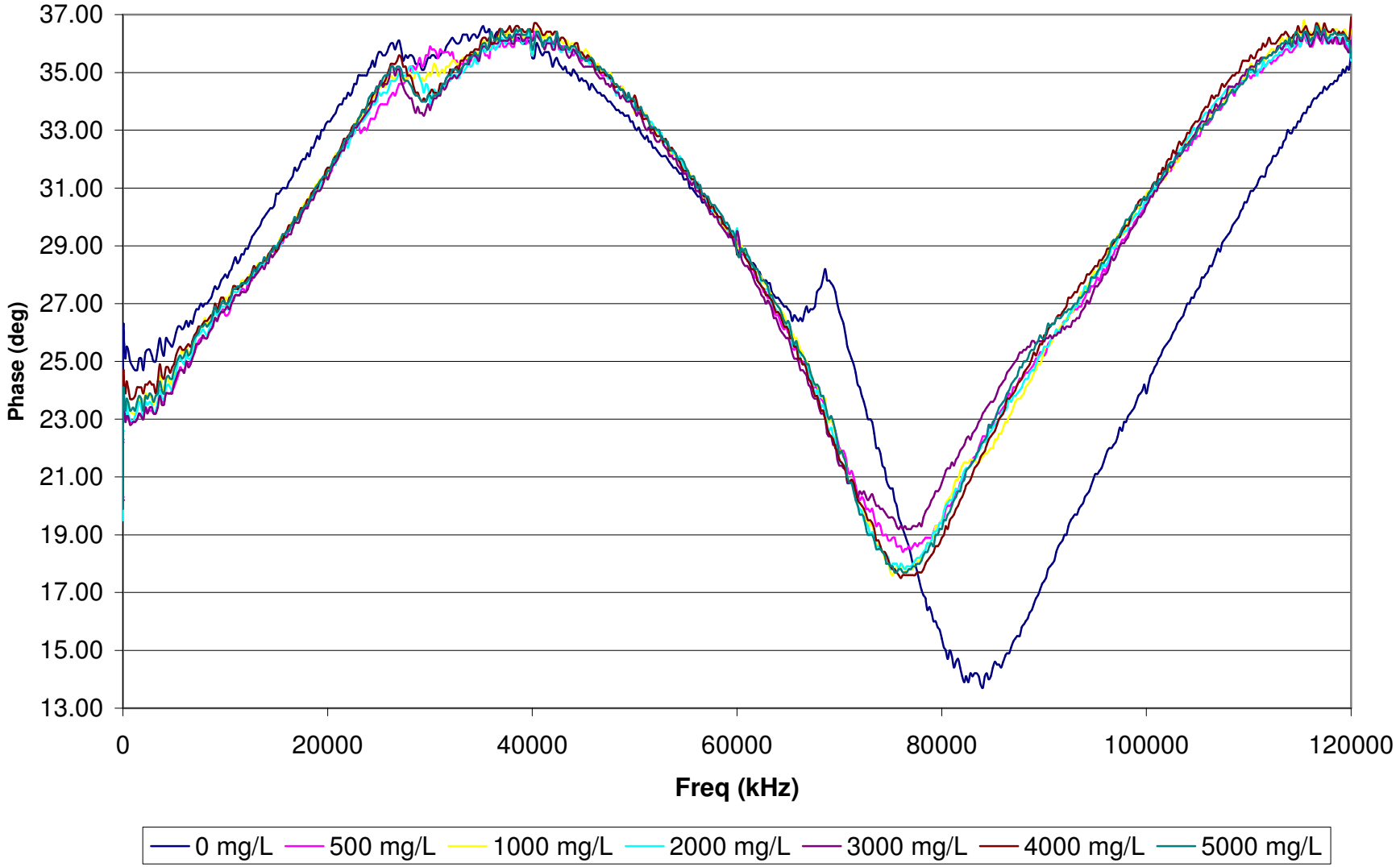

Figure A2.8. Phase data for the seven treatment levels of concentration (0-5000 mg/L) over then entire frequency range at 500 µS/cm and 20°C.

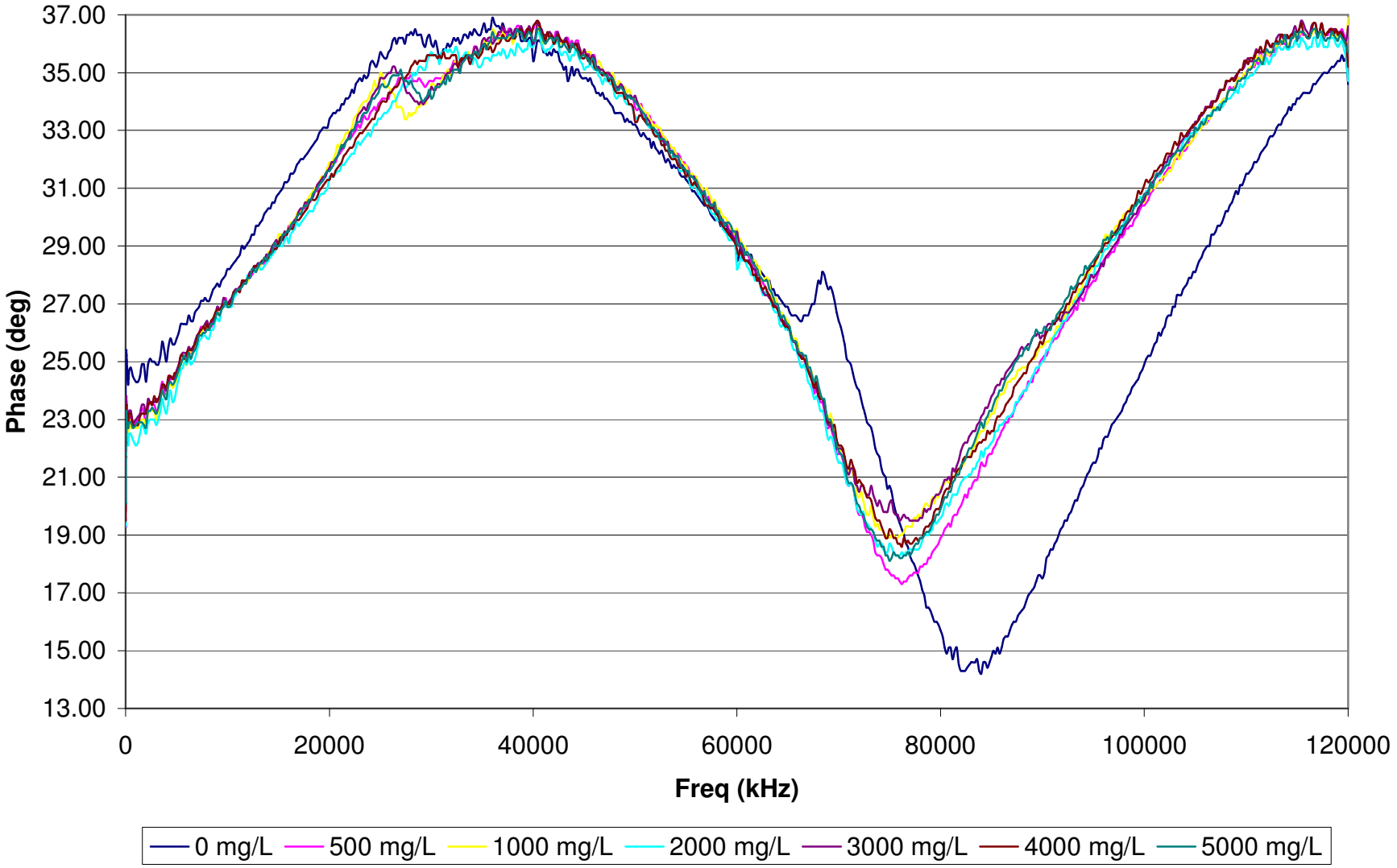

Figure A2.9. Phase data for the seven treatment levels of concentration (0-5000 mg/L) over then entire frequency range at 500 µS/cm and 30°C.

Appendix B: PLS model variables

B1. Mean and Standard Deviations for model variables of models 2A and 3A

Table B1. Mean and standard deviation for each x-variable included in PLS models 2A and 3A.

Variable Gain	Actual Freq (kHz)	St. Dev (dB)	Mean (dB)	Variable Phase	Actual Freq (kHz)	St. Dev (deg)	Mean (deg)
Intercept				p_freq1	0.05	0.694	20.500
temp		8.198*	20	p_freq2	0.3	5.406	25.836
cond		204.939**	250	p_freq3	0.55	5.553	27.840
g_freq1	0.05	0.137	5.123	p_freq4	0.8	5.510	28.238
g_freq2	0.3	0.554	2.193	p_freq5	1.41	5.385	28.823
g_freq3	0.55	0.834	1.802	p_freq6	7.94	5.380	28.999
g_freq4	0.8	0.886	1.727	p_freq7	44.67	5.186	29.433
g_freq5	1.41	0.949	1.642	p_freq8	251.19	5.118	28.280
g_freq6	7.94	0.969	1.615	p_freq9	1200	2.222	25.958
g_freq7	44.67	1.009	1.541	p_freq10	2200	1.314	24.336
g_freq8	251.19	0.911	1.618	p_freq11	3200	1.914	23.023
g_freq9	1200	0.627	1.351	p_freq12	4200	2.293	23.134
g_freq10	2200	0.229	0.992	p_freq13	5200	2.045	23.457
g_freq11	3200	0.087	0.954	p_freq14	6200	1.648	24.187
g_freq12	4200	0.127	0.881	p_freq15	7200	1.278	24.935
g_freq13	5200	0.126	1.009	p_freq16	8200	0.874	25.571
g_freq14	6200	0.108	1.161	p_freq17	9200	0.379	26.585
g_freq15	7200	0.073	1.363	p_freq18	10200	2.080	28.387
g_freq16	8200	0.054	1.598	p_freq19	11200	1.279	26.798
g_freq17	9200	0.122	1.790	p_freq20	12200	1.189	27.076
g_freq18	10200	0.223	1.980	p_freq21	13200	0.914	27.688
g_freq19	11200	0.338	1.731	p_freq22	14200	0.803	28.217
g_freq20	12200	0.165	1.979	p_freq23	15200	0.721	28.770
g_freq21	13200	0.119	2.135	p_freq24	16200	0.687	29.342
g_freq22	14200	0.106	2.274	p_freq25	17200	0.667	29.873
g_freq23	15200	0.087	2.385	p_freq26	18200	0.645	30.454
g_freq24	16200	0.079	2.481	p_freq27	19200	0.632	31.021
g_freq25	17200	0.070	2.566	p_freq28	20200	0.633	31.571
g_freq26	18200	0.065	2.645	p_freq29	21200	0.621	32.178
g_freq27	19200	0.058	2.711	p_freq30	22200	0.619	32.758
g_freq28	20200	0.052	2.772	p_freq31	23200	0.659	33.383
g_freq29	21200	0.049	2.819	p_freq32	24200	0.634	33.958
g_freq30	22200	0.045	2.858	p_freq33	25200	0.673	34.525
g_freq31	23200	0.048	2.891	p_freq34	26200	0.632	34.937
g_freq32	24200	0.050	2.906	p_freq35	27200	0.729	34.766
g_freq33	25200	0.076	2.901	p_freq36	28200	0.784	34.550
g_freq34	26200	0.141	2.838	p_freq37	29200	0.831	34.281
g_freq35	27200	0.192	2.751	p_freq38	30200	0.794	34.610
g_freq36	28200	0.194	2.720	p_freq39	31200	0.632	34.880
g_freq37	29200	0.159	2.780	p_freq40	32200	0.482	35.178
g_freq38	30200	0.093	2.853	p_freq41	33200	0.442	35.344
g_freq39	31200	0.074	2.892	p_freq42	34200	0.314	35.614
g_freq40	32200	0.071	2.919	p_freq43	35200	0.276	35.959
g_freq41	33200	0.091	2.951	p_freq44	36200	0.232	36.025
g_freq42	34200	0.072	2.978	p_freq45	37200	0.210	36.218
g_freq43	35200	0.053	3.004	p_freq46	38200	0.192	36.172

Table B1., continued. Mean and standard deviation for each x-variable included in PLS models 2A and 3A.

Variable	Actual Freq (kHz)	St. Dev (dB)	Mean (dB)	Variable	Actual Freq (kHz)	St. Dev (deg)	Mean (deg)
g_freq44	36200	0.037	3.029	p_freq47	39200	0.289	36.164
g_freq45	37200	0.027	3.045	p_freq48	40200	0.190	36.266
g_freq46	38200	0.018	3.058	p_freq49	41200	0.195	36.028
g_freq47	39200	0.045	3.066	p_freq50	42200	0.333	36.053
g_freq48	40200	0.016	3.059	p_freq51	43200	0.246	35.928
g_freq49	41200	0.012	3.059	p_freq52	44200	0.264	35.798
g_freq50	42200	0.039	3.055	p_freq53	45200	0.341	35.436
g_freq51	43200	0.015	3.043	p_freq54	46200	0.262	35.052
g_freq52	44200	0.013	3.033	p_freq55	47200	0.269	34.786
g_freq53	45200	0.041	3.020	p_freq56	48200	0.289	34.319
g_freq54	46200	0.016	3.003	p_freq57	49200	0.262	34.084
g_freq55	47200	0.015	2.985	p_freq58	50200	0.262	33.672
g_freq56	48200	0.034	2.962	p_freq59	51200	0.295	33.308
g_freq57	49200	0.016	2.933	p_freq60	52200	0.234	32.861
g_freq58	50200	0.018	2.904	p_freq61	53200	0.227	32.438
g_freq59	51200	0.044	2.875	p_freq62	54200	0.214	31.975
g_freq60	52200	0.020	2.839	p_freq63	55200	0.215	31.472
g_freq61	53200	0.021	2.799	p_freq64	56200	0.212	30.990
g_freq62	54200	0.023	2.755	p_freq65	57200	0.207	30.488
g_freq63	55200	0.043	2.711	p_freq66	58200	0.239	29.992
g_freq64	56200	0.031	2.649	p_freq67	59200	0.214	29.522
g_freq65	57200	0.035	2.588	p_freq68	60200	0.241	28.954
g_freq66	58200	0.066	2.525	p_freq69	61200	0.230	28.451
g_freq67	59200	0.048	2.448	p_freq70	62200	0.245	27.834
g_freq68	60200	0.056	2.371	p_freq71	63200	0.251	27.299
g_freq69	61200	0.063	2.284	p_freq72	64200	0.308	26.548
g_freq70	62200	0.089	2.187	p_freq73	65200	0.347	26.000
g_freq71	63200	0.082	2.072	p_freq74	66200	0.488	25.200
g_freq72	64200	0.106	1.964	p_freq75	67200	0.756	24.596
g_freq73	65200	0.095	1.818	p_freq76	68200	1.288	23.902
g_freq74	66200	0.099	1.684	p_freq77	69200	1.604	23.150
g_freq75	67200	0.125	1.524	p_freq78	70200	1.483	22.132
g_freq76	68200	0.136	1.390	p_freq79	71200	1.410	21.235
g_freq77	69200	0.213	1.257	p_freq80	72200	1.442	20.348
g_freq78	70200	0.255	1.136	p_freq81	73200	1.460	19.707
g_freq79	71200	0.259	1.003	p_freq82	74200	1.219	18.947
g_freq80	72200	0.238	0.968	p_freq83	75200	1.228	18.460
g_freq81	73200	0.219	0.804	p_freq84	76200	1.000	18.150
g_freq82	74200	0.148	0.935	p_freq85	77200	0.974	18.050
g_freq83	75200	0.127	0.791	p_freq86	78200	0.989	18.173
g_freq84	76200	0.105	0.935	p_freq87	79200	1.242	18.469
g_freq85	77200	0.056	0.901	p_freq88	80200	1.541	18.877
g_freq86	78200	0.061	1.041	p_freq89	81200	1.855	19.372
g_freq87	79200	0.096	1.125	p_freq90	82200	2.106	19.937
g_freq88	80200	0.149	1.247	p_freq91	83200	2.168	20.432
g_freq89	81200	0.204	1.372	p_freq92	84200	2.317	21.019

Table B1., continued. Mean and standard deviation for each x-variable included in PLS models 2A and 3A.

Variable	Actual Freq (kHz)	St. Dev (dB)	Mean (dB)	Variable	Actual Freq (kHz)	St. Dev (deg)	Mean (deg)
g_freq90	82200	0.238	1.516	p_freq93	85200	2.386	21.590
g_freq91	83200	0.235	1.704	p_freq94	86200	2.471	22.209
g_freq92	84200	0.257	1.845	p_freq95	87200	2.497	22.831
g_freq93	85200	0.266	1.985	p_freq96	88200	2.485	23.426
g_freq94	86200	0.279	2.110	p_freq97	89200	2.439	24.022
g_freq95	87200	0.284	2.231	p_freq98	90200	2.356	24.563
g_freq96	88200	0.276	2.339	p_freq99	91200	2.284	25.133
g_freq97	89200	0.268	2.443	p_freq100	92200	2.206	25.677
g_freq98	90200	0.248	2.533	p_freq101	93200	2.141	26.196
g_freq99	91200	0.228	2.630	p_freq102	94200	2.086	26.750
g_freq100	92200	0.206	2.721	p_freq103	95200	2.034	27.297
g_freq101	93200	0.185	2.803	p_freq104	96200	1.983	27.878
g_freq102	94200	0.166	2.878	p_freq105	97200	1.936	28.428
g_freq103	95200	0.147	2.951	p_freq106	98200	1.886	28.954
g_freq104	96200	0.132	3.016	p_freq107	99200	1.842	29.483
g_freq105	97200	0.116	3.068	p_freq108	100200	1.780	30.028
g_freq106	98200	0.102	3.117	p_freq109	101200	1.735	30.556
g_freq107	99200	0.088	3.162	p_freq110	102200	1.683	31.052
g_freq108	100200	0.076	3.191	p_freq111	103200	1.610	31.561
g_freq109	101200	0.064	3.239	p_freq112	104200	1.549	32.068
g_freq110	102200	0.067	3.275	p_freq113	105200	1.488	32.555
g_freq111	103200	0.043	3.298	p_freq114	106200	1.432	33.028
g_freq112	104200	0.035	3.325	p_freq115	107200	1.359	33.449
g_freq113	105200	0.030	3.343	p_freq116	108200	1.317	33.922
g_freq114	106200	0.028	3.356	p_freq117	109200	1.240	34.334
g_freq115	107200	0.028	3.370	p_freq118	110200	1.187	34.737
g_freq116	108200	0.035	3.382	p_freq119	111200	1.132	35.028
g_freq117	109200	0.030	3.384	p_freq120	112200	1.035	35.294
g_freq118	110200	0.030	3.383	p_freq121	113200	0.996	35.594
g_freq119	111200	0.038	3.394	p_freq122	114200	0.872	35.666
g_freq120	112200	0.036	3.385	p_freq123	115200	0.793	35.965
g_freq121	113200	0.043	3.388	p_freq124	116200	0.640	35.918
g_freq122	114200	0.040	3.389	p_freq125	117200	0.563	36.124
g_freq123	115200	0.045	3.383	p_freq126	118200	0.490	36.147
g_freq124	116200	0.049	3.366	p_freq127	119200	0.320	36.187
g_freq125	117200	0.051	3.352				
g_freq126	118200	0.059	3.346				
g_freq127	119200	0.061	3.327				

*Temperature is in degrees C

**Specific Conductivity is in µS/cm

B2. Mean and Standard Deviations for model variables of model 6B

Table B2. Mean and standard deviation for each x-variable included in PLS model 6B.

Variable Gain	Actual Freq (kHz)	St. Dev (dB)	Mean (dB)	Variable Phase	Actual Freq (kHz)	St. Dev (deg)	Mean (deg)
Intercept				p_freq1	0.05	0.687	20.510
temp		8.203*	20	p_freq2	0.3	5.439	25.762
cond		205.076**	250	p_freq3	0.55	5.607	27.734
g_freq1	0.05	0.135	5.143	p_freq4	0.8	5.565	28.121
g_freq2	0.3	0.551	2.181	p_freq5	1.41	5.446	28.701
g_freq3	0.55	0.834	1.787	p_freq6	7.94	5.431	28.887
g_freq4	0.8	0.886	1.714	p_freq7	44.67	5.255	29.292
g_freq5	1.41	0.948	1.628	p_freq8	251.19	5.156	28.145
g_freq6	7.94	0.971	1.593	p_freq9	1200	2.109	25.771
g_freq7	44.67	1.008	1.528	p_freq10	2200	1.119	24.158
g_freq8	251.19	0.909	1.602	p_freq11	3200	1.815	22.897
g_freq9	1200	0.607	1.326	p_freq12	4200	2.177	23.047
g_freq10	2200	0.179	0.961	p_freq13	5200	1.924	23.395
g_freq11	3200	0.069	0.934	p_freq14	6200	1.548	24.138
g_freq12	4200	0.126	0.872	p_freq15	7200	1.211	24.888
g_freq13	5200	0.122	1.002	p_freq16	8200	0.820	25.530
g_freq14	6200	0.097	1.152	p_freq17	9200	0.287	26.556
g_freq15	7200	0.056	1.351	p_freq18	10200	2.098	28.474
g_freq16	8200	0.036	1.586	p_freq19	11200	1.226	26.701
g_freq17	9200	0.120	1.779	p_freq20	12200	1.113	26.916
g_freq18	10200	0.233	1.970	p_freq21	13200	0.774	27.521
g_freq19	11200	0.316	1.676	p_freq22	14200	0.590	28.051
g_freq20	12200	0.117	1.939	p_freq23	15200	0.450	28.586
g_freq21	13200	0.051	2.100	p_freq24	16200	0.373	29.155
g_freq22	14200	0.026	2.239	p_freq25	17200	0.318	29.684
g_freq23	15200	0.016	2.356	p_freq26	18200	0.281	30.272
g_freq24	16200	0.014	2.456	p_freq27	19200	0.262	30.836
g_freq25	17200	0.013	2.544	p_freq28	20200	0.268	31.398
g_freq26	18200	0.015	2.623	p_freq29	21200	0.298	32.004
g_freq27	19200	0.014	2.693	p_freq30	22200	0.347	32.592
g_freq28	20200	0.016	2.755	p_freq31	23200	0.412	33.240
g_freq29	21200	0.020	2.804	p_freq32	24200	0.473	33.815
g_freq30	22200	0.021	2.844	p_freq33	25200	0.548	34.402
g_freq31	23200	0.024	2.876	p_freq34	26200	0.542	34.821
g_freq32	24200	0.038	2.894	p_freq35	27200	0.659	34.662
g_freq33	25200	0.070	2.886	p_freq36	28200	0.702	34.423
g_freq34	26200	0.140	2.826	p_freq37	29200	0.767	34.168
g_freq35	27200	0.193	2.740	p_freq38	30200	0.739	34.535
g_freq36	28200	0.198	2.709	p_freq39	31200	0.561	34.819
g_freq37	29200	0.155	2.780	p_freq40	32200	0.343	35.112
g_freq38	30200	0.079	2.856	p_freq41	33200	0.169	35.292
g_freq39	31200	0.039	2.892	p_freq42	34200	0.164	35.546
g_freq40	32200	0.062	2.911	p_freq43	35200	0.177	35.902
g_freq41	33200	0.081	2.937	p_freq44	36200	0.173	36.003
g_freq42	34200	0.072	2.968	p_freq45	37200	0.184	36.210
g_freq43	35200	0.051	2.996	p_freq46	38200	0.198	36.178

Table B2., continued. Mean and standard deviation for each x-variable included in PLS model 6B.

Variable	Actual Freq (kHz)	St. Dev (dB)	Mean (dB)	Variable	Actual Freq (kHz)	St. Dev (deg)	Mean (deg)
g_freq44	36200	0.035	3.023	p_freq47	39200	0.142	36.211
g_freq45	37200	0.022	3.040	p_freq48	40200	0.150	36.308
g_freq46	38200	0.018	3.056	p_freq49	41200	0.139	36.081
g_freq47	39200	0.015	3.061	p_freq50	42200	0.133	36.138
g_freq48	40200	0.017	3.058	p_freq51	43200	0.125	35.998
g_freq49	41200	0.012	3.059	p_freq52	44200	0.111	35.875
g_freq50	42200	0.013	3.052	p_freq53	45200	0.123	35.532
g_freq51	43200	0.014	3.044	p_freq54	46200	0.127	35.124
g_freq52	44200	0.011	3.034	p_freq55	47200	0.130	34.859
g_freq53	45200	0.014	3.018	p_freq56	48200	0.147	34.396
g_freq54	46200	0.014	3.004	p_freq57	49200	0.130	34.150
g_freq55	47200	0.013	2.985	p_freq58	50200	0.141	33.724
g_freq56	48200	0.014	2.960	p_freq59	51200	0.129	33.375
g_freq57	49200	0.014	2.934	p_freq60	52200	0.137	32.900
g_freq58	50200	0.017	2.904	p_freq61	53200	0.134	32.469
g_freq59	51200	0.015	2.872	p_freq62	54200	0.127	31.996
g_freq60	52200	0.017	2.838	p_freq63	55200	0.133	31.491
g_freq61	53200	0.018	2.795	p_freq64	56200	0.145	30.989
g_freq62	54200	0.018	2.751	p_freq65	57200	0.147	30.477
g_freq63	55200	0.021	2.703	p_freq66	58200	0.159	29.988
g_freq64	56200	0.022	2.640	p_freq67	59200	0.163	29.493
g_freq65	57200	0.025	2.579	p_freq68	60200	0.191	28.908
g_freq66	58200	0.027	2.509	p_freq69	61200	0.166	28.400
g_freq67	59200	0.031	2.433	p_freq70	62200	0.184	27.779
g_freq68	60200	0.036	2.354	p_freq71	63200	0.190	27.233
g_freq69	61200	0.035	2.263	p_freq72	64200	0.204	26.466
g_freq70	62200	0.039	2.158	p_freq73	65200	0.207	25.886
g_freq71	63200	0.044	2.044	p_freq74	66200	0.236	25.030
g_freq72	64200	0.045	1.931	p_freq75	67200	0.253	24.337
g_freq73	65200	0.050	1.785	p_freq76	68200	0.272	23.454
g_freq74	66200	0.051	1.650	p_freq77	69200	0.337	22.601
g_freq75	67200	0.056	1.484	p_freq78	70200	0.441	21.631
g_freq76	68200	0.059	1.340	p_freq79	71200	0.736	20.804
g_freq77	69200	0.062	1.176	p_freq80	72200	0.987	19.969
g_freq78	70200	0.062	1.040	p_freq81	73200	1.161	19.384
g_freq79	71200	0.059	0.906	p_freq82	74200	0.983	18.698
g_freq80	72200	0.061	0.879	p_freq83	75200	1.121	18.296
g_freq81	73200	0.054	0.725	p_freq84	76200	0.976	18.101
g_freq82	74200	0.055	0.883	p_freq85	77200	0.966	18.138
g_freq83	75200	0.047	0.748	p_freq86	78200	0.860	18.400
g_freq84	76200	0.057	0.907	p_freq87	79200	0.825	18.865
g_freq85	77200	0.051	0.894	p_freq88	80200	0.792	19.424
g_freq86	78200	0.053	1.052	p_freq89	81200	0.755	20.055
g_freq87	79200	0.046	1.158	p_freq90	82200	0.712	20.718
g_freq88	80200	0.056	1.300	p_freq91	83200	0.685	21.240
g_freq89	81200	0.053	1.448	p_freq92	84200	0.662	21.884

Table B2., continued. Mean and standard deviation for each x-variable included in PLS model 6B.

Variable	Actual Freq (kHz)	St. Dev (dB)	Mean (dB)	Variable	Actual Freq (kHz)	St. Dev (deg)	Mean (deg)
g_freq90	82200	0.054	1.605	p_freq93	85200	0.647	22.477
g_freq91	83200	0.055	1.792	p_freq94	86200	0.632	23.123
g_freq92	84200	0.058	1.940	p_freq95	87200	0.611	23.753
g_freq93	85200	0.055	2.082	p_freq96	88200	0.575	24.343
g_freq94	86200	0.060	2.210	p_freq97	89200	0.520	24.923
g_freq95	87200	0.067	2.331	p_freq98	90200	0.454	25.433
g_freq96	88200	0.075	2.435	p_freq99	91200	0.398	25.976
g_freq97	89200	0.081	2.534	p_freq100	92200	0.360	26.490
g_freq98	90200	0.081	2.615	p_freq101	93200	0.355	26.982
g_freq99	91200	0.077	2.706	p_freq102	94200	0.344	27.515
g_freq100	92200	0.069	2.788	p_freq103	95200	0.332	28.041
g_freq101	93200	0.059	2.864	p_freq104	96200	0.327	28.604
g_freq102	94200	0.049	2.933	p_freq105	97200	0.305	29.137
g_freq103	95200	0.043	2.999	p_freq106	98200	0.271	29.644
g_freq104	96200	0.037	3.058	p_freq107	99200	0.277	30.156
g_freq105	97200	0.035	3.106	p_freq108	100200	0.238	30.677
g_freq106	98200	0.037	3.149	p_freq109	101200	0.226	31.189
g_freq107	99200	0.036	3.188	p_freq110	102200	0.220	31.676
g_freq108	100200	0.033	3.214	p_freq111	103200	0.220	32.148
g_freq109	101200	0.031	3.256	p_freq112	104200	0.214	32.632
g_freq110	102200	0.028	3.285	p_freq113	105200	0.213	33.094
g_freq111	103200	0.027	3.307	p_freq114	106200	0.210	33.547
g_freq112	104200	0.026	3.330	p_freq115	107200	0.211	33.939
g_freq113	105200	0.025	3.345	p_freq116	108200	0.203	34.405
g_freq114	106200	0.025	3.356	p_freq117	109200	0.201	34.780
g_freq115	107200	0.025	3.367	p_freq118	110200	0.198	35.163
g_freq116	108200	0.025	3.376	p_freq119	111200	0.188	35.442
g_freq117	109200	0.023	3.378	p_freq120	112200	0.177	35.664
g_freq118	110200	0.021	3.376	p_freq121	113200	0.162	35.958
g_freq119	111200	0.022	3.385	p_freq122	114200	0.149	35.973
g_freq120	112200	0.021	3.375	p_freq123	115200	0.134	36.243
g_freq121	113200	0.020	3.375	p_freq124	116200	0.132	36.144
g_freq122	114200	0.020	3.376	p_freq125	117200	0.124	36.318
g_freq123	115200	0.020	3.367	p_freq126	118200	0.116	36.318
g_freq124	116200	0.021	3.348	p_freq127	119200	0.118	36.289
g_freq125	117200	0.021	3.334				
g_freq126	118200	0.020	3.324				
g_freq127	119200	0.023	3.304				

*Temperature is in degrees C

**Specific Conductivity is in µS/cm

B3. PLS Model Coefficients

Table B3. PLS model variables and coefficients for the three best-fit models.

Variable	Model 2A Coef	Model 3A Coef	Model Coef 6B	Variable	Model 3A Coef	Model 6B Coef
Intercept	0	0	0	p_freq1	0.009	0.048
temp	-0.167	0.033	-0.124	p_freq2	0.001	-0.013
cond	-0.138	-0.006	0.034	p_freq3	0.004	0.001
g_freq1	0.233		0.286	p_freq4	0.004	-0.004
g_freq2	-0.060		0.000	p_freq5	0.005	0.003
g_freq3	-0.042		-0.008	p_freq6	0.003	-0.002
g_freq4	-0.030		-0.002	p_freq7	0.005	0.018
g_freq5	-0.017		-0.005	p_freq8	0.004	0.006
g_freq6	-0.016		-0.004	p_freq9	0.009	0.026
g_freq7	-0.010		-0.008	p_freq10	0.018	0.098
g_freq8	-0.025		-0.007	p_freq11	0.008	0.023
g_freq9	-0.023		0.013	p_freq12	0.008	0.010
g_freq10	-0.092		0.036	p_freq13	0.006	0.008
g_freq11	-0.042		0.038	p_freq14	0.009	0.007
g_freq12	-0.063		-0.027	p_freq15	0.010	0.014
g_freq13	-0.034		0.022	p_freq16	0.013	-0.006
g_freq14	-0.084		-0.096	p_freq17	0.026	-0.004
g_freq15	-0.022		-0.048	p_freq18	0.010	-0.041
g_freq16	0.030		0.003	p_freq19	0.022	0.094
g_freq17	0.041		0.009	p_freq20	0.007	-0.001
g_freq18	-0.052		-0.034	p_freq21	0.007	-0.010
g_freq19	0.012		0.011	p_freq22	0.001	0.005
g_freq20	-0.052		-0.013	p_freq23	-0.006	-0.020
g_freq21	-0.102		-0.060	p_freq24	-0.010	-0.025
g_freq22	-0.099		0.053	p_freq25	-0.011	-0.041
g_freq23	-0.121		0.025	p_freq26	-0.011	0.026
g_freq24	-0.061		0.008	p_freq27	-0.014	-0.020
g_freq25	-0.050		-0.004	p_freq28	-0.019	-0.005
g_freq26	-0.009		0.076	p_freq29	-0.022	0.048
g_freq27	0.063		0.128	p_freq30	-0.033	-0.022
g_freq28	0.070		0.010	p_freq31	-0.035	-0.043
g_freq29	0.063		-0.009	p_freq32	-0.050	-0.057
g_freq30	0.034		-0.004	p_freq33	-0.048	0.011
g_freq31	-0.056		-0.141	p_freq34	-0.002	0.092
g_freq32	0.042		0.013	p_freq35	0.102	-0.010
g_freq33	0.101		0.113	p_freq36	0.097	0.014
g_freq34	0.093		0.047	p_freq37	0.032	0.038
g_freq35	0.151		-0.020	p_freq38	0.003	-0.069
g_freq36	0.047		0.050	p_freq39	0.031	0.022
g_freq37	-0.009		0.029	p_freq40	0.057	0.037
g_freq38	0.007		-0.044	p_freq41	0.025	-0.113
g_freq39	0.115		0.065	p_freq42	0.016	0.051
g_freq40	-0.026		0.046	p_freq43	0.017	0.060
g_freq41	-0.052		0.000	p_freq44	-0.040	-0.108
g_freq42	-0.050		-0.031	p_freq45	-0.027	-0.063
g_freq43	0.041		0.031	p_freq46	0.019	0.100

Table B3., continued. PLS model variables and coefficients for the three best-fit models.

Variable	Model 2A Coef	Model 6B Coef	Variable	Model 3A Coef	Model 6B Coef
g_freq44	-0.125	-0.156	p_freq47	0.027	0.148
g_freq45	0.098	0.058	p_freq48	0.073	0.126
g_freq46	0.052	-0.001	p_freq49	0.000	-0.074
g_freq47	0.032	0.092	p_freq50	0.008	0.064
g_freq48	0.086	-0.015	p_freq51	-0.001	0.029
g_freq49	-0.117	-0.054	p_freq52	0.001	-0.096
g_freq50	-0.102	-0.103	p_freq53	-0.013	-0.141
g_freq51	-0.192	-0.036	p_freq54	-0.002	-0.117
g_freq52	-0.087	-0.072	p_freq55	-0.005	-0.126
g_freq53	-0.177	-0.174	p_freq56	-0.014	-0.136
g_freq54	-0.179	-0.077	p_freq57	0.004	0.068
g_freq55	-0.085	0.021	p_freq58	-0.009	0.001
g_freq56	-0.125	-0.114	p_freq59	-0.012	0.177
g_freq57	0.078	0.018	p_freq60	-0.035	-0.077
g_freq58	-0.058	-0.032	p_freq61	-0.039	0.032
g_freq59	-0.024	-0.012	p_freq62	-0.032	-0.044
g_freq60	-0.001	0.065	p_freq63	-0.026	-0.115
g_freq61	0.051	0.069	p_freq64	-0.020	0.041
g_freq62	-0.025	-0.006	p_freq65	-0.027	0.044
g_freq63	0.012	-0.012	p_freq66	-0.008	0.054
g_freq64	0.058	-0.002	p_freq67	0.006	0.074
g_freq65	-0.030	0.018	p_freq68	-0.007	0.075
g_freq66	-0.021	0.010	p_freq69	-0.010	0.001
g_freq67	0.061	0.144	p_freq70	-0.027	-0.065
g_freq68	0.102	0.050	p_freq71	-0.016	0.019
g_freq69	0.023	-0.045	p_freq72	-0.015	-0.173
g_freq70	0.077	0.052	p_freq73	0.008	-0.049
g_freq71	0.066	0.034	p_freq74	0.015	0.043
g_freq72	0.047	0.082	p_freq75	0.014	0.085
g_freq73	0.024	-0.041	p_freq76	0.006	0.010
g_freq74	0.069	0.016	p_freq77	0.003	-0.036
g_freq75	0.098	0.073	p_freq78	0.004	-0.054
g_freq76	0.088	0.053	p_freq79	0.006	-0.027
g_freq77	0.046	0.009	p_freq80	0.011	0.064
g_freq78	0.022	-0.127	p_freq81	0.013	0.101
g_freq79	-0.003	-0.126	p_freq82	0.016	0.094
g_freq80	0.045	0.144	p_freq83	-0.003	-0.060
g_freq81	0.008	0.013	p_freq84	-0.015	-0.072
g_freq82	0.000	0.065	p_freq85	-0.022	-0.089
g_freq83	-0.118	-0.284	p_freq86	-0.016	-0.079
g_freq84	-0.081	-0.083	p_freq87	-0.007	-0.027
g_freq85	-0.149	-0.078	p_freq88	0.000	-0.023
g_freq86	-0.010	-0.009	p_freq89	0.004	-0.049
g_freq87	0.079	0.098	p_freq90	0.009	-0.015
g_freq88	0.061	-0.073	p_freq91	0.018	0.047
g_freq89	0.111	0.094	p_freq92	0.017	0.015

Table B3., continued. PLS model variables and coefficients for the three best-fit models.

Variable	Model 2A Coef	Model 6B Coef	Variable	Model 3A Coef	Model 6B Coef
g_freq90	0.108	-0.027	p_freq93	0.018	0.020
g_freq91	0.097	-0.174	p_freq94	0.017	0.034
g_freq92	0.106	0.014	p_freq95	0.020	0.076
g_freq93	0.078	0.029	p_freq96	0.022	0.110
g_freq94	0.083	0.124	p_freq97	0.021	0.096
g_freq95	0.069	0.066	p_freq98	0.018	-0.002
g_freq96	0.040	0.083	p_freq99	0.018	-0.037
g_freq97	0.016	-0.014	p_freq100	0.020	-0.055
g_freq98	-0.004	-0.069	p_freq101	0.024	-0.058
g_freq99	0.003	-0.086	p_freq102	0.028	0.089
g_freq100	0.017	-0.044	p_freq103	0.028	0.091
g_freq101	0.021	0.061	p_freq104	0.028	0.094
g_freq102	0.021	0.069	p_freq105	0.023	-0.006
g_freq103	-0.041	-0.044	p_freq106	0.019	-0.044
g_freq104	-0.042	0.106	p_freq107	0.016	-0.015
g_freq105	-0.061	0.014	p_freq108	0.016	0.048
g_freq106	-0.129	-0.166	p_freq109	0.014	0.008
g_freq107	-0.134	-0.120	p_freq110	0.013	-0.010
g_freq108	-0.099	0.019	p_freq111	0.011	-0.020
g_freq109	-0.067	0.067	p_freq112	0.007	-0.057
g_freq110	-0.128	-0.196	p_freq113	0.005	-0.138
g_freq111	-0.085	-0.148	p_freq114	0.007	0.005
g_freq112	-0.173	-0.142	p_freq115	0.008	0.105
g_freq113	-0.049	0.084	p_freq116	0.011	-0.004
g_freq114	0.134	0.167	p_freq117	0.009	0.067
g_freq115	-0.005	-0.021	p_freq118	0.013	0.001
g_freq116	0.050	0.126	p_freq119	0.014	-0.007
g_freq117	0.137	0.113	p_freq120	0.011	0.017
g_freq118	-0.082	-0.214	p_freq121	0.018	0.041
g_freq119	0.032	0.086	p_freq122	0.014	0.064
g_freq120	-0.111	-0.071	p_freq123	0.014	0.020
g_freq121	-0.027	0.014	p_freq124	0.005	-0.142
g_freq122	-0.084	-0.046	p_freq125	0.014	0.051
g_freq123	-0.102	-0.032	p_freq126	0.016	0.002
g_freq124	-0.076	0.085	p_freq127	0.004	-0.042
g_freq125	-0.170	-0.106			
g_freq126	-0.149	0.026			
g_freq127	-0.058	0.004			

Appendix C: Permission letters for copyrighted figures

Barbra C. Utley

From: Yogi Agrawal [yogi.agrawal@sequoiasci.com]
Sent: Thursday, October 08, 2009 11:02 AM
To: Barbra C. Utley
Subject: RE: permission to use a figure for my dissertation

As I recall, I did not sign any copyright release for this government gray document. Feel free to use it. Cheers

Yogi

From: Barbra C. Utley [mailto:barb@vt.edu]
Sent: Thursday, October 08, 2009 10:01 AM
To: yogi@sequoiasci.com
Subject: permission to use a figure for my dissertation

Mr. Agrawal,
I am racing to finish my dissertation with Biological Systems Engineering at Virginia Tech. I am working on a new technique for measuring suspended sediments in streams. I would like to use a copy of Figure 1 from your proceedings paper at the 7th Federal Interagency Sedimentation Conference in my literature review. I will be using it in a review of current technologies and would provide reference to your conference paper.

Please let me know if I need to ask someone else for permission as well. I just need email confirmation to submit to Virginia Tech's Graduate School. Thank you for your time and I look forward to hearing from you soon.

Barb Utley

Barbra C. Utley
Doctoral Candidate
Biological Systems Engineering
Virginia Tech
barb@vt.edu
540-808-8800

ELSEVIER LICENSE
TERMS AND CONDITIONS

Oct 13, 2009

This is a License Agreement between Barbra C. Utley ("You") and Elsevier ("Elsevier") provided by Copyright Clearance Center ("CCC"). The license consists of your order details, the terms and conditions provided by Elsevier, and the payment terms and conditions.

All payments must be made in full to CCC. For payment instructions, please see information listed at the bottom of this form.

Supplier	Elsevier Limited The Boulevard,Langford Lane Kidlington,Oxford,OX5 1GB,UK
Registered Company Number	1982084
Customer name	Barbra C. Utley
Customer address	422 N 300 E Providence, UT 84332
License Number	2287170669602
License date	Oct 13, 2009
Licensed content publisher	Elsevier
Licensed content publication	Journal of Hydrology
Licensed content title	High concentration suspended sediment measurements using a continuous fiber optic in-stream transmissometer
Licensed content author	Chris G. Campbell, Danny T. Laycak, William Hoppes, Nguyen T. Tran and Frank G. Shi
Licensed content date	15 September 2005
Volume number	311
Issue number	1-4
Pages	10
Type of Use	Thesis / Dissertation
Portion	Figures/table/illustration /abstracts
Portion Quantity	1
Format	Both print and electronic
You are an author of the Elsevier article	No
Are you translating?	No
Order Reference Number	
Expected publication date	Dec 2009

Elsevier VAT number	GB 494 6272 12
Permissions price	0.00 USD
Value added tax 0.0%	0.00 USD
Total	0.00 USD

Terms and Conditions

INTRODUCTION

1. The publisher for this copyrighted material is Elsevier. By clicking "accept" in connection with completing this licensing transaction, you agree that the following terms and conditions apply to this transaction (along with the Billing and Payment terms and conditions established by Copyright Clearance Center, Inc. ("CCC"), at the time that you opened your Rightslink account and that are available at any time at http://myaccount.copyright.com).

GENERAL TERMS

2. Elsevier hereby grants you permission to reproduce the aforementioned material subject to the terms and conditions indicated.

3. Acknowledgement: If any part of the material to be used (for example, figures) has appeared in our publication with credit or acknowledgement to another source, permission must also be sought from that source. If such permission is not obtained then that material may not be included in your publication/copies. Suitable acknowledgement to the source must be made, either as a footnote or in a reference list at the end of your publication, as follows:

"Reprinted from Publication title, Vol /edition number, Author(s), Title of article / title of chapter, Pages No., Copyright (Year), with permission from Elsevier [OR APPLICABLE SOCIETY COPYRIGHT OWNER]." Also Lancet special credit - "Reprinted from The Lancet, Vol. number, Author(s), Title of article, Pages No., Copyright (Year), with permission from Elsevier."

4. Reproduction of this material is confined to the purpose and/or media for which permission is hereby given.

5. Altering/Modifying Material: Not Permitted. However figures and illustrations may be altered/adapted minimally to serve your work. Any other abbreviations, additions, deletions and/or any other alterations shall be made only with prior written authorization of Elsevier Ltd. (Please contact Elsevier at permissions@elsevier.com)

6. If the permission fee for the requested use of our material is waived in this instance, please be advised that your future requests for Elsevier materials may attract a fee.

7. Reservation of Rights: Publisher reserves all rights not specifically granted in the combination of (i) the license details provided by you and accepted in the course of this licensing transaction, (ii) these terms and conditions and (iii) CCC's Billing and Payment terms and conditions.

8. License Contingent Upon Payment: While you may exercise the rights licensed

immediately upon issuance of the license at the end of the licensing process for the transaction, provided that you have disclosed complete and accurate details of your proposed use, no license is finally effective unless and until full payment is received from you (either by publisher or by CCC) as provided in CCC's Billing and Payment terms and conditions. If full payment is not received on a timely basis, then any license preliminarily granted shall be deemed automatically revoked and shall be void as if never granted. Further, in the event that you breach any of these terms and conditions or any of CCC's Billing and Payment terms and conditions, the license is automatically revoked and shall be void as if never granted. Use of materials as described in a revoked license, as well as any use of the materials beyond the scope of an unrevoked license, may constitute copyright infringement and publisher reserves the right to take any and all action to protect its copyright in the materials.

9. Warranties: Publisher makes no representations or warranties with respect to the licensed material.

10. Indemnity: You hereby indemnify and agree to hold harmless publisher and CCC, and their respective officers, directors, employees and agents, from and against any and all claims arising out of your use of the licensed material other than as specifically authorized pursuant to this license.

11. No Transfer of License: This license is personal to you and may not be sublicensed, assigned, or transferred by you to any other person without publisher's written permission.

12. No Amendment Except in Writing: This license may not be amended except in a writing signed by both parties (or, in the case of publisher, by CCC on publisher's behalf).

13. Objection to Contrary Terms: Publisher hereby objects to any terms contained in any purchase order, acknowledgment, check endorsement or other writing prepared by you, which terms are inconsistent with these terms and conditions or CCC's Billing and Payment terms and conditions. These terms and conditions, together with CCC's Billing and Payment terms and conditions (which are incorporated herein), comprise the entire agreement between you and publisher (and CCC) concerning this licensing transaction. In the event of any conflict between your obligations established by these terms and conditions and those established by CCC's Billing and Payment terms and conditions, these terms and conditions shall control.

14. Revocation: Elsevier or Copyright Clearance Center may deny the permissions described in this License at their sole discretion, for any reason or no reason, with a full refund payable to you. Notice of such denial will be made using the contact information provided by you. Failure to receive such notice will not alter or invalidate the denial. In no event will Elsevier or Copyright Clearance Center be responsible or liable for any costs, expenses or damage incurred by you as a result of a denial of your permission request, other than a refund of the amount(s) paid by you to Elsevier and/or Copyright Clearance Center for denied permissions.

LIMITED LICENSE

The following terms and conditions apply only to specific license types:

15. **Translation**: This permission is granted for non-exclusive world **English** rights only unless your license was granted for translation rights. If you licensed translation rights you

may only translate this content into the languages you requested. A professional translator must perform all translations and reproduce the content word for word preserving the integrity of the article. If this license is to re-use 1 or 2 figures then permission is granted for non-exclusive world rights in all languages.

16. **Website**: The following terms and conditions apply to electronic reserve and author websites:
Electronic reserve: If licensed material is to be posted to website, the web site is to be password-protected and made available only to bona fide students registered on a relevant course if:
This license was made in connection with a course,
This permission is granted for 1 year only. You may obtain a license for future website posting,
All content posted to the web site must maintain the copyright information line on the bottom of each image,
A hyper-text must be included to the Homepage of the journal from which you are licensing at http://www.sciencedirect.com/science/journal/xxxxx or the Elsevier homepage for books at http://www.elsevier.com , and
Central Storage: This license does not include permission for a scanned version of the material to be stored in a central repository such as that provided by Heron/XanEdu.

17. **Author website** for journals with the following additional clauses:

All content posted to the web site must maintain the copyright information line on the bottom of each image, and
he permission granted is limited to the personal version of your paper. You are not allowed to download and post the published electronic version of your article (whether PDF or HTML, proof or final version), nor may you scan the printed edition to create an electronic version,
A hyper-text must be included to the Homepage of the journal from which you are licensing at http://www.sciencedirect.com/science/journal/xxxxx , As part of our normal production process, you will receive an e-mail notice when your article appears on Elsevier's online service ScienceDirect (www.sciencedirect.com). That e-mail will include the article's Digital Object Identifier (DOI). This number provides the electronic link to the published article and should be included in the posting of your personal version. We ask that you wait until you receive this e-mail and have the DOI to do any posting.
Central Storage: This license does not include permission for a scanned version of the material to be stored in a central repository such as that provided by Heron/XanEdu.

18. **Author website** for books with the following additional clauses:
Authors are permitted to place a brief summary of their work online only.
A hyper-text must be included to the Elsevier homepage at http://www.elsevier.com

All content posted to the web site must maintain the copyright information line on the bottom of each image
You are not allowed to download and post the published electronic version of your chapter, nor may you scan the printed edition to create an electronic version.
Central Storage: This license does not include permission for a scanned version of the material to be stored in a central repository such as that provided by Heron/XanEdu.

19. **Website** (regular and for author): A hyper-text must be included to the Homepage of the journal from which you are licensing at http://www.sciencedirect.com/science/journal/xxxxx. or for books to the Elsevier homepage at http://www.elsevier.com

20. **Thesis/Dissertation**: If your license is for use in a thesis/dissertation your thesis may be submitted to your institution in either print or electronic form. Should your thesis be published commercially, please reapply for permission. These requirements include permission for the Library and Archives of Canada to supply single copies, on demand, of the complete thesis and include permission for UMI to supply single copies, on demand, of the complete thesis. Should your thesis be published commercially, please reapply for permission.

21. **Other Conditions**None

v1.6

Gratis licenses (referencing $0 in the Total field) are free. Please retain this printable license for your reference. No payment is required.

If you would like to pay for this license now, please remit this license along with your payment made payable to "COPYRIGHT CLEARANCE CENTER" otherwise you will be invoiced within 30 days of the license date. Payment should be in the form of a check or money order referencing your account number and this license number 2287170669602.
If you would prefer to pay for this license by credit card, please go to http://www.copyright.com/creditcard to download our credit card payment authorization form.

Make Payment To:
Copyright Clearance Center
Dept 001
P.O. Box 843006
Boston, MA 02284-3006

If you find copyrighted material related to this license will not be used and wish to cancel, please contact us referencing this license number 2287170669602 and noting the reason for cancellation.

Questions? customercare@copyright.com or +1-877-622-5543 (toll free in the US) or +1-978-646-2777.

Barbra C. Utley

From: Diefenderfer, Brian K. [Brian.Diefenderfer@VDOT.Virginia.gov]
Sent: Wednesday, October 07, 2009 7:42 AM
To: Barbra C. Utley
Subject: RE: permission to use figures from your dissertation

Barb –

You have my permission to use the figures as you described in your email.

Best of luck with wrapping up your dissertation. I'd appreciate an electronic copy, if you think about it, once it's completed.

Sincerely,

Brian

Brian K. Diefenderfer, Ph.D., P.E.
Research Scientist
Virginia Transportation Research Council
Virginia Department of Transportation
530 Edgemont Road
Charlottesville, VA 22903

434 293-1944 (phone)
434 293-1990 (fax)
brian.diefenderfer@vdot.virginia.gov

From: Barbra C. Utley [mailto:barb@vt.edu]
Sent: Tuesday, October 06, 2009 5:15 PM
To: Diefenderfer, Brian K.
Subject: permission to use figures from your dissertation

Dr. Diefenderfer,
I am racing to finish my dissertation with Biological Systems Engineering at Virginia Tech. I am working to develop a permittivity based sensor for measuring suspended sediment in streams. I found the background information on capacitance theory and polarization very help and copied a few of your figures.
Do you care if I used figures 2.1 and 2.3 with your work referenced in the captions of the figures? I believe your email response will serve as permission with the graduate school.

Thanks,
Barb Utley

Barbra C. Utley
Doctoral Candidate
Biological Systems Engineering
Virginia Tech
barb@vt.edu
540-808-8800

ELSEVIER LICENSE
TERMS AND CONDITIONS

Oct 06, 2009

This is a License Agreement between Barbra C. Utley ("You") and Elsevier ("Elsevier") provided by Copyright Clearance Center ("CCC"). The license consists of your order details, the terms and conditions provided by Elsevier, and the payment terms and conditions.

All payments must be made in full to CCC. For payment instructions, please see information listed at the bottom of this form.

Supplier	Elsevier Limited The Boulevard,Langford Lane Kidlington,Oxford,OX5 1GB,UK
Registered Company Number	1982084
Customer name	Barbra C. Utley
Customer address	422 N 300 E Providence, UT 84332
License Number	2283290492112
License date	Oct 06, 2009
Licensed content publisher	Elsevier
Licensed content publication	CATENA
Licensed content title	Capacitance sensors for measuring suspended sediment concentration
Licensed content author	Xiaoyu Li, Tingwu Lei, Wei Wang, Qichuan Xu and Jun Zhao
Licensed content date	31 March 2005
Volume number	60
Issue number	3
Pages	11
Type of Use	Thesis / Dissertation
Portion	Figures/table/illustration /abstracts
Portion Quantity	1
Format	Both print and electronic
You are an author of the Elsevier article	No
Are you translating?	No
Order Reference Number	
Expected publication date	Dec 2009
Elsevier VAT number	GB 494 6272 12
Permissions price	0.00 USD

Value added tax 0.0%	0.00 USD
Total	0.00 USD

Terms and Conditions

INTRODUCTION

1. The publisher for this copyrighted material is Elsevier. By clicking "accept" in connection with completing this licensing transaction, you agree that the following terms and conditions apply to this transaction (along with the Billing and Payment terms and conditions established by Copyright Clearance Center, Inc. ("CCC"), at the time that you opened your Rightslink account and that are available at any time at http://myaccount.copyright.com).

GENERAL TERMS

2. Elsevier hereby grants you permission to reproduce the aforementioned material subject to the terms and conditions indicated.

3. Acknowledgement: If any part of the material to be used (for example, figures) has appeared in our publication with credit or acknowledgement to another source, permission must also be sought from that source. If such permission is not obtained then that material may not be included in your publication/copies. Suitable acknowledgement to the source must be made, either as a footnote or in a reference list at the end of your publication, as follows:

"Reprinted from Publication title, Vol /edition number, Author(s), Title of article / title of chapter, Pages No., Copyright (Year), with permission from Elsevier [OR APPLICABLE SOCIETY COPYRIGHT OWNER]." Also Lancet special credit - "Reprinted from The Lancet, Vol. number, Author(s), Title of article, Pages No., Copyright (Year), with permission from Elsevier."

4. Reproduction of this material is confined to the purpose and/or media for which permission is hereby given.

5. Altering/Modifying Material: Not Permitted. However figures and illustrations may be altered/adapted minimally to serve your work. Any other abbreviations, additions, deletions and/or any other alterations shall be made only with prior written authorization of Elsevier Ltd. (Please contact Elsevier at permissions@elsevier.com)

6. If the permission fee for the requested use of our material is waived in this instance, please be advised that your future requests for Elsevier materials may attract a fee.

7. Reservation of Rights: Publisher reserves all rights not specifically granted in the combination of (i) the license details provided by you and accepted in the course of this licensing transaction, (ii) these terms and conditions and (iii) CCC's Billing and Payment terms and conditions.

8. License Contingent Upon Payment: While you may exercise the rights licensed immediately upon issuance of the license at the end of the licensing process for the transaction, provided that you have disclosed complete and accurate details of your proposed use, no license is finally effective unless and until full payment is received from

you (either by publisher or by CCC) as provided in CCC's Billing and Payment terms and conditions. If full payment is not received on a timely basis, then any license preliminarily granted shall be deemed automatically revoked and shall be void as if never granted. Further, in the event that you breach any of these terms and conditions or any of CCC's Billing and Payment terms and conditions, the license is automatically revoked and shall be void as if never granted. Use of materials as described in a revoked license, as well as any use of the materials beyond the scope of an unrevoked license, may constitute copyright infringement and publisher reserves the right to take any and all action to protect its copyright in the materials.

9. Warranties: Publisher makes no representations or warranties with respect to the licensed material.

10. Indemnity: You hereby indemnify and agree to hold harmless publisher and CCC, and their respective officers, directors, employees and agents, from and against any and all claims arising out of your use of the licensed material other than as specifically authorized pursuant to this license.

11. No Transfer of License: This license is personal to you and may not be sublicensed, assigned, or transferred by you to any other person without publisher's written permission.

12. No Amendment Except in Writing: This license may not be amended except in a writing signed by both parties (or, in the case of publisher, by CCC on publisher's behalf).

13. Objection to Contrary Terms: Publisher hereby objects to any terms contained in any purchase order, acknowledgment, check endorsement or other writing prepared by you, which terms are inconsistent with these terms and conditions or CCC's Billing and Payment terms and conditions. These terms and conditions, together with CCC's Billing and Payment terms and conditions (which are incorporated herein), comprise the entire agreement between you and publisher (and CCC) concerning this licensing transaction. In the event of any conflict between your obligations established by these terms and conditions and those established by CCC's Billing and Payment terms and conditions, these terms and conditions shall control.

14. Revocation: Elsevier or Copyright Clearance Center may deny the permissions described in this License at their sole discretion, for any reason or no reason, with a full refund payable to you. Notice of such denial will be made using the contact information provided by you. Failure to receive such notice will not alter or invalidate the denial. In no event will Elsevier or Copyright Clearance Center be responsible or liable for any costs, expenses or damage incurred by you as a result of a denial of your permission request, other than a refund of the amount(s) paid by you to Elsevier and/or Copyright Clearance Center for denied permissions.

LIMITED LICENSE

The following terms and conditions apply only to specific license types:

15. **Translation**: This permission is granted for non-exclusive world **English** rights only unless your license was granted for translation rights. If you licensed translation rights you may only translate this content into the languages you requested. A professional translator must perform all translations and reproduce the content word for word preserving the integrity of the article. If this license is to re-use 1 or 2 figures then permission is granted for

non-exclusive world rights in all languages.

16. **Website**: The following terms and conditions apply to electronic reserve and author websites:
Electronic reserve: If licensed material is to be posted to website, the web site is to be password-protected and made available only to bona fide students registered on a relevant course if:
This license was made in connection with a course,
This permission is granted for 1 year only. You may obtain a license for future website posting,
All content posted to the web site must maintain the copyright information line on the bottom of each image,
A hyper-text must be included to the Homepage of the journal from which you are licensing at http://www.sciencedirect.com/science/journal/xxxxx or the Elsevier homepage for books at http://www.elsevier.com , and
Central Storage: This license does not include permission for a scanned version of the material to be stored in a central repository such as that provided by Heron/XanEdu.

17. **Author website** for journals with the following additional clauses:

All content posted to the web site must maintain the copyright information line on the bottom of each image, and
he permission granted is limited to the personal version of your paper. You are not allowed to download and post the published electronic version of your article (whether PDF or HTML, proof or final version), nor may you scan the printed edition to create an electronic version,
A hyper-text must be included to the Homepage of the journal from which you are licensing at http://www.sciencedirect.com/science/journal/xxxxx , As part of our normal production process, you will receive an e-mail notice when your article appears on Elsevier's online service ScienceDirect (www.sciencedirect.com). That e-mail will include the article's Digital Object Identifier (DOI). This number provides the electronic link to the published article and should be included in the posting of your personal version. We ask that you wait until you receive this e-mail and have the DOI to do any posting.
Central Storage: This license does not include permission for a scanned version of the material to be stored in a central repository such as that provided by Heron/XanEdu.

18. **Author website** for books with the following additional clauses:
Authors are permitted to place a brief summary of their work online only.
A hyper-text must be included to the Elsevier homepage at http://www.elsevier.com

All content posted to the web site must maintain the copyright information line on the bottom of each image
You are not allowed to download and post the published electronic version of your chapter, nor may you scan the printed edition to create an electronic version.
Central Storage: This license does not include permission for a scanned version of the material to be stored in a central repository such as that provided by Heron/XanEdu.

19. **Website** (regular and for author): A hyper-text must be included to the Homepage of the journal from which you are licensing at http://www.sciencedirect.com/science/journal

/xxxxx. or for books to the Elsevier homepage at http://www.elsevier.com

20. **Thesis/Dissertation**: If your license is for use in a thesis/dissertation your thesis may be submitted to your institution in either print or electronic form. Should your thesis be published commercially, please reapply for permission. These requirements include permission for the Library and Archives of Canada to supply single copies, on demand, of the complete thesis and include permission for UMI to supply single copies, on demand, of the complete thesis. Should your thesis be published commercially, please reapply for permission.

21. **Other Conditions**None

v1.6

Gratis licenses (referencing $0 in the Total field) are free. Please retain this printable license for your reference. No payment is required.

If you would like to pay for this license now, please remit this license along with your payment made payable to "COPYRIGHT CLEARANCE CENTER" otherwise you will be invoiced within 30 days of the license date. Payment should be in the form of a check or money order referencing your account number and this license number 2283290492112.
If you would prefer to pay for this license by credit card, please go to http://www.copyright.com/creditcard to download our credit card payment authorization form.

Make Payment To:
Copyright Clearance Center
Dept 001
P.O. Box 843006
Boston, MA 02284-3006

If you find copyrighted material related to this license will not be used and wish to cancel, please contact us referencing this license number 2283290492112 and noting the reason for cancellation.

Questions? customercare@copyright.com or +1-877-622-5543 (toll free in the US) or +1-978-646-2777.

Barbra C. Utley

From: Academic Permissions [Academic.permissions@oup.com]
Sent: Thursday, October 08, 2009 6:57 AM
To: barb@vt.edu
Subject: FW: seeking permission to copy figure from a text book

Dear Barbra,
Thank you for your enquiry. You have our permission to use the OUP Material you list in your email below in your dissertation for submission to Virginia Tech.

If at some future date your thesis is published it will be necessary to re-clear this permission.
Please also note that if the material to be used is acknowledged to any other source, you will need to clear permission with the rights holder.

Best wishes,

Ben Kennedy
Permissions Assistant
Academic Rights & Journals
Oxford University Press
Great Clarendon Street
Oxford
OX2 6DP
Direct tel. +44 (0)1865 354728
Direct fax +44 (0)1865 353429
e mail: ben.kennedy@oup.com

From: Barbra C. Utley [mailto:barb@vt.edu]
Sent: Wednesday, October 07, 2009 2:29 PM
To: Cary - Customer Service (External)
Subject: seeking permission to copy figure from a text book

Hello,
I am seeking permission to use a figure from McBride, 1994, A Soil Chemistry text book. I am not sure where on your website to find this information. I have tried the academic permissions link and it goes to an error page. I would like to use a figure from McBride in my dissertation. I am racing to finish my dissertation for defense at the end of this month. I need to have my permissions in place before I can submit the electronic version of the document to my graduate school, so a speedy reply would be appreciated.
Thanks,
Barb Utley

Barbra C. Utley
Doctoral Candidate
Biological Systems Engineering
Virginia Tech
barb@vt.edu
540-808-8800

AMERICAN SOCIETY OF CIVIL ENGINEERS LICENSE TERMS AND CONDITIONS

Oct 06, 2009

This is a License Agreement between Barbra C. Utley ("You") and American Society of Civil Engineers ("American Society of Civil Engineers") provided by Copyright Clearance Center ("CCC"). The license consists of your order details, the terms and conditions provided by American Society of Civil Engineers, and the payment terms and conditions.

All payments must be made in full to CCC. For payment instructions, please see information listed at the bottom of this form.

License Number	2283280600009
License date	Oct 06, 2009
Licensed content title	Field Techniques for Suspended-Sediment Measurement
Licensed content author	D. G. Wren; B. D. Barkdoll; R. A. Kuhnle; R. W. Derrow
Licensed content publication	Journal of Hydraulic Engineering
Licensed content publisher	American Society of Civil Engineers
Type of Use	Doctoral Thesis
Portion used	Figure
Number of figures	4
Institution	Virginia Polytechnic and State University
Title of your work	Continuous suspended sediment monitoring using a permittivity sensor
Publisher of your work	Virginia Polytechnic and State University
Publication date of your work	12/18/2009
Website	http://twosweet.bse.vt.edu/Barb/
Usage	both
Billing Type	Invoice
Company	Barbra C. Utley
Billing Address	422 N 300 E Providence, UT 84332 United States
Customer reference info	
Total	$0.00

Terms and Conditions

A Terms and Conditions agreement is a document that describes the terms and conditions of a license to the licensee. ASCE Terms and Conditions are available during the order process, although you may review the Terms and Conditions below, before placing an order.

The publisher for this copyrighted material is The American Society of Civil Engineers (ASCE). By clicking "accept", you agree that the following terms and conditions apply to this transaction, along with the billing and payment terms and conditions established by Copyright Clearance Center, Inc. (CCC) at the time that you opened your Rightslink® account. The terms and conditions information is available when you log in to Rightslink.

One Time Permission
Each license is unique, covering only the terms and conditions specified in it. Even if you have obtained a license for certain ASCE-copyrighted content, you will need to obtain another license if you plan to reuse that content outside the terms of the existing license. For example: If you already have a license to reuse a figure in a journal, you still need a new license to use the same figure in a magazine.

Embargo
Permission will be denied if the content is requested within 3 months of the publication date.

No-Fee License
A $0 license is granted to authors who wish to reuse their own content and to authors who wish to reuse ASCE-copyrighted content in their works prepared for another ASCE publication.

Credit Lines
A full credit line must be added to the material being reprinted.

- For reuse in non-ASCE publications, add the words "With permission from ASCE" to your source citation.
- For reuse in ASCE publications, add a comma and "ASCE" after the author-date citation. For example: (Jones and Taylor 2003, ASCE)
- For online posting, add the following additional notice: "This material may be downloaded for personal use only. Any other use requires prior permission of the American Society of Civil Engineers. This material may be found at [URL/link of abstract in the Civil Engineering Database]." (Online use is a limited use that is essentially equivalent to or substitutes for the print version, and embedded material (or a specific link to it) remains in situ; it does not include use as part of a database or other uses that might conflict with or prejudice the usage of the material by ASCE.)

Online Coursepack
The site must be password protected and posted for the semester only.

ASCE Magazines
Permissions granted only for text from Civil Engineering magazine and ASCE News. Permission to use photographs, graphics, figures, or tables must be requested from the copyright owner as noted in the credit line.

Materials Not Copyrighted by ASCE
The requesting party is responsible for ensuring that the material is original to ASCE and that it does not contain the copyright of another entity or reference that it was reprinted by ASCE with permission from another source.

General
The foregoing License shall not take effect unless and until ASCE or CCC receives the

payment in accordance with the CCC Billing and Payment Terms and Conditions (including all payment provisions), which are incorporated herein by reference. Failure to fully comply with the terms of this License or the CCC Billing and Payment Terms and Conditions shall automatically render this License null and void.

ASCE or CCC may, at any time, deny the permissions described in this License at their sole discretion, for any reason or no reason, with a full refund payable to you. Notice of such denial will be made using the contact information provided by you. Failure to receive such notice will not alter or invalidate the denial. In no event will ASCE or CCC be responsible or liable for any costs, expenses or damage incurred by you as a result of a denial of your permission request, other than a refund of the amount(s) paid by you to CCC for denied permissions.

Gratis licenses (referencing $0 in the Total field) are free. Please retain this printable license for your reference. No payment is required.

If you would like to pay for this license now, please remit this license along with your payment made payable to "COPYRIGHT CLEARANCE CENTER" otherwise you will be invoiced within 30 days of the license date. Payment should be in the form of a check or money order referencing your account number and this license number 2283280600009.
If you would prefer to pay for this license by credit card, please go to http://www.copyright.com/creditcard to download our credit card payment authorization form.

Make Payment To:
Copyright Clearance Center
Dept 001
P.O. Box 843006
Boston, MA 02284-3006

If you find copyrighted material related to this license will not be used and wish to cancel, please contact us referencing this license number 2283280600009 and noting the reason for cancellation.

Questions? customercare@copyright.com or +1-877-622-5543 (toll free in the US) or +1-978-646-2777.

Barbra C. Utley

From: Tess Wynn [thwynn@vt.edu]
Sent: Wednesday, December 02, 2009 3:35 PM
To: Barbra C. Utley
Subject: copyright permission

Barb,

You have my permission to use the photos in Figures 1.1, 2.2, 2.3, and 2.6 of your dissertation.

Tess

Tess Wynn, PhD
Assistant Professor, Biological Systems Engineering
302 Seitz Hall, Virginia Tech
Blacksburg, VA 24061-0303
Phone: 540.231.2454
FAX: 540.231.3199
http://twosweet.bse.vt.edu/